UNIVERSITY OF BIRMINGHAM

CYBER-PHYSICAL MERGED LEARNING FOR ONLINE OPTIMISATION OF MULTI-MODE HYBRID VEHICLES WITH DIVERSE TIME-SCALE OBJECTIVES

by

CETENGFEI ZHANG

A thesis submitted to the University of Birmingham for the degree of
DOCTOR OF PHILOSOPHY

Department of Mechanical Engineering
School of Engineering
College of Engineering and Physical Science
University of Birmingham
03/2024

Abstract

A comprehensive investigation of the energy management and optimisation techniques used in multi-mode plug-in hybrid electric vehicles (PHEVs) is presented in this thesis. It focuses on using artificial intelligence and sophisticated control algorithms to improve multi-mode PHEV performance and efficiency. With the goal of increasing fuel efficiency and product life cycle, the research combines cutting-edge techniques for cyber-physical adaptive control schemes, real-time energy management, and battery state estimation.

This thesis first presents the development of a dedicated adaptive particle swarm optimisation (DAPSO) for offline optimisation based on a digital twin boost of the efficiency and dependability of PHEVs' energy management system (EMS) control. In terms of fuel efficiency and battery state-of-charge (SoC) maintenance, the DAPSO is superior in performance compared to traditional algorithms.

Then, regarding the electrification of multi-mode PHEVs, an intelligent digital model of a battery is developed with challenging circumstances for an automotive battery to obtain real-time status estimation. In order to improve functionality and reliability in real-time applications, this model uses both deep neural networks (NN) and Gaussian process regression with automatic relevance determination (ARD-GPR) approaches based on a modified equivalent circuit battery model (ECM) for handling health indicators throughout the charging and discharging processes.

This thesis finally develops a cuboid equivalent consumption minimisation strategy (C-ECMS) for multi-mode PHEVs. The C-ECMS provides improved performance in online optimal energy management with multiple objectives in diverse time scales. In real-world driving conditions, this strategy improves overall performance and economy by establishing a compromise between battery health, fuel efficiency, and SoC control accuracy.

The results address both the scientific and practical elements of automotive technology, providing insightful information for the development of more efficient and environmentally friendly multi-mode PHEVs.

Acknowledgements

Just like many stories, I often see myself as a Hobbit, having come from distant mountains. Since the appearances and weather of the Winterbourne garden are so similar to the Shire, and many scenes in Birmingham are said to have sparked Tolkien's inspiration in his writings for The Lord of the Rings, they have become a source of inspiration for me as well. It all began four years ago when I heard the call of research from Prof. Xu (my first supervisor) as I returned from London to Birmingham. My Gandalf, Prof. Zhou (my second supervisor), was in a restaurant at the foot of Edgbaston, sharing his vision for scientific research with me. I will try to describe our experiences in a classical and interesting manner, as if this is not an acknowledgement in a doctoral thesis, but a prelude to a novel of my life's fantastical adventure. Listening to them describe academic and industrial research like hidden treasures in a Dwarven kingdom, at that time I thought, 'Yes, I will join this journey'.

After I participated in various research projects and competitions, we celebrated new friendships and farewells at the Goose Bar and Fox Copper, we roamed endlessly through the red-brick campus. During my research time, I encountered my own 'Lonely Mountain,' crossed 'Long Lake Town,' stood firm in 'Helm's Deep'. I would like to express my most gratitude to my first supervisor, Prof. Hongming Xu, and my second supervisor, Prof. Quan Zhou, for their guidance during my doctoral studies. I am also thankful for the important advice and insights from my senior colleagues: Prof. Huw Williams and Prof. Yongjin Wang, and special thanks to Dr Lun Hua and Dr Mike Bassett for their direct support of industrial projects. I am grateful for the companionship of my fellow travellers: Dr Bin Shuai, Dr Zeyu Sun, Mr Fanggang Zhang, Ms Min Hua, Dr Guojie Deng, Mr Yiming Zhang, Mr Chengqing Wen, Mr Xu He, Mr Hongyu Sun, who have been with

me day and night. My PhD might have been finished earlier without them, but their presence made these years much happier. I would also like to thank my friends from afar: Mr Yufei Jin, Mr Xingji Xiong, Mr Jiacheng Li, Ms Zhe Zhong, Ms Ip Tsz, Ms Amora, and Ms Xina Zhang. Additionally, I'm grateful to many others who responded like distant stars when called upon in the night—those who promised to journey together with me, whether in Lothlórien, Rivendell, Gondor, or the quiet Goblin Forest. I have tried not to describe my companions with any characters we already know, as each of them is unique. Whether we're like the Fellowship of the Ring or the Dwarves seeking the Lonely Mountain, I'm sure of my luck as a Hobbit, reaching this day with the help of many friends. Thank you for sharing laughter, tears, emotions, and memories on my life's journey. Finally, I would like to thank my parents and grandparents for their unwavering support, and my dog Bubble for waiting for me every year.

I would like to extend my special thanks to Janet Hingley for her assistance for so many years in proofreading my undergraduate, master's, and doctoral theses. Additionally, I am grateful to Carl Hingley for his enlightenment in the field of automotive engineering many years ago.

Last but not least, I extend my deepest gratitude to my mentors, Prof. Xu and Prof. Zhou, for leading me into the world of academia and joining me in the excavation of research treasures. I will always cherish the moments spent in the office and laboratory, and those times of brainstorming, theorising, and calculating on scratch paper and blackboards in the basement of Costa coffee.

Now, it seems my adventure in Middle-earth may be drawing to a close. The fleet to the Undying Lands, where the elves journey, is about to set sail, and my beloved awaits me. The sound of flutes and violins calls to me again. I think I remain happy, as joyful as a Hobbit starting out from Bag End, forever embracing my gratitude and hope, looking forward to the future.

Contents

List of Figures

List of Tables

List of Publications

Journal papers

[1] **C. Zhang** et al., "Dedicated Adaptive Particle Swarm Optimization Algorithm for Digital Twin Based Control Optimization of the Plug-In Hybrid Vehicle," in *IEEE Transactions on Transportation Electrification*, vol. 9, no. 2, pp. 3137-3148, June 2023, doi: 10.1109/TTE.2022.3219290. **(Published)**

[2] **C. Zhang**, Q. Zhou, M. Hua, H. Xu, M. Bassett, and F. Zhang, "Cuboid equivalent consumption minimization strategy for energy management of multi-mode plug-in hybrid vehicles considering diverse time scale objectives," *Applied Energy*, vol. 351, pp. 121901–121901, Dec. 2023, doi: https://doi.org/10.1016/j.apenergy.2023.121901. **(Published)**

[3] M. Hua, **C. Zhang**, F. Zhang, Z. Li, H. Xu, and Q. Zhou, "Energy management of multi-mode plug-in hybrid electric vehicle using multi-agent deep reinforcement learning," *Applied Energy*, vol. 348, pp. 121526–121526, Oct. 2023. **(Published)**

[4] Q. Zhou, **C. Zhang**, Y. Li, B. Shuai, and H. Xu, "Robust optimization of energy management strategy in hybrid vehicles based on digital twin and PSO algorithm," *Journal of Automotive Safety and Energy*, vol. 13, no. 3, pp. 517–525, 2022. **(Published)**

[5] **C. Zhang**, Q. Zhou, Z. Ren, Y.Chen, A A Abdillah, and H. Xu, "A multi-kernel ARD-GPR frame for Li-ion battery SoH estimation and aging attribution based on Bayesian optimization," *IEEE Transactions on Industrial Informatics*. **(Submitted/Under reviewing)**

Conference papers

[1] **C. Zhang**, Q. Zhou, Y. Li, H. Liao, and H. Xu, "The Digital Twin Modelling of the Electrified Vehicle Based on A Hybrid Terminating Control of Particle Swarm Optimization," *IFAC-PapersOnLine*, vol. 54, no. 10, pp. 552–557, Jan. 2021. **(Published)**

[2] **C. Zhang**, Q. Zhou, M. Hua, C. Wang, and H. Xu, "Online Double-layer System Identification Scheme for Battery State-of-Health Prediction," in *Proceedings of International Conference on Applied Energy*, 2021. **(Published)**

[3] Q. Zhou, Y. Li, **C. Zhang**, L. Hua, H. Williams and H. Xu, "Transferable Representation Model Driven by Gaussion Process Regression for Real-time Energy Management of Plug-in Hybrid Vehicles," *2021 5th CAA International Conference on Vehicular Control and Intelligence (CVCI)*, Tianjin, China, 2021, pp. 1-6, doi: 10.1109/CVCI54083.2021.9661134. **(Published)**

[4] M. Hua, Q. Zhou, C. Wang, **C. Zhang**, B. Shuai, and H. Xu, "Surrogate Modelling for Battery State-of-Charge Estimation in Electric Vehicles Based on Pseudo-2-Dimensional Model and Gradient Boosting Machines," in *Proceedings of International Conference on Applied Energy*, 2021. **(Published)**

Nomenclature

GHG Greenhouse gases
NZE Net Zero Emissions
OEM original equipment manufacturers
EV electric vehicle
ADAS advanced driver-assistance system
E/E electrical and electronic components
ECU electronic control unit
EMS energy management system
BMS battery management system
BTMS battery thermal management system
MHEV mild hybrid electric vehicle
HEV hybrid electric vehicle
PHEV plug-in hybrid electric vehicle
FEV full electric vehicle
BEV battery electric vehicle
REEV range extender electric vehicle
MMHEV multi-mode hybrid electric vehicle
ICE internal combustion engine
EM electrical motor
SoC state-of-charge
SoH state-of-health
RUL remaining usable life
HiL Hardware-in-the-loop
PiL Processor-in-the-loop
SiL Software-in-the-loop
DT digital twin
IoT Internet of Things
DAQ data acquisition
SPM single particle models
P2D pseudo-two-dimensional models
ECM Equivalent circuit models
RC resistor-capacitor
ML machine learning
AI artificial intelligence
RF random forest
SVM support vector machine
PSO particle swarm optimisation
NN neural network
FNN feedforward neural networks
CNN convolutional neural networks
RNN recurrent neural networks
LSTM long short-term memory
GRU gate recurrent units
GPR Gaussian process regression
OCV open circuit voltage
KF Kalman filter
EA evolutionary algorithm
DA differential analysis
ICA incremental capacity analysis
DVA differential voltage analysis
DTV differential thermal voltammetry
DMP differential mechanical parameter
EM empirical models
RB rule-based
OB optimisation-based
LB learning-based
DOE design of experiments
DP dynamic programming
PMP Pontryagin's minimum principle
SA simulated annealing
GA genetic algorithm
MPC model predictive control
ECMS equivalent consumption minimisation strategy
EF equivalent factor
TD temporal difference
MARL multi-agent reinforcement learning
PCA principal component analysis
ARD automatic relevance determination
HI health indicators
AF ageing factor

NEDC New European Driving Cycle
UDDS Urban dynamometer driving schedule
WLTC Worldwide Harmonised Light Vehicles Test Cycle
CADC Common Artemis Driving Cycles
HWFET Highway Fuel Economy Driving Schedule
FTP Federal Test Procedure
EPA environmental protection agency
NASA National Aeronautics and Space Administration
CC constant current
CV constant voltage
BSFC brake-specific fuel consumption
EOL end of life
DoD depth of discharge
RMSE root mean square error
MAE mean absolute error
OBD onboard diagnostics
CAN controller area network
LAN local area network
PI parameter identification
DCNN deep convolutional neural network
BPTT back-propagation through time
TCCC time of constant current charge process
TCVC time of constant voltage charge process
ICP incremental capacity peak value
MAT maximum temperature
MATL maximum temperature location
SE squared-exponential
RQ rational quadratic
MLE maximum likelihood estimation
BO Bayesian optimisation
AC acquisition function
SMBO sequential model-based optimisation
EI expected improvement
PDF probability density function
CD charging-depleting
CS charging-sustaining
DAPSO Dedicated adaptive particle swarm optimisation
ODSI Online double-layer system identification
C-ECMS cuboid equivalent consumption minimisation strategy

CHAPTER 1

Introduction

1.1 Background

1.1.1 The electrification of light-duty vehicles

The automotive industry is currently experiencing a significant shift towards electrification and digitalisation. Since the beginning of the 21st century, global greenhouse gas (GHG) emissions have grown steadily in comparison to the two previous decades, mainly due to the increase in fossil CO2 emissions in previous decades, mainly due to the increase in fossil CO2 emissions. Until 2022, the global energy-related emissions of CO_2 reached a historically high level with 36.8 Giga tonnes (Gt). Specifically, from the sectors' distribution in Fig.1.1, CO_2 emissions increased in power generation and transport with 261 Mega tonnes (Mt) and 254 Mega tonnes (Mt) respectively and had a decrease in industry with 156 Mt. Overall, the CO_2 emission increased 321 Mt with a growth of 0.9% comparing with last year. [1]

More specifically, the sectoral breakdown of CO_2 emissions in 2022 reveals broadly consistent patterns to previous years. According to research by Liu et al. [2], in 2022, power accounted for 39.3% of the CO_2 emissions total, the industry took 28.9%, ground transportation took 17.9%, residential took 9.9%, international bunkers (international aviation and shipping) was 3.1%, and domestic aviation was 0.9%. Among these, the

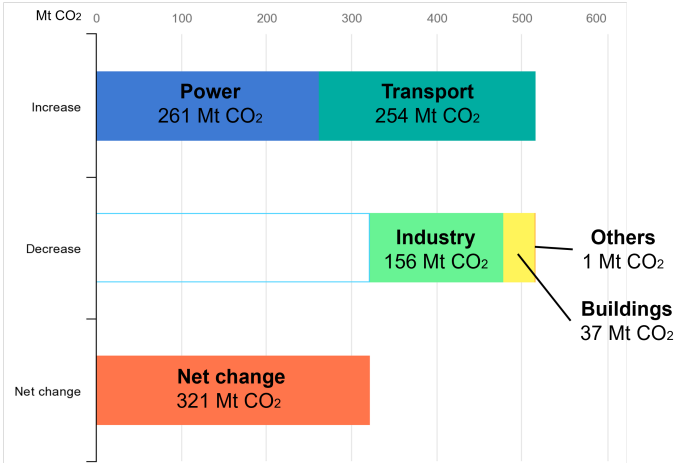

Fig. 1.1. Change in CO2 emissions by sector, 2021-2022 [1]

automotive industry is directly connected with the CO_2 emissions from power generation and ground transportation, which have played significant roles in global GHG emissions in past decades. Based on the continued growing environmental concerns with the target of Net Zero Emissions (NZE) by 2050 scenario [3], the shift to electrification for light-duty vehicles is imperative and inevitable. It is predicted that emissions of around 700 Mt CO_2-equivalents will be avoided by the use of electric cars in 2030 [4].

In such circumstances, original equipment manufacturers (OEMs) of automotive industries face upgrading vehicles in carbon reduction with high efficiency and low cost. Thus, electrification and digitalisation take two of the most significant directions for the future drive technologies. For electrification, in 2022, the European Commission raised an agreement to ensure all new cars and vans registered in Europe will be zero-emission by 2035 to fulfil the target of 'Fit for 55', where this refers to the EU's target of reducing net greenhouse gas emissions by at least 55% by 2030 [5].

In China, support has been particularly prevalent at the local level, thereby stimulating national uptake and the development of major electric vehicle (EV) companies. While in the United States, the Inflation Reduction Act (IRA) was passed in 2022, particularly on accelerating EV adoption, dedicated funding of around USD 369 billion for clean energy is allocated to climate investments. In 2022-2023, more and more countries

proposed policies to accelerate electric car adoption, either by strengthening existing plans or introducing a support mechanism for the first time, such as Japan's Green Growth Strategy or Canada's LDV deployment in 2022 [4]. In a nutshell, globally harmonised technical regulations for safer and cleaner electric vehicle deployment is the main focus of the world, as the technology continues to evolve and as societal pressures to address climate change grow, the move towards electrified transportation is expected to accelerate.

1.1.2 The digitalisation of light-duty vehicles

In recent years, digitalisation has gained widespread attention as one of the key directions for driving the automotive industry's upgrade and embracing innovative technologies. Digitalisation, as known as digital transformation, normally refers to the integration and application of digital technologies and solutions throughout the entire automotive industry value chain. The digitalisation aims to improve the efficiency of product development, drive innovations, and create a better user experience for customers for variable environments. According to a report of PwC [6], the digitalisation trends nowadays are mainly focused on such areas: 1. Digital user experience. 2. Digital in e-Mobility, Automated driving, and Smart mobility services 3. Automotive product development and manufacturing and 4. Political influences. For users, consumers desire more intelligent assistants for their digital experiences in vehicles. Automotive digital user experience (UX) and user interface (UI) are becoming increasingly important as the automotive industry continues to undergo digital transformation. By 2030, the global automotive software and electronics market is expected to reach $462 billion, representing a 5.5% CAGR from 2019 to 2030. [7] For e-mobility, automated driving and smart mobility services, the global market is expected to reach $8 billion (e-mobility) and $79 billion (advanced driver-assistance system, ADAS) after 2030 [6]. Moreover, R&D and manufacturing attracted focuses based on connected devices & sensors, predictive product analytics with AI and human-machine interfaces such as enhanced virtual reality (VR) or digital twin (DT). [8] Also, countries and

organisations are leading to support the digital transformation, for example, the UK motorsport sector has a significant real time simulation and advanced analytics capability, and the gaming industry is collaborating with manufacturers to enable new virtual product and process validation techniques [9]. The European Commission is supporting research and innovation to make Europe a world leader in connected and automated mobility (CAM) systems and services [10]. In general, the market of digitalisation for automotive can be indicated by the development of software (SW) and electrical and electronic components (E/E), where autonomous driving, connected vehicles, electrification of the powertrain and shared mobility (ACES) are significantly influenced. McKinsey & Company presented an overview of the predicted future market as Fig.1.2, the market distribution and prediction can be obtained that the future concentration of the digital transformation for the automotive industry, where automotive software, electrical unit control and power electronics play significant roles, therefore the energy management system (EMS) and its control will be focused via digitalisation path.

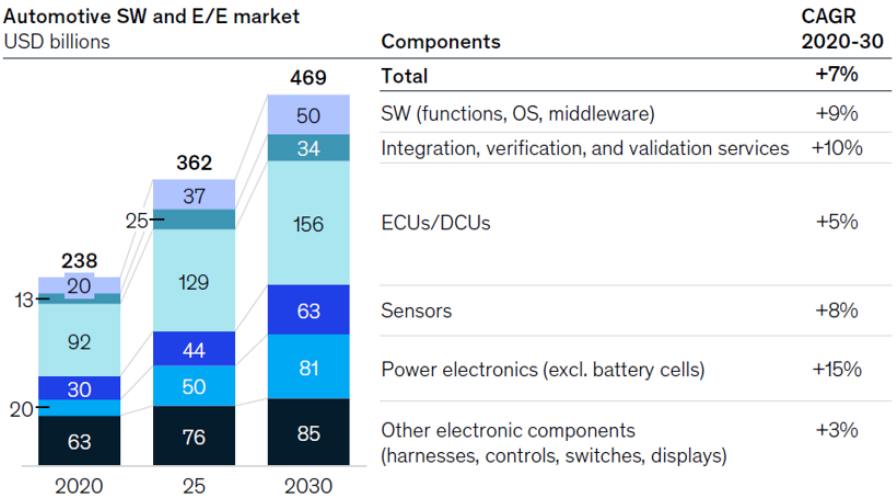

Fig. 1.2. Automotive SW and E/E market prediction [7]

1.1.3 Current development of the powertrain for electrified vehicles

The powertrain of electrified vehicles (EVs) has witnessed significant advancements in recent years as the push towards cleaner, more sustainable modes of transportation intensifies. The overarching goal is to improve efficiency, performance, reliability, and affordability. Comprehensively, notable developments in the EVs' powertrain landscape can be classified into several main categories based on their extent of electrification and frame topology according to existing research [11][12] , i.e. mild hybrid electric vehicle (MHEV), hybrid electric vehicle (HEV), plug-in hybrid electric vehicle (PHEV), full electric vehicle (FEV). The hybrid electric vehicle (as known as full hybrid electric vehicle) is the most mature powertrain technology in the present market. Generally, the HEV is classified as parallel HEV, series HEV and Series-parallel HEV. Specifically, some prominent powertrains will be introduced in below, such as range extender electric vehicle (REEV) or multi-mode hybrid electric vehicle (MMHEV).

Mild hybrid electric vehicle (MHEV)

A mild hybrid electric vehicle (MHEV) is a type of hybrid vehicle that combines an internal combustion engine (ICE), a battery, and an electric motor. The battery and motor, on the other hand, are far smaller than those seen in full hybrid electric vehicles. [13] The primary function of the additional electrical power source is to aid vehicles in modestly improving fuel efficiency and lowering emissions. However, when compared to the installation of a powertrain for a full hybrid electrified vehicle, the cost and weight penalty of MHEV are lower. When the trade-off between performance and cost is significant, the MHEV can be explored as an alternative, i.e. Honda hybrids with Integrated Motor Assist, Land Rover SUVs.

Parallel-hybrid electric vehicle

In parallel HEV topology, the driving power is supplied by the internal combustion engine (ICE) and the electrical motor (EM) via a torque coupling based on a conventional transmission possibly with a differential. This type of powertrain can be further classified into five sub-types: P_0, P_1, P_2, P_3, P_4, based on the location and size of EMs [14]. Zhuang et al. [12] further illustrated the classification as Fig.1.3. In P_0 architecture, the EM is usually installed with ICE via a belt connection, the EM is used to start ICE's work where this powertrain is also known as the belt starter generator architecture. Typically, HEV with P_0 has only a small EM for the start-stop function, i.e. Ram trucks or Jeep SUVs with the e-Torque system. A P_1 HEV is a hybrid electric vehicle that utilises an EM connected directly to the crankshaft of the engine, which is also known as an integrated starter generator (ISG). However, due to the physical limitations of the system, the ISG is normally can only provide some additional torque for acceleration-deceleration, start-stop action, or regenerative brake [15], i.e. Honda Insight. For P_2 and P_3 HEV, as in Fig.1.3, the EMs are integrated between the engine but before the transmission (P_2), and after transmission before the final drive (P_3), respectively. These setups are more adaptable than P1, allowing for longer periods of electric-only drive and stronger regenerative braking [14]. Both P_2 and P_3 can be powered solely by the electric motor under certain situations. However, when compared to P_1 or P_2, the P_3 system can operate entirely on electricity at a wider range of speeds and weights. [16] P_4 powertrain architecture usually has EMs mounted in the rear axis or in wheel hubs, with the highest extent of electrification and the highest energy recuperation potential. Moreover, P_4 is generally not used independently but is combined with other parallel subtypes, i.e. P_2 or P_3 [12], where it is typically seen in vehicles that are primarily front-wheel drive but can offer rear electric propulsion when necessary, such as a Toyota RAV4 AWD Hybrid.

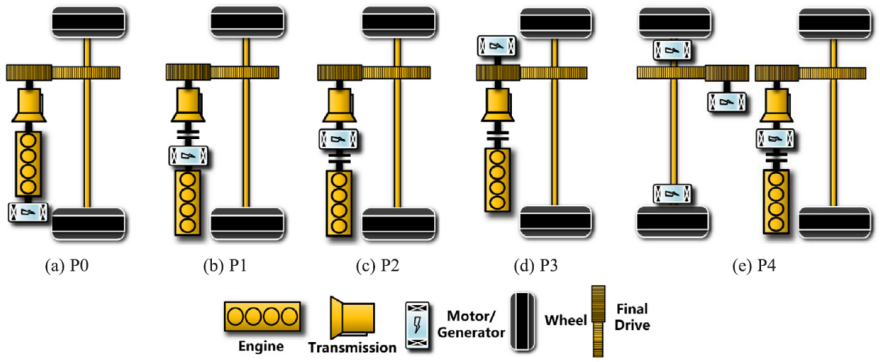

Fig. 1.3. Subtypes of P_0 to P_4 in parallel HEV [14]

Series-hybrid and Range-extender electric vehicle (REEV)

Another typical powertrain of HEVs is the series-hybrid powertrain, where series HEV normally use an EM to drive the vehicle as the traction power source with an ICE connected to an EM which acts as a generator. A typical configuration of a series-hybrid electric vehicle is shown as Fig.1.4, the EM only provides power to the wheels, and it receives electric power from either the battery pack or from a generator run by an ICE, also, a regenerative braking can be deployed to recharge the battery pack.

As a special topology of the series-hybrid electric vehicles, the range-extender EV (REEV) combines a battery-powered electric motor with an internal combustion engine (ICE) that serves primarily as a generator to produce electricity when the battery is depleted [11]. The primary propulsion of REEV is only given by the traction EM, and the ICE with a generator acts as an additional power source to provide electricity, extending the driving range, such as Chevrolet Volt or BMW-i3 REx.

Plug-in hybrid electric vehicle (PHEV)

Based on existing HEV technologies, the PHEV bridges the gap between traditional gasoline vehicles and strictly battery-powered electric vehicles. The defining feature of a PHEV is its ability to be plugged into an electrical power grid to charge its battery, with an additional ICE directly driving the powertrain or charging the electricity [17]. Thus,

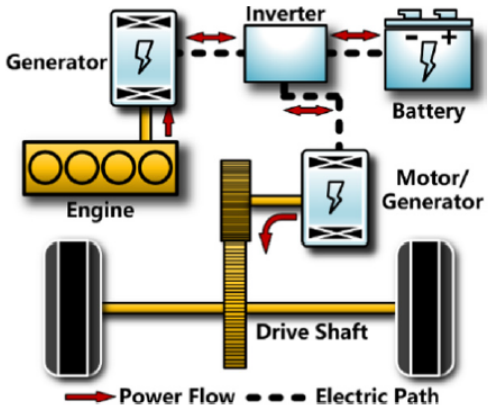

Fig. 1.4. Configuration of series HEV [14]

normally the PHEV can be regarded as a conventional HEV's powertrain with the ability to directly charge from an electrical outlet or charging station.

Series-parallel and Multi-mode hybrid electric vehicle (MMHEV)

A series-parallel-hybrid electric vehicle is a type of hybrid electric vehicle powertrain that combines elements of both series and parallel-hybrid systems. On some occasions, they are also referred to as power-split HEVs. The whole powertrain is designed to operate in either mode or a combination of both. This system dedicatedly combines the advantages of both types of hybrid systems (series-hybrid and parallel-hybrid) to achieve better energy efficiency across a broader range of complex driving conditions [18]. As is shown in Fig.1.5, the series-parallel HEV can operate with multiple types of energy flows: EV, series and parallel. If the battery's state-of-charge (SoC) is high, the vehicle can be driven only by the EM in an electricity-depleting mode. If the driving condition contains numerous start-stop or low-speed situations, i.e. urban driving area, the vehicle can operate as the series-hybrid mode as the EM covers the fast torque and speed changes with assistant power support from the engine-generator (range-extender). Moreover, if the vehicle is running with a requirement of high-speed cruising or extreme torque, the parallel mode can be deployed. It is also worth mentioning that, normally a series-parallel HEV also has plug-in charging functionality, such as Honda i-MMD.

Based on the perspective of series-parallel HEV, multi-mode HEVs are becoming increasingly popular and are available in a wide range of models and brands. The definition of multi-mode HEV (MMHEV) is raised with concentrations on multiple operational modes for optimising energy efficiency and optimally controlling performance across various driving conditions [19]. Compared to the conventional series-parallel HEVs, the scope of multi-mode HEV goes beyond just series and parallel configurations' transferring, its distinct feature are more advanced and intelligent control strategies in optimally controlling the fast-changed energy flows based on multiple power sources [20]. It is worth pointing out that series-parallel HEV and multi-mode HEV can sometimes be used interchangeably to describe advanced powertrain distribution due to their inherent overlapping functionalities.

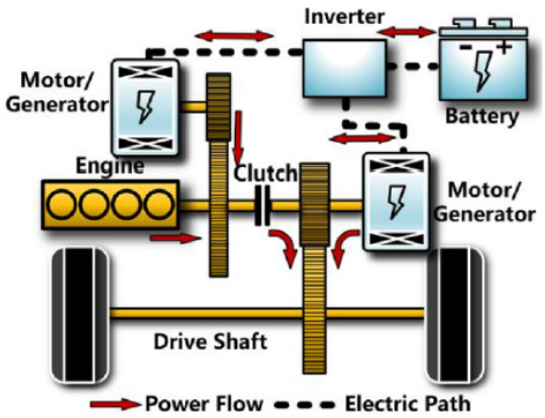

Fig. 1.5. Powertrain structure of a typical series-parallel HEV [14]

Full electric vehicle (FEV)

The full electric vehicle (FEV) is usually also known as a battery electric vehicle (BEV) or just been simplified as an electrical vehicle (EV). FEVs are powered entirely by electricity stored in on-board batteries and charged from the grid. [21] The BEV is one of the solutions to the transportation goal of zero emissions because of its environmental influences. Also, the relatively low costs of operation and maintenance provide economic benefits. However, the BEV is still suffering some negative considerations, such as

driving range anxiety, long charging times, battery degradation and side effects during the production of batteries [22].

1.1.4 The state of the art of the battery status estimation and prediction

As the process of automotive electrification deepens, electrified vehicles (including HEV, PHEV, BEV, etc.) increasingly rely on batteries as their primary source of energy. Battery application is one of the major costs for many EVs, and needs to be considered in terms of how to reduce degradation, extend their lifespan, and thereby lower the costs associated with replacement and maintenance, and also reduce the pollution of production during the automotive product's lifecycle [23]. This consideration serves as an important foundation for researching battery status and predicting future health conditions. [24] From the report of IEA [4], the demand for automotive lithium-ion (Li-ion) batteries grew by approximately 65% to 550 GWh in 2022 from around 330 GWh in 2021, mostly due to an increase in the sales of electric passenger cars, with new registrations rising by 55% in 2022 compared to 2021.

This logical trend illustrates the expectation that batteries, particularly lithium-ion batteries, will progressively take the lead in the upcoming automobile industry sub-markets. Furthermore, because of the problems with battery degradation (as known as ageing) and disposal that have arisen in large-scale battery manufacture over the past few decades, stakeholders usually take two actions into account when taking market economics, environmental concerns, and climate change into account [25]: For those existing battery applications, the battery recycling industry is investigated in order to address the problems related to the degradation and disposal of current batteries. For future automotive battery applications, research efforts on batteries are being intensified in order to improve the entire product lifecycle of car batteries in terms of cost and performance. Fig. 1.6 provides an overview of the demand for automotive batteries in

previous years and projects the expansion of the battery recycling market until 2040. It illustrates the emergence and demand for technologies that lower the overall cost of vehicle batteries across their lifecycle.

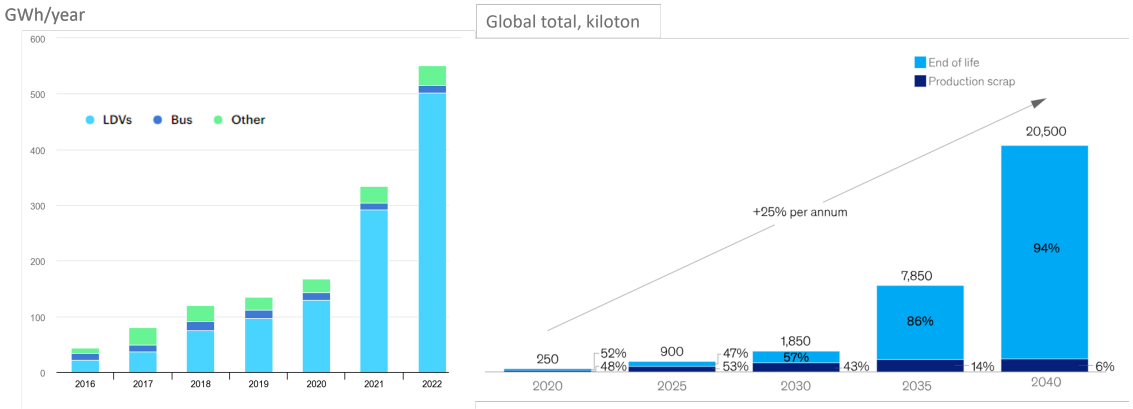

Fig. 1.6. Automotive battery demand and recycling market value comparison [4], [25]

1.2 | Motivations

This PhD focuses on the most recent advancements in hybrid vehicle technology, specifically on a variety of research linked to multi-mode plug-in hybrid electric vehicles. This program intends to optimise the control and develop the intelligent features of existing plug-in hybrid vehicle powertrains and cutting-edge industrial prototypes with the help of both the academic and industrial sectors. Several factors underscore the critical nature of this PhD can be summarised as:

1) The digital twinning of automotive product development represents a transformative shift in how vehicles are conceived, designed, tested, and brought to market. This transition towards digital approaches has not only streamlined processes but has also introduced new paradigms that redefine the product development of automotive engineering.

2) To prolong the product life and lower the auxiliary cost for such electrified vehicles, it is critical that the battery conditions, including both short-term status and long-term health, be investigated for integration with the energy management systems.

3) As electrification becomes more advanced, multi-mode plug-in hybrid electric vehicles (MM-PHEVs) control techniques need to become more complex and intelligent to adapt to the constantly changing operating parameters, such as driving conditions or the status of power sources.

4) The EMS must react quickly to driver inputs such as steering, braking, and acceleration on the shortest time scale (milliseconds to seconds) for instantaneous power supply. Also, with the attention moving to battery lifetime and health over the longest time periods (days to years), the EMS must control charging cycles, steer clear of extreme states of charge, and maintain the battery at ideal working ranges to increase battery life and retain capacity. The EMS needs to effectively respond to immediate power demand, preventing malfunctions and extending the life of the vehicle by examining long-term trends in battery degradation.

1.3 Aim and objectives

The aim of this PhD project is to provide an artificial intelligence approach for multi-mode hybrid powertrains in online optimal energy management control, which will aid OEM's product development in achieving maximum energy efficiency for vehicle operations. Furthermore, this research will contribute to improving the total product life cycle of EVs by effectively balancing the instant power consumption in a short operational period and the accumulating cost of batteries during long-term usage. The precise objectives are as follows:

1) To build a digital twin model of the multi-mode PHEV especially in series-hybrid working conditions, with a dedicated adaptive particle swarm optimisation algorithm that determines the fatal control factors of EMS offline.

2) To develop a data-driven model of battery by sensing multiple signals of real-time performance from instant battery state-of-health status, which can be implemented into online health monitoring estimation with battery ageing explainability.

3) To develop an online optimal control method for real-time optimal energy management control for multi-mode PHEVs while taking into account multi-objective optimisation across diverse time scales.

4) To evaluate both the offline global optimised digital twin model and the online optimal control strategy for vehicle performance in each stage, as well as to demonstrate the advancement of the proposed artificial intelligent methodology for multi-mode hybrid vehicle energy management control and optimisation of battery applications.

1.4 Thesis outline

The remaining portion of the thesis is divided into six parts: a literature review, an introduction to the methodology, three primary chapters devoted to the research contributions, and an ending chapter with conclusions.

Chapter 2 reviews the development and use of digital twin technology in the automobile industry, as well as the evolution and significance of electric vehicles and current control methods and optimisation techniques. Additionally, literature of battery status estimation will be presented for later integration with EMS. Then, contemporary offline optimisation for product development and cutting-edge online optimal control techniques with multiple objectives are described with highlights. Lastly, all the existing research is discussed and summarised with the corresponding research gaps based on the logic of this thesis.

Chapter 3 describes the methodology and experimental facilities of this PhD program. The methodology includes digital twin platform set-up, data collection, vehicle modelling, and simulation environments are introduced. Followed by the illustration of the offline

optimisation and the online optimal control strategy. Lastly, the experimental facilities, which compromise a Hardware-in-the-loop (HiL) facility for the implementation of online optimal control and a battery test facility for data-driven modelling, are introduced.

Chapter 4 carries out the research into an advanced offline evolutionary optimisation approach based on the digital twin. Based on conventional particle swarm optimisation (PSO), a novel dedicated adaptive particle swarm optimisation (DAPSO) algorithm for digital twin based control optimisation is proposed by the author, with the term 'dedicated' referring to the specialised design based on powertrain used in this study. The outcomes of this chapter have been published with IEEE Transactions on Transportation Electrification (TTE) [26]. Utilising the global information gleaned from the swarm, a novel particle swarm optimisation (PSO) algorithm with an adaptive swarm control approach is created to manage the exploration and exploitation of each individual particle agent. In order to identify the unified settings of the EMS, extensive cross-validation testing under three simulated real-world driving circumstances is conducted after applying the DAPSO algorithm to DT-based optimisation of a PHEV controlled by charging-depleting/ charging-sustaining (CD/CS) strategy, where the HiL is applied to validate the determined control thresholds.

Chapter 5 studied data-driven approaches for digital modelling of the battery health status and its integration for vehicle's real time application. The main content of this chapter is published in the Energy Proceedings of International Conference on Applied Energy 2021 [27]. In order to calibrate a battery model for state-of-health (SoH) estimation using measured data, an novel online double-layer system identification (ODSI) approach is proposed by the author. The ODSI approach first uses offline particle swarm optimisation (PSO) to perform robust optimisation in the lowest layer in order to establish the unified settings for the basic battery model. After that, a deep convolutional neural

network (DCNN) is added to the base model to allow for the transfer of knowledge from offline optimisation to online adaptation for the estimation of SoH under various operating environments. Then, an asynchronous system of joint status estimation based on two long short-term memories (LSTM) are proposed to have SoC and SoH co-estimations during the battery uncompleted discharge process. Finally, a multi-kernel automatic relevance determination based Gaussian process regression (ARD-GPR) frame is proposed for estimating battery SoH based on real-world automotive scenarios. Bayesian optimisation is used to identify the ARD parameters and to better understand battery's degradation.

Chapter 6 presents the research of an online optimal control with consideration of diverse time scale objectives based on the multi-mode PHEV of an industrial prototype, and the contribution of this chapter is published with Applied Energy[28]. With the new notion of the 'Hamiltonian matrix' based on the conventional cost status (Hamiltonian function in optimal control) of conventional ECMS, a novel approach named cuboid equivalent consumption minimisation strategy (C-ECMS) for multi-mode plug-in hybrid electric vehicles (PHEVs) is given, where the 'cuboid' is referred to as the 3-dimensional knowledge base. This technique adds an extra control degree of freedom to the conventional status vector of the cost function (Hamiltonian function), allowing for efficient dual motor control in the multi-mode PHEV. In order to produce three Hamiltonian matrices that establish a cuboid knowledge base for optimal control taking into account various time scale objectives, such as instant energy consumption, instant battery status, and long-term battery health condition. An ageing factor (AF) is introduced in conjunction with the equivalent factor (EF), where their Pareto frontier is conducted and analysed. Finally, the HiL is implemented to validate the proposed C-ECMS with its best parameters' setting.

Chapter 7 summarises the results and implications of the research undertaken in this thesis and recapitulates the major findings of the study. This chapter ends with an in-depth discussion and a suggestion for potential research in the future.

CHAPTER 2

Literature review

This chapter primarily covers some recent literature from the viewpoints of electrification and digitalisation of electrified vehicles. Firstly, the development and application of vehicle product development in digitalisation are presented, especially in the aspect of digital twinning. In terms of vehicle electrification, the section begins by introducing the ways for state assessment and prediction as well as the digital modelling methods for batteries, which are crucial energy sources for electric vehicles. The energy management strategies for multi-mode plug-in hybrid electric vehicles (PHEVs) are finally covered from different modelling aspects, along with the mathematical fundamentals of optimal control. The literature review in this chapter forms a logical foundation for this PhD research project.

2.1 | Digital twinning in the automotive industry

In the automotive sector, digital twins are becoming more and more significant since they improve the consumer experience, promote sustainability, and enable more inventive and efficient design, production, and maintenance operations; their growing use in the automobile industry is being driven by these advantages. This section mainly introduces the components of the digital twin, including physical entity, virtual entity, connectivity, database and services, with their corresponding functionality. Later, the digital twin applications in the automotive sector are further introduced.

2.1.1 Digital twins' components and functionalities

A digital twin (DT) is a virtual representation of a physical entity or system. It is used in a variety of industries to mimic, anticipate, and optimise performance by simulating real-world processes, systems, or objects. Digital twins frequently combine real-time data from sensors on the physical entity to update and change the virtual model, allowing for continuous feedback and adaptation. At present, the most widely recognised digital twin model is the one proposed by Tao Fei et al. [29] in 2018, where normally the digital twin contains a physical asset, a digital representation, connectivity, database, and services model.

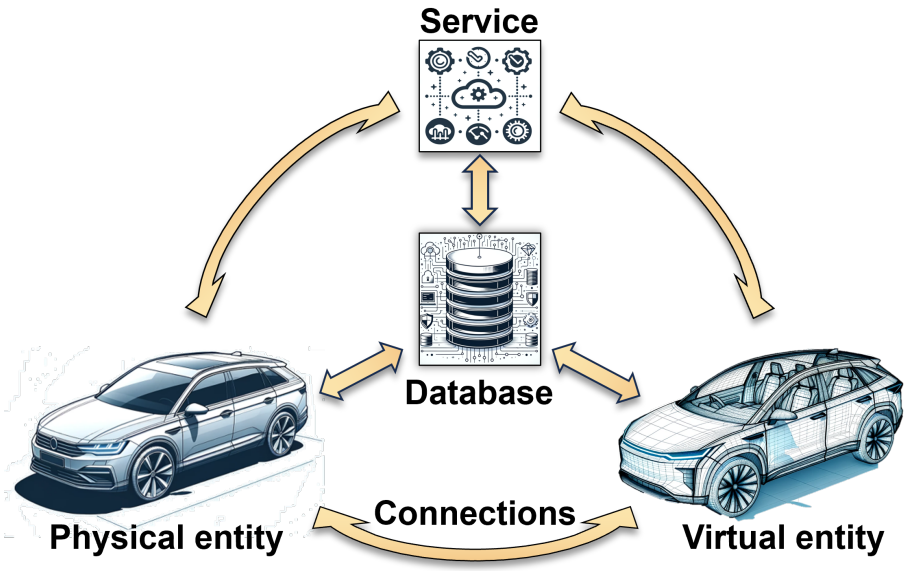

Fig. 2.1. General digital twin frame in automotive engineering

Physical entity

Firstly, a physical entity (known as a physical asset) of the digital twin is regarded as the true entity in the real world. It can range from tiny pieces of equipment to sophisticated complex systems. Research from both Sun et al. [30] and Zhang et al. [31] point out that the physical assets include themselves as well as auxiliary resources like the surrounding environment and materials that are connected to them. It is worth mentioning that the

sensors attached to the testing target are also regarded as a part of the physical assets [32]; where sensors play roles in physical information perception for either the status [33] and operation [34] of the physical target or environmental information [35].

Virtual entity

The virtual entity, known as the digital representation/modelling, on the other hand, is a virtual counterpart in representing the physical assets from multiple perspectives of comprehensive performances, which are normally based on continuous data updating and iterative simulations [29]. Existing research has conducted classifications for digital modelling from different perspectives, i.e. based on variable-scale topologies [36] or based on functionalities [37]. Among these, recent research by Tao et al. [38] further comprehensively classified the digital representation into four main categories:

1. Geometric model: geometric models normally outline the dimensions, internal organisation, orientation and position in space, as well as interactions between physical components. Zheng et al. [39] proposed a three-level virtual modelling approach of the element-behaviour-rule to the vehicle's body-in-white (BIW) based on the geometrical model for real-time inspection.

2. Physical model: the physical model is used for quality assurance as well as the study and forecasting of physical properties. There are examples such as static models, which are quantitative models of physical property, state, and behaviour determined solely by physical entities; and dynamic models, which determine the physical state distribution of the entire system, calculations must be made and performed on the spatiotemporal solution domain. Wei et al. [40] developed a finite element model for real-time wear modelling, in order to facilitate the dynamic evaluation of CNC machine tool performance attenuation by digital twin models.

3. Behavioural model: the behavioural model portrays physical objects' correlated, random, periodic, sequential, and simultaneous activities. For example, Boulfani et al.

[41] created a more accurate behavioural model by extracting and analysing the amount of abnormal temperature change from physical generator misbehaviours and removing the anomalous behaviours from the generator's digital twin model.

4. Rule model: the rule model depicts the evolutionary tendencies and patterns of physical items and reveals latent knowledge, where data mining, analysis, and formal representation of experience and knowledge across the life cycle are included. Scheffel et al. [42] made it possible for the digital twin model to discover faults based on the pre-processing of raw data from various stages of the machine's lifetime.

Connectivity

Connectivity, normally represents the networks and communication protocols that transport data from the physical world to the digital one, such as the Internet of Things (IoT) platforms, wireless networks, and cloud infrastructures [43]. A conclusive definition presented by Tao's group [44] classifies the connectivity of DT into two main categories: the external connection and the internal connection. The external connection emphasises the link between the DT with the surrounding environment [45], [46] and human interaction [47]; while the internal connections are established among DT's components, i.e. between the physical entity and virtual entity, [48] between entities, database and services [49], [50].

Data acquisition and storage

The DT's database transforms and saves raw data to produce relevant insights. Once acquired, data must be processed and stored by relevant facilities such as edge computing devices, data centres, or cloud storage.

In data gathering approaches, data acquisition (DAQ) is the process of sensing an electrical or physical phenomenon, such as voltage, current, temperature, pressure, or sound, and converting it to a digital form. A DAQ normally contains an analog-to-digital converter, software, signal conditioning circuitry, and sensors [51].

Research by Zhang et al. [52] classified the data storage of DT as mainly six categories: physical-entity related data, which refers to the data generated during operations of a physical entity, including both the static and dynamic situations; virtual model-related data, which describe a physical entity in the digital space with respect to different aspects, such as geometric property, physical parameter, dynamic behaviour, operation and maintenance rules [52]; service-related data, which mainly includes performance data, scheduling data, and quality data for application scenarios; domain knowledge data, which contains common knowledge such as expert experience, predefined rules, and industry standards. [53] Eventually, all data can be combined into fusion data, which requires DTs to process enormous amounts of data gathered from many sources, including the real world, virtual worlds, and historical databases, and to shrink the dimensions of the large amounts of data so they can be used in the right applications [51].

Services

The services approach enables collaboration between physical assets and digital representations. It may also include analytics and AI algorithms that evaluate data from the digital twin in order to gain insights, forecast behaviours, or detect abnormalities. Machine learning models can be trained to predict maintenance needs or optimise operations based on the patterns they identify. Driven by multidimensional models and fusion data, the digital twin service can be summarised as monitoring, evaluation, simulation, prediction, optimisation and control [54].

For the monitoring service, Lei et al. [55] designed and implemented a DT of a DC-DC converter, where the service function of this DT could monitor and detect the failure of the system in real time. Also, Zhou et al. [56] proposed a DT with a monitoring service for a rail-mounted gantry crane (RMGC), where the virtual model could test the control algorithm and map the movement process of the physical asset.

For the evaluation service of DT, Wang et al. proposed a DT model of a rotor system to investigate its ability for unbalanced quantification and localisation of fault diagnosis. [57] Liu et al. [58] presented a DT system for power transmission and transformation equipment, which realised the status evaluation differentiation and fault diagnosis.

The simulation services of DT focus more on the virtual models' verification and validation. Research done by Yang et al. [59] proposed a DT platform based on a combination of ROS, MATLAB and SimIDE, to achieve multi-dimensional and multi-scale simulation. Furthermore, Schluse et al. [60] outlined a general frame of a DT integrated with simulation, and summarised the multiple uses of DT models and simulations in various scenarios.

The prediction of DT's service is important for the entire system, as it indicates the operational features and performance of the product life cycle. Liu et al. [61] presented a general frame of the DT for aircraft systems; based on numerous data fusions, the platform can achieve predictive maintenance. Another prominent case by Yang et al. [62] focuses on a prediction of lithium-ion battery life based on a DT system.

The service of DTs also comprises a system optimisation process, which often includes optimisation of design, configuration, performance, energy efficiency, or operation. Zhang et al. [63] proposed a DT platform based on an aerospace electric thruster, where the optimal design is conducted by iterative optimisations of the closed-loop simulation and adjustment between the physical assets and digital modelling.

Finally, DT system services include control functions (particularly for real-time control objectives) based on bidirectional interactions between physical assets and digital models. A typical example from research carried out by Ward et al. [64] gave a machining digital twin system based on a large-scale CNC machine tool designed for high-speed machining of aero-structural parts. The DT predicted and controlled machine-induced residual stress by a closed loop feedback which updated the spindle speed and feed rate in real time.

2.1.2 Digital twins in automotive application

Conventional design of experiments-based (DoE-based) models are believed to be enhanced by the DT [65], [66] since DTs are not only digital models of the physical entities but also have AI functions embedded to enable self-understanding, learning, and reasoning for research and development tasks [67]. According to the outlook from two recent review papers for DTs [68], [69], research into DT-based robust design with self-adaption is in high demand. There are several successful applications of DTs in the design, control, and maintenance of automotive products.

For vehicles' power sources, Li et al. [70] incorporated an H-infinity filter with a particle swarm optimisation (PSO) algorithm to improve the model accuracy of the digital counterpart of batteries for EVs; while Zhou et al.[71] proposed a human-knowledge-augmented Gaussian process regression method to build a battery DT for state-of-health estimation. Another study carried out by Li et al. [72], developed a digital twin paradigm for the battery management system (BMS) to estimate the battery status based on a voltage sensor, with a prominent accuracy of over 90%.

For vehicles' powertrain and drivetrain components, Venkatesan et al. [73] developed a DT based on the artificial neural network (ANN) algorithm for energy efficiency optimisation of an EV motor system; while research presented by Toso et al. [74] focused on a motor's real-time monitoring and evaluation.

The advanced driver assistance systems (ADAS) have also drawn concentrated focus on DT's applications, e.g., Liu et al. [75] developed a DT of a transport system to help autonomous vehicle decision-making with fused sensor data; while Yu et al. [76] developed a practical autonomous driving system development paradigm, which generates an integral, comprehensive, precise, and reliable representation of the physical environment to minimise the need for physical testing.

There has also been the focus on other vehicle systems, such as vehicle dynamics [77], [78]; cyber security [79], [80]; and driving safety [81], [82].

Specifically, it is essential for OEMs to attain a robust and reliable design for the energy management system in the research and development stage of harnessing the DT, because it is impossible for vehicle manufacturers to monitor and control all vehicles centrally through centralised cloud computing [68]. Therefore, robust and reliable control optimisation of PHEVs for automotive OEMs through research on DT-based vehicle product development is desired. Based on this motivation, Gao et al. [83] proposed a cyber hierarchy and interactional network (CHAIN) concept control method formed with the ability of environmental perception, analysis, decision-making, as well as execution, realising the overall goal of the system. Yang et al. [84] proposed a cyber-physical optimisation-based fuzzy EMS for a plug-in hybrid electric bus (FHEB) to eliminate the conflict between parameter optimisation and real-time operation, where fuel consumption is reduced with a mitigation of battery capacity loss. Ye et al. [85] applied reinforcement learning (RL) to DT, where an enhanced Q-learning EMS using a digital twin model for an electric vehicle with both a battery and an ultracapacitor, was proposed with an improvement of fuel efficiency and a slower rate of battery degradation, the overall operating cost was reduced. Moreover, Li et al. [86] developed digital twins by GT-Power software, MATLAB, and Simulink software based on multi-objective evolutionary optimisation, to develop a higher performance Atkinson cycle gasoline engine and explore its fuel-saving potential on series-hybrid electric vehicles. Research from Zhang et al. [87] focuses on DT-based optimisation of an EMS for a plug-in hybrid vehicle (PHEV); where a dedicated adaptive particle swarm optimisation (DAPSO) algorithm was developed to enhance the optimality and trustworthiness of the DT-based EMS optimisation in a variety of driving conditions.

2.2 Battery status estimation and prediction

Battery status estimation and prediction in PHEVs are crucial since the battery plays a significant role in the power source of electrified vehicles with modern transportation gradually moving towards electrification. The lithium battery is popular in particular the automotive industry because of its notable dynamic performance [88]. As one of the primary sources of energy for future electric vehicles, batteries play a crucial role in the powertrain. In the product development and optimisation maintenance of vehicles, it's essential to understand the operational status of batteries and predict their potential behaviours in the future [89]. Additionally, in the context of digital twins, the performance of a battery's digital model directly impacts various aspects of the overall performance of the electric vehicle powertrain. Typically, in the development of energy management and control systems for electric vehicles, battery state estimation and future behaviour prediction are among the most widely addressed aspects. This section provides a review of the state-of-the-art for battery modelling, status estimation and status prediction based on different modelling approaches.

2.2.1 Battery digital modelling

Digital modelling techniques for batteries entail building a virtual model of a battery to mimic its behaviour in different scenarios. Instant status, including state-of-charge (SoC) and numerous other critical aspects of battery performance can be predicted by these models. Battery modelling can be done in a variety of ways, each with a unique set of methods and degrees of complexity. Generally, the digital modelling of batteries mainly falls into three main categories, according to the research of Wang et al.[88]: the physical-based electrochemical models [90]; the electrical equivalent circuit models[91]; and the data-driven models [92].

Physical-based electrochemical models

These models, which are typically sophisticated and based on the electrochemical processes occurring inside the battery, can offer in-depth explanations of concepts like reaction kinetics and ion diffusion that shed light on the inner workings of the battery [93]. Specifically, the electrochemical models can be classified as single particle models (SPM) and pseudo-two-dimensional (P2D) models. The SPM simulates the diffusion of lithium ions in the active material and simplifies the electrodes as single particles, [94] e.g. Cen et al. [95] developed a simple SPM with an adaptive model observer to estimate battery parameters in the solid surface phase, including a SoC state meaning normalised lithium-ion concentration, and a SoH parameter implying maximum lithium-ion surface concentration. Liu et al. [96] proposed a nonlinear observer with terminal voltage feedback injection based on the electrochemical single particle model to monitor the SoC of a lithium-ion battery.

The P2D model is a more thorough model that takes into account the spatial distribution of electrochemical processes and potentials within the electrodes, where it is also known as the Doyle-Fuller-Newman (DFN) model [97]. For battery SoC estimation, Gao et al. [98] used a scheme based on the reduced-order P2D model and the dual nonlinear filters for the reliable co-estimations of cell SoC and SoH. Yang et al. [99] developed a rapid SoC estimation approach based on the simplified P2D model and genetic algorithms without restricting the initial equilibrium state of batteries; then a fast SoC estimation scheme was proposed using the constrained optimisation method with a current pulse.

Electrical equivalent circuit models

Equivalent circuit models (ECM) depict the battery as a collection of resistors, capacitors, and voltage sources, where the passive electrical components, such as resistors and capacitors, are used to mimic the behavioural response of a battery [100].

Typically, a resistor-capacitor (RC) network is used to simulate the dynamic characteristics of the battery. From the simplest Rint model to the 1-RC model (known as the Theverin model), and the 2-RC model (known as the dual polarization model), a more complex ECM uses resistor-capacitor (RC) networks to characterise the battery transient responses with various time constants connected to the diffusion and charge-transfer processes [101].

These models are generally basic and need minimal processing resources, making them suited for real-time applications such as battery management systems (BMS). Liaw et al. [102] presented an equivalent-circuit-based battery model, capable of simulating charge and discharge behaviour of lithium-ion batteries when applied to vehicles. Moreover, Xia et al. [103] applied a second-order resistor-capacitor (2-RC) ECM of a battery for accurate and reliable SoC estimation based on a cubature particle filter (CPF). While Piarro et al. [103] compared 1-RC, 2-RC and 3-RC ECMs of electrified vehicles based on parametric identification of genetic algorithm (GA) based optimisations.

Data-driven models

In recent years, with the development of multi-discipline modelling, the data-driven approach (also referred to as the machine learning approach) of battery modelling has been widely researched. Data-driven battery models make predictions about battery behaviour based on past and present data by utilising machine learning (ML), artificial intelligence (AI), or statistical techniques. Data-driven models, in contrast to physics-based models, which necessitate an in-depth understanding of the battery's internal workings, use data to anticipate battery conditions like state-of-charge (SoC), state-of-health (SoH), and remaining usable life (RUL). Because these models can manage intricate, non-linear relationships and can adjust to new data, making them resilient to a range of operating circumstances and battery kinds, they are becoming more and more significant. [104] Generally, data-driven methods of battery modelling in SoC estimation

are mainly classified as linear regression approaches, in which the simplest model that can be created is probably the basic fitting of a smooth line (one input dimension) or a hyperplane (multiple input dimensions) to the data, with insights into the physics indicated by the underlying data [105], [106]; Random forest (RF) is a technique for ensemble learning that can shed light on the relative importance of various features and applies several decision trees to regression or classification tasks [107], [108]; A support vector machine (SVM) is an extension of the random forest where the functions to be trained are simultaneously classified in a multidimensional space instead of being divided along a single input direction [109]. This technique can lead to better-fit quality in cases where training data is low, but the computational needs are substantially higher. [110] A neural network (NN), in battery modelling makes use of a variety of topologies to forecast, mimic, and comprehend battery behaviour. These models take advantage of the neural networks' capacity to mimic intricate non-linear functions, which makes them especially useful for problems in which the relationships between variables are not obvious: i.e. feedforward neural networks (FNN) [111]; convolutional neural networks (CNN) [112]; recurrent neural networks (RNN) [113], including long short-term memory networks (LSTM) or gate recurrent units (GRU) [114]; A Gaussian process regression (GPR) is a sophisticated machine learning technique that is used to predict intricate battery behaviours without requiring a particular model form [115]. It is probabilistic, adding a degree of uncertainty to its forecasts, and non-parametric, deriving a function straight from the data. Because of this, GPR is extremely flexible and accurate when used for activities such as determining the batteries' relative performances [116].

2.2.2 Battery SoC estimation

Estimating the battery state-of-charge (SoC) is a crucial aspect of managing battery systems, especially for lithium-ion batteries used in portable gadgets, energy storage

systems, and electric vehicles (EVs). The SoC serves as the battery's equivalent of a fuel gauge, showing the percentage of the battery's overall capacity that is still charged [89].

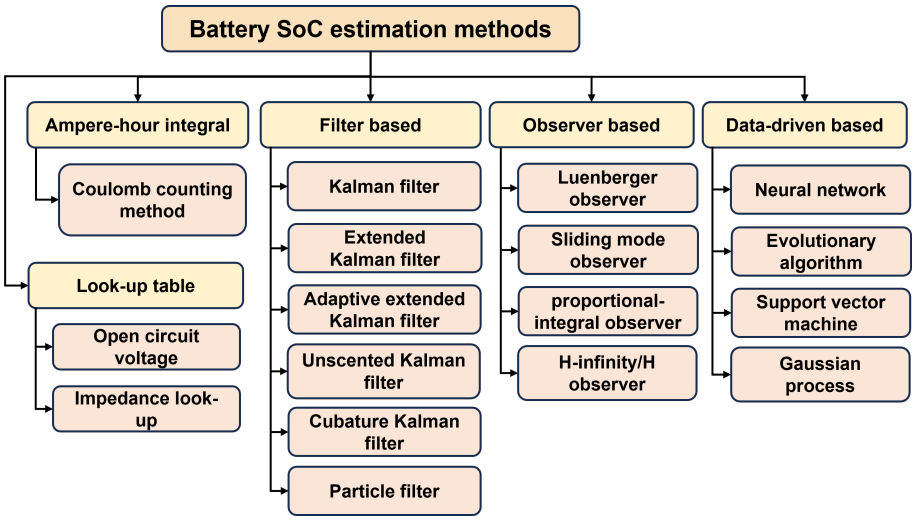

Fig. 2.2. Classification of battery SoC estimation methods

Look-up table method

Look-up table techniques use an equation or relationship to determine the SoC after analysing and measuring physical battery properties including voltage, current, and temperature. Generally, the open circuit voltage (OCV) method and the impedance look-up table method are the most widely researched. The former is one of the most straightforward approaches for estimating the state-of-charge (SoC), which depends on the relationship between a battery's voltage and its state of charge when it is in a stable open circuit situation (not supplying or receiving current) [117], [118]; while the latter approach makes use of the connection between the battery's impedance and SoC [119]. The battery's resistance to the passage of AC current is measured by its impedance, which varies depending on the battery's age, condition, temperature, and charge level [120].

Ampere-hour integral method

The Ampere-hour integral method is a common approach for determining a battery's state-of-charge (SoC), often known as charge counting or the Coulomb counting method. It is founded on the idea that a battery's state of charge (SoC) is directly correlated with the amount of electrical charge it contains [121]. Specifically, the SoC of a battery can be monitored by measuring the flow of charge into and out of the battery. This is done by directly measuring the electric current entering or leaving the battery over time [122].

Filter-based method

Battery state-of-charge (SoC) estimate techniques based on filters evaluate observed data and forecast the SoC using mathematical algorithms when the SoC cannot be measured directly, and must instead be inferred from indirect measures such as voltage, current, and temperature [88]. The impacts of estimating mistakes and measurement noise are also reduced with the use of filters. Several popular filter-based techniques include the Kalman filter (KF) [123]; Extended Kalman filter (EKF) [124]; Adaptive extended Kalman filter (AEKF) [125]; Unscented Kalman filter (UKF) [126]; Cubature Kalman filter (CKF) [127]; and the particle filter (PF) [128].

Observer-based method

Similarly, based on the measured values of the system's external variables, the state observer can calculate the estimated values of the state variables. Luenberger [129] developed the concept and construction method of a state observer to realise state feedback or other needs for control systems. The introduction of the state observer not only gives a practical means of realising state feedback technology but it has also been used in many fields of control engineering. For battery state estimation, observer-based methods such as the Luenberger observer (LO) [130]; the sliding mode observer (SMO) [131]; the proportional-integral observer (PIO) [132]; and the H-infinity/H observer (HIO) [133] have been widely used in recent years.

Data-driven-based method

The utilisation of data-driven techniques to estimate a battery's state-of-charge (SoC) is growing in popularity since these methods can manage complex nonlinearities and fluctuating battery properties without requiring sophisticated electrochemical models. These techniques use historical and present data to determine the correlation between SoC and measurable battery characteristics including voltage, current, and temperature [88]. The commonly used data-driven methods for SoC estimation include the neural network (NN)[134]; fuzzy logic [135]; evolutionary algorithm (EA) [136]; support vector machine (SVM) [137]; Gaussian processes (GP) [138].

2.2.3 Battery health condition estimation and prediction

For the practical automotive engineering applications of lithium batteries, one of the factors that cannot be ignored is the degradation problem [139]. Typically, this problem is assessed using the state of health (SoH) of the battery for two reasons: 1) increase of the internal resistance. 2) loss of capacity [140]. Since it is impossible to measure the battery impedance in real-world driving, regular battery ageing evaluation focuses on capacity loss in practical applications [141]. Generally, battery degradation can be evaluated by differential analysis (DA) methods, model-based methods and data-driven methods [141].

Differential analysis methods

The DA methods rely heavily on direct measurements of battery performance (mostly voltage curves) to obtain sensitive SoH-related features, and DA methods are classified into four groups: incremental capacity analysis (ICA); differential voltage analysis (DVA); differential thermal voltammetry (DTV); and differential mechanical parameter (DMP) estimation.

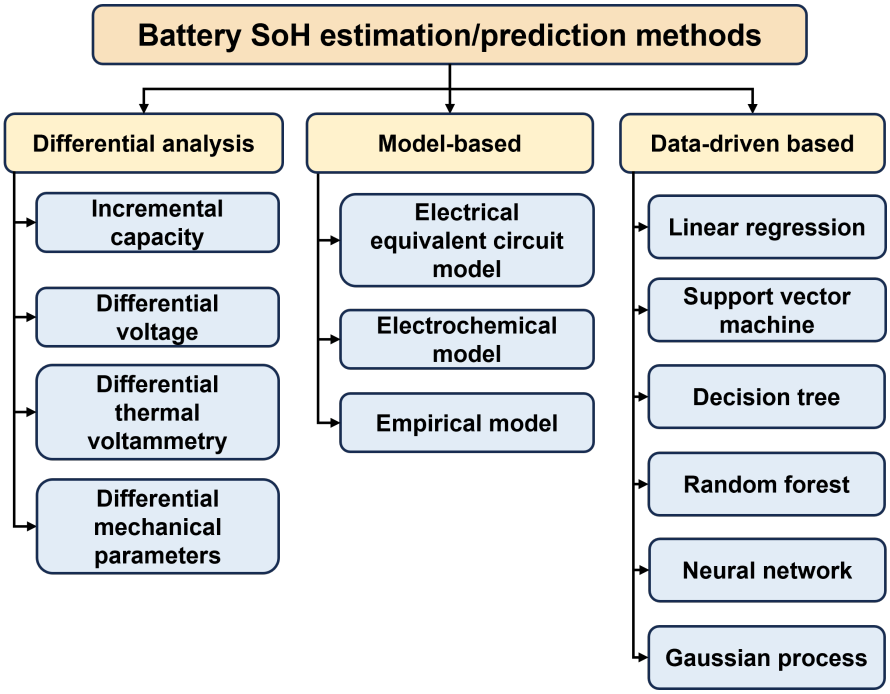

Fig. 2.3. Classification of battery SoH estimation/prediction methods

The incremental capacity analysis (ICA) reveals that when the battery capacity fades, the peak amplitudes decrease [142]. In the work of Maures et al. [143] with an extension to high C-rates of State of Health (SoH) diagnostic methods based on incremental capacity (IC) peak tracking, two features were extracted from IC curves and showed logarithmic correlations with the SoH, both during the charge and discharge processes. Some research of Tian et al. [144] proposed an ageing mechanism identification method, based on the identified open-circuit voltage, where the battery ageing mechanism can be analysed by means of an incremental capacity analysis; then the normalised incremental capacity peak is used to estimate the remaining capacity.

In contrast to the ICA, the differential voltage analysis (DVA) observed peak positions of voltage change [145], where the battery charge voltage curve (charge voltage vs.charged capacity, V–Q) can be conducted. Wang et al. [146] proposed a new method for battery SoH estimation using the location interval between two inflection points or the transformation parameter of the differential based on a new algorithm to obtain the

DV curve according to the centre least squares method. Zhang et al. [147] proposed a model-free SoH calculation method by fusion of the coulomb counting method and differential voltage analysis (DVA), where the rapid online SoH calculation under constant current discharging stage can be realised.

The DTV approach measures temperature and voltage simultaneously while galvanostatically charging and discharging a cell, where the DTV metric about health indicators is then obtained by calculating the ratio of the temperature and voltage differentials with respect to time [148].

Wang et al. [149] proposed an advanced filter method could be used to smooth differential thermal voltammetry (DTV) curves, where the relationship between battery degradation and the DTV curves was determined with extraction of the health factors from the DTV curves. The intercalculation of ions causes stress on the materials inside batteries during charging and discharging, notably the electrodes, which results in volume changes. These stresses have the potential to cause mechanical degradation over time [150]. To assess the mechanical characteristics that are measurable and correlate with SoH, the differential mechanical parameter (DMP) estimation can be used to assess the health of the battery [151].

Model-based methods

Utilising mathematical depictions of the battery's behaviour, model-based techniques for evaluating the state of health (SoH) of batteries assess the battery's present state in comparison to its initial state [152]. Model-based methods are widely used as online methods for estimating SoH from resistance characteristics and capacity loss. Generally, the model-based methods are classified as [141] the electrical equivalent circuit model (EECM), where Huang et al. [153] developed a self-adaptive piecewise equivalent circuit model (PECM) for SoH based on the extended Kalman filter (EKF), which can establish itself as a combination of linear and nonlinear piece-wise functions with continuously

adjusting parameters from voltage, current, and temperature, among other things, and can adapt itself to any working condition in real time. While Amir et al. [154] employed a 2-RC model to simulate the degradation of the Li-ion battery while taking into account both the temperature effect and time-dependent degradation; this approach predicts the SoH accurately and is also very adaptable for a variety of cells of different chemistry.

Futhermore an electrochemical model (ECM) can mimic the behaviour of the battery under various situations and estimate the SoH by analysing changes in parameters like diffusion coefficients, reaction rates, or electrolyte conductivity, where ECMs are normally highly precise but frequently computationally costly [152]. For simply reducing the computation cost, Gao et al. [155] developed a reduced-order electrochemical model with a dual nonlinear filter for co-estimations of cell SoC and SoH; the P2D electrochemical model was first simplified with Padé approximation to obtain the state-space expressions while guaranteeing model. Bartlett et al. [156] proposed a reduced-order electrochemical model for a composite, which could estimate the current split between the materials in the composite electrode as well as the bulk and surface lithium concentrations of each material.

Empirical models (EM) depict the relationship between quantifiable battery parameters (such as voltage, current, and temperature) and the SoH using mathematical equations obtained from experimental data. To estimate the SoH, for instance, EMs can link the quantity of charge/discharge cycles with the observed capacity fade. Jiang et al. [157] constructed an empirical degradation model of a lithium-ion battery SoH with charge-discharge cycles, then the empirical degradation model was fused with a data-driven method to give an accurate SoH estimation. Besides, the EM is always implemented with other modern techniques for practical applications, e.g. Li et al. [158] integrated EMs with various deep learning networks to estimate the state of health (SoH) of batteries under various operational circumstances in ambient temperature.

Data-driven methods

Battery State of Health (SoH) can be estimated using data-driven techniques, which apply statistical and machine learning algorithms to analyse historical and current battery operating data to identify trends and gain new insights [159]. Data-driven models are growing in popularity because these techniques can manage intricate, non-linear connections that are challenging to explicitly characterise with physics-based models.

Generally, the data-driven methods for battery SoH estimation are classified as follows. Linear regression is a basic yet successful method for simple linear relationships between input characteristics and SoH, especially when the connections between the SoH and the input features are linear or nearly linear. Lee et al. [160] designed and analysed multiple regression models for deterioration parameters in order to quantify the impact of parameters on degradation based on a 2-RC ECM; while Ang et al. [161] provided a straightforward multiple linear regression approach that uses a brief voltage measurement segment from a battery's continuous current discharge curve to precisely calculate its SoH.

Another strong and adaptable machine learning technique that can be used to estimate the state of health (SoH) of batteries is support vector machines (SVM), because of its ability to handle high-dimensional data and non-linear relationships [139]. A SoH estimation method based on SVM models and virtual standard performance tests was proposed by Klass et al. [162] The virtual tests for battery SoH estimation show quick testing times appropriate for online use, and the number of support vectors for the proposed SVM models is controllable and allows for storage in on-board memory. Moreover, Feng et al. [163] proposed a support vector machine (SVM) based predictive diagnosis model for battery SoH estimation, where the support vectors are derived from the charging data of new cells and represent the inherent properties of the Li-ion battery.

Decision trees are a useful tool for estimating the state of health because of their ease of use and interoperability; they are especially helpful for a preliminary exploratory study that aims to determine how various factors affect battery health. [141] After extracting the features of battery ageing tests from National Aeronautics and Space Administration (NASA) and performing dimensionality reduction on them, Qian et al. [164] utilised the decision tree method to group the features and applied an original support vector machine algorithm simulation for the battery SoH estimation. Furthermore, using the gradient boosting decision tree (GBDT) algorithm in conjunction with a two-stage transformation-based feature extraction method, Pan et al. [165] demonstrated extracting time-domain and frequency-domain health features from battery data through the use of fast Fourier transform (FFT) and singular spectrum analysis (SSA) for battery health estimation.

As an upgraded alternative, a random forest is an ensemble of decision trees, often more robust and accurate than individual trees. Mawonou et al. [166] proposed a novel approach to battery age prediction, utilising the random forest (RF) algorithm while accounting for actual user behaviour and environmental factors. Whilst Yang et al. [167] used the random forest technique to generate the final SoH estimate by using the indicators from extract indicators for both SoH and changes in SoH between two consecutive charge/discharge cycles by the CNNs.

Another significant cluster is the neural networks, especially deep learning networks, which are capable of learning complex patterns in large data sets: feedforward neural networks (FNN) [168]; convolutional neural networks (CNN) [169]; recurrent neural networks (RNN), including long short-term memory (LSTM) [170]; moreover, hybrid models, which combine advanced methods to obtain a better performance, i.e. empirical mode decomposition and LSTM combined SoH estimation [171]; AdaBoost-PSO-SVM model [172]; ICA-Bi-LSTM-combined model [173]; CNN-BiLSTM fused network[173]; and CNN-BiLSTM model [174].

Automotive applications with battery health status considered

Applications for vehicles cover a wide range of technologies and capabilities when considering the battery state as a key factor. These applications are especially relevant to electric and hybrid vehicles (HEVs), as battery performance has a direct impact on the efficiency and operation of the vehicle. For example, based on the battery's SoH, the control system of vehicles modifies the charging and discharging rates, where lower SoH batteries might not be able to withstand high discharge rates or fast charging as effectively as modern batteries [175]. Consequently, the control algorithms are designed to have a gentler approach in order to increase the useable life of older batteries [176]. Moreover, vehicle batteries with lower SoH are more sensitive to temperature extremes; hence, the battery thermal management system of the vehicle uses SoH data to more accurately adjust the cooling or heating of the battery pack, ensuring it runs within an optimal temperature range [177], [178]. By continuously monitoring the SoH, the vehicle's control system can provide timely maintenance information, which is more straightforward for battery maintenance or replacement before the degradation [179].

Among all applications, the most crucial is instantaneous energy management in cars which considers the instant SoH of the battery; a more thorough comprehension of the SoH aids in energy management for the vehicle [180]. In order to preserve battery life and functionality, the system may limit power to non-critical systems or alter acceleration behaviour if the SoH is low [181]. Intelligent automotive energy management methods that take into account many factors, such as the condition of the battery and energy consumption for the long term and also instantly, are now possible with the help of data connection and modern computational resources, [182] where implementations of such EMSs for connected vehicles [183] or fleets [184] are also widely researched.

In conclusion, the operational effectiveness, security, and dependability of electric and hybrid cars in automotive applications all depend critically on the state of the batteries.

It affects every aspect of the car, including safety features, maintenance schedules, and driving range and performance. It is becoming more and more crucial to precisely monitor and control battery state as the automotive sector continues to move towards electrification.

2.3 Optimal control approaches of energy management system for electrified vehicles

Optimal control approaches in the EMS of EVs (including multi-mode PHEVs) are vital to maximise efficiency, performance, and sustainability. For the last decades, a large variety of research has focused on how to improve energy efficiency and reduce the overall cost of electrified vehicles. Specifically, the energy management system plays the most critical role in the powertrain system, which can lead to a higher fuel economy or better electricity utilisation, reducing emissions, ensuring drivability, and mitigating the degradation of components to improve product life cycles. This section presents an overview of modern EMS optimal control approaches of PHEVs, including rule-based (RB) approaches, optimisation-based (OB) approaches and learning-based (LB) approaches [185].

2.3.1 Rule-based approaches

The rule-based (RB) method is most applicable and implementable for EVs' practical engineering problems, which directly controls the actions of components by following certain pre-set rules during the operation of the vehicle. Some certain advantages of this approach are presented as follows: firstly, its simplicity and transparency are more convenient for engineering applications based on heuristic logic. Also, it is computationally low and can immediately respond to real-time conditions; this reduces the cost of product development while increasing the robustness of the EMS [185]. Moreover, RB methods are

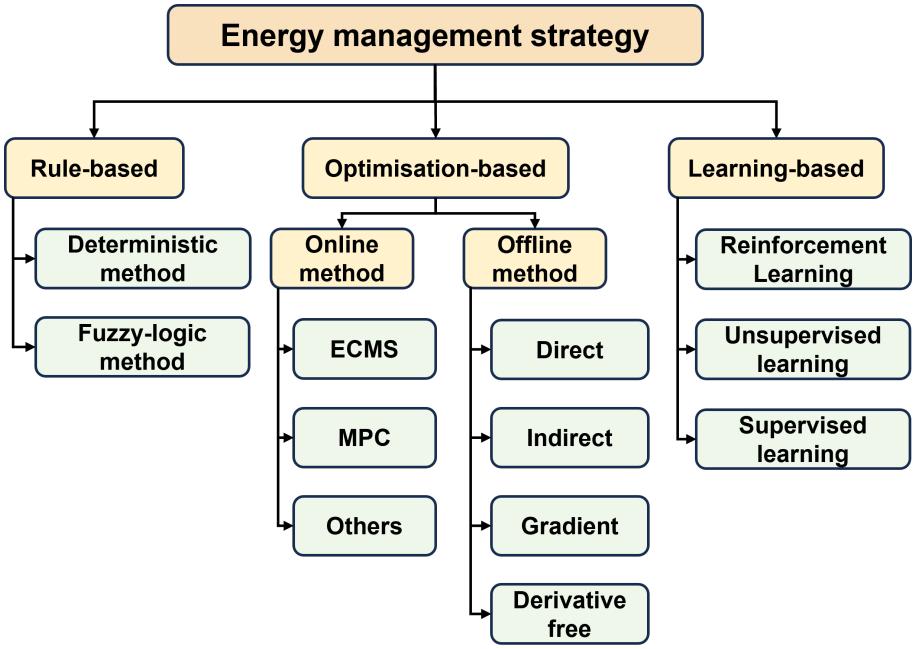

Fig. 2.4. Classification of energy management strategies

always conveniently customised and tuned by users for their desired functions. Generally, RB methods are classified as deterministic methods and fuzzy logic methods. For the former approaches, the deterministic strategy can be developed based on continuously adjusting certain thresholds by the iterative design of experiments (DOE) [186]; also, those certain rules can be tuned by some advanced technologies, such as neural networks [187] or reinforcement learning [188]. However, vehicles hardly perform prominently in dealing with complex real-world driving conditions without the implementation of a set of appropriate thresholds. In most conditions, the thresholds are fixed during the operation of vehicles, which may have poor performances when the driving environment varies.

2.3.2 Optimisation-based approaches

From the perspective of application scenarios, optimisation-based methods are normally classified as offline optimisation-based approaches (also known as global optimisation approaches) and online optimisation-based approaches, according to prior knowledge or driving conditions. It is worth mentioning that the global constraint for offline optimisation

and the local (instant status) constraints for online optimisation are different, due to known information; their cost functions are different to lead to optimal performances [185].

Offline optimisation approaches

Offline optimisation methods for plug-in hybrid vehicles (PHEVs) are used to discover optimal control strategies and vehicle characteristics in order to achieve specific goals such as minimising fuel consumption, lowering emissions, or maximising performance, with known global information [189]. To discover the ideal settings for the vehicle's components and control tactics, these methods often utilise simulations and mathematical models with different approaches: direct algorithms, like dynamic programming (DP) and its variations, are often used to solve complex optimisation problems for energy management systems (EMS) when all information is known beforehand [190]. The DP simplifies these complex problems by breaking them down into smaller sub-problems, making it easier to find solutions, particularly when dealing with many variables and constraints, i.e. distributing the power flows between engine and motors [191], [192]. In contrast, indirect algorithms, such as Pontryagin's minimum principle (PMP), address the theoretical foundations before solving the target problem, where the necessary conditions for optimality are determined first then mathematical formulations are solved to find the optimal solution based on the Hamilton-Jacobi-Bellman equation [193]. The core idea of the PMP is that the constrained global optimisation problem is reduced to the local Hamiltonian function minimisation problem, i.e. by considering the engine and battery constraints, the energy management system of a parallel HEV is optimised by iterative calculation of the co-state variable based on partial derivative of the Hamiltonian function [194].

Gradient algorithms represent another direction of optimisation for vehicles' EMS; they iteratively move to the desired maximum (minimum) values by utilising the objective

function's derivative information within mathematical constraints like differentiability and continuity [185]. Some prominent approaches are widely applied to electrified vehicles' optimal energy management because of their ability to converge to the optimal solution efficiently, i.e. linear programming (LP) [195]; quadratic programming (QP) [196]; sequential quadratic programming (SQP) [197]; and convex programming (CP) [198].

Derivative-free algorithms, also known as meta-heuristic algorithms, are essential for use in electrified vehicles' EMS due to their flexibility in handling non-differentiable functions with discontinuities or discrete variables; their robustness to noisy data; their ability to manage discrete variables; and their computational simplicity [199]. Compared to previous optimisation approaches, derivative-free algorithms can often lead to a global optimisation result. The major derivative-free algorithms mainly consist of the genetic algorithm (GA), simulated annealing (SA), particle swarm optimisation (PSO) and their relative variants.

The genetic algorithm (GA) is a stochastic search method inspired by natural selection and genetic evolution, where reproduction, crossover information, and mutation are the three primary stages of the GA principle [200]. By eliminating the local optima traps, the GA can find the global optima in nonlinear, non-convex, multi-modal, and discontinuous-time optimisation problems of vehicles' EMS. Panday et al. [201] applied the GA to both the battery digital model and EMS of hybrid electric vehicles to optimise the modelling parameters and relative control thresholds for better energy performances. Lü et al. [202] analysed the GA applications in fuel-cell hybrid vehicles while considering multiple targets of vehicles' dynamic performance, economy and components' durability. The GA is also widely applied with the other advanced approaches, such as deep learning [203] or reinforcement learning [204]. Furthermore, the variants of the GA for multiple objective optimisations, such as non-dominated sorting genetic algorithm II (NSGA-II), are also widely researched: Li et al. [205] applied the NSGA-II to optimise the HEV's operation map with complex variables to improve engine efficiency with reduced emission;

Deng et al. [206] utilised the NSGA-II for a parallel HEV to optimise the EMS efficiency while considering emissions, fuel consumption, and drivability.

Simulated annealing (SA) was originated by Kirkpatrick in 1983, inspired by the metal annealing process [207]. EMS of hybrid vehicles can benefit from the appropriate application of SA to optimise a number of vehicle performance factors, where the objective is to determine the optimal approach for controlling the energy flow between various sources, such as the internal combustion engine, electric motor, and battery [208]. The SA is also used in multi-mode PHEVs to limit the frequency of mode switching and to avoid the battery's abrupt high power output [209].

Particle swarm optimisation (PSO) is a computational method for tackling optimisation issues that was inspired by the social behaviour of birds flocking or fish schooling [210]. When applied to the energy management system (EMS) of hybrid vehicles, it thrives in multidimensional and nonlinear problem environments and offers a robust and efficient way to optimise the vehicle's energy consumption and performance. The most direct application of PSO in hybrid vehicle energy management is the optimisation of control parameters. Boujneh et al. [211] and Cheng et al. [212] both applied PSO to determine the control thresholds of hybrid electric vehicles to get better energy performance with fewer emissions. Also, the PSO's variants are widely researched when dealing with hybrid vehicles' EMS. Chen et al. [213] developed a dynamic PSO (PDSO) of the hybrid electric vehicles with considering the battery SoC, engine speed and instant demand torque to determine the power split ratio and gear shifting mode in EMS. Rahman et al. [214] proposed an accelerated PSO (APSO) to determine the charging strategy based on charging time, battery capacity, and SoC level of a PHEV to improve the energy distribution. Furthermore, a modern PSO is also applied alongside many other advanced technologies in intelligent hybrid vehicle energy management systems and related components, i.e. Zhou et al. [215] developed a DT of an energy-harvesting shock absorber to optimise its design parameters using a PSO; Li et al. [216] incorporated an

H-infinity filter with a particle swarm optimisation (PSO) algorithm to improve the model accuracy of the digital counterpart of batteries for EVs; while Geng et al.[217] combined a PSO with an ECMS for multiple objectives optimisation for PHEVs. Chen et al. [213] developed a system based on a PSO with fuzzy logic recognising the driving condition to improve the driving efficiency. The PSO can also help with the autonomous driving to improve energy efficiency [218].

Online optimisation approaches

Plug-in hybrid electric vehicles (PHEVs) employ online optimisation techniques in their energy management systems (EMS) to dynamically optimise the vehicle's energy consumption in real time, taking into account the driver's inputs, the vehicle's present status, and the external environment. These methods are crucial for improving the performance, sustainability, and efficiency of PHEVs. Generally, online optimisation-based energy management strategies can be represented by for example model predictive control (MPC), or equivalent consumption minimisation strategy (ECMS).

In practical vehicle applications, obtaining a global driving profile in advance is unrealistic. Therefore, based on the principles of dynamic programming (DP), the model predictive control (MPC) has been proposed to address real time optimisation problems over a specific time horizon with further prediction [219]. An MPC-based energy management system (EMS) typically consists of two main parts. The prediction module is the first module, which forecasts future data for a given time horizon based on information that has been available for a given amount of time. Different intelligent approaches are applied in this module, e.g. the frozen-time MPC (FTMPC) [220]; prescient MPC [221]; exponential varying MPC [222]; stochastic MPC [223]; artificial intelligence MPC [224]; telematics MPC [225]. Based on the acquired predictions, the control module, which is the second module, optimises control. With the help of sensors, the prediction module can gather pertinent data on vehicle dynamics (speed, position, driving conditions, etc.)

or vehicle energy (energy demand, battery condition, engine conditions, etc.) and forecast the relevant areas of interest for the given time period [185]. On the other hand, using the prediction data that was collected, the control module optimises the existing vehicle energy distribution and sends the optimised results to the appropriate components for implementation. This enables the prediction module to refresh the incoming data by allowing the vehicle system to produce fresh responses [226]. In a nutshell, with its dynamic and predictive approach to optimising energy management, improving vehicle performance, lowering emissions, and extending battery life, the MPC is a potent tool in the EMS of hybrid electric vehicles.

Another promising online optimal control approach is the equivalent consumption minimisation strategy (ECMS), which is commonly used in hybrid electric vehicles to reduce fuel consumption while maintaining optimal vehicle performance [227]. Since the ECMS has a greater level of technical readiness, it is attracting the attention of numerous automobiles nowadays. The ECMS seeks to simultaneously reduce fuel and electrical power usage while dividing the global optimisation issue into several instantaneous local optimisation sub-problems. Additionally, it is more computationally efficient than systems based on extensive computations since complex training conditions are not required [228]. Inspired by the calculation of the co-state of the PMP approach, the ECMS operates by calculating the most efficient way to distribute power demand between power sources instantly based on the equivalent factor (EF). The EF's determination is the focus when the ECMS is applied to vehicles' EMS [229].

According to the determination and adjustment of the EF, the ECMS is generally categorised into: ECMS with offline estimation of the EF (EF is constant through the entire driving process) and ECMS with online adjustment of the EF (EF is tuned dynamically according to instant status) [185], [228]. The former approach necessitates prior information of driving conditions, such as trip distance or speed distribution, in order to achieve global optimality. This is achieved by employing numerous advanced

approaches, mainly including the DP [230]; GA [231]; PSO [232]; PMP [233]; GWO [234]; and direct numerical analysis [235] to find the most appropriate EF value. However, the final EF value can normally be guaranteed after iterative calibrations for various driving cycles. The ECMS with adjusting the EF in real time is an advanced approach that further enhances the effectiveness, where the EF value significantly depends on instant information about both environmental factors, i.e. speed prediction [236], travelling distance [237], or driving pattern recognition [238]; and vehicle status factors, i.e. engine working condition [239], battery status's estimation and further prediction [240], [241] or transmission efficiency [242]. To achieve an adaptive EF with various driving conditions in real time, multiple advanced methods are applied to help the determination of the EF value, i.e. Onori et al. [243] introduced the basic ECMS applications of hybrid electric vehicles with EF adaptions based on weight functions. While Yang et al. [244] applied the PID controller to control the EF value in real time in order to adopt different driving conditions. For simplicity of practical applications, look-up tables of EF values can also be generated in advance and then applied in real time, i.e., EF adaptation with consideration of the SoC of the battery [245] and look-up table of EF values by considering both the power demand and battery SoC [246]. Furthermore, fuzzy logic is also applied to help the EF online determination [247]; and its derivatives have also been extensively researched, e.g. Singh et al. [248] proposed an ECMS system based on the adaptive neuro-fuzzy inference system (ANFIs) to optimally control the HEV. Artificial intelligence is also widely applied to thereal-timee EF tuning of the ECMS, i.e. artificial neural network (ANN) based EF tuning [249] and learning vector quantization neural network (LVQNN) recognition based on the online adjustment of the EF. Conclusively, the ECMS, which combines economy, adaptability, and environmental responsibility, is a monument to the advances in automotive technology. It is indisputable that it will have a major impact on hybrid vehicle technology in the future, contributing to the development of smart and sustainable transportation solutions.

2.3.3 Learning-based approaches

The hybrid vehicle learning-based EMS can be categorised according to the kind of learning algorithms being used as well as how they are utilised. By employing a range of machine learning and artificial intelligence methodologies, learning-based approaches optimise the energy distribution between the internal combustion engine and electric motor; thereby enhancing the overall performance and economy of the vehicle. Generally, the most widely adopted learning-based approaches can be categorised into reinforcement learning, unsupervised learning (i.e. clustering) and supervised learning (i.e. neural networks)

Reinforcement learning

Hybrid electric vehicles use an EMS with reinforcement learning (RL) as a sophisticated method of powertrain optimisation. The EMS, functioning as the RL agent, learns from interactions with the environment, or the car and its operational settings in order to maximise a cumulative reward, where the reward is usually connected to goals like fuel economy, lower emissions, and battery management [250]. The multiple RL methods are widely applied to the EMS, such as temporal difference (TD) learning [251]; Q-learning [252]; double Q-learning [253]; multi-step Q-learning [254]; dyna Q-learning [255] and their variants based on deep learning: deep Q-network (DQN) [256] and deep deterministic gradient policy (DDPG) [257]. While decentralised learning, typically associated with multi-agent reinforcement learning (MARL), involves isolated agents with local central consoles, its reinforcement learning algorithms are comparable to those used in centralised learning [258]. Despite using less processing power and offering more flexibility, they exhibit a similar performance [259]. Furthermore, by integrating predictive modelling into the reinforcement learning framework to the EMS, predictive RL methods aim to enhance the decision-making process regarding energy distribution between different power sources

(like an internal combustion engine and electric motor) by anticipating future conditions and requirements [260].

In conclusion, reinforcement learning in hybrid vehicle EMSs is an iterative process that uses environmental information to help the system decide how best to use energy. Although it necessitates careful consideration of algorithm design, data management, and system integration, this technique can considerably improve vehicle performance and efficiency.

Unsupervised learning

In vehicle energy management, the primary application of unsupervised learning is clustering. More specifically, C-means [261] and K-means clustering [262] are widely researched and applied to intelligent EMS, e.g. Wei et al. [263] applied a K-means clustering algorithm to develop a frame of driving pattern recognition, helping the intelligent EMS appropriately allocate the power distribution with driving conditions recognised. The clustering can also be combined with the other advanced approaches to help the EMS, e.g., Wang et al. [264] proposed a fuzzy logic control strategy based on global optimisation and considering the recognition of driving cycles to advance the fuel economy, where the parameter tuning of the fuzzy logic is decided by both the GA and K-means clustering. Furthermore, the operation conditions of vehicles are also considered for the implementation of K-means clustering, e.g. Liu et al. [265] developed a frame utilising principal component analysis (PCA) and K-means clustering to construct a functioning condition recognition model, which involves a thorough consideration of several criteria such as accessory status, road and environmental information, driving profile fragment information, and fundamental vehicle attributes. To determine how different electric vehicles operate under the combined influence of their internal control strategy characteristics and external influences, feature extraction and cluster analysis of various operating scenarios should be carried out.

Supervised learning

Using historical or labelled data, supervised learning offers an organised method for forecasting and optimising different components of a vehicle's energy management system, enabling decision-making. The choice of a supervised learning algorithm depends on the specific task at hand, the features of the data, and the desired outcome. Generally, linear regression (LR), support vector machines (SVM), neural networks (NN) and Gaussian process regression (GPR) are the approaches used mostly in academia and industry.

In an energy management system (EMS), particularly for vehicles, a regression model is essential for forecasting continuous variables using past data. This makes it possible to manage the vehicle's energy resources more effectively and efficiently, as the linear regression is widely applied to the powertrain, i.e. directly implemented on the EMS [266] or applied to power components [267].

Vehicle energy management systems that use support vector machines (SVM) provide a reliable and effective means of optimising energy use, anticipating maintenance requirements, and improving overall vehicle performance and lifetime. The current automotive systems' diversified and data-rich environment is a particularly good fit for it because of its capacity to manage complicated, high-dimensional data. Application of SVM in electrified vehicles includes power-train condition identification [268], battery status estimation and prediction [269], energy consumption optimisation [270], speed prediction [271], and route pattern recognition [272]. Also, SVM can be applied with the other advanced methods [273].

The main benefit of integrating a neural network into an energy management system for a car is that it can greatly increase energy efficiency. Optimal energy usage patterns can be predicted by a neural network through the analysis of complicated data from multiple vehicle sensors. During this process, multiple NNs are applied to different applications of

vehicles' EMS, including emission minimisation [274]; energy consumption optimisation [275]; determination of control thresholds [276]; diving condition prediction [277]; braking system optimal control [278]; and battery optimal management [279]. In addition, various forms of neural networks and their derivatives are also widely applied in the EMS of electric vehicles, e.g. CNN [278], [280], conventional RNN [274], [278], LSTM [279], [281] or combinations of multiple NNs [282].

As a research direction with immense potential, probability machine learning is extensively studied and applied in today's applications of vehicle energy management, where Gaussian process regression (GPR) is one of the most successful approaches. The GPR is a powerful tool for EMS in vehicles because it can accurately predict and optimise energy usage while also dealing with noisy data and small training sets by its uncertainty quantification, e.g. Morlock et al. [283] proposed a framework for an economical cruise controller for electric vehicles in order to achieve real time applicability, where the GPR is applied by using traffic speed data from a cloud server; Bae et al. [284] presented an energy-efficient supervisory control method for power management in parallel (P)HEVs strategy by using an adaptive DP and Gaussian process regression to build a stochastic estimation of the value function. This method has one-step look-ahead horizon control and takes real-time learning and prediction uncertainty into account. For the energy management of plug-in hybrid electric vehicles (PHEVs), Zhou et al. [285] developed a novel transferable representation control model of a real-time controller by merging Gaussian process regression and an adaptive neural fuzzy inference system, which results in much better control efficiency and algorithm learning capabilities; moreover, the GPR is applied to the other auxiliary energy system in the vehicle. With an emphasis on the battery cooling refrigeration cycle and inside cooling of electric vehicles, Guo et al. [286] presented a real-time benchmarking technique based on GPR that allows for the ongoing assessment of the energy efficiency of numerous electric vehicle air conditioning systems.

2.3.4 Optimal control approaches for multi-mode hybrid vehicles

A hybrid electric vehicle that can run in multiple separate modes to maximise performance and fuel efficiency is known as a multi-mode PHEV or HEV. It normally includes two electric motors, a battery, an internal combustion engine, and a power electronics system that can smoothly switch between the various operating modes in response to road conditions and driver demand. Multi-mode hybrid vehicles always have four different and functional modes of operation: pure electric mode, pure combustion mode, charging the battery while driving in combustion mode, and boost mode, which combines electric and combustion engines [287]. Among these conditions, how to control the mode switch and optimally distribute the power becomes the primary concentration, e.g. Wu et al. [288] proposed a predictive energy management strategy based on multi neural networks for a multi-mode plug-in hybrid electric vehicle with an offline frame optimising the control thresholds and an online platform to recognise and respond to the instant driving conditions. Similarly, Li et al. [289] proposed a strategy including an offline section and an online section, where the former applies the PSO to optimise the thresholds of mode switching, the EF value in ECMS and the components' map of operations. While the online part optimally controls the instant operation of the powertrain based on the trained results from the offline section in advance. Furthermore, Zhuang et al. [290] analysed HEV configurations with different planetary gear (PG) compromises to determine the operation mode switching based on mode number, normalised efficiency and maximum output torque. Besides the single vehicles, a multi-mode hybrid electric vehicle routing problem (MM-HEVRP) was introduced by Seyfi et al. [291] as an extension of the hybrid electric vehicle-travelling salesman problem (HEV-TSP). Based on a homogeneous fleet of HEVs operating in four optimally chosen drive modes to minimise total travel cost, the problem takes into account customer demands, vehicle cargo capacities, and mandatory returns to the depot at the end of the day.

In a nutshell, automotive technology has advanced significantly with the development of multi-mode vehicles, which not only reduce environmental effects but also offer drivers a flexible option for satisfying their changing requirements during the driving process.

2.4 | Summary and research gaps

This chapter offers a thorough analysis of three key topics: 1) digital twin modelling for the development of electrified vehicles; 2) battery modelling, including status estimate and prediction; and 3) optimal control strategies for the EMS of HEVs, especially for multi-mode PHEVs. The current literature suggests that the following can be used to summarise the above areas' projected trends with their research gaps:

1) For automotive digitalisation, in the realm of automotive product development for design and engineering, digital twins are used to create virtual prototypes of vehicles and their components, which are aimed to simulate and optimise vehicle performance under complex conditions. However, there is a potential research gap in exploring the limits of accuracy and fidelity in these simulations, with the gap lying in how closely these virtual prototypes can mimic real-world behaviours under extreme or unusual conditions, and how they can incorporate unpredictable human factors or environmental changes.

2) For automotive electrification, current research in automotive lithium-ion battery modelling focuses on enhancing battery understanding and performance from the electrical, chemical, mechanical, and control principles. Regarding the progress in applying machine learning to improve lithium-ion battery performance and sustainability, there is still a research gap in comprehensively understanding and predicting battery degradation across a wide range of real-world scenarios. This includes investigating how diverse usage patterns, temperatures, and charging behaviours affect battery efficiency and lifespan.

3) In particular, the improvement of the multi mode hybrid vehicle is a major advancement in hybrid technology, but there is a research gap in seamless integration and real-time adaptability of these systems in unpredictable, rapidly changing driving environments. Research could focus on how these systems respond to unexpected changes in driving circumstances or power demands while maintaining efficiency and vehicle performance.

4) For those multi-objective optimisation applications in automotive EMS control, it is important to take these different time-scale objectives into account when optimising vehicle EMSs due to complicated operations and demands on the energy system fluctuating over time. While for current approaches, there is still a considerable research gap in developing models that can estimate status and adapt to future driving situations based on past and present data. This includes developing more dynamic and anticipatory models that can adapt methods in real time in response to unexpected changes in driving performance, optimising efficiency, extending battery life, and guaranteeing the dependability and safety of the vehicle.

CHAPTER 3

Methodology and Facilities

This PhD thesis focuses on the development of cyber-physical merged learning for online optimisation of multi-mode hybrid vehicles with diverse time-scale objectives: including PHEV digital frame formulation, battery data-driven digital modelling, and optimal energy management control for multi-mode hybrid vehicles. This chapter describes the research methods for data collection, digital modelling and optimal energy management after introducing the study goal and technological path for technology development. Furthermore, the chapter will go on to show the research facilities, hardware-in-the-loop (HiL) test subsystems, and the multi-mode hybrid vehicle system for real-time simulation.

3.1 | Research target and methods

The main focuses of this research are based on a multi-mode PHEV prototype with its power components and control system. An overview of the research is shown in Fig.3.1. The development of the multi-mode PHEV EMS consists of three main parts: 1) digital twin-based global optimisation control; 2) data-driven battery digital modelling; and 3) online optimal control with diverse time scale objectives. This research first aims to improve the efficiency of commercial vehicle product development and optimise energy management by using an offline global optimisation algorithm and a digital twin platform. Then, for highly electrified plug-in hybrid electric vehicles or multi-mode hybrid vehicles that frequently use batteries, real time application and ageing pattern improvement of the

corresponding battery digital models are developed to enhance the model's performance and functionality. Ultimately, an online optimal control energy management system is developed that takes into account both short-term instantaneous energy consumption and long-term power loss. This system is based on the previous offline optimisation results and key parameter calibration for the powertrain of multi-mode prototype vehicles and the hardware-in-the-loop testing is used to verify the system.

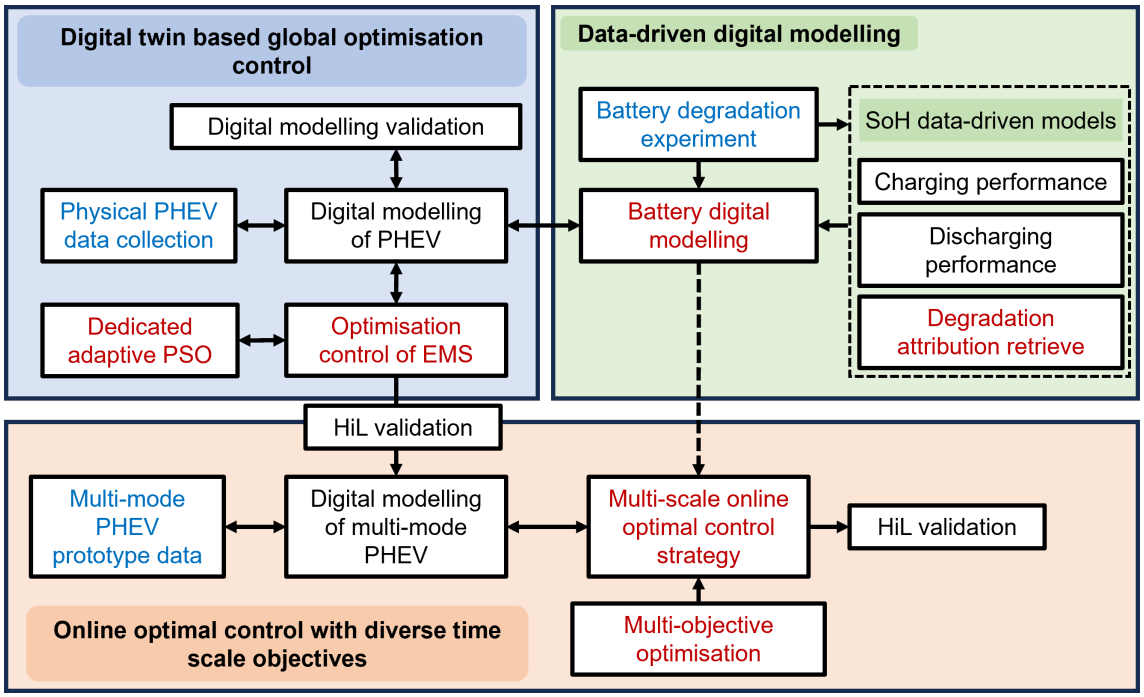

Fig. 3.1. The overview frame of the whole PhD research scope

3.1.1 Research method for DT-based offline optimisation

A digital twin frame was established based on the multi-mode PHEV in series-hybrid mode, which was developed based on chassis dynamometer test data of a conventional vehicle. To improve the DT-based EMS optimisation's optimality and reliability under various driving circumstances, a dedicated adaptive particle swarm optimisation (DAPSO) algorithm was developed by the author. Specifically, the conventional particle swarm optimisation (PSO) algorithm was combined with an adaptive swarm control approach to

construct the DAPSO, which managed the exploration and exploitation of each individual swarming particle in accordance with the global information acquired from the swarm.

3.1.2 Research method for battery digital modelling

Later, by considering the most significant power source of EVs in the second part, data-driven automotive battery digital modelling, an equivalent circuit model (ECM) was built based on offline parameter identification. Then, by concentrating on the battery's real time performance, the battery health models were developed based on the charging and discharging process via data-driven approaches. Firstly, an novel online double-layer system identification (ODSI) scheme to calibrate a battery model for state-of-health (SoH) prediction was firstly developed by focusing on the battery charging process. Then, an asynchronous system of joint estimation for batteries' SoH based on long short-term memory (LSTM) was proposed by focusing on the battery discharging process. Finally, to ensure the battery health estimation, a multi-kernel Gaussian process regression with automatic relevance determination (ARD-GPR) was proposed. The ARD was used to capture five health indicators (HIs) relevance during the battery charging-discharging process, and the estimated multiple-dimensional length scales of ARD-GPR demonstrate how the degradation process varies throughout the different phases.

3.1.3 Research method for EMS online optimal control based on diverse time scales

In the final stage of the third part, online optimal control with diverse time scale objectives, using a novel interpretation of the "Hamiltonian matrix," which is based on conventional instant cost status vector of ECMS. A cuboid equivalent consumption minimisation strategy (C-ECMS) for multi-mode PHEV is presented, which adds a second control degree of freedom to the traditional Hamiltonian vector, allowing for the best possible dual motor control in these vehicles. Next, an ageing factor (AF) was introduced and

coupled with the equivalent factor (EF), in order to create three Hamiltonian matrices that construct a cuboid knowledge base for optimal control taking into account various time-scale objectives.

3.2 Research facilities and resources

This study was conducted at the Advanced Engine and Vehicle Technology Research Centre at the University of Birmingham. Hardware and software facilities for HiL testing provided by ETAS were used for testing validation and demonstration. Additionally, a battery cycler for degradation testing was introduced for the battery experiments and relative ageing data collection.

3.2.1 Hardware-in-the-loop testing facilities

Automotive engineering relies extensively on hardware-in-the-Loop (HiL) testing, especially with current automobiles that have sophisticated software systems and electronic control units (ECUs). Ensuring the dependability, security, and effectiveness of automotive systems and parts requires the use of this technique.

hardware facilities

The HiL testing platform was constructed as shown in Fig. 3.2. For this research, a HiL testing system was constructed by utilising the hardware supplied by the ETAS company, which consists of a host PC, a prototype controller (ES910), and a real time computer (LABCAR) with controller area network (CAN) interfaces and multiple I/Os. The host PC is set based on a Windows 10 64-bit system with a CPU of 11th Gen Intel Core i7-11850H @ 2.50GHz, 16 GB RAM, and a graphic processor of NVIDIA GeForce GTX 3070. Via an Ethernet connection, the host PC downloaded the digital model of the automobile to the LABCAR. Subsequently, the algorithm was loaded into a code compiler and integrated into the LABCAR controller unit for instantaneous validation. In order

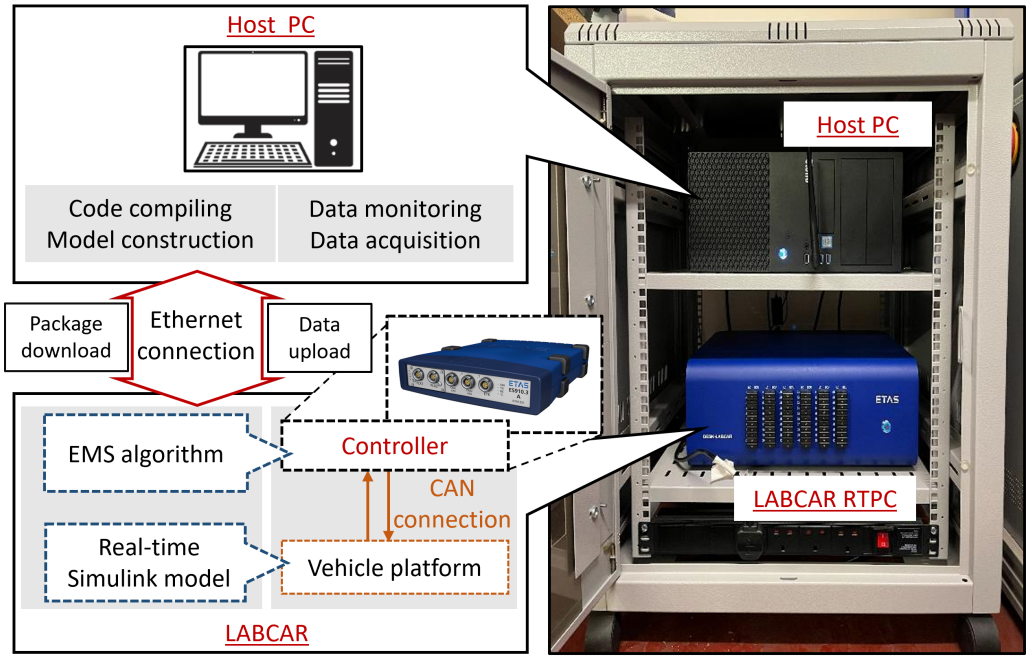

Fig. 3.2. Hardware-in-the-loop platform

for the LABCAR to reflect the CAN connection in the vehicle, a CAN connection was established between the control unit and the vehicle platform. In the HiL test, real time data transfer took place between the controller and the vehicle platform; and the vehicle's performance was ultimately captured in a data file. Using real-time models, LABCAR simulated the signals seen in actual cars and used the CAN bus to connect with the ES910.

software application

Also provided by the ETAS company, the software ETAS Experiment Environment (EE) and INCA, which set up the virtual environments (instrumentation, parameterization, etc.) and conducted simulations, were used to implement complied models of vehicles and controllers in the LABCAR and controller, respectively. The software offers functions such as signal conversion, sensor/actuator modelling, signal path tracing, and instrument creation to display measure variables and adjust experiment parameters, data logger recording, signal generator stimulating inputs, and more. Using an Ethernet connection,

the host PC downloaded the vehicle model to the LABCAR. The C code for the energy management algorithms was then implemented in the controller of the LABCAR for real time validation.

3.2.2 Driving cycles

For simulation to be effective, driving cycles are essential because they offer a reliable, consistent framework for comparing and assessing vehicle performance in different scenarios. Fuel consumption, emissions, and other performance factors are measured using these standardised cycles, which mimic a variety of driving situations such as mixed circumstances, urban traffic, and highway driving.

Standard driving cycle

By utilising these benchmarks OEMs and researchers can make well-informed decisions based on standardised performance indicators to evaluate and optimise vehicle designs in a reliable and efficient manner, where fairness is guaranteed when evaluating the performance of the vehicles. Generally, several typical standard driving cycles are introduced as below. The New European Driving Cycle (NEDC) [292] is shown in Fig.3.3 a). The NEDC was a driving cycle created to evaluate fuel efficiency and engine emissions in passenger cars that are put through controlled testing. The official fuel consumption and CO2 emissions of new automobiles are determined by the EU using the NEDC, which was first adopted in the 1980s. However, it has been criticised recently for attempting to faithfully replicate actual driving circumstances.

The Worldwide Harmonised Light Vehicles Test Cycle (WLTC) [293] are dynamometer tests conducted on the chassis to measure fuel consumption and emissions in light-duty cars, shown in Fig. 3.3 b). As the process for European car homologation, it seeks to replace the earlier and regional New European Driving Cycle (NEDC). More realistic driving scenarios, such as faster acceleration rates, higher maximum speeds, and shorter stop periods, are included in the WLTC as opposed to the NEDC and because of this, it

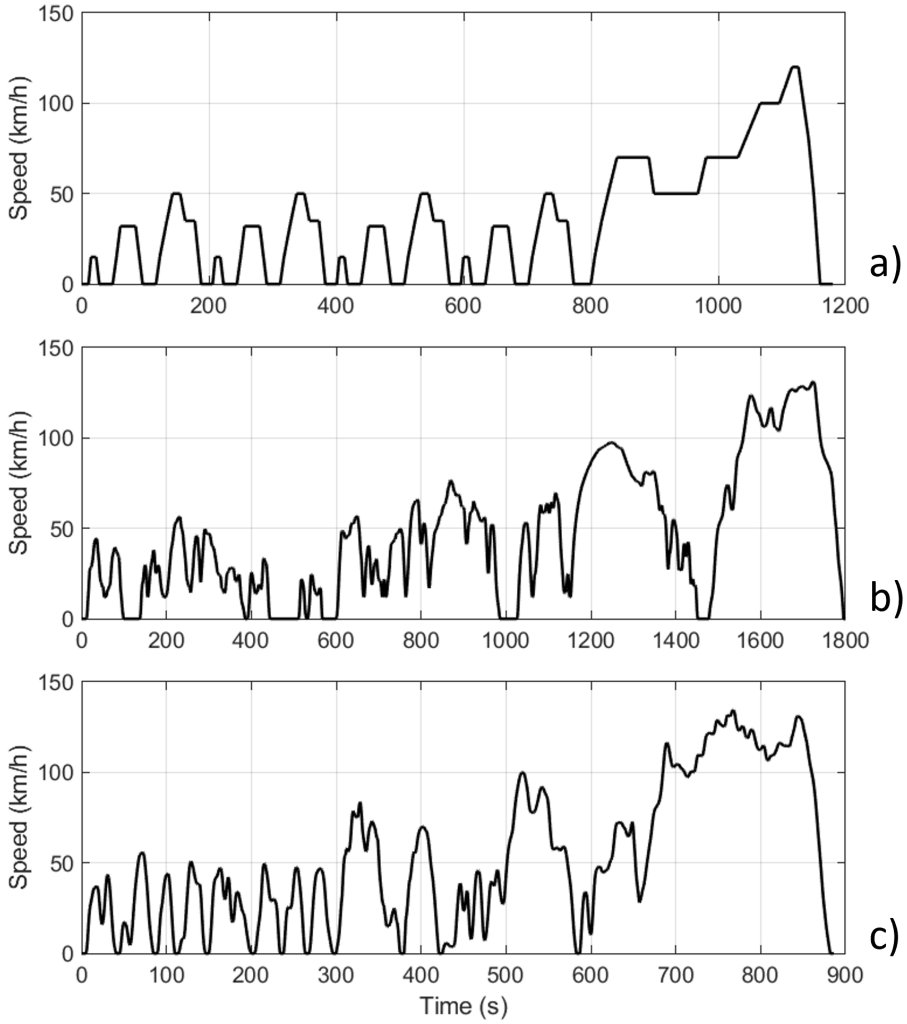

Fig. 3.3. Comprehensive driving cycles: a) NEDC; b) WLTC; c) RTS95

more closely resembles contemporary driving habits. The four segments of the WLTP driving cycle—low, medium, high, and extra high—each have a varied average speed to accommodate a variety of vehicle driving circumstances.

The RTS 95 [294] (Fig. 3.3 c)), sometimes referred to as RTS Aggressive or RTS 95 Aggressive, is a chassis dynamometer test cycle that represents aggressive driving, including urban, rural, and motorway segments. It is based on a subset of the Worldwide Harmonised Light Vehicles Test Procedure (WLTP) database, with a high representation of high-speed and load engine operating points.

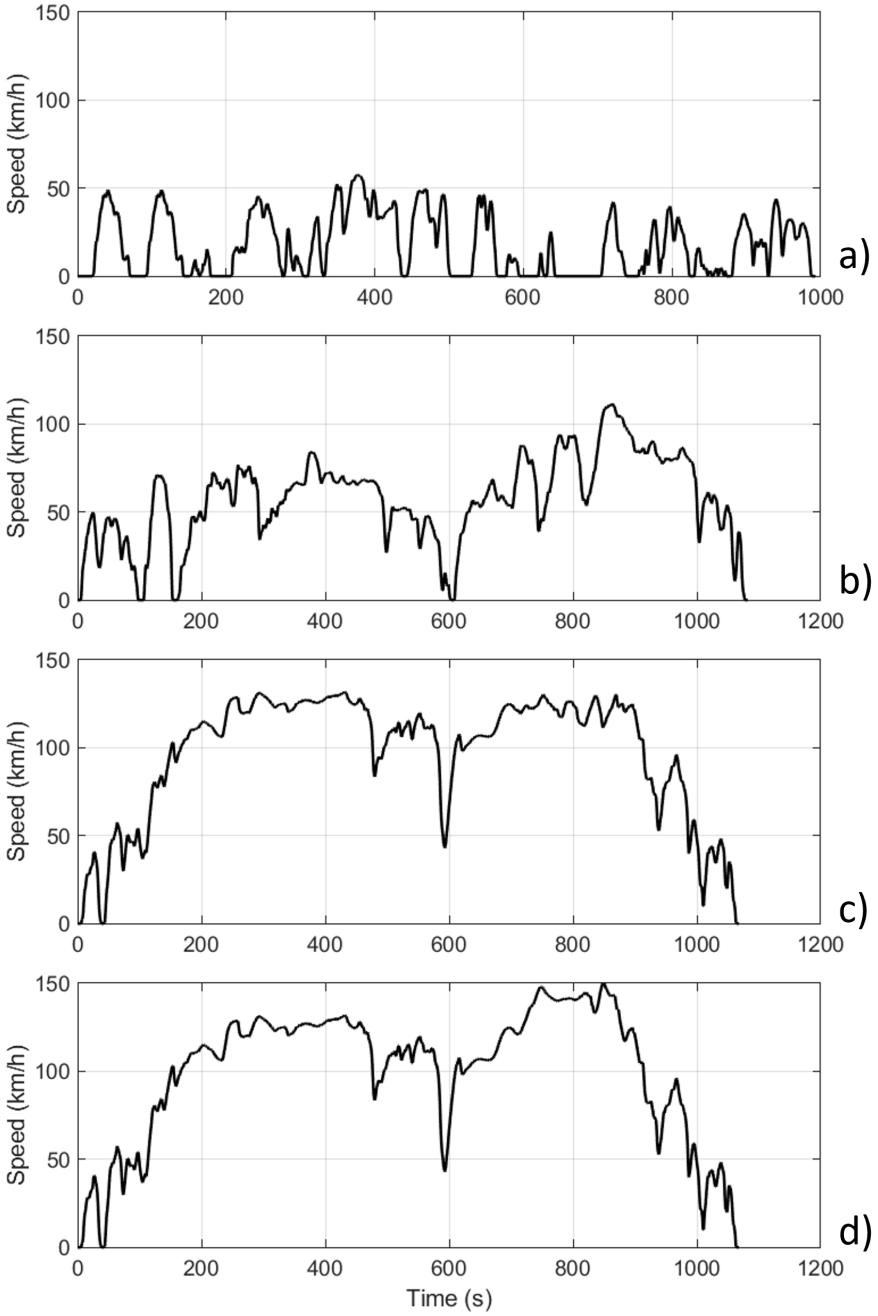

Fig. 3.4. Common Artemis Driving Cycles: a) Artemis-Urban; b) Artemis-Rural Road; c) Artemis-Motorway 130; d) Artemis-Motorway 150

The European Artemis (Assessment and Reliability of Transport Emission Models and Inventory Systems) project [292] produced the Common Artemis Driving Cycles (CADC), which are chassis dynamometer processes based on statistical analysis of a vast database of real-world driving patterns in Europe. Three driving schedules are included in the

cycles as shown in Fig. 3.4: a) urban, b) rural road, and two variations of the motorway cycle, with top speeds of c) 130 km/h and d) 150 km/h. The CADC was created to simulate a variety of driving scenarios and vehicle applications, such as gearbox usage and starting circumstances. Based on a statistical examination of a large database of actual driving patterns around Europe, the cycles were created to be indicative of real-world driving circumstances in the EU.

The FTP-72 (Federal Test Procedure) cycle, which is also called Urban Dynamometer Driving Schedule (UDDS) or LA-4 cycle, is applied to mimic the tradiational urban driving conditions; Additionally, two more cycles from the FTP-75 series test by the United States environmental protection agency (EPA) are applied [292]: The Highway Fuel Economy Test Cycle as in Fig.3.5 a), also called the Highway Fuel Economy Driving Schedule (HWFET), as one of its driving cycles for assessing a vehicle's fuel efficiency on a highway. The HWFET was created expressly to replicate highway driving including faster average speeds and fewer stops in comparison to urban driving cycles. The US06 is a supplementary fuel economy test (as in Fig. 3.5 b))that is used to calculate the EPA's on-road fuel economy ratings. It is distinguished by faster speeds, quick acceleration, and forceful braking, all of which indicate aggressive driving behaviour. To sum up, the HWFET evaluates a vehicle's performance under typical highway driving situations, while the US06 cycle is intended to test a vehicle's limits in terms of speed, acceleration, and driving aggression.

In a nutshell, Table 3.1 gives all the information about the operating circumstances, such as the duration, total length, average speed, and maximum speed of each condition. This makes it easier to intuitively compare the basic properties of the imposed standard conditions.

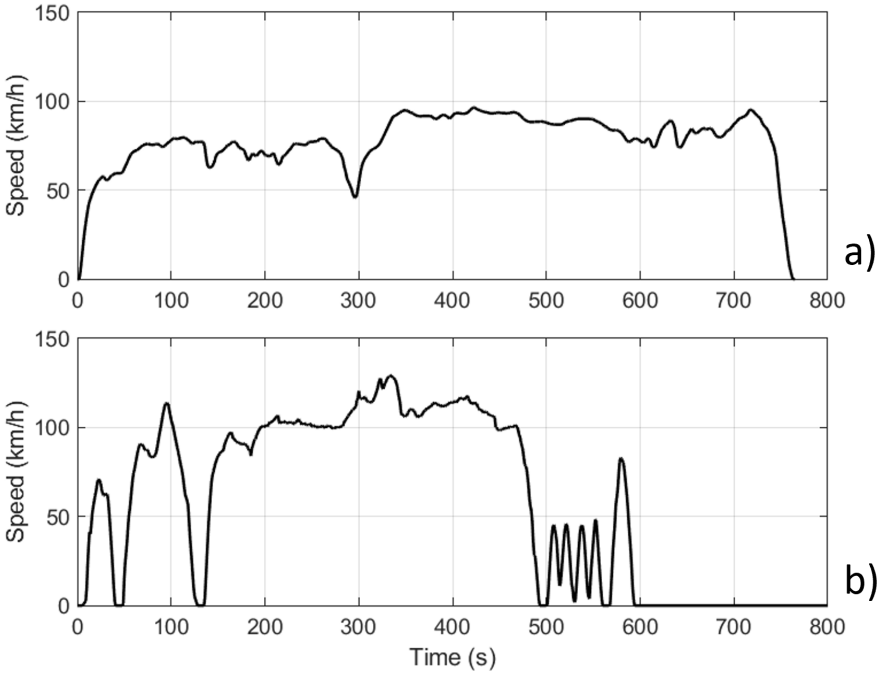

Fig. 3.5. FTP-75 series cycles: a) HWFET; b) SFTP-US06

Random driving cycle

A random WLTP cycle generating software developed by Kooijman et al.[295], is deployed to analyse driving energy consumption in real life over a wide range of driving behaviours as shown in Fig. 3.6. Random driving cycles are a crucial tool in research and development because they allow the testing of novel technologies—such as the intelligent EMS or system optimum control—under a wide range of circumstances. In this tool, the relative parameter set of the vehicle can be predefined for those key configurations of the powertrain. This random driving cycle generator generates more varied and unpredictable driving scenarios, closely simulating real-world conditions, and offering continued value in vehicle testing and development as driving patterns alter with changes in urban architecture, traffic management, and driver behaviour. The generated random driving cycles will be applied to validate the functionality of the EMS via HiL in later sections.

Table 3.1
Driving cycles profile

Driving cycle	Duration (s)	Distance (km)	Average speed (km/h)	Max speed (km/h)
NEDC	1180	10.93	33.35	120
WLTP3	1800	23.27	51.78	131.3
RTS95	886	12.93	52.52	134.45
Artemis-Urban	993	4.874	17.7	57.3
Artemis-Rural Road	1082	17.275	57.5	111.1
Artemis-Motorway130	1068	28.737	96.9	131.4
Artemis-Motorway150	1068	29.547	99.6	150.4
UDDS	1372	12.07	31.5	91.25
HWFET	765	16.45	77.7	97
US06	596	12.8	77.9	129.2

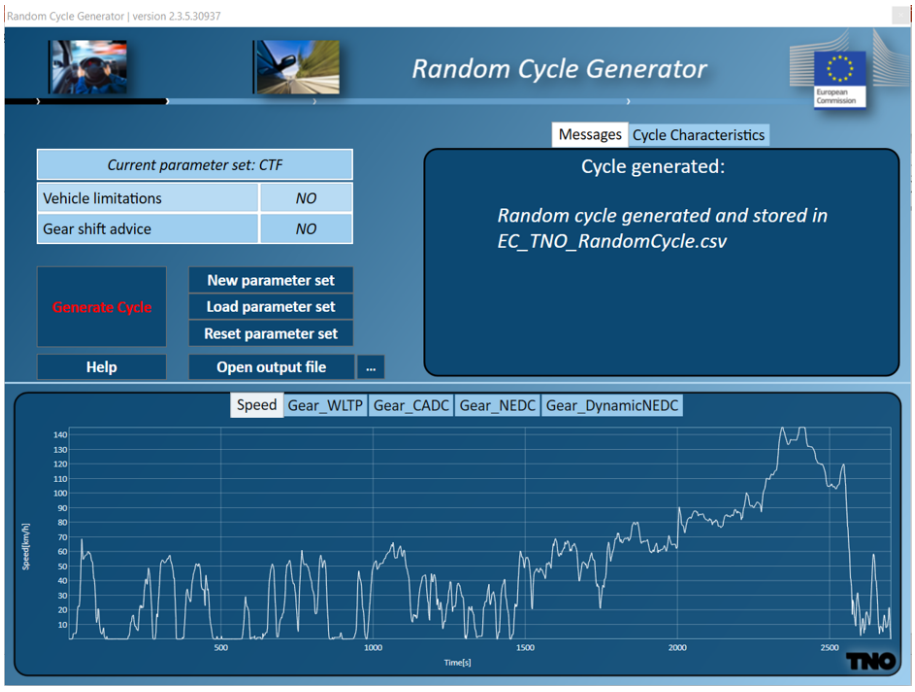

Fig. 3.6. WLTP random cycle generator [295]

3.2.3 Battery experiment and data collection

Besides previous research, two types of lithium-ion battery cells (SAMSUNG INR18650-29E and SAMSUNG INR21700-30I) were tested to create a validation database beacuase of their widely applications in automotive engineering. The equipment utilised to perform

the battery cycle testing is depicted in Fig. 3.7, where the battery cells were kept in an ESPEC temperature chamber (Su-642) and tested by a Series 4000 MAccor tester (A190721), with a computer monitoring and saving the battery data. The Series 4000 consists of a test cabinet, PC, and test software. The PC computer and test cabinet are linked by a fast 10 Base T communications network. The test system is immediately operational as soon as AC power is applied to it. The ESPEC SU-642 bench-top temperature chamber provides environmental testing performance in a small package. It has an inner volume of 64 litres and a temperature range of -40 °C to 150 °C. The chamber is designed to provide accurate temperature control and is ideal for a wide range of environmental testing applications, such as battery testing.

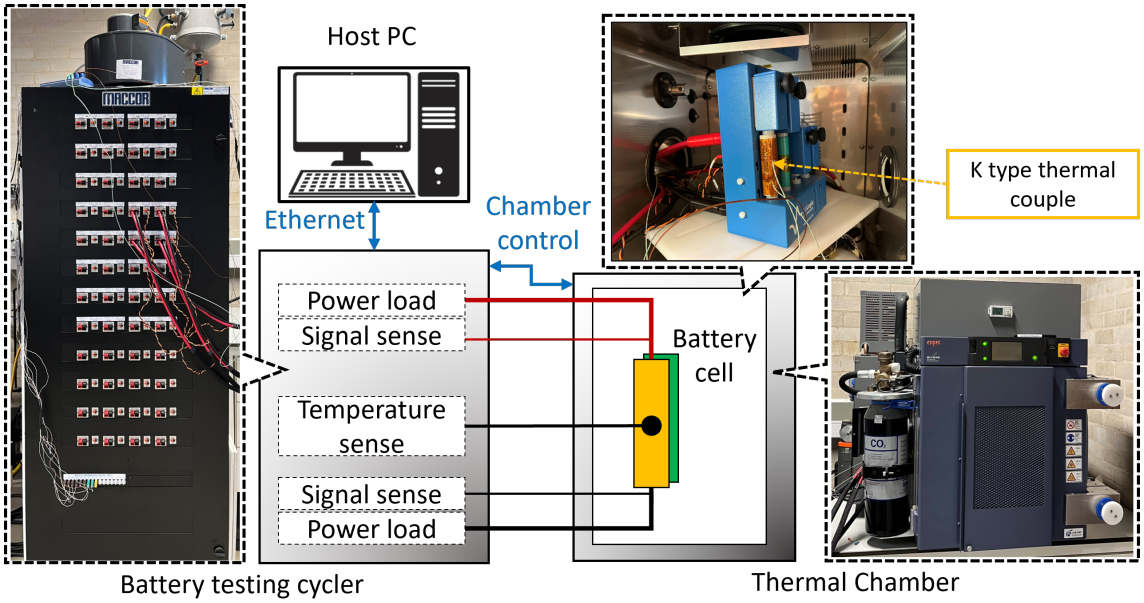

Fig. 3.7. Battery degradation test facility

Open source battery database

A widely used data set from NASA [296] was applied first to help the model train. In this data set, 34 Li-ion 18650 cells with a nominal capacity of 2 Ah were included. They were tested under a variety of ambient temperatures (4 °C, 24 °C, and 43 °C), while the battery cells were charged using a standard constant current and constant voltage (CC-CV)

charging methodology and discharged using various discharging scenarios. The data set contains recorded battery performances of cycling iterations for discharge capacity with in-cycle measurements of terminal current, voltage, and cell temperature. The data is recorded until cells' capacity drops below 30% of their nominal capacity. The details of the data sets applied in this research are shown in Table 3.2.

Table 3.2
NASA database

data set name	Nominated capacity	Temperature	ageing rate
B0005, B0006, B0007, B0018	2Ah	24 ^oC	30%
B0029, B0030, B0031, B0032	2Ah	43 ^oC	30%
B0053, B0054, B0055, B0056	2Ah	4 ^oC	30%

3.3 | Multi-mode PHEV powertrain and its digital modelling

Digital modelling for vehicle systems is a critical aspect of modern automotive engineering, leveraging the power of computational tools and simulation to optimise the design and functionality of these systems. It enables the R&D process to innovate and evolve rapidly in order to meet the problems of efficiency, performance, environmental requirements, and the electrification transition. In this section, a backward model of a plug-in PHEV is presented with specifications of vital components, such as the engine, motor, battery.

3.3.1 Multi-mode PHEV powertrain and working modes

Fig.3.8 depicts the architecture of the powertrain of multi-mode PHEVs. An internal combustion engine (ICE), two motor/generators (MG1 and MG2) with integrated gear-boxes, and a battery package make up this powertrain's primary power units. The solid black lines represent the mechanical ties in the powertrain; while the dashed green line

represents the electric links, and the dotted green line represents the regenerative brake, respectively. The clutch controls the connection between the gear box and MG1.

The multi-model PHEV operates in multiple modes, as seen in Fig.3.8: pure-EV mode (power flow indicated by the yellow arrow), series-hybrid mode (power flow indicated by the blue arrow), and parallel mode (power flow indicated by the red arrows).

Pure-EV mode

In the pure-EV mode, the MG1 and ICE are totally shut down. The battery package is the only power source that supports the MG2 to meet the power demands during the driving process. Mathematically, they are presented as

$$\left.\begin{aligned} P_{\mathrm{req}} &= \eta_{\mathrm{MG2}} P_{\mathrm{MG2}} \\ T_{\mathrm{req}} &= i_{\mathrm{RD}} \cdot i_{\mathrm{R2}} \cdot T_{\mathrm{MG2}} \\ P_{\mathrm{Batt}} &= P_{\mathrm{MG2}} \end{aligned}\right\} \tag{3.1}$$

where P_{Batt} and P_{MG2} are the power offered by the battery and MG2, respectively; η_{MG2} is the corresponding efficiency of the MG2; T_{MG2} is the torque offered by MG2, and this torque is transmitted to the wheels through the gearbox integrated with MG2 (with the gear ratio i_{R2}) and the final differential (with the gear ratio i_{RD}).

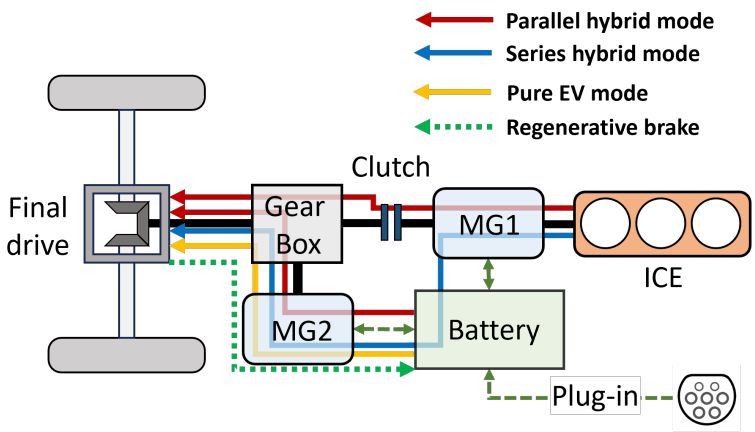

Fig. 3.8. The powertrain of the multi-mode PHEV

Series-hybrid mode

In series mode, the battery's state of charge (SoC) determines how the range extender (ICE+MG1) functions; the clutch is deactivated, and the MG2 still powers the entire powertrain, with a part of the energy being compensated by the range extender. When operating in series mode, the PHEV's energy flow yields

$$\left.\begin{aligned} P_{\mathrm{req}} &= \eta_{\mathrm{MG2}} P_{\mathrm{MG2}} \\ T_{\mathrm{req}} &= i_{\mathrm{RD}} \cdot i_{\mathrm{R2}} \cdot T_{\mathrm{MG2}} \\ P_{\mathrm{Batt}} &= \eta_{\mathrm{MG1}} P_{\mathrm{MG1}} - P_{\mathrm{MG2}} \\ P_{\mathrm{ICE}} &= P_{\mathrm{MG1}} \\ \omega_{\mathrm{ICE}} &= \omega_{\mathrm{MG1}} \end{aligned}\right\} \tag{3.2}$$

where P_{ICE} and P_{MG1} are the power offered by the engine and MG1, respectively; η_{MG1} is the corresponding efficiency of the MG1; ω_{ICE} and ω_{MG1} are the rotation speed of the ICE and MG1, and they are the same at this time.

Parallel-hybrid mode

In parallel mode, the ICE can compensate for the MG2 by providing some driving torque through the engaged clutch. The PHEV's energy flow in parallel mode produces

$$\left.\begin{aligned} P_{\mathrm{req}} &= \eta_{\mathrm{MG2}} P_{\mathrm{MG2}} + \left(\eta_{\mathrm{ICE}} P_{\mathrm{ICE}} - P_{\mathrm{MG1}}\right) \\ T_{\mathrm{req}} &= i_{\mathrm{RD}} \cdot i_{\mathrm{R2}} \cdot T_{\mathrm{MG2}} + i_{\mathrm{R1}} \cdot \left(T_{\mathrm{ICE}} - T_{\mathrm{MG1}}\right) \\ P_{\mathrm{Batt}} &= \eta_{\mathrm{MG1}} P_{\mathrm{MG1}} - P_{\mathrm{MG2}} \\ \omega_{\mathrm{ICE}} &= \mathrm{MG1} \end{aligned}\right\} \tag{3.3}$$

where η_{ICE} is the engine efficiency; T_{ICE} and T_{MG1} are the torque outputs of the engine and MG1, respectively; i_{R1} is the transmission ratio of the gearbox to MG1.

Multi-mode PHEV powertrains combine the advantages of electric vehicles (EVs) and standard HEVs, enabling greater flexibility, increased fuel efficiency, and lower emissions. The capacity to function in different modes enables these vehicles to adapt to a variety of driving situations and requirements.

3.3.2 Digital modelling for a multi-mode PHEV

Due to the intricate layout of a multi-mode PHEV's powertrain, a detailed analysis of powertrain models for multi-mode PHEVs is required. In this research, both forward-facing and backward-facing vehicle models are applied to the powertrain applications to reveal the instant power flow during driving conditions.

Forward-facing vehicle model

A forward-facing vehicle model [297] is necessary to fulfil the speed trace from a drive cycle, where a driver model in a forward-facing vehicle model supplies torque demand in the form of the required ICE torque and brake torque. In a basic driver model, the torque requirement is often achieved by using one or more proportional-integral (PI) controllers in relation to the required speed trace. Afterwards, the driver model sends the pedal actions (which correlate to the power demands) to the EMS control, which then distributes the power flow from the motor and ICE properly. Prior to being applied to the wheels, the torque generated by the executors is routed via the final drive ratio and gearbox. Following the transmission of power to the wheel, the vehicle's performance—primarily its speed-is determined by the longitudinal model of the vehicle. The vehicle speed that emerges from the force exerted serves as the driver model's feedback for speed tracking. It also returns to the gearbox as angular velocity after passing through the drivetrain. A typical forward-facing vehicle model is shown in Fig.3.9.

Backward-facing vehicle model

The other specific method used in vehicle analysis and simulation is a backward-facing model of a plug-in PHEV, where the estimation of energy usage and the evaluation of the effectiveness of different PHEV powertrain components are the main uses of this modelling technique [297]. As is shown in Fig. 3.10, backward modelling involves starting the simulation from the demand side, i.e. the model vehicle's wheels, and working its way back to the energy power sources, i.e. ICE, battery, etc.

Generally, if the speed and time distribution are obtained from a driving cycle, the instant force needed at the wheels of a vehicle to overcome rolling resistance, aerodynamic drag, inertia, and gravity forces (when climbing hills) would calculated by the vehicle model (known as the vehicle longitudinal model). As a result, the power demand of the vehicle at each time point can be identified, and the demand is then communicated to the EMS control model to suitably allocate actions to those components in the powertrain. The EMS controller will then send control commands to each executor, such as the gearbox, ICE, or battery. Their respective performance and overall energy consumption (including efficiency losses) of the powertrain will provide feedback for both the vehicle model and the EMS control unit to make further control adjustments. By starting from the power demand side (normally the wheels) and processing backwards through the powertrain, the backward-facing vehicle model provides insights into the efficiency of various components and the overall energy requirements of the vehicle under different driving conditions.

Vehicle model

A longitudinal vehicle model is used in automotive engineering to simulate and analyse a vehicle's straight-line motion while taking forces along the vehicle's axis of motion into account. This type of model is essential for comprehending and predicting a vehicle's acceleration, deceleration, and cruising behaviour under a variety of scenarios. Mathematically, the vehicles' dynamics can be presented as

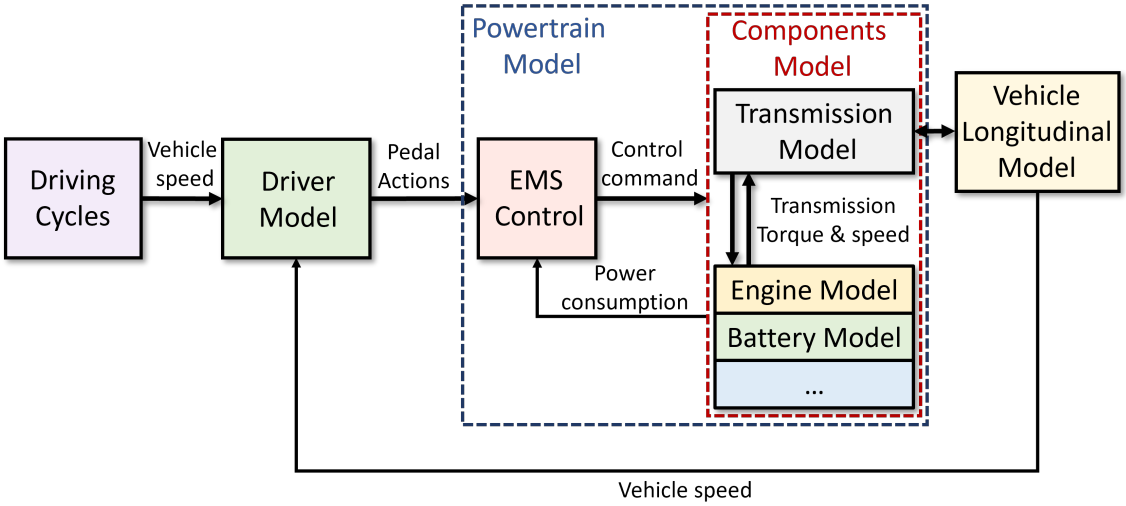

Fig. 3.9. Forward-facing model of a vehicle system

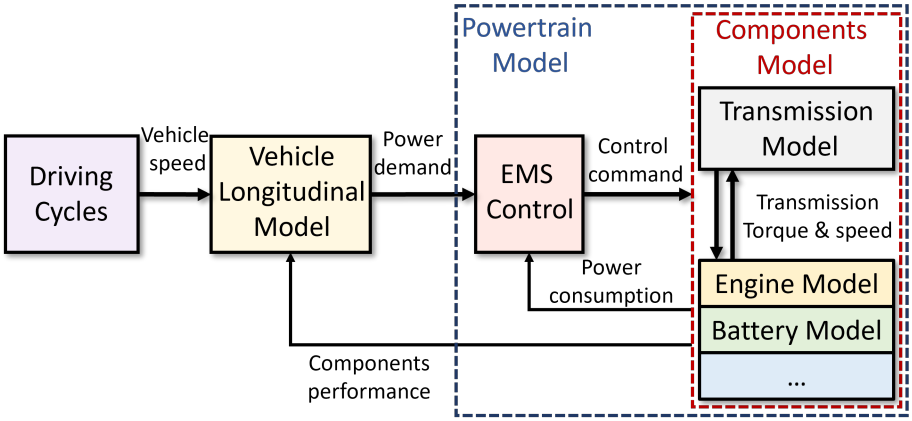

Fig. 3.10. Backward-facing model of a vehicle system

$$\left.\begin{aligned} P_{\text{req}} &= F_{\text{tot}} \cdot v = \left(ma + F_f + F_a + F_g\right) \cdot v \\ T_{\text{req}} &= F_{\text{tot}} \cdot R \end{aligned}\right\} \tag{3.4}$$

where P_{req} is the vehicle's instant power demand; while F_{tot} is the vehicle's total force demand; v is the vehicle speed; F_f, F_a and F_g are the rolling resistance (friction), the air resistance and the gradient resistance, respectively. The torque needed at the wheel is denoted by T_{req}; while the tyre radius is denoted by R. Specifically, the F_f, F_a and F_g can be further explained by

$$\left.\begin{aligned} F_f &= C_f mg\cos\theta \\ F_a &= \frac{1}{2}\rho v^2 C_d A \\ F_g &= mg\sin\theta \end{aligned}\right\} \tag{3.5}$$

where m is the vehicle mass and a is the vehicle acceleration; C_f is the vehicle's rolling friction coefficient; g is the gravity acceleration; θ is the angle of the terrain slope; and ρ is the air density; C_d is the aerodynamic drag coefficient, and A is the vehicle's frontal area.

Since the following research is based on different layouts of powertrains, particular data and information on the vehicles will be presented in the corresponding chapters.

Generic ICE model

As a typical sort of mathematical model in the fields of control systems and automotive engineering, the map-based model depicts the most common characteristics of an internal combustion engine. In order to create a map-based engine model, extensive data from an engine running in different scenarios must be gathered, mostly from steady and transient dynamometer tests. Important performance indicators, including power, torque, fuel consumption, and emissions, are carefully tracked. After that, the data is filtered to eliminate abnormalities and normalised for uniformity. The engine's performance is then visually represented throughout its operating range through the use of comprehensive maps, usually in three dimensions. As is shown in Fig. 3.11, the map, which was created using the relationship between engine speed and torque as axes for determining brake-specific fuel consumption (BSFC), illustrates how different operating conditions affect significant fuel economy results.

With insights that help drive efficiency gains and fuel consumption reductions, the map-based model is a valuable tool for optimising the powertrain design, engine performance, and EMS control strategies.

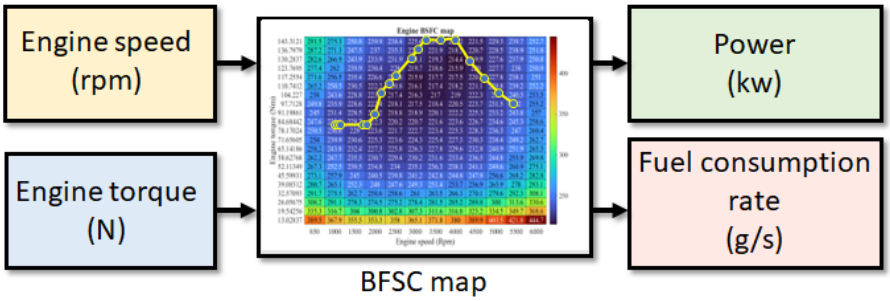

Fig. 3.11. Map-based ICE consumption model

Generic motor model

Similarly, creating a map-based motor model requires a methodical approach to data collection and analysis, especially for electric motors. To collect vital information such as torque, power output, and efficiency, rigorous testing is first carried out under a range of operating situations, including diverse loads, speeds, and temperatures. After carefully cleaning and normalising the data, multi-dimensional performance maps are created, usually displaying power, torque, and efficiency against variables such as load and speed, as demonstrated in Fig. 3.12.

The performance characteristics of the motor are comprehensively visualised throughout its working range by means of these maps. It is also notable that the yellow line is the maximum torque line of the motor, as this shows the limit of its ability according to speed and torque.

These maps provide the final model, which is crucial for improving design efficiency, leading the development of novel motor applications, and optimising motor control strategies—all of which ensure optimal performance under a variety of conditions.

Generic battery model

Based on the demand for fast responses with reliable simulation results, a 2-RC equivalent circuit battery model (ECM) in MATLAB/Simulink was created, as shown in Fig. 3.13.

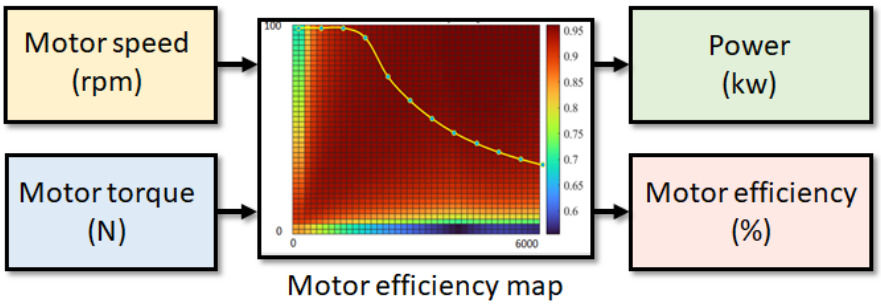

Fig. 3.12. Map-based motor model

According to the power relations, the 2-RC model determines battery current, I_{Batt}, at every sampling time based on the powertrain power requirement, P_{Batt} and the instant available battery voltage, U_t. Generally, they obey the governing equations as below:

$$\left.\begin{aligned} U_o &= I_{\mathrm{Batt}} R_o \\ U_s &= \frac{I_{\mathrm{Batt}}}{C_s} - \frac{U_s}{R_s C_s} \\ U_l &= \frac{I_{\mathrm{Batt}}}{C_l} - \frac{U_l}{R_l C_l} \\ U_t &= U_{\mathrm{ocv}} - U_s - U_l - U_o \end{aligned}\right\} \tag{3.6}$$

where R_o is the ohmic resistance of the battery and U_o is the voltage drop brought on by the ohmic resistance; U_s is a representation of the voltage drop throughout the charging process. The short-term equivalent capacitance is represented by C_s, and the resistance by R_s. The voltage that indicates the battery diffusion process is called U_l; the open circle voltage, or U_{ocv}, is dependent on the battery state of charge (SoC); long-term equivalent capacitance is represented by C_l and equivalent resistance by R_l.

Besides, according to Seaman et al. [298] and Chen et al. [299] a sensitivity analysis on the battery equivalent circuit is used to define a set of relative parameters directly relating to the SoC, which is then given to the equivalent circuit model equations. The following equations were obtained, indicating the sensitivity of the models to parameter uncertainty or variation with the SoC's change:

$$
\left.
\begin{aligned}
C_{\text{cap}} &= P_1 \\
U_{\text{ocv}} &= P_2 \exp\left(P_3 SoC\right) + P_4 + P_5 SoC + P_6 SoC^2 + P_7 SoC^3 \\
R_o &= P_8 \exp\left(P_9 SoC\right) + P_{10} \\
R_s &= P_{11} \exp\left(P_{12} SoC\right) + P_{13} \\
C_s &= P_{14} \exp\left(P_{15} SoC\right) + P_{16} \\
R_l &= P_{17} \exp\left(P_{18} SoC\right) + P_{19} \\
C_l &= P_{20} \exp\left(P_{21} SoC\right) + P_{22}
\end{aligned}
\right\} \tag{3.7}
$$

where the sensitive parameters, denoted as P_1 to P_{22}, are all determined by the battery's instantaneous state of charge. In order to more correctly depict the battery's operating performances in practical applications, those parameters can be adjusted by sophisticated algorithms, such as PSO or GA, taking into account the various batteries' varying electrochemical properties. Based on the previous governing equations, the SoC of the battery can be further presented mathematically as:

$$
\mathrm{SoC}(t) = \mathrm{SoC}\left(t_0\right) - \frac{\int_{t_0}^{t} I_{\mathrm{Batt}} dt}{C_{\mathrm{Batt}}(t)} \tag{3.8}
$$

where I_{Batt} is the battery's current, determined from Eq. 3.6; $SoC(t_0)$ indicates the starting SoC, and $C_{\mathrm{Batt}}(t)$ indicates the battery's capacity. As a result, Eqs. 3.6 to 3.8 effectively offer a thorough summary of the fundamental working theories and essential performance criteria of a power battery for PHEVs.

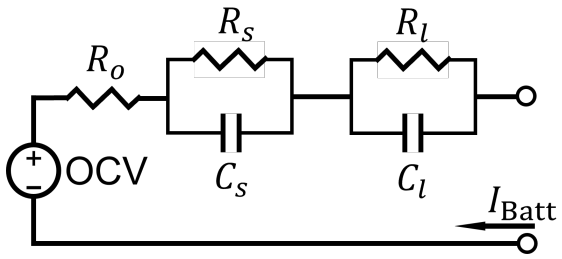

Fig. 3.13. The 2-RC battery model

3.3.3 Modelling of SoH estimation for the lithium-ion battery

Various computational and algorithmic techniques are used in the state of health (SoH) estimate process for lithium-ion batteries in order to evaluate the batteries' functioning and overall health over time. For lithium-ion batteries, which are frequently used in electric vehicles, to be reliable, secure, and have a long lifespan, this evaluation is essential. Generally, when the battery's capacity drops to a particular value (i.e. 20%), the battery is considered to be at the end of life (EOL) and needs to be significantly maintained or replaced directly. In this section, two major estimation approaches are introduced which are also the main concentrations of the later research of this PhD program.

Empirical model

From the studies by Wang et al. [300] and Song et al. [301] taking into account time, temperature, discharge rate, and depth of discharge (DoD), a semi-empirical model can be mathematically formulated as follows:

$$Q_{\mathrm{Loss}} = Ae^{-\left(\frac{E_a + B\cdot \mathrm{C_{Rate}}}{R_g\ \mathrm{T_{batt}}}\right)} \cdot {A_h}^{z} \tag{3.9}$$

where Q_{Loss} is the battery's capacity loss; and pre-exponential factor A, activation energy E_a, gas constant R_g, and battery temperature T_{batt} are all represented. The C-rate of discharge, or C_{Rate}, is accompanied by a compensating factor, or B; Z is the power-law factor, and A_h is the Ah-throughput. Those variables can be further determined according to different battery types with variable mechanisms. Furthermore, the Ah-throughput, A_h, and the C-rate, C_{Rate}, can be calculated by

$$\left.\begin{aligned} A_h &= \tfrac{1}{3600}\int_{t_k}^{t_{k+1}} |I_{\mathrm{Batt}}|\, dt \\ \mathrm{C_{Rate}} &= \tfrac{I_{\mathrm{Batt}}}{C_{\mathrm{Batt}}} \end{aligned}\right\} \tag{3.10}$$

Later, this empirical model will be used in conjunction with the battery's 2-RC model to provide a real time response in the PHEV simulation.

Data-driven model

The battery's data-driven model of SoH estimation and prediction follows a path of development of a supervised machine learning model as shown in Fig. 3.14. Using complicated data sets, the data-driven technique for battery SoH estimation analyses and forecasts battery health using sophisticated algorithms. The history data, which includes important characteristics such as charge/discharge cycles, voltage, current, temperature, and battery age, among others, is first gathered from the testing cycler or battery management system.

Subsequently, the data undergoes various processing techniques, such as noise reduction, dimension reduction, or normalisation. Additionally, the features that are most relevant to the regression results-also referred to as the health indicators (HIs) in battery SoH estimation-are chosen and taken out of the database in order to train and validate the model later. Typically, 30% of the data is used for training the model, while the remaining 70% is used for validation, and model accuracy is typically measured using performance measures like mean absolute error (MAE), root mean square error (RMSE), or R-squared. Finally, the trained SoH model with relative parameters defined can be applied to the corresponding battery health estimation and prediction scenarios.

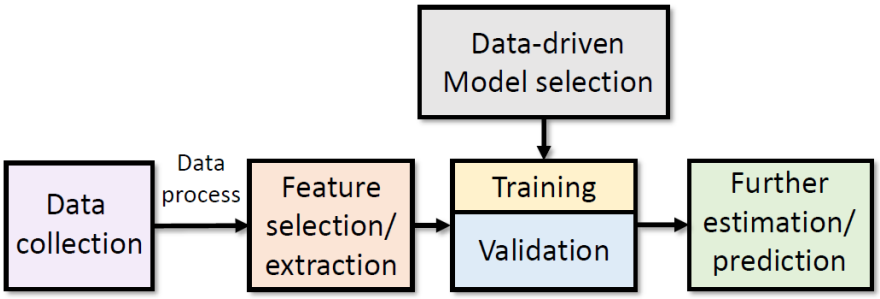

Fig. 3.14. Process of a data-driven model

3.4 Chapter summary

Conclusively, the research techniques and facilities are introduced in this chapter. The primary studies that are pertinent to this chapter are:

1. The technical path for the development of cyber-physical merging learning for optimising multi-mode PHEVs is presented in this chapter, which covers digital twin-based global optimisation control, data-driven battery digital modelling, and online optimal control with diverse time-scale objectives. Data collection, digital modelling, and the deployment of energy management systems are among the research methodologies used. A multi-mode PHEV prototype is a key area of focus.

2. This chapter additionally discusses the significance of driving cycles in vehicle simulation, focusing on typical driving cycles such as NEDC, WLTC, RTS 95, and CADC, as well as random driving cycles generated by the software. The hardware-in-the-loop (HiL) testing facilities and battery test equipment are also highlighted, with an emphasis on their importance in automotive engineering.

3. Finally, the chapter demonstrates digital modelling for multi-mode PHEV systems, including a longitudinal vehicle model, ICE and motor models, battery models, and lithium-ion battery state of health (SoH) assessment that comprises empirical and data-driven SoH estimate models. The study utilises computational methods and simulation to verify the design and functionality of vehicle systems, notably in terms of efficiency and performance.

CHAPTER 4

Dedicated APSO for offline optimisation based on the digital twin of EVs

Currently, the majority of DT research for vehicle applications is focused on enhancing model accuracy [302] and data connectivity [303]. To increase the model accuracy of the digital equivalent of batteries for EVs, Li et al. [302] combined an H-infinity filter with a particle swarm optimisation (PSO) algorithm. Venkatesan et al. [304] created a DT based on the ANN algorithm for optimising the energy efficiency of an EV motor system. While Liu et al. [305] created a transport system DT to aid autonomous vehicle decision-making using fused sensor data. Zhou et al. [306] used a PSO to optimise the design parameters of an energy-harvesting shock absorber. Furthermore, Zhou et al. [307] developed a human-knowledge-augmented Gaussian process regression technique for developing a battery DT for estimating the state of health.

It is critical for OEMs to achieve robust and dependable design using DT at the research and development stage because vehicle makers cannot remotely monitor and manage all vehicles using centralised cloud computing [308]. According to two recent DT review publications [309] and [310], research into DT-based resilient design with self-adaption is in high demand. As a result, this chapter intends to provide automotive OEMs with robust and dependable control optimisation of PHEVs through research on a specific AI algorithm for DT-based vehicle product development. Following the authors' recent work

in hybrid vehicle design and control [311]–[313], a specific AI algorithm based on the PSO method's high robustness and self-adaptation ability will be built.

Compared to the other approaches for the EMS optimal control, PSO leverages many advantages: PSO can be naturally adaptive, and it can continuously alter control techniques depending on real-time data from the digital twin, resulting in greater EMS optimisation. The PSO has fewer tuning parameters than its counterparts, such as the non-dominated sorting genetic algorithm (NSGA), strength Pareto evolutionary algorithm-II (SPEA-II), and multiple objective evolutionary algorithm (MOEA), [314] because it is a widely used derivative-free algorithm that can solve optimisation problems with nonlinear constraints and high-dimensional searching spaces [315], [316]. Besides, PSO searches for the global optimum by considering numerous candidate solutions at the same time, making it more effective in identifying the optimal solution than approaches that may become caught in local optima compared to those sub-optimal approaches (i.e. rule-based control or the fuzzy logic control). Some global optimisation approaches (i.e. DP) are suffered by the curse of dimensionality, where the computational requirements grow exponentially with the increase in state and decision variables. In contrast, PSO is less affected by this problem and can handle the complexity and high-dimensional nature of the EMS optimisation problem in a more scalable manner. Nonetheless, the PSO parameters must be fine-tuned to attain the optimum optimality and resilience for various applications; also, the calculation efficiency for PSO in system optimisation is not thoroughly investigated, as described [317]. Because the intelligent algorithm is so important in the AI-based DT system, a well-designed PSO with high computing performance is required.

This chapter offers the proposed DAPSO algorithm for DT-based PHEV energy management optimisation to overcome the foregoing concerns in terms of robustness and computing efficiency in the application of AI-based optimisation on DT platforms. It describes a procedure for transferring testing data to vehicle DT and optimising control

using DT. In this chapter, a vehicle test is performed first using the chassis dynamometer. The data is then collected in order to create a digital car model. The proposed DAPSO is applied to the digital model to conduct simulation experiments in order to obtain optimised control threshold findings. Finally, a processor-in-the-loop (PiL) test is performed to validate the optimised results' performance. Following the introduction of the DT application for PHEV energy management optimisation, the process can be applied to the R&D of other vehicle types, such as battery electric vehicles.

4.1 Digital twin of PHEV

This section describes the DT system in this study, which consists of a physical object (the PHEV), a digital model of the PHEV, a service model for EMS optimisation, a database, and interfaces between each component. The physical entity in this study is the vehicle itself, and a database is created based on data received from vehicle tests, as shown in Fig. 4.1. This chapter will cover the details of digital modelling and EMS optimisation, as well as a workflow for transferring testing data to vehicle DT and DT-empowered control optimisation.

4.1.1 Digital modelling of the PHEV

The physical asset in this section is the PHEV, and the digital model of the PHEV is constructed using MATLAB/Simulink. The cyber-physical connection between the vehicle and the digital model is formed through data transfer from the dynamometer and onboard diagnostics (OBD) based on a test of the BMW-i3 REx. The digital model consists mostly of a virtual vehicle plant and a prototype energy management system that employs an empirical rule-based technique with adjustable thresholds.

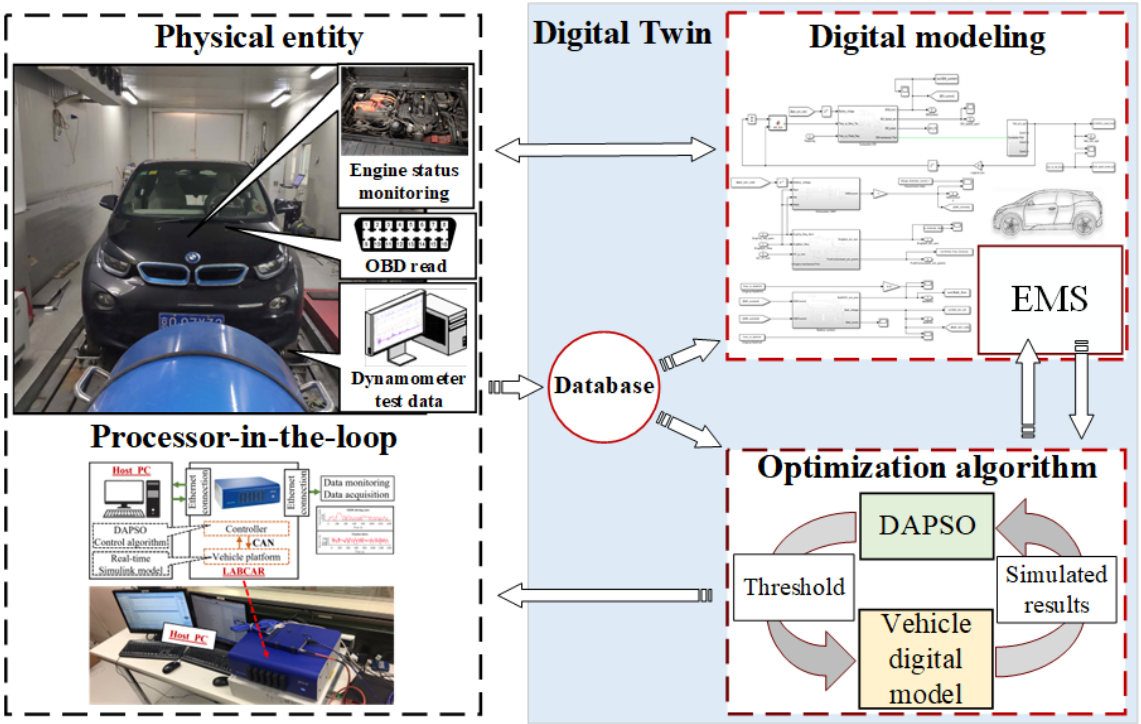

Fig. 4.1. Demonstration of DT

Vehicle plant and technical specifications

Based on the introduction in section 3.3, a forward-facing framework is used to model the virtual vehicle plant. To enable the virtual car to follow the speed profile (specified by the driving cycles) with fewer than 5% tracking errors, a PID-type driver model is utilised. A 125-kW traction motor powers the virtual vehicle's plug-in hybrid engine. The powertrain's major source of power is a 60-Ah battery pack. The alternate power unit is a 26.6-kW range extender, which provides power for battery charging. Table 4.1 summarises the vehicle specs utilised for DT modelling.

EMS of Powertrain

Specifically, the EMS is considered the only series-hybrid mode of the multi-mode powertrain, as in section 3.3.1, with an empirical rule-based EMS drawn from BMW-i3 REx testing data. First, the PHEV's chassis dynamometer was tested by conducting driving cycles, while the traction motor, range-extender, and battery operating data were

Table 4.1
Specifications of the vehicle [318]

Vehicle specifications	Parameters	Values
Vehicle body	Weights	1400 kg
	Wheelbase	2570 mm
	Length/Width/Height	3398/2040/1577 mm
	Front area	2.38 m^2
	Coefficient of air drag	0.3
Tyres	Size F/R	175/70 R19
ICE (DOHC-8 valve 12)	Displacement	0.647 L
	Maximum power	25 kW
Traction motor (PM AC Synchronous)	Maximum power	125 kW
	Maximum torque	250 Nm
Battery package (Lithium-ion)	Number of cells	96
	Nominal system voltage	355 V
	Pack capacity	60 Ah
	Pack energy	22 kWh
Drivetrain (Rear wheel drive)	Final drive ratio	9.7

measured in real time. The operating region of the engine and motors was classified based on the test data, and the EMS is inferred and validated. This approach is described in detail in some previous research [319].

The traction motor drives the vehicle in this powertrain, and the EMS controls the range extender for battery charging and provides additional electric power. When the battery state-of-charge (SoC) is high, the vehicle operates as a pure EV, according to the basic control logic. When the SoC level falls below 16%, the range-extender turns in and steadily raises its power output to keep the battery SoC level stable. The range-extender's operating mode is determined by three separate SoC level thresholds, namely the SoC low limit, SoC medium limit, and SoC high limit, which are also referred to as the SoC_1, SoC_2, and SoC_3 in the rest of this chapter.

The rule bases, as shown in Algorithms 1 and 2, determine the operating speed and torque of the range-extender based on observations of the battery SoC and vehicle speed. When the vehicle's speed falls below 16.1 km/h, the range-extender is turned off fully.

Algorithm 1 Range-extender working speed control logic

```
if vehicle speed < 16.1 km/h then
  range-extender is OFF
else
  if SoC < SoC_1 then
    if vehicle speed < 55 km/h then
      range-extender works in low speed
    else if vehicle speed > 96.6 km/h then
      range-extender works in high speed
    else
      range-extender works in transition speed
    end if
  else if SoC_1 < SoC < SoC_3 then
    if vehicle speed < 55 km/h then
      range-extender works in low speed
    else if vehicle speed > 80 km/h then
      range-extender works in medium speed
    else
      range-extender works in transition speed
    end if
  else
    range-extender is OFF
  end if
end if
```

Algorithm 2 Range-extender working torque control logic

```
if SoC < SoC_2 then
  if vehicle speed < 24 km/h then
    range-extender works in low torque
  else if vehicle speed > 51.5 km/h then
    range-extender works in high torque
  else
    range-extender works in transition torque
  end if
else if SoC_2 < SoC < SoC_3 then
  if vehicle speed < 51.5 km/h then
    range-extender works in low torque
  else
    range-extender works in transition torque
  end if
else
  range-extender is OFF
end if
```

Otherwise, the range-extender has normally six working conditions, three work speeds: low speed, medium speed, and high speed, respectively being allocated with two working torques: low torque and high torque.

4.1.2 Energy management strategy optimisation

Following the findings of [320] three battery SoC thresholds, SoC_1, SoC_2, and SoC_3, will be modified to achieve the lowest equivalent fuel and power use while maintaining battery SoC. The mathematical representation of the optimisation problem can be formulated as

$$\begin{aligned} [SoC_1, SoC_2, SoC_3] \quad &= \arg\min\left(J_{\text{com}}\right) \\ \text{s.t.} \quad &\left\{ \begin{array}{c} J_{\text{com}} = \varphi \cdot \left| \frac{\text{SoC}_{\text{final}} - \text{SoC}_{\text{std}}}{\text{SoC}_{\text{ref}}} \right| + (1-\varphi) \cdot \frac{\text{EC}_{\text{final}}}{\text{EC}_{\text{ref}}} \\ SoC_1 < SoC_2 < SoC_3 \\ SoC_1, SoC_2, SoC_3 \in \left[SoC^-, SoC^+\right] \end{array} \right\} \end{aligned} \tag{4.1}$$

where J_{com} is the objective function; SoC_{final} and EC_{final} are the final SoC and equivalent consumption at the end of a given driving cycle, respectively; φ is the weight factor used to balance the preference for cycle-end SoC control versus the cycle's equivalent consumptions; and SOC_{std} is a desired final SoC level derived from rule-based control. The SoC_{ref} and EC_{ref} are normalisation factors, with $SoC_{ref} = SoC^+ - SoC^-$ and EC_{ref} equalling the same fuel usage under traditional rule-based regulation. The battery SoC lower and upper boundaries are $SoC^- = 13.5\%$ and $SoC^+ = 60\%$, respectively. The equivalent consumption of fuel and electricity can be calculated by

$$\left. \begin{array}{c} EC_{\text{final}} = \int_0^T \left(\dot{m}_{\text{ice}}\left(P_{\text{ice}}(t)\right) + \dot{m}_{\text{em}}\left(P_{\text{em}}(t)\right) \right) dt \\ \left[P_{\text{ice}}(t), P_{\text{em}}(t)\right] = \mathbf{DT}\left(SoC_1, SoC_2, SoC_3\right) \end{array} \right\} \tag{4.2}$$

where $\dot{m}_{\text{ice}}$ is the fuel consumption rate in g/s and P_{ice} and P_{em} are the engine and traction motor power demands in kW, respectively; $P_{\text{ice}}(t)$ and $P_{\text{em}}(t)$ can be derived using the

DT with various SoC threshold values, and $\dot{m}_{\mathrm{em}}$ is the equivalent fuel consumption transmitted from electricity in g/s, and may be computed using [321]

$$\left.\begin{aligned}\dot{m}_{\mathrm{em}}\left(P_{\mathrm{em}}(t)\right) &= \gamma \cdot S_{\mathrm{dis}} \frac{1}{\eta_{\mathrm{batt}}\eta_{\mathrm{em}}} \frac{P_{\mathrm{em}}(t)}{H_{\mathrm{LVH}}} + (1-\gamma) \cdot S_{\mathrm{chg}} \cdot \eta_{\mathrm{batt}}\eta_{\mathrm{em}} \frac{P_{\mathrm{em}}(t)}{H_{\mathrm{LVH}}} \\ \gamma &= \frac{1+\mathrm{sign}\left(P_{\mathrm{em}}(t)\right)}{2}\end{aligned}\right\} \tag{4.3}$$

where H_{LVH} is the lower heating value of the fuel, S_{dis} and S_{chg} are the equivalent factors for battery discharging and charging, and $S_{\mathrm{dis}} = S_{\mathrm{chg}} = 2.5$ is predefined as in [321]. Additionally, the efficiency of the battery and motor are represented by η_{batt} and η_{em}, respectively.

4.2 | The proposed dedicated adaptive particle swarm optimisation (DAPSO)

This part introduces the proposed dedicated adaptive PSO (DAPSO) algorithm, which is firstly designed and developed to deal with the DT-based optimisation outlined in section 4.1.2. As shown in Fig. 4.2, the DAPSO iteratively performs a rolling optimisation with the DT of the PHEV.

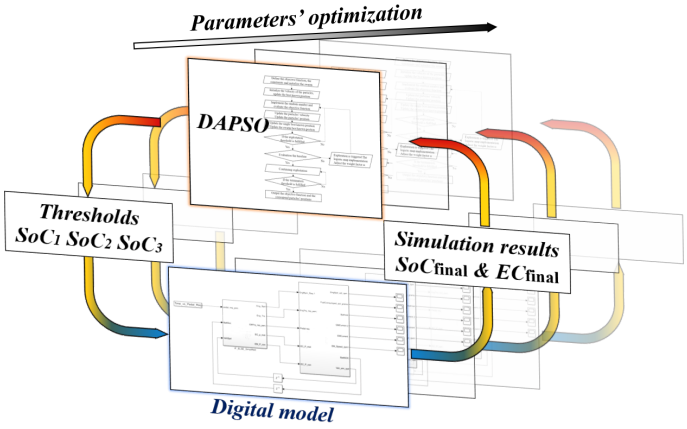

Fig. 4.2. Frame of the iterative optimisation process

4.2.1 Iterative optimisation process

The DAPSO algorithm, like the conventional PSO algorithm, employs computer agents (particles) to retrieve the optimal objective function values and return the best particle position. Initially, the DAPSO assigns p at random inside the search space defined in Eq. 4.1. The position of each particle is $x_i^t = \left[SoC_1^{i,t}, SoC_2^{i,t}, SoC_3^{i,t}\right]^{\mathrm{T}}$, where $i = 1, 2, 3, ..., p$ is the index number for individual particles; $k = 1, 2, 3, ..., \tau$ is the number of iterations; and τ is the maximum number of iterations. Each particle will compute its objective function using the DT based on the position information, and the best positions will be returned to update the particles' positions using the PSO process [322]. Mathematically, this process can be expressed as

$$\left.\begin{aligned} v_i^{k+1} &= \omega \cdot v_i^k + \alpha \cdot \epsilon_1 \left[g^* - x_i^k\right] + \beta \cdot \epsilon_2 \left[x_i^{*(k)} - x_i^k\right] \\ x_i^{k+1} &= x_i^k + v_i^{k+1} \end{aligned}\right\} \tag{4.4}$$

where v_i^k and x_i^k indicate the velocity and position of the i-th particle at the k-th state; g^* denotes the best particle overall across all findings; $x_i^{*(k)}$ is the current swarm's local best at the k-th iteration; ϵ_1 and ϵ_2 are two random numbers between 0 and 1; α and β are the two attraction factors, and $\alpha = \beta = 2$ meet the most general instances; ω is the inertia factor used to balance exploration and exploitation, and it is generally set between 0.6 and 0.9, [322] although in this research it is initially set at 0.65 by repeated trials.

4.2.2 Adaptive control of the swarm

The proposed DAPSO is built around an adaptive swarm control technique, as indicated by the red dashed rectangle in Fig. 4.3. A state machine is used to implement adaptive swarm control, based on observing swarm information, such as DT outputs (fuel usage and SoC level) and relative particle locations and velocities. The state machine controls the DAPSO parameters based on three modes: 1) exploration, 2) exploitation, and

3) termination. DAPSO differs from traditional PSO in that it can investigate the optimum swarm movement strategy during the heuristic optima search process using a new exploration and exploitation method.

The DAPSO will attempt new search areas in the exploration mode; while DAPSO individuals will follow the inertia to move in the exploitation mode. The detailed parameters for the three modes are shown as below.

1) Exploitation mode: if the criteria indicated in threshold 1 are met, the algorithm will move to the exploitation mode. Threshold 1 determines the state of charge of the battery and the equivalent consumption by

$$\frac{\left|SoC^k_{\text{opt}} - SoC_{\text{ref}}\right|}{SoC_{\text{ref}}} \leq 5\% \text{ and } EC^k_{\text{opt}} \leq EC_{\text{ref}} \tag{4.5}$$

where SoC^k_{opt} and EC^k_{opt} are the battery state of charge and equivalent energy consumption obtained by the DT with the best particle location at iteration t, respectively; SoC_{ref} is the reference battery SoC level, which in this section is 16%, and EC^k_{opt} is the reference equivalent consumption for each cycle.

The fulfilment of both conditions shows that the current process is on the right track, so the exploitation proceeds with the ω being constant. The particles' velocity and position will be updated as shown in Fig. 4.3.

2) Exploration mode: to prevent the algorithm from becoming trapped in local optima, the DAPSO adds an early exploration mechanism based on variations in the cost function value in five neighbouring iterations (before the first 20 iterations).

$$\epsilon = \left|J^k_{\text{com}} - J^{k-1}_{\text{com}}\right| + \left|J^{k-1}_{\text{com}} - J^{k-2}_{\text{com}}\right| + \cdots + \left|J^{k-4}_{\text{com}} - J^{k-5}_{\text{com}}\right| \tag{4.6}$$

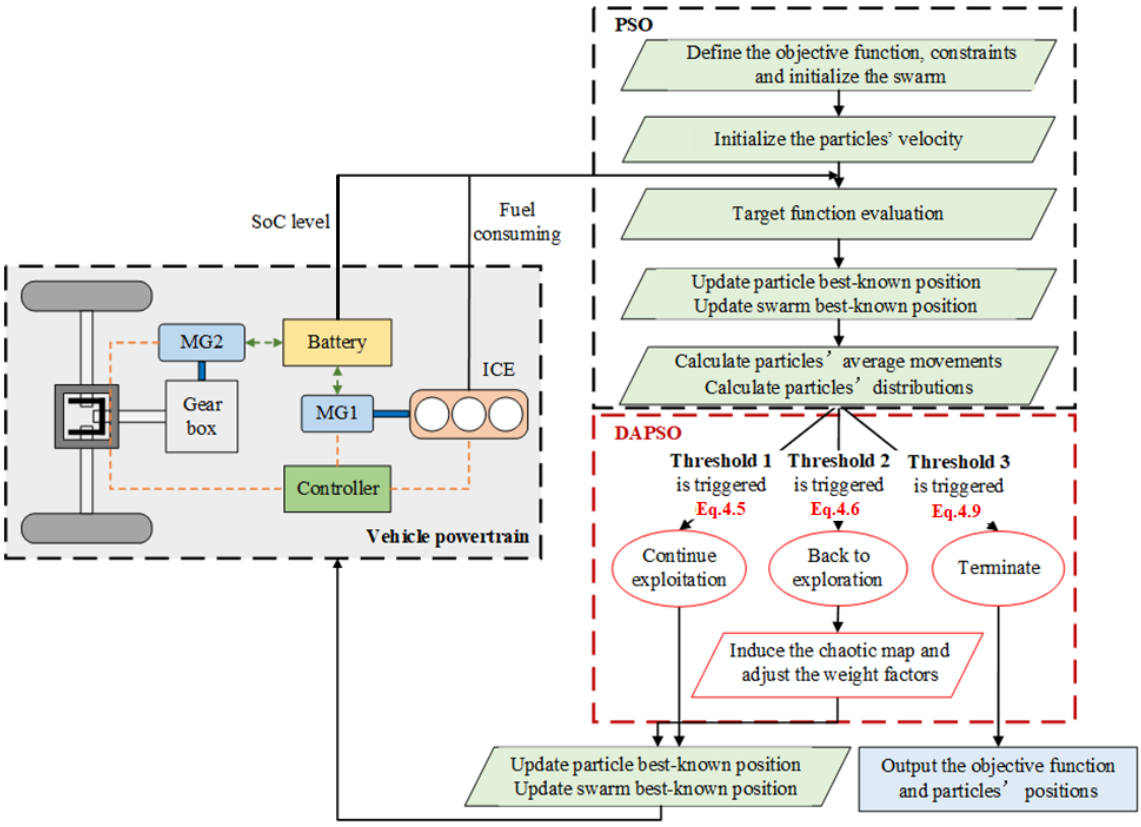

Fig. 4.3. Flowchart of the DAPSO

If $\epsilon = 0$, the exploration will be activated, and the inertia factor will be reset to its initial value (at the first iteration after the reset) as

$$\omega^1 = 0.3 \tag{4.7}$$

Otherwise, the DAPSO will generate the inertia factor using a logistic chaos map as follows:

$$\omega^k = 2.6 \cdot \omega^{k-1} \cdot (1 - \omega^{k-1}) \tag{4.8}$$

3) Termination mode: in Table 4.2, the termination conditions were traditionally classified into four types of criteria based on the work of Zielinski and Laur. [323] The algorithm may be terminated immediately following a certain number of iterations (θ_{iter}), regardless

of the optimised results, or if the improvement of the objective function does not reach a given threshold (θ_{imp}) within a certain range of iterations, or if the movement (dimensionless quantity in search spaces) of single particles is less than a certain threshold θ_{mov}. The distances of each particle to the instant best particle (which indicates the position of the best solution) are calculated, and this indicates how near the particles gather to the optimal position. The process will be terminated if the average distance falls below a particular threshold limit.

All four criteria are taken into account in this research. The exploration and exploitation actions are decided using the improvement-based termination condition, where $\theta_{\text{imp}} = \epsilon$. The last three criteria are the termination threshold (threshold 3), the algorithm will terminate when the termination threshold (threshold 3) meets the criteria, as indicated by any of the three conditions:

$$\left.\begin{aligned} k &\geq \theta_{\text{iter}} \\ \bar{P}_{\text{mov}} &\leq \theta_{\text{mov}} \\ \bar{P}_{\text{dis}} &\leq \theta_{\text{dis}} \end{aligned}\right\} \tag{4.9}$$

where k is the number of iterations; $\bar{P}_{\text{mov}}$ is the average particle movement; and $\bar{P}_{\text{dis}}$ is the average distance between each individual particle's position and the position of the best particle, with their related thresholds θ_{iter} , θ_{mov}, and θ_{dis}, respectively. The $\bar{P}_{\text{mov}}$ and $\bar{P}_{\text{dis}}$ can be further expressed mathematically as

$$\left.\begin{aligned} P_{\text{mov}} &= \sum_{i=1}^{N} \left(v_i^{k+1} - v_i^k \right) \\ P_{\text{dis}} &= \sum_{i=1}^{N} \left(x_i^k - x_i^{*(k)} \right) \\ \bar{P}_{\text{mov}} &= \frac{P_{\text{mov}}}{N} \\ \bar{P}_{\text{dis}} &= \frac{P_{\text{dis}}}{N} \end{aligned}\right\} \tag{4.10}$$

where v_i^k , x_i^k, and $x_i^{*(k)}$ are from Eq. 4.4, and N is the number of particles in the swarm; P_{mov} represents the velocity increment of each particle from the k-th to the $(k+1)$-th iteration. The average value $\bar{P}_{\text{mov}}$ represents the magnitude of particle movement; P_{dis} is the distance between the positions of each particle x_i^k and the best particle $x_i^{*(k)}$ at the k-th iteration. Similarly, P_{dis} represents the magnitude of the distribution for particles close to the optimal solution.

Table 4.2
Different termination conditions of PSO

Termination conditions	Considered criteria	Thresholds
Maximum-iteration-based	Number of iterations	θ_{iter}
Improvement-based	The improvement of objective function	θ_{imp}
Movement-based	The movement of single particles	θ_{mov}
Distribution-based	The average distance of the swarm	θ_{dis}

4.3 | Comparable research with conventional PSO

A series of simulation runs and processor-in-the-loop (PiL) tests were performed to illustrate the benefits of the suggested approach for PHEV energy optimisation. Additionally, experiments were carried out to investigate the optimal configuration of the suggested DAPSO algorithm. Both the PiL test platform and the software-in-the-loop (real-time simulation) platform were used for the experimental investigation. Initially, the DAPSO method was implemented offline. The baseline techniques for the comparison study were four PSO versions. With the ETAS-LABCAR, the powertrain's performance was evaluated in real time as the control parameters were optimised. The basic PHEV model was created in MATLAB/Simulink, and its parameters were adjusted using data gathered from chassis dynamometer testing at Tingshua University.

4.3.1 Baseline methods comparison

To assess the proposed mechanism, standard PSOs with general parameter values are compared with this DAPSO, as the suggested approach examines both termination conditions and adaptive attraction techniques. As per the previously discussed termination methods, four PSO variations were selected as baseline approaches for DT-based control optimisation, each with a distinct inertia factor setting and terminating circumstance. Table 4.3 provides an overview and comparison of the DAPSO with the terminology and parameters of the baseline techniques.

The PSO1, PSO2, and PSO3 all use the same inertia factor value, $\omega = 0.65$, which is the standard setting for PSO [323], [324]. The PSO4 follows a chaotic map with a dynamic inertia factor, as shown in Eq. 4.8. The starting inertial factor value in this study is 0.7, in accordance with Yang's suggestion [322].

Both PSO1 and PSO4 were ended when the maximum iteration requirement was fulfilled, i.e. $\theta_{\text{iter}} = 50$ is used in this study. The PSO2 was terminated by the minimal movement condition with the $\theta_{\text{mov}} = 0.001$; while PSO3 was terminated by the minimum distribution condition with the $\theta_{\text{dis}} = 0.05$. The values of θ_{iter}, θ_{dis}, and θ_{mov} are obtained from a collection of compiled samples using the standard PSO optimised outcomes. In accordance with the earlier research [311], [312], the other relative parameters are empirically determined. In a nutshell, the DAPSO is compared with PSO1, PSO2, and PSO3 for the termination mechanism and PSO4 and DAPSO are compared for the implementation of swarm adaptive control. The values for the remaining parameters are the same, with the exception of those stated above.

4.3.2 Dynamic programming approach

Dynamic programming (DP) is a numerical approach to tackling multistage decision-making problems, and it is capable of offering the global optimised solution to issues of any

complexity level (within the certain mathematical constraints and computer capability) based on Bellman's concept[16]. In hybrid vehicles, DP optimises control algorithms to achieve optimal fuel efficiency and electricity utilisation. The procedure involves: 1. Establishing the problem via state variables that represent the system's current status (as is shown in Eq. 4.2); 2. Identify the decision variables for control actions (i.e. power split between engine and motor), an objective function to minimise (Eq. 4.3), and constraints such as battery SOC limits and vehicle physical limits; 3. Divide the driving cycle into discrete stages (time steps); 4. Set the cost function J_{com} at the final stage, considering terminal costs; 5. For each time step, a backward calculation is executed from terminal step to the beginning step with all possible control actions, their instant cost between single steps; 6. Determine the best solution based on each state with minimal cost function J_{com}. The final solution computed by the DP method is the global optimised results with corresponding actions of each component in the powertrain. The optimally controlled result by DP will be regarded as the best solution in the later comparison with different methods.

4.3.3 Performance indicators

The three key performance metrics for assessing AI algorithms are computational efficiency, reliability, and optimality [325]. This section establishes a thorough scoring system by figuring out the weighted sum value of the functions influencing these three parameters.

Table 4.3
Comparison of the DAPSO with baseline methods

Name of PSO variant	Inertial factor ω	Termination methods
PSO1	Fixed ($\omega = 0.65$)	Maximum-iteration
PSO2	Fixed ($\omega = 0.65$)	Minimum-movement
PSO3	Fixed ($\omega = 0.65$)	Minimum-distribution
PSO4	Chaotic dynamic	Maximum-iteration
DAPSO	Adaptive chaotic dynamic	Selected machine

The overall score S is defined as the weighted sum of three components that assess optimality, computation efficiency, and success rate, respectively, in order to gauge the effectiveness of the DT system:

$$S = w_1 \underbrace{(1 - J_{\text{com}})}_{\text{Optimality}} + w_2 \underbrace{\left(1 - \frac{T_{\text{opt}} - T_{\text{ave}}}{T_{\text{ave}}}\right)}_{\text{Computation efficiency}} + w_3 \underbrace{\left(\frac{\aleph_{\text{opt}}}{\aleph_{\text{total}}}\right)}_{\text{Success rate}} \tag{4.11}$$

where J_{com}, the core component that embodies the optimality of the DT-based system, is the vehicle performance measure, or the objective function specified in Eq. 4.1. The time consumption of a single optimisation is represented by T_{opt} in the second component (which represents computing efficiency); while the average time consumption of all PSO algorithms under study is represented by T_{ave}. The better the computing efficiency, the smaller T_{opt}. The third component, which indicates the success rate, has two values: $\aleph_{\text{total}}$, which is the total number of trials (in this case, 20,) and $\aleph_{\text{opt}}$, which is the number credited for the success, where the robustness of the DT-based system is measured by the ratio of $\aleph_{\text{opt}}$ to $\aleph_{\text{total}}$. Then w_1, w_2 and w_3 are weighting factors for optimality, computation efficiency, and success rate, respectively. The weighting factor settings of $w_1 = 0.5$,$w_2 = 0.25$, and $w_3 = 0.25$ are chosen as an example to show how DAPSO can determine the greatest value of the overall score function. To accommodate varying optimisation tastes, the weighting parameters can be modified.

4.3.4 Fourfold cross-validation testing

In Table 4.4, the cycles on the horizontal axis validate the learning outcome of local optimisation, i.e., in the first row, all PSOs are applied to optimise the UDDS cycle, and the optimised results (thresholds) are then validated by the Highway, US06, and NEDC cycles. The cycles on the vertical axis represent the local optimisation by various PSO types. A fourfold cross-validation is established when the optimisation findings from one selected driving cycle are validated by the remaining driving cycles. The highway

Table 4.4
Set-up of fourfold cross-validation based on driving cycles

All PSO variant	UDDS	Highway	US06	NEDC
UDDS	**Learning**	Validation	Validation	Validation
Highway	Validation	**Learning**	Validation	Validation
US06	Validation	Validation	**Learning**	Validation
NEDC	Validation	Validation	Validation	**Learning**

cycle shows the fuel efficiency of automobiles on the motorway; the UDDS cycle was selected to reflect the average driving condition in cities; the US06 cycle is representative of aggressive driving behaviours; and the NEDC cycle was selected due to its extensive research and typical driving conditions. The majority of the driving scenarios for the PHEV use were covered by the selection of these four cycles.

4.3.5 Random real-world driving validation

In order to assess the proposed approach, three simulated random driving cycles from the real world were tried as shown in Fig. 4.4. In a publication by Kooijman and Yuan. ([326]), the cycles were produced by an open-source random cycle generator that created uncertainty to mimic actual driving situations. Table 4.5 displays the general data for these three cycles.

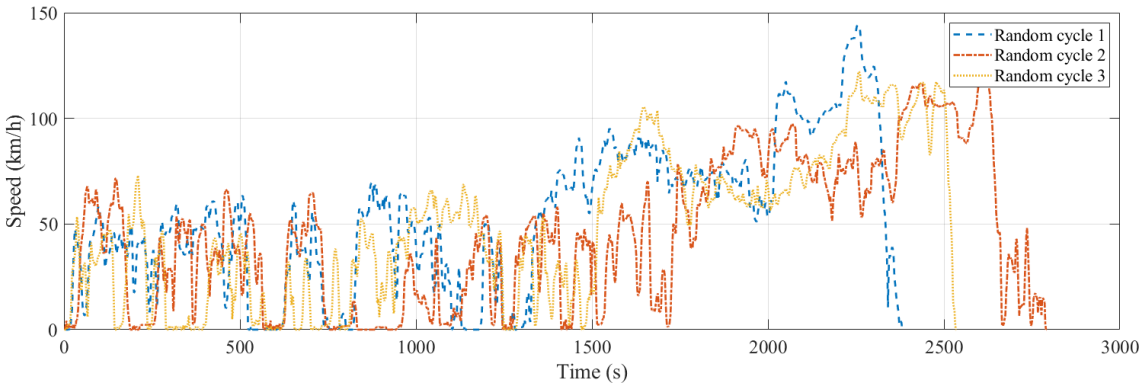

Fig. 4.4. Driving profiles of the three simulated real-world driving cycles

Table 4.5
Information about the three random driving cycles

Cycles	Infomation				
	Distribution	Distance	Cycle time	Max speed	Average speed
Cycle 1	Urban part	11.6	1404	60.0	35.2
	Rural part	13.3	648	89.9	73.6
	Motorway part	10.2	331	144.1	110.8
	Total	35.1	2383	144.1	58.2
Cycle 2	Urban part	13.0	1862	60.0	27.6
	Rural part	11.5	559	89.9	74.3
	Motorway part	10.6	370	127.0	103.3
	Total	35.2	2791	127.0	48.2
Cycle 3	Urban part	11.3	1557	59.9	29.9
	Rural part	11.7	586	89.9	71.6
	Motorway part	11.5	392	122.2	105.3
	Total	34.4	2535	122.2	53.0

4.3.6 Processor-in-the-loop (PiL) test

The PiL testing platform was constructed as shown in Fig. 3.2. Via an Ethernet connection, the host PC directly downloaded the digital model of the automobile to the LABCAR without using an ES910 controller. The algorithm was then loaded into a code compiler and added to the LABCAR controller unit for real-time validation. In order for the LABCAR to reflect the CAN connection in the vehicle, a CAN connection was established between the control unit and the vehicle platform. In the PiL test, real-time data transfer took place between the controller and the vehicle platform, and the vehicle's performance was ultimately captured in a data file.

4.4 | Results and discussion

4.4.1 Dynamics of particles during the optimisation process

The average movement ($\bar{P}_{\mathrm{mov}}$) and average distribution ($\bar{P}_{\mathrm{dis}}$) of the optimisation systems based on the suggested DAPSO algorithm and the traditional PSO method need to be examined in order to evaluate their dynamics. A comparison of the mobility and distribution of particles is demonstrated in Fig.4.5, respectively. Based on the optimisation under the UDDS condition, the outcomes are obtained. It can be demonstrated that by varying the inertia factor to obtain larger values of movement and distribution after the tenth iteration, the DAPSO particles are encouraged to explore. When threshold 1 is reached, the DAPSO optimises faster than the traditional PSO by employing a greater inertia factor value to follow the chaotic map and quickly converge to the best solution. After threshold 2 is enabled, the DAPSO has an 8.2% higher $\bar{P}_{\mathrm{dis}}$ and 5.17% higher value of $\bar{P}_{\mathrm{mov}}$ than the traditional PSO algorithm. The algorithm then moves to its exploitation step, till it terminates when threshold 1 is reached.

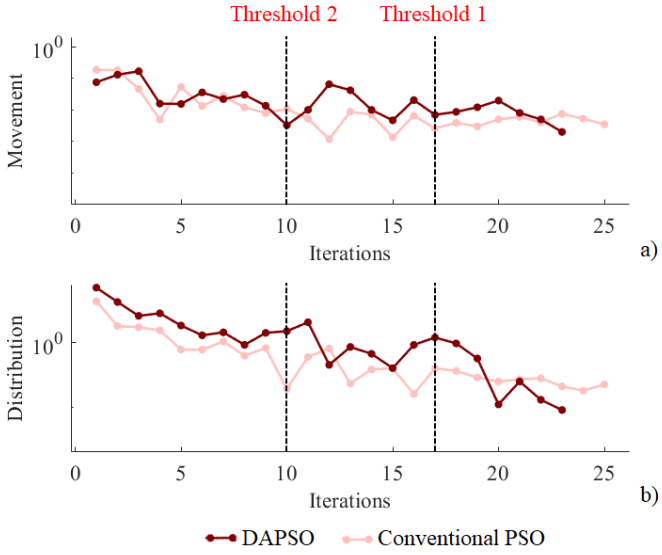

Fig. 4.5. Flowchart of the DAPSO

4.4.2 Local optimisation performance in learning cycles

Table 4.6 displays the optimisation outcomes from the local learning cycle, with the top optimisation outcomes highlighted. The objective function (specified in Eq.4.1) value used in Table 4.6 to assess the system optimality analyses the vehicle performance by taking into account two factors: 1) the difference between the final and goal SoCs; and 2) the rate of improvement in equivalent fuel consumption (EC). The optimality value will rise with improved vehicle performance. The second component of Eq.4.11 is used to calculate computing efficiency; the higher the computation efficiency, the faster the calculation. Table 4.6 compares the number of iterations required for convergence.

By simultaneously taking into account the DT system's optimality, computation efficiency, and success rate, the overall score, or S, indicates how well the system performed overall. The PSO4 produces the best optimality of 0.617 for the UDDS cycle and PSO3 takes the least amount of time—548.5 s; while DAPSO and PSO1 have the highest success rates—100%. The PSO1 has the most optimality for the highway driving cycle, but its success rate is only 40%. With the lowest average time consumption of 445.4 s, the DAPSO has the highest success rate of 90%. The DAPSO achieves the maximum optimisation (0.543), the lowest time consumption (412.7 s), and the highest success rate (80%) for the US06 cycle learning process.

The fourth section of Table 4.6 displays the results of the local optimisation for the NEDC cycle. Once more, the DAPSO has the highest success rate of 90%, the least average time consumption of 676.9 s, and the best optimality of 0.575. Table 4.6 displays the overall results for the DAPSO and PSO1-4. The DAPSO has the greatest overall scores, which are 0.864, 0.836, 0.906, and 0.890 for the UDDS, Highway, US06, and NEDC cycles, respectively.

4.4.3 Cross-validation in standard cycles

In order to examine global performance, the best local strategy found during each driving cycle is verified by the remaining three driving cycles following the local learning process. The optimal threshold values for SoC1, SoC2, and SoC3 under the highway cycle are, according to the cross-validation, 9.65%, 14.80%, and 16.02%, respectively. Fig. 4.6 compares the total scores attained in the validation and optimisation processes. Similar results are obtained in cycles of optimisation and validation for the techniques optimised

Table 4.6
Local learning results

Cycle	PSO type	Single scoring targets					Scores
		Optimality	Converged iteration	Time spent (s)	Computation efficiency	Success rate (%)	
UDDS	PSO1	0.606	50	989.5	0.77	100	0.745
	PSO2	0.586	36	724.6	1.10	65	0.730
	PSO3	0.610	27	548.5	1.32	65	0.797
	PSO4	0.617	47	947.7	0.82	80	0.713
	DAPSO	0.610	30	611.0	1.24	100	0.864
Highway	PSO1	0.506	50	650.9	1.43	40	0.709
	PSO2	-0.020	103	1343.8	0.82	70	0.369
	PSO3	-0.074	117	1533.7	0.65	60	0.275
	PSO4	0.349	77	1010.8	1.11	85	0.664
	DAPSO	0.419	34	445.4	1.61	90	0.836
US06	PSO1	0.497	50	662.8	1.58	65	0.806
	PSO2	0.485	117	1554.9	1.01	70	0.671
	PSO3	0.500	253	3364.6	-0.13	60	0.366
	PSO4	0.162	54	724.6	1.54	50	0.591
	DAPSO	0.543	31	412.7	1.74	80	0.906
NEDC	PSO1	0.019	50	866.7	1.37	40	0.453
	PSO2	0.392	59	1037.3	1.25	80	0.708
	PSO3	0.487	153	2653.8	0.08	65	0.426
	PSO4	0.111	55	969.5	1.30	80	0.580
	DAPSO	0.575	39	676.9	1.51	90	0.890

*The largest data is underlined

by the DAPSO and PSO1. To demonstrate the stability of the heatmaps, the average optimality is computed [using Eq.4.11] and shown in Table 4.7, where a SoC-corrected fuel consumption control is assessed. It is evident that the DAPSO stands out from its competitors by attaining the maximum optimality value (0.6180).

The performances (fuel consumption and battery SoC trajectory) of the PHEV optimised by DAPSO under the highway cycle are compared with the theoretical best performance (obtained by dynamic programming, DP) and the baseline rule-based method in order to illustrate the efficacy of the proposed approach. The findings (as displayed in Fig.4.7) demonstrate the effectiveness of the proposed DAPSO algorithm in optimising PHEV control performances. When compared to the rule-based method, fuel consumption is reduced by more than 11.4%. Using only 6% more fuel than the theoretical best performance, the DAPSO-optimised PHEV can maintain comparable SoC levels with DP outcomes (error within 0.63%).

Table 4.7
Average optimality of different EMS control settings by the five methods

PSO type	PSO1	PSO2	PSO3	PSO4	DAPSO
Optimality values	0.6004	0.5580	0.4983	0.5948	0.6180

4.4.4 Global performance in simulated real-world driving

In this part, three random driving cycles under simulated real-world driving situations were used to assess the robustness of the optimisation outcomes. Table 4.8 compares the outcomes of implementing EMSs with thresholds optimised by DAPSO based on cross-validation under standard cycles on a vehicle operating under random driving cycles. The PHEV's optimality calculations demonstrate the efficacy of the proposed DAPSO. As stated in Eq.4.1 and Eq.4.11, the optimality scores are determined by taking into account the fuel economy and the final SoC control, which shows the EMS performances that

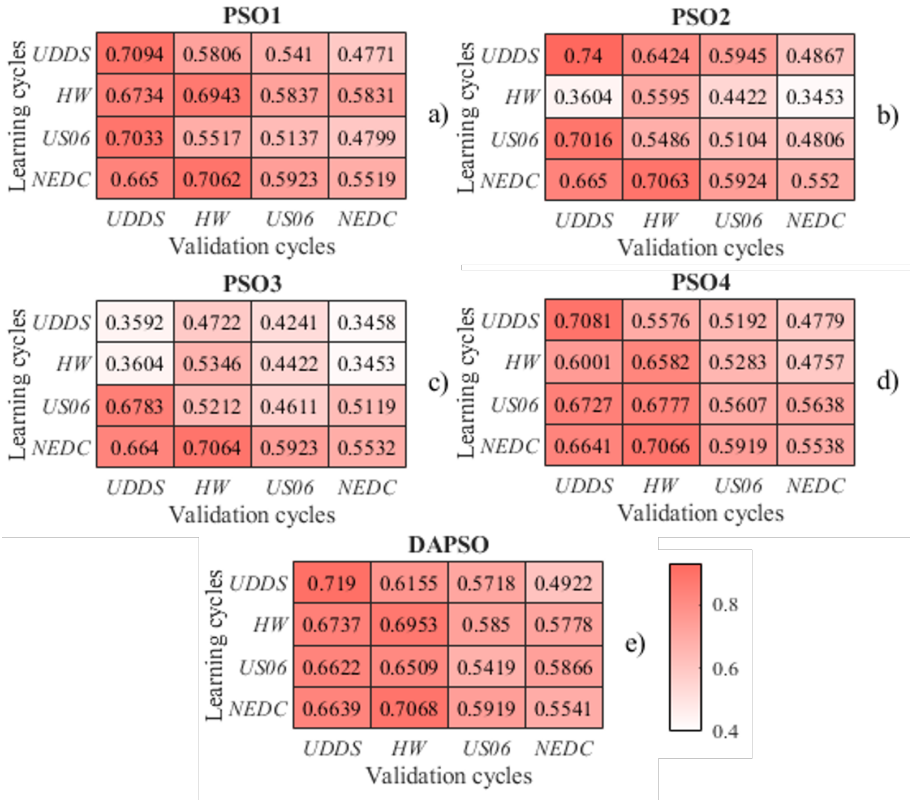

Fig. 4.6. Heatmap of optimality for the cross-validation results obtained: (a) PSO1; (b) PSO2; (c) PSO3; (d) PSO4; (e) DAPSO

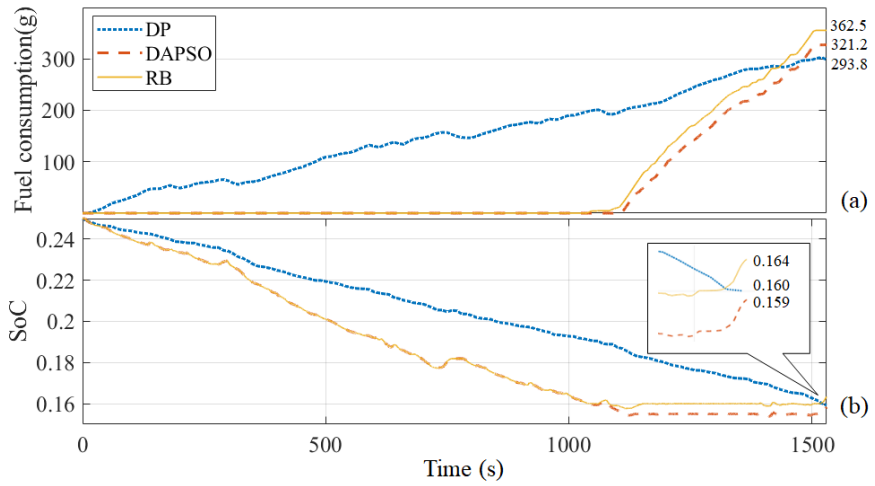

Fig. 4.7. Control performances under the highway cycle: (a) accumulated fuel consumptions; (b) SoC trajectories.

are refined by the DAPSO. The greatest average optimality value of any EMS optimised using the Highway cycle has been found with a value of 0.5954, which is 2.6% higher

than the average of the UDDS (0.5803), US06 (0.5537), and NEDC (0.5752) cycles. In ordinary driving conditions, the highway cycle-based DAPSO-generated EMS threshold settings are found to have the maximum level of robustness.

Real-time control capabilities were validated by PiL experiments and Fig.4.8 shows the vehicle's real-time performances under the three chosen driving cycles. For the charging-sustaining scenario for the car with high electricity use, the initial battery SoC was set at 16%. Since cycles 2 and 3 of the random driving process are kinder than cycle 1, the range extender's working circumstances are less taxing during these cycles, which led to slighter changes in their SoC (as illustrated in Fig.4.8(b)). It is also evident that the EMS keeps the battery voltage within a respectable range (4.5%) when the SoC dramatically declines in Fig.4.8 (b) over the 2000–2600 s interval. Figs.4.8 (c) and (d) show that, under most urban and rural driving situations, changes in SoC and voltage are moderate. This suggests that the battery functions best in mild conditions, which helps to slow down battery degradation [327].

Table 4.8
Global optimisation comparison

Optimality	DAPSO optimised thresholds			
	UDDS	Highway	US06	NEDC
Simulated real-world driving cycle 1	0.5723	0.5935	0.5556	0.5735
Simulated real-world driving cycle 2	0.5812	0.6001	0.5492	0.5794
Simulated real-world driving cycle 3	0.5875	0.5925	0.5562	0.5726
Average optimality score	0.5803	0.5954	0.5537	0.5752

4.5 | Chapter summary

To improve the optimality and reliability of the DT-based optimisation of a plug-in hybrid electric vehicle (PHEV) with rule-based control, a DAPSO method is presented in this chapter. In order to maximise the performance of the plug-in hybrid electric vehicle

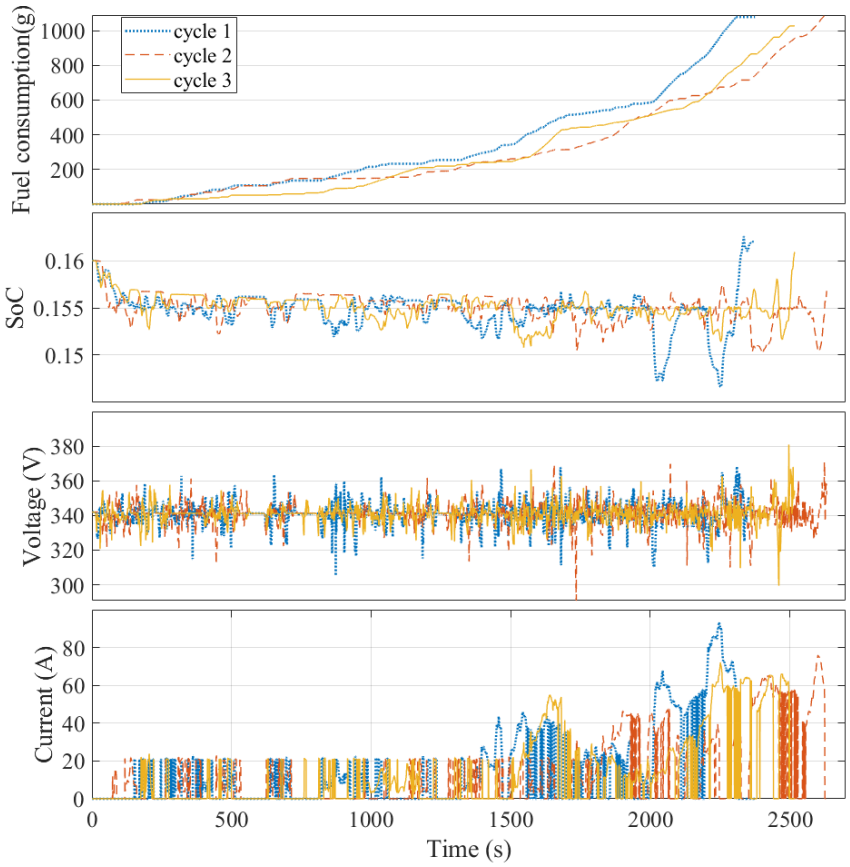

Fig. 4.8. PiL results for the three validation cycles: (a) fuel consumption of each cycle; (b) SoC level; (c) battery voltage variation; (d) current generation of range-extender

(PHEV) based on an objective function that assesses fuel usage and maintaining battery SoC, the DAPSO enhances the PSO algorithm with an adaptive swarm control method. Based on a thorough assessment of the system's optimality, computation efficiency, and success rate, an overall score (S) is defined for the DT system. The DAPSO algorithm determines the unified settings of the EMS through cross-validation testing under three worldwide driving circumstances. The DAPSO and traditional PSO algorithms' optimal control settings were used to monitor the performance of the plug-in hybrid electric vehicle (PHEV) during experimental assessments. The following is a summary of the study's conclusions:

1) The DAPSO algorithm can lead to up to 24% improvements in optimality over the PHEV's optimised by the baseline algorithms by encouraging more local searching for the

best threshold with an adaptive inertia factor controlled by observing the swarm's instant results. This suggests that the DAPSO has better performance in controlling the final SoC while saving fuel consumption.

2) The DAPSO can save up to 49.1% processing time over the baseline approaches by implementing a state machine that manages the exploitation-to-exploration ratio and the termination of the DT-based PHEV optimisation.

3) The EMS settings acquired under the highway cycle using the DAPSO can be the unified setting for the researched PHEV, according to the cross-validation testing of the simulated real-world driving. When comparing the EMS settings obtained under different driving cycles, greater optimality values (an indication measuring fuel consumption and final battery SoC level) of 4.5% can be attained.

Future study plans to employ the DAPSO for more DT-based PHEV optimisation problems, such as multiple objective optimisations of battery deterioration with instantaneous energy consumption. For DT-based PHEV optimisation tasks, the optimisation of PHEV equivalent consumption minimisation techniques and theoretical research on focused creation of alternative evolutionary algorithms, such as the bees algorithm, NSGA, will also be carried out. Additionally, research will be done on the application of the DAPSO for real-time control of automotive systems, such as energy management systems.

CHAPTER 5

Intelligent digital model of a battery and real-time status estimation

Modern transportation is moving towards the electrification of vehicles in order to reduce the dependence on fossil fuels. The focus of vehicle power sources has steadily shifted from engines to power batteries as electrification progresses. In order to improve the intricate energy management plans of highly electrified hybrid systems, it is essential to consider the health and functioning of batteries as a crucial component of powertrain product development. Because of their exceptional dynamic capabilities, lithium batteries are especially popular in the automotive sector [328]. A great deal of research has been done on digital modelling of lithium batteries [88]. especially for degradation problems [139], [159]. For two reasons, the state of health (SoH) of the battery is typically used to evaluate battery degradation: the rise in internal resistance and the loss of capacity [140]. Model-based and data-driven techniques are used in the regular assessment of battery ageing since the internal resistance cannot be evaluated directly. While machine learning may effectively accomplish the latter, the former is dependent on substantial empirical experiences [141].

This chapter mainly focuses on the research of digital models of multi-mode PHEVs' batteries and their ageing performance while in use. It aims to model and assess the ageing of batteries based on direct/indirect indications from charging and discharging

behaviours and data during operation, achieving evaluation and prediction. The main work is divided into three parts:

1) Workload 1: A double-layer battery identification system is built to assess end-of-life issues based on the battery's intuitive signal of the charging process. This method only addresses voltage and current battery performance when identifying the battery modelling parameters. The battery's performance data is then taken from the digital model and used as the input for battery cycle testing for assessment and learning in order to estimate and predict SoH.

2) Workload 2: In order to handle the SoC and SoH estimations during the battery discharge process, an asynchronous system of joint status estimation based on two long short-term memories (LSTM) is proposed. One LSTM continuously monitors the battery's performance in terms of current, voltage, and temperature in order to create an open-loop estimation for the SoC, while the other LSTM continuously tracks the incomplete voltage drop in order to create a closed-loop prediction using partial time series data up until the cut-off voltage. Both methods can be used to the dynamic battery real-time operating scenarios, and they solely address the voltage, current, and temperature performance of the battery.

3) Workload 3: A multi-kernel automatic relevance determination (ARD)-GPR frame for battery SoH estimation is proposed based on the battery performances mentioned above. Multiple indirect health indicators in the charging process are taken into account in accordance with real-world automotive scenarios, and by using Bayesian optimisation to help identify the ARD parameters, the degradation reasoning is concentrated to help improve designs and operational strategies, resulting in reduced environmental impact, enhanced performance, and cost savings.

To summarise, the accompanying graphic below shows the technical location (Fig.5.1) and pathways (Fig. 5.2) of the three modules in this chapter. This will be a graphic

summary of the tactics and techniques used in the various sections at the end of the chapter, offering a clear and succinct overview of the technical approaches discussed.

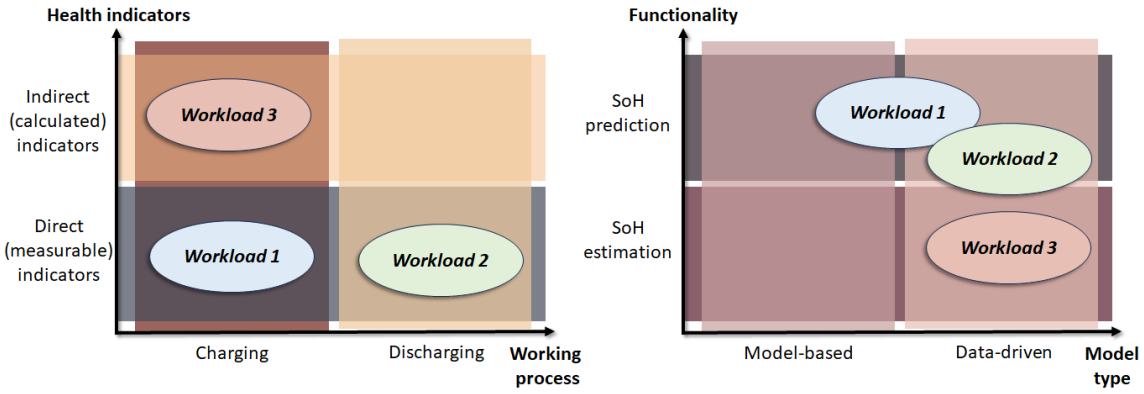

Fig. 5.1. Workloads' technical positioning

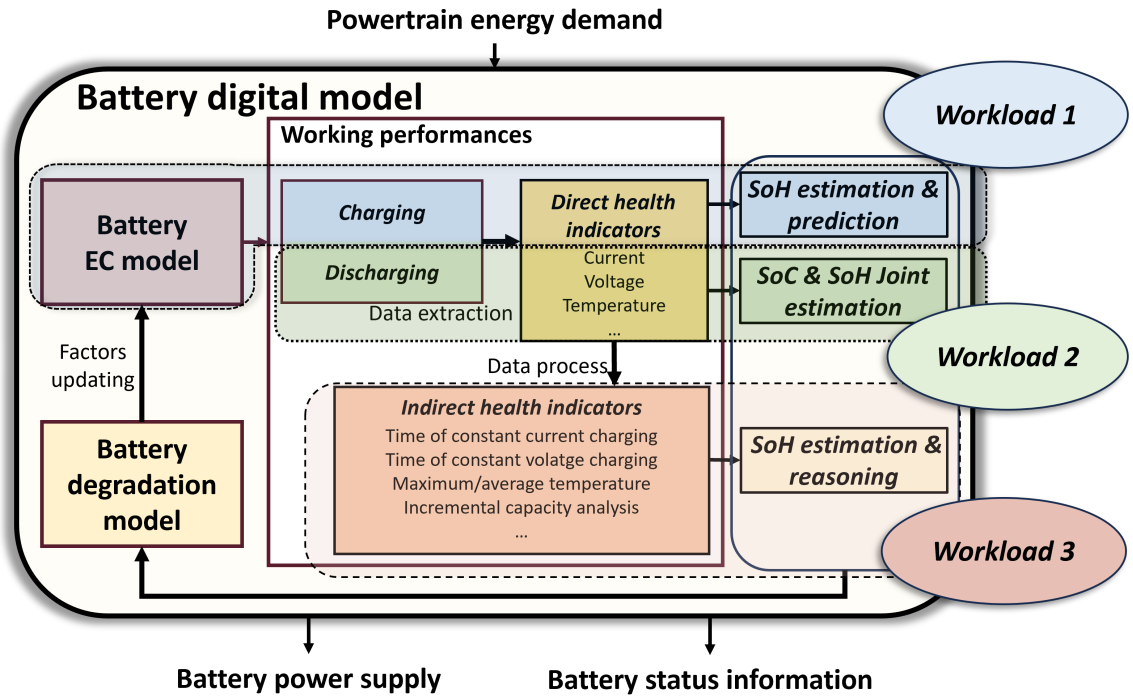

Fig. 5.2. Workloads' technical pathway

5.1 | Online double-layer system identification scheme

Digital models of batteries are constantly created from scratch for the intricate automobile engineering environment, necessitating a large computational resource. Then, additional data will be manually handled in the forecast process for the end-of-life issue. To meet this need, a double-layer battery identification system is built in this study. This method solely addresses the voltage and current performance of the battery for battery parameter identification (PI). Next, in order to anticipate SoH, the battery's performance data is acquired from the digital model and fed into a battery cycle test for assessment and learning.

5.1.1 The mechanism of the double-layer structure

This system is composed of two layers: the top layer and the bottom layer. A digital model of a battery with a PSO-based PI optimisation is found in the top layer. A battery SoH estimation model with a DCNN structure for real-time prediction resides in the lower layer. Fig.5.3 depicts the overall system architecture.

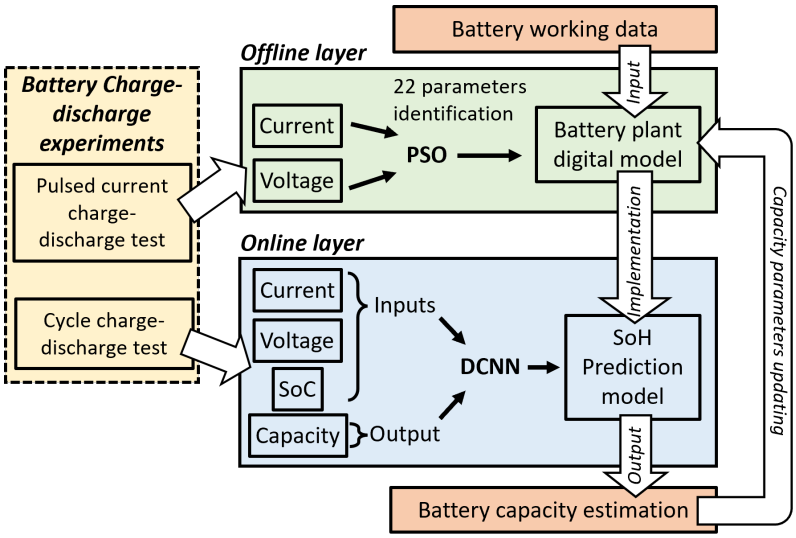

Fig. 5.3. The ODSI structure

The offline PI optimisation of a digital model of a battery

As in the general battery digital modelling introduced in section 3.3.2, the parameter identification for the 22 dimensions is a large-scale numerical problem. For its prominent ability to deal with large-dimension, nonlinear optimisation problems, the PSO is chosen to calibrate the model with the 22 parameters of the battery (as Eq.3.7). The digital model uses the recorded current data from the battery's pulse charge-discharge trials as input. The PI optimisation uses its associated voltage data as a comparison target. The PI optimisation can be expressed mathematically as follows:

$$
\begin{aligned}
&[\mathrm{X}_1, \mathrm{X}_2, \ldots \mathrm{X}_{22}] = \operatorname{argmin}\left(\mathrm{J}_{\mathrm{vlt}}\right) \\
&\text{s.t.} \left\{ \begin{array}{c} \mathrm{J}_{\mathrm{vlt}} = \sqrt{\frac{\sum_{\mathrm{i}=1}^{\mathrm{T}} \left(\mathrm{V}_{\mathrm{sim}} - \mathrm{V}_{\mathrm{ref}}\right)^2}{\mathrm{T}}} \\ \mathrm{X}_1 \in [0.5\mathrm{X}_{1\mathrm{ref}}, 1.5\mathrm{X}_{1\mathrm{ref}}] \\ \ldots \\ \mathrm{X}_{22} \in [0.5\mathrm{X}_{22\mathrm{ref}}, 1.5\mathrm{X}_{22\mathrm{ref}}] \end{array} \right\}
\end{aligned}
\tag{5.1}
$$

where the 22 numerical parameters in Eq. 5.1 are represented by $X_1, X_2, \ldots, X_{22}$. The J_{vlt} represents the root mean square error (RMSE) of the voltage V_{ref} reference data and the simulated voltage V_{sim}.The parameters for $X_{1\mathrm{ref}}, X_{2\mathrm{ref}}, \ldots, X_{22\mathrm{ref}}$ come from the reference for the mathematical model extraction of Li-ion batteries [298]. For every numerical parameter, the upper and lower bounds of the search spaces are empirically determined, with a 50% variance from the reference values. The PSO is employed with searching spaces to optimise the parameters in order to produce an accurate battery model with the lowest root mean square error (RMSE). Then, recalling the updating mechanism of the PSO algorithm (Eq. 4.4), x_k is a 20×22 matrix with 20 group sizes and 22 dimensions ($X_1, X_2, \ldots, X_{22}$ in this chapter), this matrix represents the positions of all individual particles at the k-th ($k = 1, 2, \ldots, j-1, j, \ldots$).

The online prediction of the battery SoH

Owing to the challenge of accurately measuring internal resistance, the SoH of capacity loss is the primary focus of this research. When a battery reaches a specific point in its capacity, such as 80%, it is deemed to be beyond its useful life. This section uses a deep convolutional neural network (DCNN) to evaluate and predict the battery's state of deterioration, drawing inspiration from recent studies [329]–[331].

The overall DCNN structure of the online prediction part is shown in Fig. 5.4, where the inputs are the battery's voltage, current, and Coulomb counting, which show the battery's state of charge. The output is the instantaneous capacity of the discharge phase, which shows the SoH of the battery. Mathematically, the inputs are expressed by a matrix as:

$$\text{Input} = \begin{bmatrix} I_1^k & V_1^k & C_1^k \\ I_2^k & V_2^k & C_2^k \\ \vdots & \vdots & \vdots \\ I_t^k & V_t^k & C_t^k \end{bmatrix}_{t\times 3} \tag{5.2}$$

where the tested current value, voltage value, and Coulomb counting value at the t-th in the k-th iteration of the charge-discharge test are, respectively, represented by the values I_t^k, V_t^k, and C_t^k. The matrix in this work has a size of $t \times 3$, where t represents the time steps for each iterative test (t=3500).

This DCNN, which is located in the right portion of Fig.5.4, is made up of two completely connected stages and three convolution stages. The input size is defined as 3500×3×1 by using Eq.5.2 from an earlier study [330]. The size of the first convolutional layer is 2×1, and there are 20 filters (kernels) in total. The stride has a padding of [0,0,1,1] and a size of 1×1. After that, the data is passed into a batch normalisation layer, which lowers the gradient vanishing and speeds up computation. A max-pooling layer

receives the processed data after the rectified linear unit (ReLU). In a comparable manner, there are 32 kernels in the second convolution stage and 40 kernels in the third with convolutional layers that share a 3×1 stride size. Then, there are 50 layers in the last two fully connected layers. Ultimately, the output is the single capacity value following a regression. These parameters are first established using the reference, and they are then empirically adjusted through a degree of experimental simulation in an effort to balance calculating speed and accuracy. The experimental data will be used to train this DCNN before it is integrated into an online application for battery SoH calculation.

The integration of two layers

Data is passed between the two layers with two subsections through an integration process. Feedback will be distributed for the purpose of updating the capacity parameter of battery's digital model, which will produce the voltage and state of charge data that the battery needs as inputs for the online layer. This closed-loop system uses data from longer time spans to forecast future capacity fluctuations based on the input of present requirements.

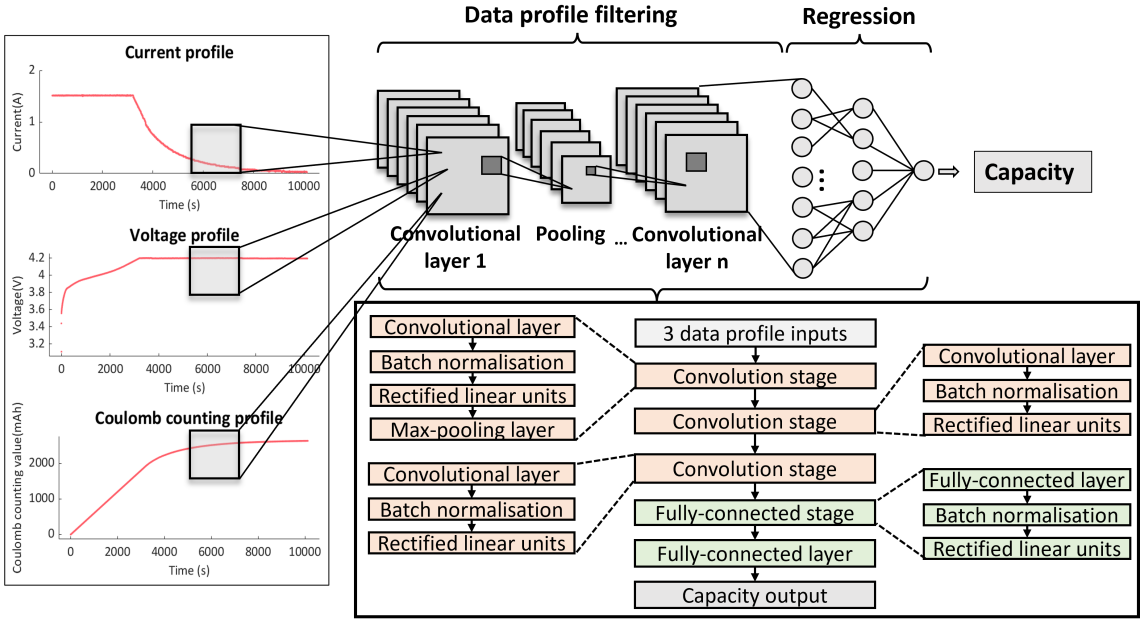

Fig. 5.4. The DCNN structure

5.1.2 Database implementation

The 18650 Li-ion battery database is selected for this section from the NASA database. [332] specifically B007, B0005, and B0006. There are two types of tests carried out in this database: the first is a standard charge-discharge cycle test involving charging the battery with a continuous current of 2 amps until it reaches the cut-off value of 4.2 volts, and then discharging it at a constant current of 2 amps until the voltage reaches 3.2 volts. The second is the battery undergoing a pulsed charge-discharge cycle test, in which it is discharged from 4.2V for 10 minutes at a pulse current of 1A, followed by a 20-minute rest period.

Among these tests, the battery digital plant model is developed using the pulsed charge-discharge data, while the DCNN for battery degradation evaluation and prediction is trained using the normal charge-discharge data. Ultimately, the information is utilised to verify the learning outcomes of the preceding two frameworks. The database is displayed as Table 5.1 in the following. These three experimental data (B0005, B0006, and B0007) are utilised to train the DCNN for the battery SoH estimation model. The data ratio, as shown in Table 5.2, represents the percentage of data used in neural network learning. The network is trained using three sets of data, each with a distinct data ratio. Ultimately, a cross-validation will be carried out to investigate the system's resilience. The system's prediction findings will be contrasted with experimental data on battery capacity loss by cutting the DCNN's training set.

Table 5.1
Data implementation usage

Data types	Usage
Pulsed charge-discharge	2-RC model training/validation
Regular charge-discharge	SoH estimation model training/validation

Table 5.2
Offline learning set-up for DCNN SoH estimation

Data ratio	Database		
0.5/ 0.6/ 0.7/ 0.8	B0005	B0006	B0007

Table 5.3
Cross-validation set-up for battery SoH estimation

B0005	B0006	B0007
Learning	Validation	Validation
Validation	Learning	Validation
Validation	Validation	Learning

5.1.3 Workload 1 results and discussion

Battery digital modelling

Fig.5.5 displays the voltage performance of the battery model in the pulsed discharge simulation following the PSO-optimised relative parameters. It is computed that the root-mean-square error (RMSE) is 0.0045. This is seen as a 2-RC model that can be used for the later merged platform.

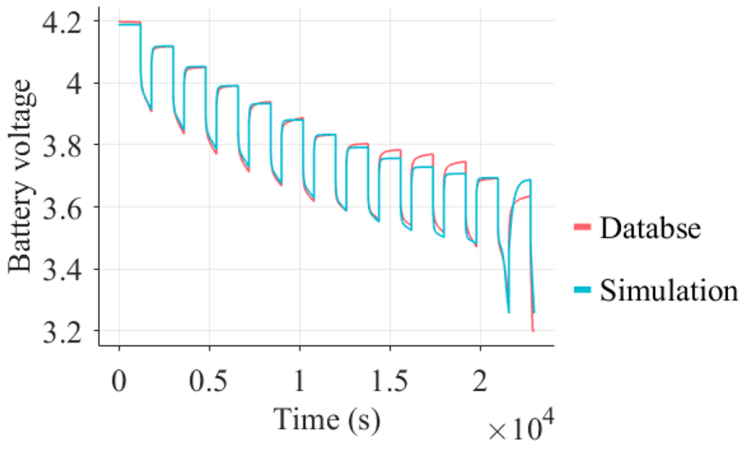

Fig. 5.5. Performance validation for battery modelling

Table 5.4
Learning result in RMSE

Data ratio	RMSE		
	B0005	B0006	B0007
0.5	0.0245	0.0210	0.0156
0.6	0.0166	0.0154	0.0133
0.7	0.0185	0.0151	0.0120
0.8	0.0121	0.0134	0.0115

Battery SoH estimation

The DCNN is primarily trained and tested in this section to produce an accurate result for the capacity estimation of the battery. The local learning outcomes for the DCNN in the proposed ODSI for each learning database (B0005, B0006, and B0007) are displayed in Fig. 5.6 a), b), and c). The results show that the B0005 database's local learning process exhibits the greatest variability in capacity loss estimation (5.6 a), and 5.6 b) and c) show comparable learning outcomes. The RMSE for the DCNN's learning results are displayed in Table 5.4. The biggest RMSE is found in the B0005 database. However, once the learning data ratio is bigger than 0.6, it rarely affects the performance of this DCNN in the B0006 and B0007 databases. The outcomes of the estimation were utilised to update the capacity variation value in the battery's digital model.

Model prediction for cross-validation

The created platform from each battery data set is used to cross-validate with each database following the local training. Figs.5.7 a), b), and c) shows the cross-validation findings. Three battery databases are used to pre-train the system (see sections 4.1 and 4.2), after which each database is compared for predictions. Fig.5.7 a) shows the validation of the pre-trained ODSI from B0005, B0006, and B0007 for the B0005 experimental database. It is possible to determine that there are differences between the B0005 experimental database and the three prediction outcomes. Two criteria are

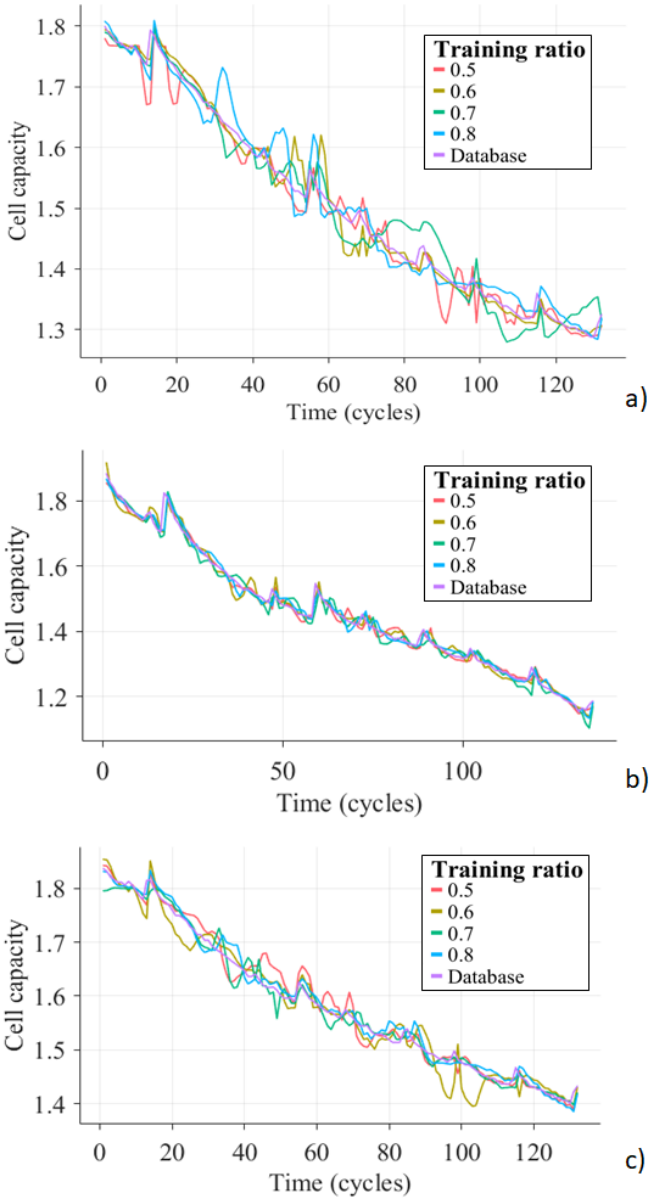

Fig. 5.6. The DCNN learning result for battery SoH estimation for B0007 validation data set

used to determine the reason: first, the dynamic training environment causes the 2-RC model's cumulative system error. Secondly, the training database of B0005 is thought to have more noise and less data than usual for training purposes. These could lead to low accuracy but high precision in subsequent forecast outcomes. The ODSI pre-trained by B0007 has the highest accuracy in predicting the decrease of battery capacity in

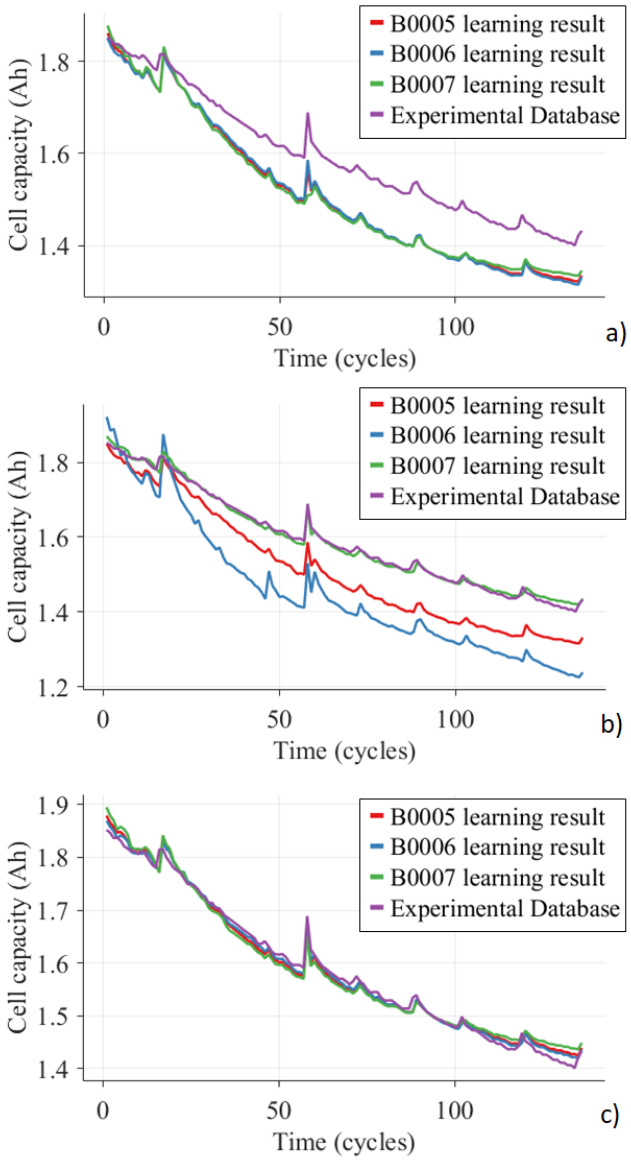

Fig. 5.7. The DCNN learning result for battery SoH estimation for cross-validation data set

Fig.5.7 b). The system that was pre-trained by B0005 yields mistakes at the middle stage, whereas the system that was pre-trained by B0006 has the most error. All of the systems that were pre-trained using the three experimental databases clearly forecast the loss of battery capacity (see Fig.5.7 c)). The database B0007 is thought to represent the most typical scenario involving battery deterioration and capacity loss. All things

considered, the ODSI platform demonstrates the capacity to forecast battery capacity decrease with just a current input.

5.1.4 Workload 1 summary

With experimental research based on cross-validation, this work provides an online double-layer system identification scheme for SoH estimation and prediction. The following conclusions can be drawn: 1. the battery can be modelled for real-time applications by introducing the proposed ODSI. The system's closed-loop method provides immediate feedback between the neural network and the 2-RC model, in contrast to the generic RC model that takes SoH into account. 2. The suggested system has an advantage over the pure neural network battery models in that it does not require starting from scratch with model training. Through direct support from the offline layer's 2-RC model, the online DCNN can reduce computation time while estimating health. 3. Furthermore, the instantaneous feedback between the two levels of this ODSI allows the system to predict a capacity loss for battery degradation even further by adding additional existing data to the system.

5.2 An asynchronous system of joint estimation

There are still difficulties with co-estimating battery state in real-time applications with complicated working conditions. A model-based technique can respond quickly for battery co-estimation, but it is inaccurate because capacity fluctuates constantly. While data-driven approaches can provide accurate estimation results, they are not appropriate for online applications since they are always restricted to a single prediction objective with fixed parameters and require a well-prepared database in order to be trained beforehand. In order to address both the SoC and the SoH estimation, an asynchronous system of joint battery status estimation based on two long short-term memories (LSTM) is proposed in this section. One LSTM continuously monitors the battery's performance in terms of

current, voltage, and temperature in order to make an open-loop prediction for the SoC; while the other LSTM continuously monitors the incomplete voltage drop in order to make a closed-loop prediction using partial time series data up until the cut-off voltage. Both methods can be used with the dynamic battery operating settings as the real time scenario, and they solely address the voltage, current, and temperature performance of the battery.

5.2.1 Frame statement of the joint estimation

A full-time LSTM and a partial-time LSTM make up the framework of this system, as shown in Fig.5.8. In order to determine the current SoC level, the previous LSTM continuously records all battery electrical performances. The later LSTM just keeps track of the battery's partial performance during the discharging phase; if the procedure isn't completed, forecasts are generated. After analysing the data using a time evaluation, the capacity is determined using a relative time ratio.

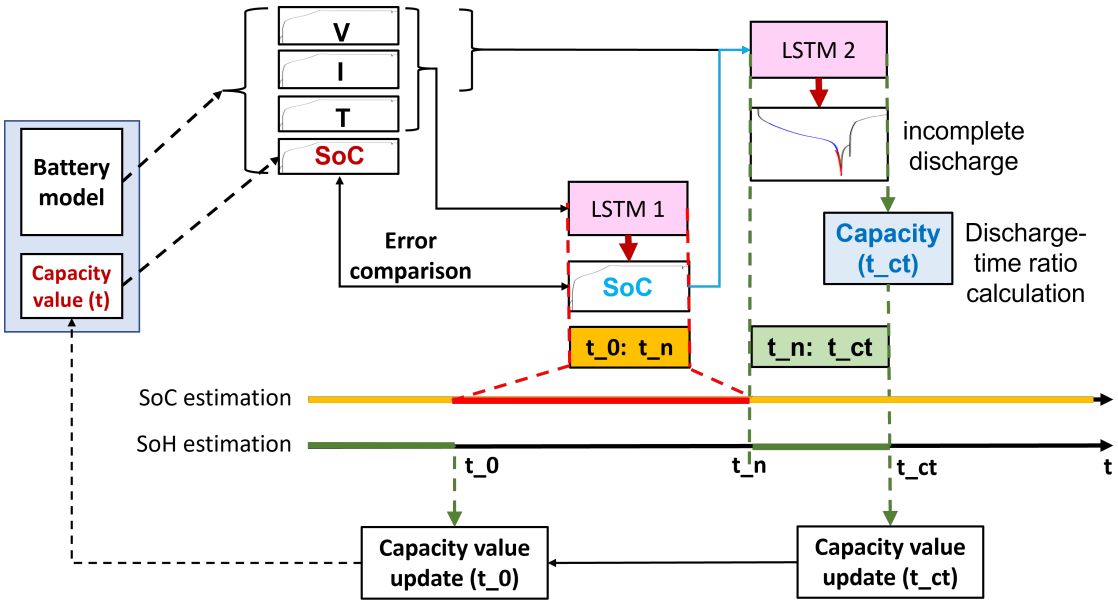

Fig. 5.8. Frame of the asynchronous LSTM system

Long short-term memory

The long short-term memory (LSTM) was first developed by Hochreiter et al. to solve the information decay during the algorithm back-propagation through time (BPTT). Most gradient-based learning algorithms, such as conventional recurrent neural networks (RNN), suffer either gradient vanishing or gradient explosion when the information is transferred by the backflow through a long time period. To overcome the time dependence problem, the LSTM is proposed with a cell state (memory cell), a hidden state, a forget gate layer, an input gate layer and an output gate layer, as Fig. 5.9 shows below.

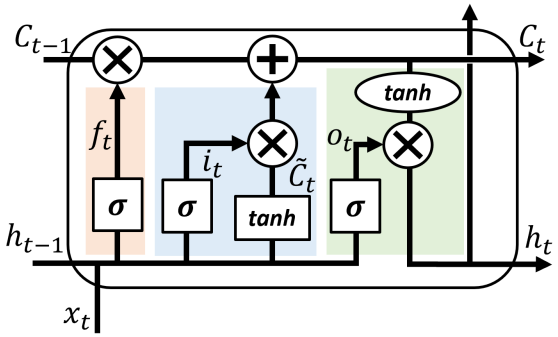

Fig. 5.9. The structure of the LSTM

In the standard LSTM structure, the forget gate (orange part) is defined as

$$f_t = \sigma\left(W_f \cdot [h_{t-1}, x_t] + b_f\right) \tag{5.3}$$

where σ is the sigmoid function which decides if the information need to be transferred; W_f is the weighting factor during the data transfer; h_{t-1} is the hidden state at the t-1 step; x_t is the instant input at the t step; finally, b_f is the bias in this process. Then the input gate layer i_t with a candidate memory cell $\tilde{C}_t$ is indicated by the blue part, which is defined as

$$\left.\begin{aligned} i_t &= \sigma\left(W_i \cdot [h_{t-1}, x_t] + b_i\right) \\ \tilde{C}_t &= \tanh\left(W_c \cdot [h_{t-1}, x_t] + b_c\right) \end{aligned}\right\} \tag{5.4}$$

where W_i is the weighting factor and is the bias for the instant input and the last hidden state. W_c and b_c are the weighting factors and bias for the candidate memory cell calculation. The green part shows the output gate layer o_t, it is expressed as

$$\left.\begin{aligned} o_t &= \sigma\left(W_o \cdot [h_{t-1}, x_t] + b_o\right) \\ h_t &= o_t \cdot \tanh\left(C_t\right) \end{aligned}\right\} \tag{5.5}$$

where W_o and b_o are the weighting factor and the bias for the output, respectively; h_t is the hidden state at the t step, which is calculated by the output o_t and the memory cell C_t; C_t is demonstrated as

$$C_t = f_t \cdot C_{t-1} + i_t \cdot \tilde{C}_t \tag{5.6}$$

where in this mechanism, the memory cell C_{t-1} in the last time step is updated to C_t. This is designed to mitigate the gradient vanishing and capture the information during a long time period.

The full-time LSTM for SoC estimation

The immediate SoC is the output of the LSTM 1, and its inputs in Fig. 5.9 are the battery's temperature (T), voltage (I), and current (V). The inputs are mathematically described by a matrix as follows:

$$\text{Input } 1 = \begin{bmatrix} I_{t_0} & V_{t_0} & T_{t_0} \\ I_{t_0+1} & V_{t_0+1} & T_{t_0+1} \\ \vdots & \vdots & \vdots \\ I_{t_n} & V_{t_n} & T_{t_n} \end{bmatrix}_{(t_n - t_0)\times 3} \tag{5.7}$$

where, depending on the battery's charge-discharge activities, the V, T, and C are the current, voltage, and temperature values at the th during the interval from v_0 to v_U (the red line in Fig. 5.9). The matrix has a size of $(t_n - t_0) \times 3$, and the $t_n - t_0$ can be seen

as a time window that starts at any point during the LSTM 1 estimation. The instant SoC value SoC_t, as predicted by the LSTM based on the inputs, is the output.

The LSTM 1's construction is depicted in Fig.5.10. It is made up of three LSTM layers, three dropout layers, and a fully linked layer. By referring to the earlier research [330] and using Eq. 5.6, the input size is defined as $t \times 3 \times 1$. There are 80, 60, and 40 hidden units in each of the three LSTM layers. According to earlier studies, a dropout layer comes after each LSTM layer to avoid over-fitting [333]. After that, the data is put into a 40-unit layer that is entirely connected. The instantaneous SoC level is the output in this frame after the result data has been generated and output in a single channel.

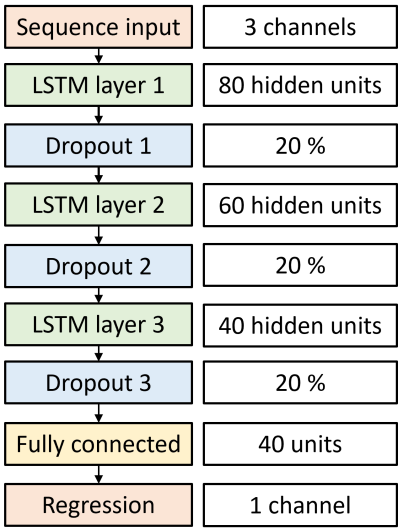

Fig. 5.10. The structure of the LSTMs

The partial-time LSTM for SoH estimation

A role for the incomplete discharge prediction is played by the LSTM 2 in Fig.5.8. Motivated by study [334], there exists a strong correlation between the capacity fluctuation and the battery's discharge duration from the high voltage to the cut-off voltage. The LSTM can be used to anticipate incomplete discharging cycles up until the voltage approaches the cut-off voltage, according to research by Qu et al [335].

The LSTM 2 is used to forecast the partial discharge process and provide an immediate capacity value for the battery's parameter update. The LSTM 2 input is displayed as

$$\text{Input } 2 = \begin{bmatrix} I_{t_0+1} & V_{t_0+1} & SoC_{t_0+1} \\ I_{t_0+2} & V_{t_0+2} & SoC_{t_0+2} \\ \vdots & \vdots & \vdots \\ I_{t_n} & V_{t_n} & SoC_{t_n} \end{bmatrix}_{(t_n-(t_0+1))\times 3} \tag{5.8}$$

where the SoC value, voltage, and current are represented by the letters SoC_t, V_t, and I_t. In the last time step, LSTM 1 predicts the SoC value. The input of LSTM 2 is received one time step after that of the LSTM 1, and LSTM 2 updates its status till the time reaches the t_n. Next, the closed-loop prediction begins with the outcome at t_n, indicating that each input at t is the output of $t-1$ step. Only the data from the most recent time step is taken into account by the LSTM 2, and the iterative prediction process won't stop until the cut-off voltage is achieved. Subsequently, the closed-loop prediction calculation time is evaluated, yielding a ratio between the initial discharge time and the iterative prediction time. The instant capacity value is thereafter determined by applying this ratio.

The asynchronous co-estimation

As stated in the previous introduction, the system as a whole is an asynchronous co-estimation framework. As the yellow line in Fig.5.8 illustrates, the SoC estimation in LSTM 1 is a full-time procedure that uses an open-loop prediction of the SoC value based on instantaneous battery performances of current, voltage, and temperature. When calculating capacity for a SoH estimate, a partial time procedure is employed. First, the time window is utilised to update the LSTM 2's status. The LSTM 2 then makes a closed-loop prediction for any incomplete discharging process up until the cut-off

voltage is acquired. The entire frame operates in an asynchronous manner, and versatile applications allow for the customisation of the time frames.

5.2.2 The training and validation of the frame

In this section, the NASA database is also utilised. Three numbers in the set—B0005, B0006, and B0007—have been selected to obtain data-driven learning. A standard charge-discharge cycle test involves charging the battery at a continuous current (2A) until it reaches a cut-off value of 4.2 V, then discharging it at a current of 2 A until the voltage drops to 3.2 V, as per the tests in this database. Of these, the charge-discharge data is initially used to create the LSTM 1 for the instantaneous SoC estimation; these three experimental databases (B0005, B0006, and B0007) are used to train the network for the battery SoC estimation. The network trained by one set is then tested by the remaining two sets in a cross-validation process, as shown in Table 5.5, to assess the resilience. Next, the LSTM 2 is trained for the online battery degradation assessment using the data from frequent charge-discharge cycles and capacity variations. Test and analysis are done on the time window spans for the LSTM 2 to obtain the closed-loop prediction of the incomplete discharging process (Table 5.6). After analysing the data, the most suitable time window length will be selected and applied to the entire frame going forward. Ultimately, a cross-validation will be carried out to investigate the system's resilience. The asynchronous system only implements temperature, current, and voltage. The LSTM 1 then provides the estimated SoC and serves as the input for the LSTM 2, which generates capacity fluctuations at different stages. After that, the outcome will be contrasted with a traditional ANN.

Table 5.5
Cross-validation set-up for LSTM 1 based on the open-loop prediction

B0005	B0006	B0007
Learning	Validation	Validation
Validation	Learning	Validation
Validation	Validation	Learning

Table 5.6
Span of time window analysis for LSTM 2 based on the closed-loop prediction

Time window	Database		
8% 16% 24% ... 96%	B0005	B0006	B0007

5.2.3 Workload 2 results and discussion

Full time SoC estimation

Fig.5.11 displays the performance of the SoC estimation for the battery based on the open-loop calculation contrasted with the experimental result in a single charging-discharging procedure after the relevant parameters were adjusted. The learning and validation results for the various test sets are displayed in Table 5.7. The database being used to train the LSTM 1 is the first column in Table 5.7, which is used to calculate the root-mean-square error (RMSE). The other two data sets serve as validation. An average error of 0.0694 is found in the B0005 and B0006 data sets for both of the outcomes from the LSTMs trained on these data sets; however, in the database B0007, this error increased to an average value of 0.0979. Because the fluctuation in the data is harsher in the B0007, the validation RMSEs of the LSTM based on the B0005 and B0006 are greater with 0.0852 and 0.0789, respectively, when the B0007 is employed to train the LSTM.

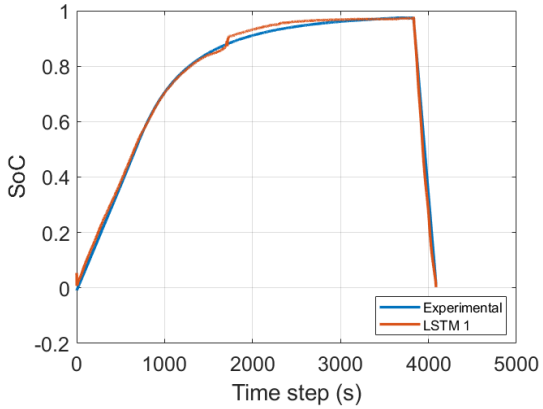

Fig. 5.11. The performance of the SoC estimation for the LSTM 1

Partial time SoH estimation

The time window size, or time span, is examined to assess the network's performance in order to train the LSTM 2 for online SoH estimation. The original experimental discharge time and the predicted findings for each time frame are compared in Fig. 5.12. The average RMSEs in Table 5.8 represent the discrepancy between the time estimated by LSTM 2 and an incomplete discharging procedure. Table 5.8 illustrates that the average RMSE increases as the time window increases. First, when the time window is set to 100 seconds (i.e. 40% of the total data length for the experimental discharge procedure), the RMSE reaches its maximum value of 0.1248. Subsequently, the RMSE decreases when the time span is larger.

Table 5.7
Learning and cross-validation result of LTSM 1

RMSE			
	B0005	B0006	B0007
B0005	0.0702*	0.0821	0.1052
B0006	0.0602	0.0651*	0.0906
B0007	0.0852	0.0789	0.0640*

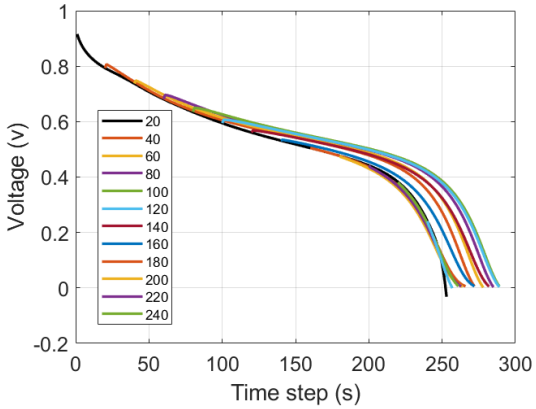

Fig. 5.12. The prediction of incomplete discharging of the LSTM 2

Table 5.8
Learning and cross-validation result of LTSM 2

RMSE of variable time span												
Span percent (%)	8%	16%	24%	32%	40%	48%	56%	64%	72%	80%	88%	96%
Time window (s)	20	40	60	80	100	120	140	160	180	200	220	240
Average RMSE (%)	6.57	8.65	11.07	12.46	12.48	10.03	6.58	4.50	3.81	3.46	2.77	1.38

Dynamic battery joint-estimation

The pre-trained parameters with the highest accuracy in battery SoC estimation are applied in the asynchronous system following the independent trainings for both the LSTM 1 and LSTM 2. Next, the real time input for this asynchronous system is applied to the database including the current, voltage, and temperature. 0.008 is the average relative error between the experimental data and the SoH estimation for each charging-discharging cycle. The asynchronous system, in short, demonstrates the ability to jointly estimate in real time simulation. All that is required to estimate the SoC and SoH is temperature, voltage, and current.

5.2.4 Workload 2 summary

In this section, a novel asynchronous system for SoC-SoH co-estimation based on the LSTM frame is presented, along with an experimental analysis using cross-validation. The following conclusions can be drawn: 1. With the introduction of this asynchronous system, real-time applications can predict and monitor the battery only while discharging, which allows for flexibility in response to the demands of online applications. 2. Real-time data can be directly applied to the SoC estimation with notable accuracy thanks to LSTM 1's open-loop prediction. In order to save computing resources, an additional battery model is not required. In addition, the LSTM 2 is utilised to forecast the possible duration required for the battery to completely discharge to the cut-off voltage by focusing on the incomplete charging-discharging process, then the SoH can be estimated easily through the correlation. For real time applications where uncertainties arise while driving, this is more adaptable and reliable.

5.3 The multi-kernel ARD-GPR frame

This section concentrates on GPR techniques for battery SoH estimation that are based on the automatic relevance determination (ARD) mechanism. Several health indicators throughout the charging process are taken into account based on real-world automotive circumstances. In order to embrace the dynamic conditions of the battery's SoH estimation, the Bayesian optimisation is employed to iteratively optimise the ARD length distribution.

This section includes several contributions of the battery's modelling and SoH estimation. First, using a selection of health indicator (HI) inputs from an open-source database with various temporal horizons, four kernel functions with their ARD frame are tested. In order to reveal the mechanism underlying the battery fading process, the relative parameters are investigated. Second, the deterioration of two different kinds of lithium battery cells

is examined, and the results are gathered in less than a hundred days. This database is then used for the construction and validation of the model.

Ultimately, a multi-kernel GPR frame based on automated relevance determination (ARD) is suggested to handle dynamic working conditions that resemble real-world automobile applications. The suggested framework is verified using various battery kinds and instantaneous temperatures to replicate the charging process in any given amount of time under actual driving circumstances.

5.3.1 Battery performance analysis

In this section, to accommodate the practical vehicle application, since the discharging process is random and arbitrary in the charging-depleting stage of the vehicle, [336] the HIs are extracted from the charging process. A set of typical battery charging direct performances is shown in Fig.5.13, where the constant current charging process (CC), constant voltage charging process (CV) and relative temperature are demonstrated. Those signals can be directly monitored and recorded for a later numerical operation. Also, the increment capacity (IC) curve is another significant factor in battery health condition, it is based on the differentiation of the battery capacity over the battery voltage, for a full or a partial cycle regarding the experimental conditions [337]. A set of curves of B0005 database is shown as Fig. 5.14, where the ICP values are compared against the voltages in the figure.

5.3.2 Health indicators extraction and data pre-process

Based on existing research, [338] the HIs are classified as measured health features and calculated health features. The former typically consists of signals for voltage variation, current variation, temperature variation, and time performance. Those signals can be directly monitored and measured during the battery's real time performances [339]–[346]; while the calculated health features are often generated by the first or second differential

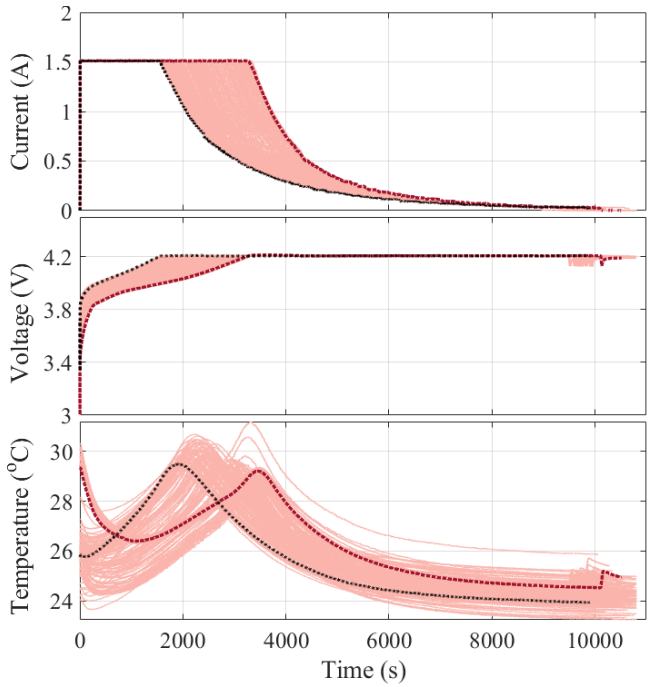

Fig. 5.13. Battery performances in iterative charging process

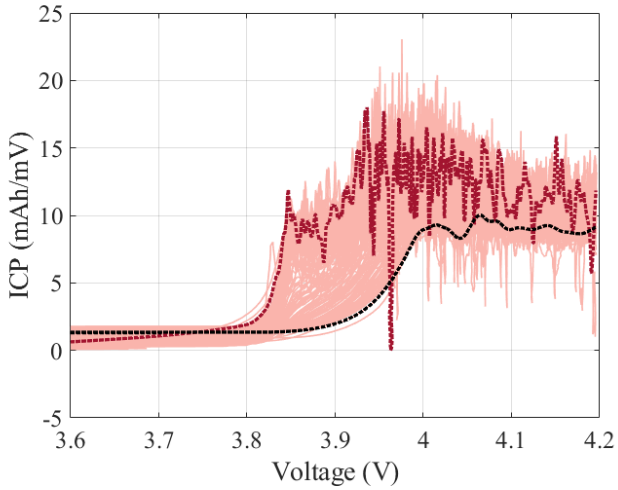

Fig. 5.14. IC curves in iterative charging process

of signals with respect to different targets, where the potential changing is analysed [347]–[350]. Inspired by existing research [338], [351]–[353], five HIs are selected as: 1.time of constant current charge process (TCCC) ; 2. time of constant voltage charge process (TCVC); 3. incremental capacity peak value (ICP); 4. maximum temperature

Table 5.9
Health indicators being analysed

HIs	Property	Classification
HI1	TCCC	Direct measurable features
HI2	TCVC	Direct measurable features
HI3	ICP	Calculated features
HI4	MAT	Direct measurable features
HI5	MATL	Direct measurable features

(MAT); and 5. maximum temperature location (MATL). The HIs are summarised in Table 5.9

Then, to avoid distortion of the analysis results due to abnormal data, pre-processing is necessary to exterminate unsuitable data for the following applications. In this section, data with any of the following issues will be deemed erroneous and removed from the database: 1. scarce data with discontinuity causes calculation singularity; 2. data that surpasses algorithms' limits and constraints; 3. data with severe fluctuations which cause extreme derivation conditions. The data has also been normalised to improve the training performances.

5.3.3 Mechanism of GPR and Bayesian optimisation

Due to the advantages of practical and flexible qualities for creating models without specific functional forms, the GPR technique has been widely used in statistics and machine learning. The GPR describes the regression function using the probabilistic technique to quantify uncertainties. This section presents a general formulation of GPR, its kernel functions and ARD modifications.

The standard GPR

Gaussian process regression (GPR) is widely applied to non-parametric regression modelling. A GPR first confirms a priori based on obtained data, then through a Bayesian inference process, a posterior probability can be defined for data distributions [354]. Its

general formulation of GP is denoted by

$$f(\mathbf{x}) \sim GP\left(m(\mathbf{x}), \mathbf{K}\left(\mathbf{x}, \mathbf{x}^*\right)\right). \tag{5.9}$$

where $m(\mathbf{x})$ indicates the mean functions of the obtained data distribution; $\mathbf{K}\left(\mathbf{x}, \mathbf{x}^*\right)$ is the kernel function (as known as covariance function) between the obtained set $\mathbf{x}$ and the set to be predicted $\mathbf{x}^*$. Specifically,

$$m(\mathbf{x}) = \mathbb{E}[f(\mathbf{x})] \tag{5.10}$$

$$\mathbf{K}\left(\mathbf{x}, \mathbf{x}^*\right) = \mathbb{E}\left[\left(f(\mathbf{x}) - m(\mathbf{x})\right)\left(f\left(\mathbf{x}^*\right) - m\left(\mathbf{x}^*\right)\right)^T\right] \tag{5.11}$$

By considering practical scenarios, the observed data are often expressed with an implicit formulation:

$$\mathbf{y} = f(\mathbf{x}) + \epsilon \tag{5.12}$$

where $\mathbf{y}$ is the observed vector $\mathbf{y} = [y_1, y_2, ...]$; ϵ is an artificial noise which obeys a Gaussian distribution $\epsilon \sim N\left(0, \sigma_n^2\right)$. This yields

$$\mathbf{y} \sim N\left(0, \mathbf{K}(\mathbf{x}, \mathbf{x}) + \sigma^2\mathbf{I}\right) \tag{5.13}$$

where $\mathbf{I}$ is an unit matrix and $\sigma^2\mathbf{I}$ represents the noise covariance matrix. It is worth mentioning that they are the same dimension with $\mathbf{K}(\mathbf{x}, \mathbf{x})$. Also, it is commonly defined as $m(\mathbf{x}) = 0$. Now assume a training set $\{\mathbf{x}, \mathbf{y}\}$ from a certain domian $\mathbf{D}$ is observed. Furthermore, a test set $\mathbf{x}^*$ and its corresponding function output $\mathbf{y}^*$ (values to be predicted) are defined. Then, their joint distribution can be denoted by further yielding Eq.5.13 as

$$\begin{bmatrix} \mathbf{y} \\ \mathbf{y}^* \end{bmatrix} \sim \mathcal{N}\left(0, \begin{bmatrix} \mathbf{K}(\mathbf{x},\mathbf{x}) + \sigma^2\mathbf{I} & \mathbf{K}(\mathbf{x},\mathbf{x}^*) \\ \mathbf{K}(\mathbf{x},\mathbf{x}^*)^T & \mathbf{K}(\mathbf{x}^*,\mathbf{x}^*) \end{bmatrix}\right) \tag{5.14}$$

Then the predictions can be made by considering the posterior (also known as a conditional distribution) as

$$p\left(\mathbf{y}^* \mid \mathbf{x}^*, \mathbf{x}, \mathbf{y}\right) = \mathcal{N}\left(\mathbf{y}^* \mid \mathbf{m}^*, \boldsymbol{\Sigma}^*\right) \tag{5.15}$$

with

$$\mathbf{m}^* = \mathbf{K}\left(\mathbf{x},\mathbf{x}^*\right)^T \mathbf{K}\left(\mathbf{x},\mathbf{x}^*\right)^{-1} \mathbf{y} \tag{5.16}$$

$$\boldsymbol{\Sigma}^* = \mathbf{K}\left(\mathbf{x}^*,\mathbf{x}^*\right) - \mathbf{K}\left(\mathbf{x},\mathbf{x}^*\right)^T \mathbf{K}\left(\mathbf{x},\mathbf{x}^*\right)^{-1} \mathbf{K}\left(\mathbf{x},\mathbf{x}^*\right) \tag{5.17}$$

where $\mathbf{m}^*$ is estimation mean and Σ^* is estimation covariance.

Kernel functions and ARD formulation

The kernel function is employed in GPR to describe the covariance between pairs of input data points. The assumptions made about the data's underlying structure are based on the kernel function selected, and this decision can significantly affect GPR performance. In this section, four types of kernel functions are applied according to suggestions [355], [356] and their mechanisms are introduced in the following: the first is the squared-exponential (SE) function, which is also known as the radial basis function kernel or the Gaussian kernel. [354] Its general formulation is given as

$$\mathbf{K}_{SE}\left(x, x^* \mid \theta\right) = \sigma_f^2 \exp\left(-\frac{1}{2}\frac{r^2}{\sigma_l^2}\right) \tag{5.18}$$

where θ is the set of kernel parameters, where $\theta = [\sigma_f, \sigma_l]$; σ_f is the signal standard deviation and σ_l is the characteristic length scale; r is the kernel distance between x and x^*, specifically

$$r = \sqrt{(x - x^*)^T (x - x^*)} \tag{5.19}$$

The second kernel function applied is Matérn covariance function, which is recommended because it offers a versatile method to represent spatial dependency that may capture various degrees of smoothness in the underlying process. In contrast to the SE kernel, it does not experience the concentration of measure problem for high-dimensional inputs. Specifically, the alternatives of the Matérn kernel are applied as Matérn 3/2 (M32) and Matérn 5/2 (M52). Matérn 3/2 is expressed as

$$\mathbf{K}_{M32}\left(x, x^* \mid \theta\right) = \sigma_f^2 \left(1 + \frac{\sqrt{3}r}{\sigma_l}\right) \exp\left(-\frac{\sqrt{3}r}{\sigma_l}\right) \tag{5.20}$$

The Matérn 5/2 is denoted by

$$\mathbf{K}_{M52}\left(x, x^*\right) = \sigma_f^2 \left(1 + \frac{\sqrt{5}r}{\sigma_l} + \frac{5r^2}{3\sigma_l^2}\right) \exp\left(-\frac{\sqrt{5}r}{\sigma_l}\right) \tag{5.21}$$

The last function is the rational quadratic (RQ) kernel , which is defined as

$$\mathbf{K}_{RQ}\left(x, x^* \mid \theta\right) = \sigma_f^2 \left(1 + \frac{r^2}{2\alpha\sigma_l^2}\right)^{-\alpha}, \tag{5.22}$$

where σ_l is the characteristic length scale; α is a positive-valued scale-mixture parameter. From the parameters introduced above, the length scale can be further defined as a vector σ_{l_i} for each predictor i, where i = 1, 2,...,d (according to the dimension of inputs). The built-in kernel (covariance) functions, each with its own length scale, provide automated relevance determination (ARD). In contrast, the original GPR kernels with the same length-scale parameters are named isotropic (ISO) kernels. The ARD can be used to determine the correlating length scales in a covariance function, for battery applications, it is used to capture the underlying mapping among different variables, i.e. instant

voltage, operation temperature, and capacity. To this end, the Euclidean distance of the original kernels is upgraded to higher dimensions, and the distances defined in the Hilbert space are expressed by the norm formulation as

$$r = \sqrt{\sum_{i=1}^{d} \frac{\left(x_i - x_i^*\right)^2}{\sigma_{l_i}^2}} \tag{5.23}$$

Conventionally, the last step is the hyperparameters identification, for computation efficiency and practicality, the Type-II maximum likelihood estimation (MLE) is often applied [357] with general default settings. In this section, for accurately monitoring and estimating the battery's behaviours, in later sections Bayesian optimisation will be applied to optimally obtain the best compromises of the hyperparameters mentioned above.

Fundamentals of Bayesian optimisation

For the purpose of determining the ideal set of parameters for a certain objective function, as a sequential model-based optimisation technique, Bayesian optimisation (BO) is applied when the objective function is expensive to evaluate and its assessment results are based on noisy or stochastic databases. Concretely, it is useful when there is no closed-form expression for the objective function but the observations (potentially noisy) of this function at sampling values can be obtained. The BO is especially beneficial when these assessments are expensive, when derivatives are unavailable, or when the problem at hand is non-convex. [358]

Particularly, the general BO consists of three key components: 1. objective function, which is the target function to be optimised with defined input and output; 2. surrogate model, which normally is a probabilistic model that can represent the behaviour of the objective function based on existing observations. In this paper, the Gaussian process (GP) is applied for its prominent flexibility and ability for uncertainty quantification; 3. acquisition function (AC), which quantifies the utility or desirability of sampling a

particular point in the search space. It also balances exploration and exploitation. Typical acquisition functions are expected improvement (EI), probability of improvement (PI), and upper confidence bound (UCB). In this section, the EI approach is applied based on its practical ability. Based on the formulation of the sequential model-based optimisation (SMBO), the pseudo-code of the BO is presented as Algorithm 3.

Algorithm 3 Bayesian optimisation

Define the objective function $f(x)$ to be optimised.
Define the search space X for the input variables x.
Initialize the surrogate model $M(x)$ using an initial set of observations.
for t $= 1$ to T **do**
  Select the next point x_t by optimising the acquisition function $\alpha(x|M_{(t-1)})$.
  Evaluate the objective function $f(x_t)$ to obtain the corresponding output y_t.
  Augment the set of observations with the new pair (x_t, y_t).
  Update the surrogate model $M_{(t)}$ using the augmented set of observations.
end for
Return the best-observed input x^* that maximizes the objective function.

Acquisition functions expected improvement

In this section, the ARD length scales are determined by applying the EI based on practicality and simplicity. In addition to the chance of increasing the existing best, it is also desirable for the improvement's magnitude to be taken into account. Accordingly, the "expectation of distributions" is the basis for the suggested expected improvement acquisition function. For the improvement $I(x)$, the expected value of $I(x)$ is

$$\mathrm{EI}(x) \equiv \mathbb{E}[I(x)] = \int_{-\infty}^{\infty} I(x)\varphi(z)\mathrm{d}z \tag{5.24}$$

where $\varphi(z)$ is the probability density function of the normal distribution $\mathcal{N}(0,1)$, i.e., $\varphi(z) = \frac{1}{\sqrt{2\pi}} exp(-z^2/2)$. Actually, $\mathrm{EI}(x)$ is a kind of a weighted average of "value" multiplied by the "probability of getting that value.". Thus, the $\mathrm{EI}(x)$ is expressed as

$$\mathrm{EI}(x) = \int_{-\infty}^{\infty} I(x)\varphi(z)\mathrm{d}z = \int_{-\infty}^{\infty} \underbrace{\max\left(f(x) - f\left(x^{\star}\right), 0\right)}_{I(x)} \varphi(z)\mathrm{d}z \tag{5.25}$$

Then the $\max(f(x) - f(x^{\star})$ is considered as two parts: 1. $\max(f(x) - f(x^{\star}) > 0$ and 2. $\max(f(x) - f(x^{\star}) < 0$. If the point x is the next point of best solution with $f(x) = f(x^{*})$, then

$$f(x) = f(x^{*}) \Rightarrow \mu + \sigma z = f(x^{*}) \Rightarrow z = \frac{f(x^{*} - \mu)}{\sigma} \tag{5.26}$$

Then, this point can be called back to PI with $z_0 = \frac{f(x^{*}) - \mu}{\sigma}$ and break up the integral mathematically,

$$\mathrm{EI}(x) = \underbrace{\int_{-\infty}^{z_0} I(x)\varphi(z)\mathrm{d}z}_{\text{Zero since } I(x)=0} + \int_{z_0}^{\infty} I(x)\varphi(z)\mathrm{d}z \tag{5.27}$$

Then, a long mathematical process can be presented as

$$\begin{aligned}
\mathrm{EI}(x) &= \int_{z_0}^{\infty} \max\left(f(x) - f\left(x^{\star}\right), 0\right)\varphi(z)\mathrm{d}z = \int_{z_0}^{\infty} \left(\mu + \sigma z - f\left(x^{\star}\right)\right)\varphi(z)\mathrm{d}z \\
&= \left(\mu - f\left(x^{\star}\right)\right) \underbrace{\int_{z_0}^{\infty} \varphi(z)\mathrm{d}z}_{1-\Phi(z_0)\equiv 1-\mathrm{CDF}(z_0)} + \frac{\sigma}{\sqrt{2\pi}} \int_{z_0}^{\infty} z e^{-z^2/2}\, \mathrm{d}z \\
&= \left(\mu - f\left(x^{\star}\right)\right)\left(1 - \Phi\left(z_0\right)\right) - \frac{\sigma}{\sqrt{2\pi}} \left[e^{-z^2/2}\right]_{z_0}^{\infty} \\
&= \left(\mu - f\left(x^{\star}\right)\right) \underbrace{\left(1 - \Phi\left(z_0\right)\right)}_{\Phi(-z_0)} + \sigma\varphi\left(z_0\right) \\
&= \left(\mu - f\left(x^{\star}\right)\right) - (\mu - f(x^{*}))\Phi\left(\frac{f(x^{*}) - \mu}{\sigma}\right) + \sigma\varphi\left(\frac{f(x^{*}) - \mu}{\sigma}\right) \\
&= \left(\mu - f\left(x^{\star}\right)\right)\Phi\left(\frac{\mu - f\left(x^{\star}\right)}{\sigma}\right) + \sigma\varphi\left(\frac{\mu - f\left(x^{\star}\right)}{\sigma}\right)
\end{aligned} \tag{5.28}$$

For the last equation, in fact, the probability density function (PDF) of the normal distribution is symmetric, therefore $\varphi(z_0) = \varphi(-z_0)$. Many methods can be applied to optimise the Eq.5.28, by using continuous first- and second-order optimisation such as quasi-Newton method L-BFGS-B. Conclusively, the $\mathrm{EI}(x)$ obtains high values when $\mu - f(x^*) > 0$ and $\theta > 1$ which indicates the improvement of the value and improvement of the uncertainty. It is notable to point out that the formula works when $\sigma(x) > 0$, otherwise if $\sigma(x) = 0$, $\mathrm{EI}(x) = 0$ since the point is being observed (without uncertainty). The last step is to introduce a hyperparameter, namely, ξ, where this hyperparameter is applied to control the trade-off between exploration and exploitation, mathematically,

$$\mathrm{EI}(x;\xi) = \left(\mu - f\left(x^\star\right) - \xi\right)\Phi\left(\frac{\mu - f\left(x^\star\right) - \xi}{\sigma}\right) + \sigma\varphi\left(\frac{\mu - f\left(x^\star\right) - \xi}{\sigma}\right) \tag{5.29}$$

If $\xi = 0$, where EI continues exploiting the current formula. The larger ξ, the smaller the improvement will be, which leads the algorithm towards more exploration. A trade-off between $(\mu - f(x^*)$ and $\sigma(x)$, balances between evaluating at points with high expected quality (high $(\mu - f(x^*)$) versus high uncertainty (high $\sigma(x)$). In the context of optimisation, evaluating at points with high expected quality relative to the previous best point is valuable because good approximate global optima are likely to reside at such points. On the other hand, evaluating at points with high uncertainty is valuable because it teaches about the objective in locations about which there is little knowledge and which tend to be far away from that which has previously been measured. A point that is substantially better than that which has previously been seen may reside there. It is often called the "exploration vs. exploitation trade-off.".

5.3.4 Frame assessmemt

This section describes the experimental technique as well as the assessment process. In addition, the construction of the multi-kernel ARD-GPR approach is described, followed by an analysis and discussion of hyperparameter estimation using MLE first, then the

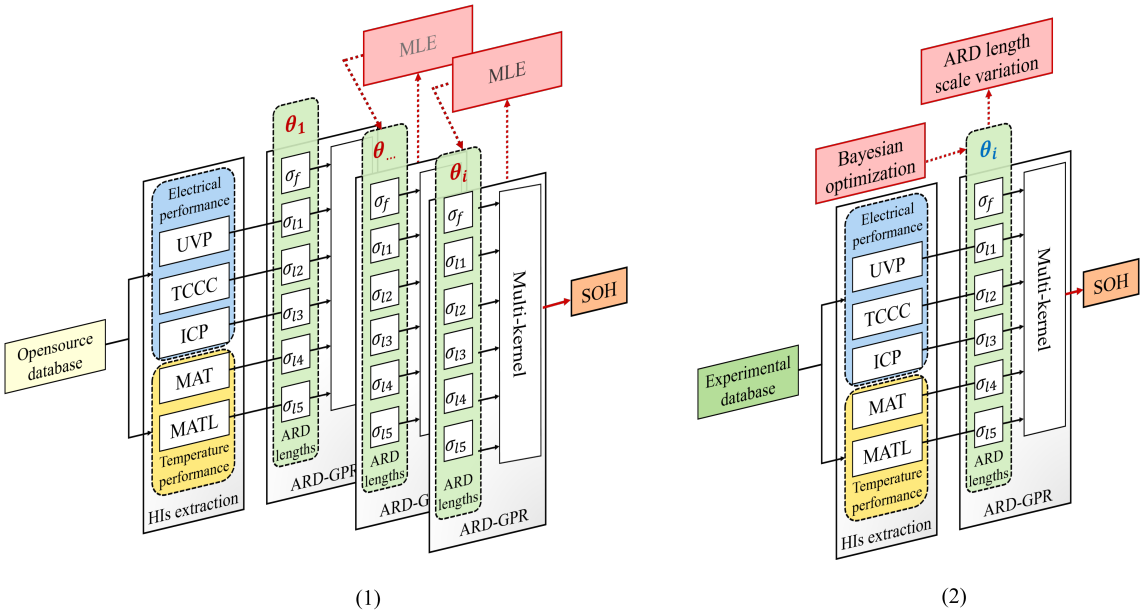

Fig. 5.15. The proposed multi-kernel ARD-GPR frame: (1) the learning process based on open-source databases; (2) Validation process based on experimental databases

Bayesian optimisation is applied to confirm the ARD length scales. The establishment of the multi-kernel ARD-GPR is shown as Fig.5.15.

General evaluation

Three main steps are applied to test the different GPRs based on the database. First, based on nine battery databases with the operating ambient temperatures of 4°C, 25°C and 44°C (three groups of data sets of each certain temperature), their charging processes are focused. Then, with each cycle iteration the five HIs mentioned previously are extracted as training inputs with corresponding instant battery capacity as a training output, the ratio of learning (obtained) data to validation data is 0.7/0.3. The GPR frame is trained based on extracted data to explore the best compromise of the best performance. Table 5.11 presents the test settings with relative contents: $T_{Ambient}$ represents the battery data sets under three temperature conditions; kernel functions contain SE, M32, M52, RQ; construction methods represent the construction methods of compound kernels, where 'single' means only a single kernel applied, 'Add' means two base kernels are added

Table 5.10
Battery database

Database feature	Database name
NASA battery database of $T_{Mid}(25°C)$	B0005, B0006, B0007, B0018
NASA battery database of $T_{High}(44°C)$	B0029, B0030, B0031, B0032
NASA battery database of $T_{Low}(4°C)$	B0053, B0054, B0055, B0056
Experimental database of 18650	EXP1
Experimental database of 21700	EXP2

Table 5.11
Kernels' construction plan

Test setting	Content
Kernel functions	SE/M32/M52/RQ
Construction methods	Single/Add/Multiply
Length scale	ISO/ARD

and applied (i.e. SE+M32), 'Multiply' means two kernel functions are combined with multiplication (i.e. SE*M32). Then, the length scale decides if the ARD is applied. If ARD-kernel is applied, then $\theta = [\sigma_f, \sigma_{l_1}, ..., \sigma_{l_5}]$, else $\theta = [\sigma_f, \sigma_l]$ in ISO-kernel application. The kernel combination plans are shown in Table 5.11. The overall battery database is shown in Table 5.10.

To evaluate the estimation performance of the data-driven models, the root-mean-square-error (RMSE) is applied. It is widely used to measure the difference between expected and actual values in quantitative data, by taking the square root of the average squared difference between predicted values y^* and actual values y. Mathematically,

$$\mathrm{RMSE} = \sqrt{\frac{1}{N}\sum_{j=1}^{N}\left(y - y^*\right)^2} \tag{5.30}$$

Kernels' construction

Then, the best compromise of the GPRs with the average least RMSEs of NASA battery databases under different temperatures is selected. Mathematically, the combined GPR

frame is expressed as

$$\mathbf{K}_{Hybrid}\left(x, x^{*} \mid \theta\right) = R * \mathbf{K}_{Reg} + (1 - R) * \mathbf{K}_{Abn} \tag{5.31}$$

where $\mathbf{K}_{Reg}$ is the kernel function that been used to deal with HI inputs under the most general situation ($25°C$); $\mathbf{K}_{Abn}$ is the kernel function to solve the inputs from those abnormal conditions of temperature ($4°C$ or $44°C$); R is the ratio to control the balance of both kernels to achieve the best regression performances. Then, to adopt the real temperature conditions of a battery in vehicles, three sets of databases are randomly chosen from all databases of each temperature. These three sets compromise a comprehensive database to evaluate the multi-kernel GPR. The comprehensive evaluation is equally distributed to the RMSE generated by different data, mathematically,

$$\mathbf{E}_{Com}\left(x, x^{*} \mid \theta\right) = (\mathbf{E}_{25°C} + \mathbf{E}_{44°C} + \mathbf{E}_{4°C})/3 \tag{5.32}$$

where $\mathbf{E}_{Com}$ is the comprehensive evaluation; $\mathbf{E}_{25°C}$ is the RMSE generated by the multi-kernel GPR from the $25°C$ database; similarly, $\mathbf{E}_{44°C}$ and $\mathbf{E}_{4°C}$ are RMSEs evaluated by the multi-kernel GPR based on the $44°C$ database and $4°C$ database, respectively. The comprehensive evaluation $\mathbf{E}_{Com}$ of the constructed GPR will be tested based on test sets drawn randomly from databases of three temperatures. Finally, the best R is confirmed after iterative tests to control the bias of selected kernel sets.

ARD length-scale hyperparameter identification

Finally, to reveal the mechanism of battery degradation, the variations of the length scales (as the σ_{l_i} in Eq. 5.23) in ARD kernels are concentrated. The time horizon is defined as the length of the data set of battery performances obtained in the iterative cycles. When the size of the time horizon changes, the inputs of the GPR frame are changed accordingly, which causes the variation of the ARD length scales estimated

by Bayesian optimisation. Since the length scales of an ARD-kernel function represent correlations between multiple inputs and the estimation results, thus the variation of the hyperparameters indicates the impact of each HI on the predicted capacity. In this section, the GPR is fed by variable lengths of training data under different time horizons from the NASA battery database and the experimental battery database, from 100% to 90% battery capacity degradation process. The variation of ARD hyperparameters is recorded and analysed to attribute the explanation.

5.3.5 Workload 3 results and discussion

General testing under variable temperatures

In this section, 16 types of kernels (including single kernels and combined kernels) are tested with 12 NASA battery databases under 3 different environmental temperatures ($5°C$, $25°C$ and $44°C$, respectively). The results are shown in Fig. 5.16, where the y-axis indicates normalised RMSE values (scaled all RMSE values into 0 to 1 for a better comparison) and the ticks on the x-axis are compromises of kernel functions. In the results of the $25°C$ condition, it can be shown that the RMSEs generated by multiplications of kernel functions are significantly lower than those combined by addition. Averagely, the multiplication compromises can achieve a lower RMSE of 0.043, which is 33.8% lower than the RMSE of the addition compromises (0.065), and 29.4% lower than the single kernel functions (0.061). From the perspective of kernel hyperparameters, the GPR with ARD frame leads to an average RMSE of 0.055, which is 3.51% lower than the RMSE generated by those ISO-GPRs (0.057).

For those results generated in $44°C$, a reversed distribution of RMSE is presented compared to the results of $25°C$. The average RMSEs generated by single kernels (0.056) and addition kernels (0.089) are 38.5% and 2.2% lower than those caused by multiplication kernels (0.091). In this circumstance, both ISO-GPRs and ARD-GPRs lead

to similar RMSEs of estimation; the average RMSE of the former is 0.078, which is 1.3% lower than the latter (0.079).

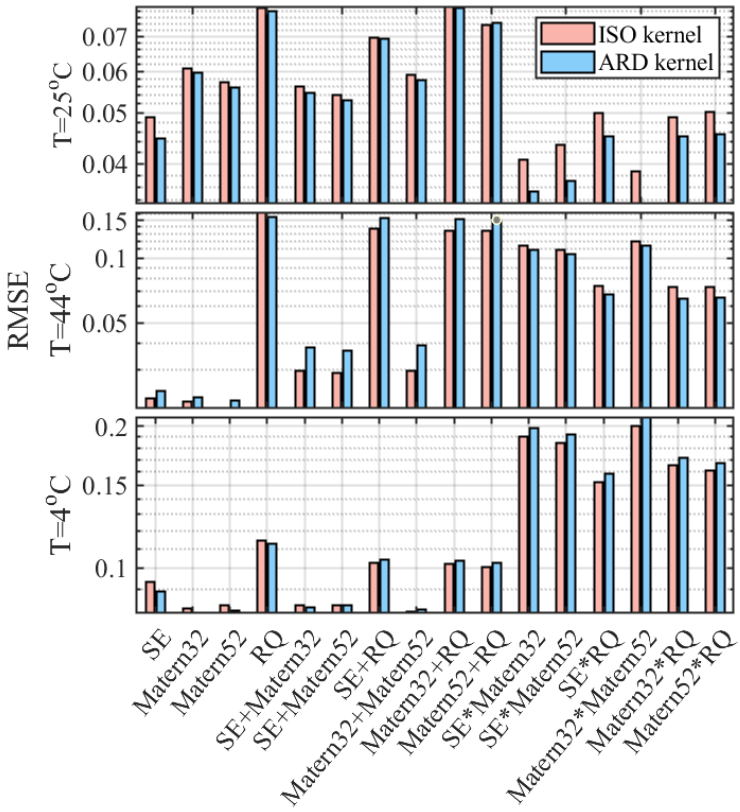

Fig. 5.16. Performances of GPR compromises with three different temperatures

When the temperature of the working condition is reduced to $4°C$, both single kernels and addition kernels produce small values of RMSE, which are 0.092 and 0.093, respectively. The average RMSE generated by multiplication kernels with a value of 0.180 is much larger than the previous two approaches. At this temperature, the performances of ARD-GPR and ISO-GPR are the same, with RMSE values of 0.120 and 0.122, respectively. Conclusively, when the environmental temperature is near to the room temperature, the multiplication kernels give a better performance among the three types of kernels. Later when the temperature is increased higher or reduced to a very low level, the single kernels and addition kernels show superiority in estimation accuracy. Also, generally, the ARD-GPRs outperform in room temperature for the battery capacity SoH estimation

but behave similarly with the ISO-GPRs in the other two circumstances with different temperatures.

According to this analysis, a part of the combination of additive kernel functions and single kernel functions shows a lower RMSE in regression performance at extreme temperatures; thus the SE × M52 will be selected as $\mathbf{K}_{Abn}$. but the combination of multiplicative kernel functions performs better overall around the typical battery temperature (about 25 degrees Celsius).

Consequently, for the comprehensive kernel function assembly, the $\mathbf{K}_{Reg}$ will be selected from the multiplicative kernel functions; whereas $\mathbf{K}_{Abn}$ will be selected from the range of additive kernel functions and single kernel functions.

Determination and optimisation of multi-kernel ARD-GPR

In this section, as introduced in Eq.5.31 and Eq.5.32, there are three groups of NASA battery data under different temperatures, each with four data sets, divided for training and validation in a 0.7/0.3 ratio. The value R is set as 0.5 at this stage for the initial trials.

Table 5.12
Multi-kernel ARD-GPR cross-testing results

RMSE		$\mathbf{K}_{Reg}$ candidates					
		SE×M32	SE×M52	SE×RQ	M32×M52	M32×RQ	M52×RQ
$\mathbf{K}_{Abn}$	SE	0.0469	0.0476	0.0506	0.0462	0.0511	0.0512
	M32	0.0496	0.0503	0.0532	0.0489	0.0538	0.0538
	M52	0.0489	0.0496	0.0526	0.0482	0.0531	0.0532
	RQ	0.0545	0.0552	0.0582	0.0538	0.0587	0.0588
	SE+M32	0.0488	0.0495	0.0525	0.0481	0.0530	0.0531
	SE+M52	0.0485	0.0492	0.0522	0.0478	0.0527	0.0528
	SE+RQ	0.0528	0.0535	0.0565	0.0521	0.0570	0.0571
	M32+M52	0.0493	0.0501	0.0530	0.0487	0.0536	0.0536
	M32+RQ	0.0546	0.0553	0.0583	0.0539	0.0588	0.0589
	M52+RQ	0.0537	0.0544	0.0574	0.0530	0.0579	0.0579

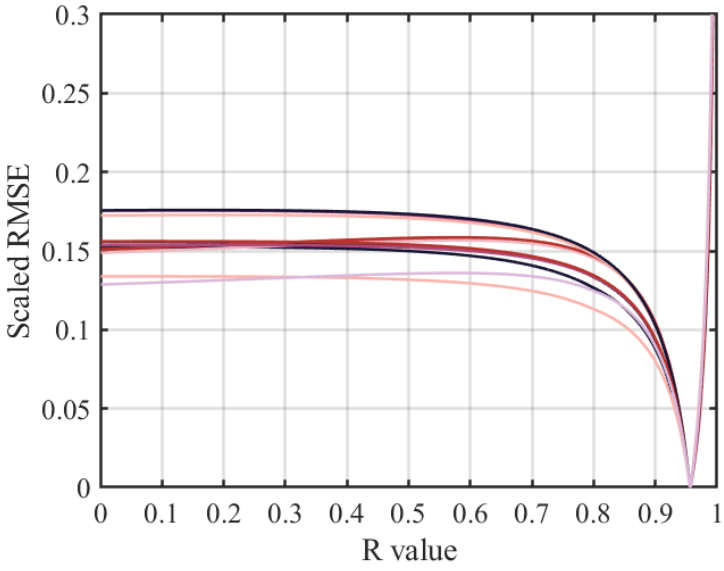

Fig. 5.17. Performances of GPR compromises with different R values

The goal is to test and verify the different compositions of the ARD-GPR kernel function: that is, the $\mathbf{K}_{Reg}$ is chosen from multiplication kernels (6 kernels), and those based on addition and single kernels as $\mathbf{K}_{abn}$ (10 kernels), totalling 60 multi-kernel pairing methods. For the final test RMSE is calculated using Eq.5.32, which takes the average of the four battery data sets at every temperature into account. The results of the cross-complication test are shown in Table 5.12. In this table, it can be observed that when the $\mathbf{K}_{Reg}$ is chosen as $M32 \times M52$ and the $\mathbf{K}_{Abn}$ is chosen as SE, the validation RMSE achieves its minimum at 0.0462. This signifies a reduction of 7.6% in comparison to the average RMSE (0.0501) of other schemes with $\mathbf{K}_{Reg} = M32 \times M52$, and a reduction of 12.42% in comparison to the average RMSE (0.0528) of all schemes included in the table.

To have the highest robustness (lowest RMSE) in the scenario based on this method, more optimisation of the value of R is required. To verify the estimated effectiveness of the current optimal kernel function combination, 40 groups of randomly paired data are employed, each group containing a random set of normal-temperature battery databases, a random set of high-temperature battery databases, and a random set of low-temperature battery databases. The value of R grows at intervals of 0.01 over the entire testing

process, going from 0 (totally the effect of $\mathbf{K}_{Abn}$ = SE) to 1 (entirely the function of $\mathbf{K}_{Reg}$ = M32 × M52), where each kernel function is weighted from dominance to irrelevance. Fig. 5.17 illustrates how the RMSE findings from the 40 groups of data tests are normalised for simpler analysis in order to lessen the influence of data inconsistency. The y-axis is the corresponding scaled RMSE with values being normalised to give a better indication, where the minimum value of RMSE of each test of a group is the lower boundary of scaling (scaled range starts from zero). It is obviously seen that the minimum scaled RMSE occurs when $R = 0.96$, and this means the multi-kernel GPR performs the highest robustness when the compromise of M32 × M52 dominates with a ratio of 0.96 and an SE dominates the remaining 0.04 considering three types of working environments.

Validation of the multi-kernel ARD-GPR and batteries degradation analysis

Finally, the proposed multi-kernel ARD-GPR and the traditional ARD-GPR methods were validated based on test data of two test batteries, with the results as in Table 5.13. From the table, it can be observed that the proposed multi-kernel ARD-GPR, in the validation of actual battery data, achieved estimated RMSEs of 0.014 and 0.025 for battery experimental data EXP1 (18650) and EXP2 (21700), respectively. Moreover, the RMSE of the proposed multi-kernel ARD-GPR frame for EXP1 is relatively 6.7% lower than the least RMSE (0.015) of conventional kernel methods . For EXP2, the RMSE of the proposed multi-kernel ARD-GPR (0.025) is 7.4% lower than the least RMSE (0.027) of conventional kernel methods.

Based on the proposed frame, the ARD parameters are also analysed in the time domain. Ultimately, this suggested approach notwithstanding, more analysis of the numerical fluctuations of ARD parameters in every dimension is required to disclose the degree to which different health issues influence the battery during its ageing phase. On the other hand, if the accuracy and precision of the battery health estimation are guaranteed,

Table 5.13
Multi-kernel ARD-GPR validation compared to conventional methods

Kernel functions	RMSE	
	EXP1 (18650)	EXP2 (21700)
ARD-SE	0.022	0.031
ARD-M32	0.015	0.027
ARD-M52	0.017	0.029
ARD-RQ	0.030	0.051
ARD Multi-kernel	0.014	0.025

the battery's ageing stages and time points can be verified by examining the numerical changes in each ARD, which is very helpful in directly revealing the texture of the battery ageing process through electrical signals. Four batteries' estimated SoH data are examined in this section: the 18650 and 21700 batteries from the experiments in earlier sections, as well as two from the NASA public database, B0005 and B0007 (both at a temperature of 25 degrees Celsius). Taking into account that the battery thermal management system (BTMS) actively tracks and controls the batteries' operating temperature during actual vehicle operation, this imposes arbitrary influences on the battery's natural temperature variations. As a result, temperature health indicators (HI4 and HI5) are now omitted in this section. After Bayesian optimisation of parameters to guarantee that the estimation accuracy at each time point has an error RMSE less than 0.05, the suggested framework is utilised to assess the health indicators relating to the three electrical performance of the batteries, as shown in Fig.5.18. In Particular, L1, L2, and L3 show the effect of ARD lengths that have been normalised for health indicators that correlate to TCCC, TCVC, and ICP, respectively.

In this graph, the y-axis represents the dimensionless, normalised ARD parameters, while the x-axis represents the degree of battery capacity loss, ranging from 100% (fully healthy) to 90% (partially degraded). (For the number of cycles in battery operation, NASA's public data is approximately 60 cycles, while the experimental data is approximately 300 cycles.) The graph shows that the variations in ARD parameters for B0005 and B0007

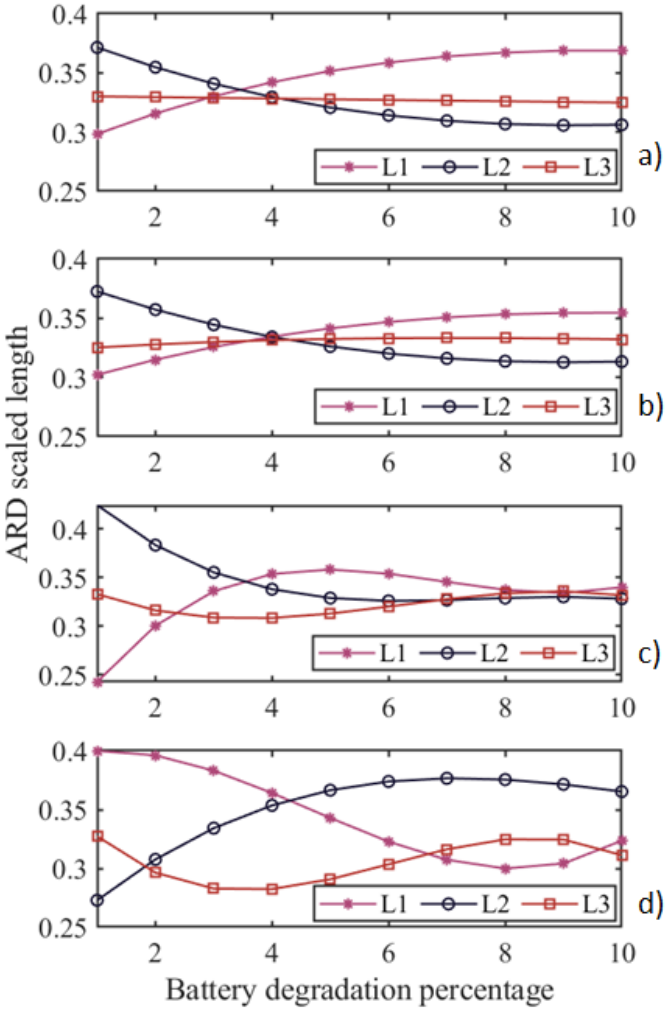

Fig. 5.18. ARD length variations comparison of 4 batteries in different dimensions. a) B0005 data set. b) B0007 data set. c) Experimental 18650 data set. d) Experimental 21700 data set.

are fairly similar, which can be attributed to the highly consistent testing environment and battery type (both are the same type of 18650 lithium-ion batteries). A rough similarity in the trend of ARD parameter changes may be seen by comparing the experimental 18650 battery data (Fig.5.18 c)) in this section with NASA's publicly available data; however, slight differences exist, which are considered because of the upgrading of battery technologies in both material and manufacturing process nowadays. However, in contrast to the other three, the results of the experiment using the 21700 battery (Fig.5.18 d)

Table 5.14
Pearson correlation of ARD length scales of each battery in different dimensions

ARD length scale 1 (L1)				
	B0005	B0007	EXP1	EXP2
B0005	1.0000	0.9998	0.8896	-0.8530
B0007	0.9998	1.0000	0.8961	-0.8536
EXP1	0.8896	0.8961	1.0000	-0.6193
EXP2	-0.8530	-0.8536	-0.6193	1.0000
ARD length scale 2 (L2)				
	B0005	B0007	EXP1	EXP2
B0005	1.0000	0.9999	0.9477	-0.9716
B0007	0.9999	1.0000	0.9494	-0.9732
EXP1	0.9477	0.9494	1.0000	-0.9892
EXP2	-0.9716	-0.9732	-0.9892	1.0000
ARD length scale 3 (L3)				
	B0005	B0007	EXP1	EXP2
B0005	1.0000	-0.8853	-0.5309	-0.3920
B0007	-0.8853	1.0000	0.3792	0.0012
EXP1	-0.5309	0.3792	1.0000	0.9761
EXP2	-0.3920	0.0012	0.9761	1.0000

)are somewhat different. This could be due to differences in the material's composition and physical dimensions, adding even more uncertainty.

Table 5.14 displays the results of the Pearson correlation analysis that was performed on the L1, L2, and L3 ARD lengths for four batteries: B0005, B0007, experimental 18650 (EXP1) and experimental 21700 (EXP2). The L1 and L2 health indices for B0005 and B0007 have very strong correlations, with Pearson coefficients of 0.9999 and 0.9998, respectively, but L3 has a negative correlation value of -0.8853 (actually they almost did not vary during the degradation process). This once again demonstrates that under the same working conditions, identical batteries will exhibit consistent patterns during the cyclic ageing process.

For the experimental 18650 (EXP1) battery experiment performance, concerning the L1 ARD parameter, it exhibited a certain level of correlation with B0005 and B0007,

with correlation coefficients of 0.8896 and 0.8961, respectively. Also, L2 shows a strong correlation, with Pearson correlation coefficients of 0.9477 and 0.9494 with respect to B0005 and B0007, respectively. On the other hand, L3 does not demonstrate a significant correlation with values of -0.5309 for B0005 and 0.3792 for B0007.

The experimental 21700 (EXP2) battery's comparison results are really quite distinct from the 18650 series, showing a clear negative correlation. The experimental 21700 battery and B0005, B0007, and the experimental 18650 battery (EXP1) have Pearson correlation coefficients of -0.8530, -0.8536, and -0.6193 for ARD length scale 1 (L1). These three correlation coefficients in the L2 dimension: -0.9716, -0.9732, and -0.9892 indicate a very strong negative association. The main finding in the L3 dimension is that, when it comes to the ICP health indicator (HI3), the 21700 battery and the experimental 18650 battery show the greatest correlation.

In a nutshell, the four batteries show consistent patterns and a highly correlated performance in the TCVC health factor throughout the degradation process, according to the proposed multi-kernel arD-GPR framework. If the battery type is known, this pattern can be used to analyse the distribution of ARD length scales and identify the time and level of battery degradation. Additionally, variations of ARD length scales for HIs are important for assessing the reasons behind battery ageing and offer important insights into the ageing process.

5.3.6 Workload 3 summary

In this section, effective battery SoH estimation with charging conditions in variable temperature environments was presented. The Gaussian process regression with ARD kernels was implemented and modified to conduct a battery SoH estimation based on data-driven approaches. In particular, two li-ion batteries were tested as databases for the later validation of the algorithm. Based on 16 collocations of kernels, the M32 $\times$ M52 and SE are chosen as the best compromises, with the most appropriate allocation

ratio of 0.96 for the multi-kernel ARD-GPR in complex temperature environments. The proposed multi-kernel ARD-GPR shows an average 7.1% lower RMSE compared to the conventional GPR methods with the validation of the experimented data.

Finally, the variation of the ARD lengths was analysed with the degradation process. By the correlation analysis of different dimensions of HIs, the multi-kernel ARD-GPR frame has shown that its estimation results were able to locate a certain degradation level based on ARD length scales and attribute the importance of the operation performances without any additional information, where it is practically and easily implemented to the EV's application.

5.4 | Chapter summary

This chapter primarily focuses on the establishment of digital models for electric vehicle batteries, aiming to support intelligent energy management in advanced hybrid vehicles through real-time applications. The main work is based on publicly available databases and experimental data, and it includes the following:

1. An online double-layer system identification scheme was proposed with an equivalent circuit model for batteries using PSO for parameter identification (with a RMSE=0.0045) and a battery health estimation and prediction system is developed by using deep convolutional neural networks (DCNN) based on data characteristics derived from the battery's direct health indicators of charging behaviour, which can achieve an average RMSE of 0.0152 with a learning/validation ratio of 0.7/0.3.

2. Based on the equivalent circuit model created in the first section, an asynchronous LSTM-based mechanism was designed to forecast the incomplete discharging process for simultaneous estimation of battery state of charge (SoC) and state of health (SoH) by focusing on direct health indicators in random discharge processes.

3. A frame of multi-kernel gaussian process regression (GPR) and its automatic relevance determination (ARD) mechanism was developed by concentrating on the indirect health

indicators for a robust battery health estimation based on open-sourced data, then the proposed multi-kernel ARD-GPR showed an average 7.1% lower RMSE compared to the conventional GPR methods with the validation of the experimented data. Furthermore, Bayesian optimisation was employed to analyse ARD parameters for revealing the battery's ageing stages and signal attribution.

In summary, this chapter combines optimisation, neural networks, and data analysis techniques to investigate several models and methodologies to assess battery health and ageing for intelligent energy management in multi-mode PHEVs.

CHAPTER 6

Online optimal control of cuboid-ECMS for multi-mode PHEVs considering multiple objectives in diverse time scales

Optimising the useful battery life of electrified cars (EVs), particularly plug-in hybrid electric vehicles (PHEVs), is crucial due to the potential environmental consequences associated with battery recycling. An emerging subject in PHEV energy management is upgrading the standard ECMS to minimise battery degradation [359]. For single-mode PHEVs, there are a number of methods to introduce battery ageing models in the ECMS, such as series PHEVs [360] and parallel PHEVs [361], [362]. In order to operate a multi-mode plug-in hybrid electric vehicle (PHEV), Liang et al. developed a battery degradation considered ECMS based on a lookup table [363]. However, extra empirical rules were added to control the engine's working mode. For a parallel HEV, Sarvaiya et al. created an ECMS based on empirical equations for battery ageing [364]. For a series HEV, Suri et al. designed an ECMS while taking into account a battery severity map [365]. The primary distinction between single-mode and multi-mode plug-in hybrid electric vehicles (PHEVs) is that the latter can operate in pure electric mode, series-hybrid mode, or parallel mode thanks to a coupling device, such as a clutch or planetary gearset. This gives power splitters greater flexibility for improved fuel economy, but it also presents

design issues for ECMSs as additional control variables must be coordinated for the best possible control.

Furthermore, due to their ability to switch between modes, multi-mode plug-in hybrid electric vehicles (PHEVs) are more practical for driving in real-world situations and have a vast potential for energy savings over single-mode vehicles. However, since the impact of two motors on the state of the battery cannot be fully reflected in the typical Hamiltonian function, the normal ECMS cannot be easily applied for the multiple mode energy management of the PHEV [366], [367]. Developing an ECMS for a multi-mode plug-in hybrid electric vehicle (PHEV) is more challenging due to the long-term cumulative nature of battery ageing and the necessity for the EMS to balance optimisation objectives across several time scales [365]. Up to now, little ECMS research has taken into account a variety of power sources over a range of time scales.

To do this, energy management strategies need to be tailored to individual driving conditions using a variety of sophisticated techniques for optimising both long-term and short-term objectives. The energy management system may maintain battery health over the course of the vehicle's lifespan; optimise energy use for individual journeys; respond fast and effectively to driving demands; and effectively integrate with wider energy systems by addressing these various time-scale objectives.

This study has proposed a new cuboid equivalent consumption minimisation strategy (C-ECMS) for the multi-mode PHEV that has two primary improvements over the current ECMSs in order to address their shortcomings. Firstly, in order to enable optimal control of two motors in multi-mode plug-in hybrid electric vehicles (PHEVs), a new concept known as a "Hamiltonian matrix" is introduced. Secondly, an ageing factor (AF) is introduced in conjunction with the equivalent factor (EF) to generate three Hamiltonian matrices that establish a cuboid knowledge base for optimal control taking into account diverse time-scale objectives. A Pareto study of the effects of the EF and AF values on

the vehicle's energy efficiency, the accuracy of the SoC control, and the loss of battery capacity leads to a unified setting for the EF and AF.

6.1 | PHEV powertrain and battery systems

The technical details of the PHEV under study are described in this part, together with information on its powertrain architecture, important modelling factors, and battery degradation. The MATLAB/Simulink digital model of the powertrain and baseline techniques are available from the MAHLE firm and have been verified for actual application.

6.1.1 Multi-mode powertrain modelling

Based on the introduction in section 3.3, a backward model is created to mimic the power flow of the PHEV in MATLAB/Simulink. Fig. 3.8 depicts the architecture of the multi-mode PHEV powertrain. A 70 kW internal combustion engine (ICE), two motor/generators (MG1 with a nominal power of 21 kW and MG2 with a notional power of 135 kW) with integrated gearboxes, and a 20 kWh battery make up this powertrain's primary power units. Table 6.1 lists the important parameters utilised in the modelling. Furthermore, the working modes of this powertrain follow the rules in section 3.3.1.

6.1.2 Battery equivalent circuit model and degradation model

To emulate the internal dynamics that affect battery ageing, this section builds a 2-RC equivalent circuit battery model in MATLAB/Simulink. The corresponding digital model is established based on Eq.3.6 in section 3.3.2, then the battery package parameters' identification is done based on the approach of Section 5.1.1 in chapter 5. Recalling the empirical model of the battery SoH condition in Eq.3.3.3 and Eq.3.10, $A = 0.0032$,$E_a = 15162$, $B = 1516$, and $z = 0.824$; these are calibrated comprehensively by work conducted by Song et al. [368], [369] and the work in previous chapters.

Table 6.1
Specifications of the multi-mode powertrain

Component parameters	Values
Vehicle mass (m)	1700 kg
Tyre rolling radius (R)	0.337 m
Rolling resistant coefficient (C_f)	0.011
Front area (A)	2.5 m^2
Aerodynamic drag coefficient (C_d)	0.32
Engine displacement (D)	1 L
Battery capacity (C_{batt})	54.3 Ah
Battery nominal open-circuit-voltage (U_{OCV})	350 V
Differential ratio (i_{RD})	4.14
Transmission ratio of gearbox-MG1 (i_{R1})	0.95
Transmission ratio of gearbox-MG2 (i_{R2})	3.91

6.2 | Energy management problem statement

The multi-objective optimisation problem for the multi-mode PHEV considering fuel consumption, Q_{Fuel}, battery SoC control error, Q_{SoC}, and battery capacity loss, $Q_{\text{Loss(t)}}$, is formulated mathematically by

$$\begin{aligned}\left\{P_{\text{ICE}}(t), P_{\text{MG1(t)}}, P_{\text{MG2(t)}}\right\} &= \operatorname{argmin}\left(Q_{\text{Fuel}}, Q_{\text{SoC}}, Q_{\text{Loss}}\right), t = 0, \ldots, T \\ \text{s.t.} &\left\{\begin{array}{c} Eq.3.1-3.8, 6.1, 6.2 \\ \text{SoC}_{\min} \le \text{SoC}(t) \le \text{SoC}_{\max} \\ 0 \le P_{\text{ICE(t)}} \le P_{\text{ICE}\max} \\ 0 \le P_{\text{MG1(t)}} \le P_{\text{MG1}\max} \\ P_{\text{MG2}\min} \le P_{\text{MG2(t)}} \le P_{\text{MG2}\max} \end{array}\right\}\end{aligned} \tag{6.1}$$

where $SoC_{\min}$ and $SoC_{\max}$ are the lower and upper limitations of the battery SoC level, respectively; the power outputs of the engine ($P_{\text{ICE(t)}}$), motor 1 ($P_{\text{MG1(t)}}$), and motor 2 ($P_{\text{MG2(t)}}$) are constrained by their restrictions, and Q_{Loss} is the battery capacity

loss described by Eq.3.3.3. Furthermore, because this PHEV operates as a pure EV in charging-depleting (CD) mode, the emphasis is on the charging-sustaining (CS) process. Thus, the PHEV's battery SoC at the conclusion of driving is desired to be the same as the initial value; to this aim, energy differences can only be displayed depending on fuel usage. The energy consumption over the driving, Q_{Fuel}, is calculated by

$$Q_{\mathrm{Fuel}} = \int_0^T \dot{m}_{\mathrm{ICE}} \left(T_{\mathrm{ICE(t)}}, \omega_{\mathrm{ICE}}(t) \right) H_{\mathrm{LHV}} dt \tag{6.2}$$

where T is the total driving duration; $\dot{m}_{\mathrm{ICE}}$ is the immediate fuel flow rate at the t-th step, which is determined by a fuel mass flow rate map of engine speed, $\omega_{\mathrm{ICE}}(t)$, and engine torque $T_{\mathrm{ICE(t)}}$; and H_{LHV} is the fuel's lower heating value, which is typically 43.4 MJ/kg for petrol [370]. The relative SoC error Q_{SoC} is defined as

$$Q_{\mathrm{SoC}} = \left| \frac{SoC_{\mathrm{final}} - SoC_{\mathrm{target}}}{SoC_{\mathrm{target}}} \right| \tag{6.3}$$

where SoC_{final} is the SoC level at the end of the drive; and SoC_{target} is the SoC level to be achieved. The SoC_{target} is set to 0.3 in this section since it is a commonly acknowledged number for PHEV control in terms of battery operation safety [363] [371].

6.3 | The mechanism of the C-ECMS

Based on ordinary ECMS, this part firstly proposes a novel cuboid equivalent consumption minimisation technique (C-ECMS). Section 6.3.1 introduces the mechanism of the standard ECMS. The proposed C-ECMS is then developed by converting the standard Hamiltonian state vector into a two-dimensional state matrix (named Hamiltonian matrix) to represent the potential energy distributions from multiple dimensions in the optimal control of the multi-mode PHEV in section 6.3.3, as shown in Fig. 6.1. Based on the battery deterioration model created in section 6.1.2, the ageing factor (AF) is introduced to build three Hamiltonian matrices that comprise a cuboid knowledge base for energy

management of the multi-mode PHEV in collaboration with the equivalent factor (EF). The working process is shown in Fig. 6.2, where the 'cuboid' is referred the 3-dimensional knowledge base being indicated in the figure.

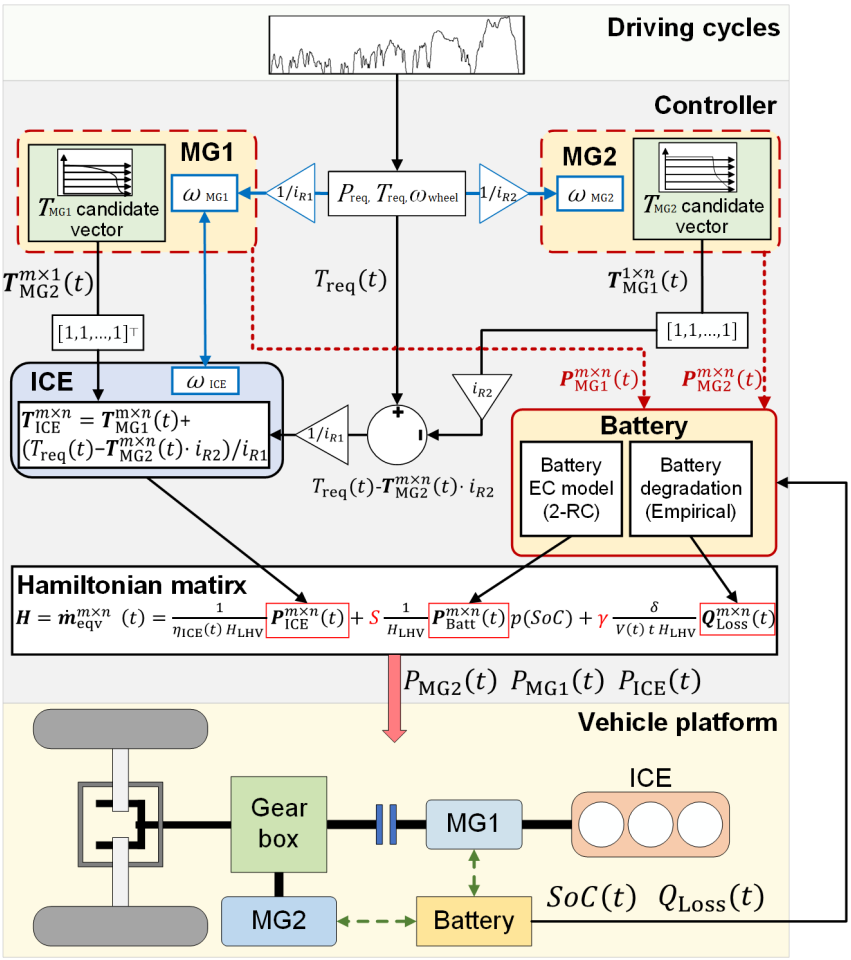

Fig. 6.1. The architecture of C-ECMS

6.3.1 The standard ECMS

Conventional global optimisation process is normally offline with all information known, i.e. PMP, the Hamiltonian function is therefore applied and described by both dynamic equations and co-state functions of optimisation to represent the instant status of the system [372]. Later, for practicality and simplicity in automotive engineering, the idea of equivalent consumption minimisation strategy (ECMS) is come out with a core concept

that electrical energy can be roughly translated to fuel consumption using an instant cost function centred on a single equivalent factor (EF) rather than original co-state functions [359]. Then a global optimisation is reduced by a local (instaneous) optimal control with an approximate best solution, which is mathematically proofed [372].

Specifically, the Hamiltonian state function is therefore adapted into an instant status vector of ECMS, which represents potential solutions of different power distributions in an instant time step. The instant cost status of the Hamiltonian function for standard ECMS can be represented by

$$\left.\begin{aligned} H(t) = \dot{m}_{\text{eqv}}\ (t) &= \dot{m}_{\text{ICE}}(t) + \dot{m}_{\text{Batt}}(t) \\ \dot{m}_{\text{ICE}}(t) &= \frac{P_{\text{ICE}}(t)}{\eta_{\text{ICE}}(t) H_{\text{LHV}}} \\ \dot{m}_{\text{Batt}}(t) &= \frac{S}{H_{\text{LHV}}} P_{\text{Batt}}\ (t) \end{aligned}\right\} \tag{6.4}$$

where S is the equivalent factor (EF), which represents the tendency of equivalent power translating, it normally needs to be adjusted for various driving cycles; $\dot{m}_{\text{Batt}}$ denotes the equivalent fuel consumption from electrical energy; H_{LHV} is the lower heating value of the fuel; and $\dot{m}_{\text{eqv}}(t)$ is the instant equivalent consumption (EC) of fuel at the t-th time step.

A vector of candidate power values for batteries is generated by using a candidate vector with a set of indices, $\overrightarrow{n} = [0, 1, 2, 3, \ldots, (n-1)]$, in order to discretise the battery's candidate power with finite numbers as in the equations below,

$$\vec{P}_{\text{Batt}}\ (t) = P_{\text{Batt, min}}(t) + \overrightarrow{n} \times \frac{\left[P_{\text{Batt,max}}\ (t) - P_{\text{Batt,min}}\ (t)\right]}{n} \tag{6.5}$$

where $P_{\text{Batt,min}}\ (t)$ and $P_{\text{Batt,max}}\ (t)$ represent the lower and higher bounds of the battery's potential power output at the t-th time, respectively.

Because the typical ECMS only considers a motor, the vector of candidate ICE power values, $\vec{P}_{\text{ICE}}$, and the vector of candidate MG power values, $\vec{P}_{\text{MG}}$, can be determined by

$$\left.\begin{aligned}\vec{P}_{\mathrm{ICE}}(t) &= P_{\mathrm{req}}\ (t) - \vec{P}_{\mathrm{Batt}}\ (t)\\ \vec{P}_{\mathrm{MG}}(t) &= \vec{P}_{\mathrm{Batt}}\ (t)\end{aligned}\right\} \tag{6.6}$$

By incorporating Eqs. 6.4, 6.5, and 6.6, the vector of cost status for Hamiltonian can be obtained at each instant time as

$$\vec{H} = \frac{\vec{P}_{\mathrm{ICE}}}{\eta_{\mathrm{ICE}}(t) H_{\mathrm{LHV}}} + \frac{S}{H_{\mathrm{LHV}}} \vec{P}_{\mathrm{Batt}} \cdot p(SoC) \tag{6.7}$$

where $p(SoC)$ is a penalty function that is used to manage the SoC level during the control process [372]. Its formulation is as follows:

$$p(SoC) = 1 - \left(\frac{SoC(t) - SoC_{\mathrm{target}}}{SoC_{\max} - SoC_{\min}} \right)^{\alpha} \tag{6.8}$$

where $SoC(t)$ is the battery's SoC level; $SoC_{\max}$ and $SoC_{\min}$ are the operating limits of the battery during the driving process. In this section, $SoC_{\max} = 0.8$, $SoC_{\min} = 0.2$, and $\alpha = 3$ are widely recognised PHEV control settings [373]. The ECMS will discover an index value, $opt \in [1, n]$, that satisfies the condition at each sampling period as

$$\vec{H}(\ \mathrm{opt}\ ) \leq \vec{H}(j), i \in [1, n] \tag{6.9}$$

and will output the values of $\vec{P}_{\mathrm{Batt}}(\mathrm{opt})$, $\vec{P}_{\mathrm{MG}}(\mathrm{opt})$, $\vec{P}_{\mathrm{ICE}}(\mathrm{opt})$ for real time control.

6.3.2 The novel Hamiltonian matrices for multiple motors

To enable dual-motor controls in the multi-mode PHEV, two torque candidate vectors for MG1 and MG2 are established by inserting two index vectors: $\overrightarrow{\boldsymbol{n}} = [0, 1, 2, 3, \ldots, (n-1)]$, $\overrightarrow{\boldsymbol{m}} = [0, 1, 2, 3, \ldots, (m-1)]^{\intercal}$,

$$\left.\begin{aligned}\boldsymbol{T}_{\mathrm{MG1}}^{1\times n}(t) &= T_{\mathrm{MG1,min}}(t) + \overrightarrow{\boldsymbol{n}} \times \frac{\left[T_{\mathrm{MG1,max}}(t) - T_{\mathrm{MG1,min}}(t)\right]}{n}\\ \boldsymbol{T}_{\mathrm{MG2}}^{m\times 1}(t) &= T_{\mathrm{MG2,\ min}}\ (t) + \overrightarrow{\boldsymbol{m}} \times \frac{\left[T_{\mathrm{MG2,max}}(t) - T_{\mathrm{MG2,min}}(t)\right]}{m}\end{aligned}\right\} \tag{6.10}$$

where $\boldsymbol{T}_{\mathrm{MG1}}^{1\times n}(t)$ and $\boldsymbol{T}_{\mathrm{MG2}}^{m\times 1}(t)$ are the torque candidate vectors of the MG1 and MG2. Then the corresponding candidate power matrices of MG1 and MG2 at time t is given as

$$\left.\begin{aligned}\boldsymbol{P}_{\mathrm{MG1}}^{m\times n}(t) &= \frac{\omega_{\mathsf{wheel}}(t)}{i_{R1}\cdot i_{RD}}\cdot \underbrace{[1,1,\ldots,1]}_{m}^{\top}\times \boldsymbol{T}_{\mathrm{MG1}}^{1\times n}(t)\\ \boldsymbol{P}_{\mathrm{MG2}}^{m\times n}(t) &= \frac{\omega_{\mathsf{wheel}}(t)}{i_{R2}\cdot i_{RD}}\cdot \boldsymbol{T}_{\mathrm{MG2}}^{m\times 1}(t)\times \underbrace{[1,1,\ldots,1]}_{n}\end{aligned}\right\} \tag{6.11}$$

The potential power offered by the battery is calculated by

$$\boldsymbol{P}_{\mathsf{Batt}}^{m\times n}(t) = \boldsymbol{P}_{\mathrm{MG1}}^{m\times n}(t) + \boldsymbol{P}_{\mathrm{MG2}}^{m\times n}(t) \tag{6.12}$$

The ICE bridges the power gap between the instant power demand and the power provided by the battery. It is shown mathematically as

$$\boldsymbol{P}_{\mathrm{ICE}}^{m\times n}(t) = P_{\mathsf{req}}(t) - \boldsymbol{P}_{\mathsf{Batt}}^{m\times n}(t) \tag{6.13}$$

Based on Eqs. 6.10- 6.13 the Hamiltonian matrix is formulated as

$$\boldsymbol{H}_{\mathrm{mtx}}^{m\times n}(t) = \dot{\boldsymbol{m}}_{\mathrm{eqv}}^{m\times n}(t) = \frac{1}{\eta_{\mathrm{ICE}}(t)H_{\mathrm{LHV}}}\boldsymbol{P}_{\mathrm{ICE}}^{m\times n}(t) + \frac{S}{H_{\mathrm{LHV}}}\boldsymbol{P}_{\mathrm{Batt}}^{m\times n}(t)\cdot p(SoC) \tag{6.14}$$

6.3.3 Cuboid knowledge base for energy management

Based on Eqs.3.8, 3.9, 3.10 two matrices for battery capacity loss, $\boldsymbol{Q}_{\mathrm{Loss}}^{m\times n}$, and the Ah-throughput, $\boldsymbol{Ah}_{\mathsf{Batt}}^{m\times n}$, can be formulated as

$$\left.\begin{aligned}\boldsymbol{Ah}_{\mathsf{Batt}}^{m\times n} &= \frac{1}{3600}\int_{t_k}^{t_{k+1}}\left|\frac{\boldsymbol{P}_{\mathsf{Batt}}^{m\times n}(t)}{U(t)}\right| dt\\ \boldsymbol{Q}_{\mathsf{Loss}}^{m\times n} &= A\exp\left(-\left(\frac{E_a+B\cdot\frac{\boldsymbol{I}_{\mathsf{Batt}}^{m\times n}(t)}{C_{\mathsf{batt}}}}{R_g T_{\mathsf{batt}}}\right)\right)\left(\boldsymbol{Ah}_{\mathsf{Batt}}^{m\times n}\right)^{z}\end{aligned}\right\} \tag{6.15}$$

By combining Eq.6.14 and Eq.6.15, the cuboid knowledge base, as illustrated in Fig.6.2, is formulated by the Hamiltonian matrix as

$$H(t) = \underbrace{\frac{1}{\eta_{\mathrm{ICE}}(t) H_{\mathrm{LHV}}} \boldsymbol{P}_{\mathrm{ICE}}^{m\times n}(t)}_{\text{Actual consumption by ICE}} + \underbrace{\frac{S}{H_{\mathrm{LHV}}} \boldsymbol{P}_{\mathrm{Batt}}^{m\times n}(t) \cdot p(SoC)}_{\text{EC by battery}} + \underbrace{\gamma \frac{\delta}{U(t) t H_{\mathrm{LHV}}} \boldsymbol{Q}_{\mathrm{Loss}}^{m\times n}(t-1, t)}_{\text{battery capacity loss penalty}} \tag{6.16}$$

where the first item on the right-hand side represents the ICE's actual fuel usage. The second figure is the battery's comparable gasoline consumption. The third item is the penalty of equivalent fuel consumption caused by capacity loss (the capacity loss Ah is converted into fuel flow rate); γ is an ageing factor; and δ is a gain factor used to align the magnitude of battery capacity loss with the other components. According to the magnitude of values in the Hamiltonian function of C-ECMS, $\delta = 106$ in this section.

A cuboid knowledge base is built for the C-ECMS by calculating the total Hamiltonian values based on Eq.6.16 for various combinations of clutch state (determining the operating mode) and power outputs of MG1, MG2, and ICE, as shown in Fig. 6.2. Based on the power demand of the multi-mode PHEV, an indicator with the lowest EC value

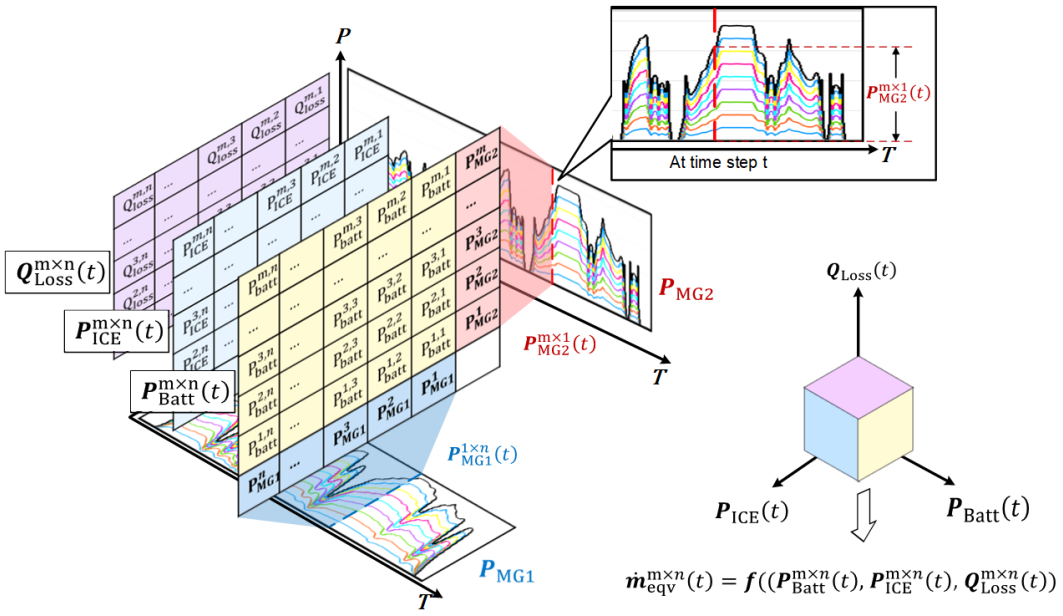

Fig. 6.2. The cuboid knowledge base for C-ECMS

can be retrieved from the three state matrix generated by the ICE, battery and battery degradation, where they are named as the cuboid knowledge base (in three dimension) in each control time step. The indicator can be used to determine the clutch status as well as the power outputs of the MG1, MG2, and ICE for real time control.

6.4 Results and discussion

Experiments are carried out over five driving cycles to investigate 1) the effect of the number of elements in Hamiltonian matrices on SoC control accuracy; and 2) the effect of EF and AF settings on the Pareto frontier while accounting for fuel efficiency, SoC accuracy, and battery ageing. The WLTP3, Artemis Urban, Artemis Rural Road, Artemis Motorway 130, and RTS95 driving cycles were used for the study to cover the majority of the PHEV's driving circumstances. The Artemis series of driving cycles may reflect the most real-world driving situations with transitory speed variations; while the RTS95 cycle portrays aggressive driving styles, and WLTP3 offers full driving scenarios for PHEVs with low, medium, and high speed ranges. The driving cycles' information can be reviewed in Table 3.1. The unified setting for C-ECMS is obtained based on the experimental investigation, and the result is validated by a comparison study with the rule-based strategy and the standard ECMS implemented in the same PHEV.

6.4.1 Impact of number of elements in the Hamiltonian matrices on SoC control accuracy

The number of elements in the Hamiltonian matrices influences the knowledge base information for MG1 and MG2 control. More information in the Hamiltonian matrix will theoretically result in a more accurate control performance (i.e. less SoC control error), but will necessitate more computer resources. As a result, the values of n and m that determine the size of the Hamiltonian matrices must be chosen carefully. The

significance of the variables n and m resides in their vital role in establishing optimal energy distribution between the motors (MG1 and MG2) and the engine (ICE) during the control process. Through the selection of these parameters, the power allocation among the various components of the powertrain can be efficiently balanced, resulting in improved fuel economy and decreased energy consumption. This section optimises the following mathematical problem in order to arrive at the ideal setting of n and m,

$$\left.\begin{aligned} \{n, m\} &= \operatorname{argmin}\left(Q_{\mathrm{SoC}}\right) \\ Q_{\mathrm{SoC}} &= \left|\frac{SoC_{\mathrm{final}} - SoC_{\mathrm{target}}}{SoC_{\mathrm{target}}}\right| \times 100\% \\ &\text{s.t.n, } m \in \mathbb{Z}^{+} \end{aligned}\right\} \tag{6.17}$$

where n and m stand for the number of elements in the power distributions of MG1 and MG2, respectively; Q_{SoC} is the relative error between the target SoC (SoC_{target}= 0.3 in this study) and the final SoC at the end of the driving cycle (SoC_{final}). Since the power discretisation below such a limit is extremely harsh for the calculation, the lowest number of elements in the Hamiltonian matrices is fixed at 10. Based on the instant power

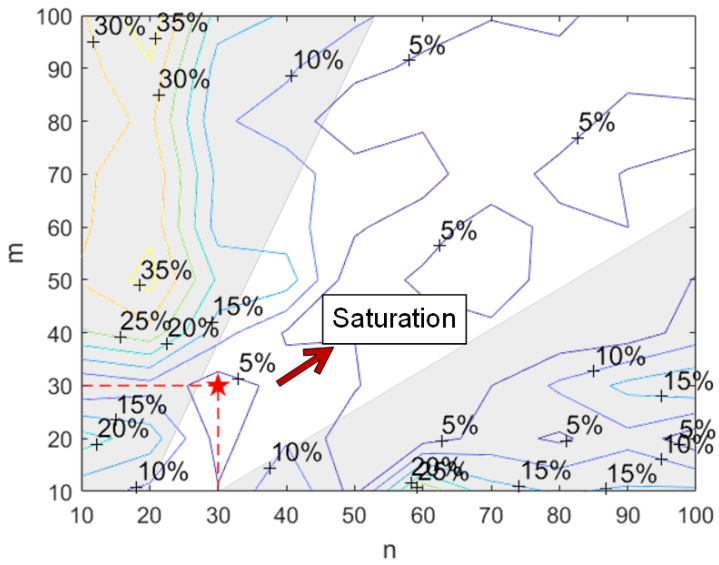

Fig. 6.3. The numerical analysis of power discretisation

matrix computation constraint in timed seconds, the maximum number of elements is set at 100. Additionally, the "saturation" in Fig.6.3 indicates that the SoC error will stop decreasing further when the combination of n and m increases in the white area that is not covered by the shadow, along the direction of the arrow. The computational accuracy has achieved saturation at this point. According to Fig.6.3, the C-ECMS may operate at peak efficiency in SoC sustaining at $n = 30$ and $m = 30$, resulting in a minimum SoC inaccuracy of less than 5%. Fig.6.3 further emphasises that the C-ECMS cannot ensure stable management of battery SoC, i.e. SoC error is greater than 10%, when the values of n and m are not chosen appropriately, for example, in the grey area.

6.4.2 Impact of the equivalent factor and the ageing factor on control performances

The impact of the values of the AF and EF factors on the control performances are examined in this section because the suggested C-ECMS added an additional ageing factor (AF) to address the multi-objective optimisation issue in real time control. First, using varied AF and EF settings (AF values from 0 to 2 with an interval size of 0.025 and EF values from 0.5 to 4 with an interval size of 0.05), an orthogonal experiment is created to produce 5600 sample points for the C-ECMS.

Subsequently, the multi-mode PHEV under study was equipped with 5600 groups of settings, and its performance was assessed under five driving cycles, namely WLTP3, Artemis-Urban, Artemis-Rural Road, Artemis-Motorway 130, and RTS95, with respect to fuel economy, SoC sustaining error, and battery capacity loss. Using the definition of Pareto domination, which is based on the 5 $\times$ 5600 groupings of outcomes acquired under the five driving cycles, five Pareto frontiers (PFs) are obtained by:

$$P(\boldsymbol{Y}) = \left\{ \boldsymbol{y}' \in \boldsymbol{Y} : \left\{ \boldsymbol{y}' \in \boldsymbol{Y} : \mathbf{y}' \succ \mathbf{y}'', \mathbf{y}'' = \mathbf{y}' \right\} = \varnothing \right\} \tag{6.18}$$

where $P(\boldsymbol{Y})$ is the solutions on the PF; $\boldsymbol{y}$ is feasible set of objective functions in $\mathbb{R}^3$, as

$$\boldsymbol{Y} = \left\{ \boldsymbol{y} = [\mathrm{Q_{Fuel}}, \mathrm{Q_{Loss}}, \mathrm{Q_{SoC}}]^{\boldsymbol{T}} \in \mathbb{R}^3; [\mathrm{Q_{Fuel}}, \mathrm{Q_{Loss}}, \mathrm{Q_{SoC}}]^T = \mathscr{M}(\mathrm{AF}, \mathrm{EF}, \mathrm{DC}) \right\} \tag{6.19}$$

where $\mathbf{y}' \succ \mathbf{y}''$ denotes that the values of all the elements in the vector$\mathbf{y}''$ dominate the values of enlacements in $\mathbf{y}'$; and $\mathscr{M}$ is the PHEV model running with different AF and EF values under a given driving condition, DC. In Fig.6.4, five Pareto frontiers (PFs) acquired under five standard cycles with varying AF and EF values are displayed. The PFs are projected onto the 2D planes for analysis and can be seen in 3D. The links between any two of the three optimisation objectives—fuel economy, ultimate SoC error, and battery capacity loss—are shown in Fig.6.4(b), (c), and (d).

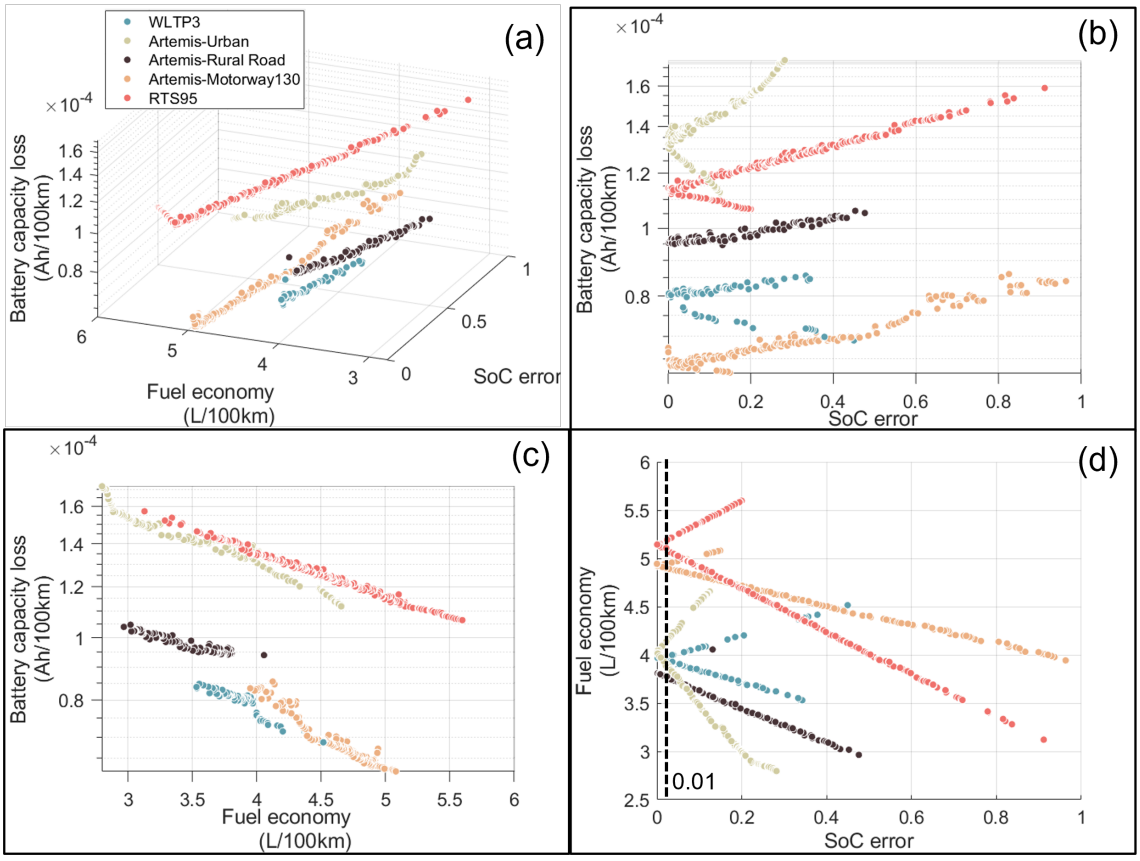

Fig. 6.4. Pareto frontier in five cycles: (a) PF in 3D space; (b) Projection on fuel economy-battery capacity loss coordinates; (c) Projection on SoC error-battery capacity loss coordinates; (d) Projection on SoC error-fuel economy coordinates

There exists a clear trade-off between battery capacity loss and fuel economy, as Fig. 6.4(c) illustrates. Essentially, fuel efficiency must be sacrificed in order to reduce battery capacity loss further. The battery capacity loss is not always linearly connected with the SoC sustain error, as shown in Fig. 6.4(b), for the majority of cases (4 out of the 5 driving cycles that were analysed). This implies that minimising the SoC sustaining faults does not always result in a reduction in battery capacity loss. Furthermore, Fig. 6.4(c) demonstrates the lack of a significant association between the fuel economy and the SoC sustaining error. Due to the fact that it is not possible to simply add the duty of battery capacity loss mitigation into either SoC sustaining control or fuel-saving control as in the previous research [364] [373] [374], the proposed 3D Hamiltonian matrix is required.

Establishing unified EF and AF settings is crucial for practice since real time control settings that provide a high degree of robustness should be fixed. Based on the Pareto frontiers found in Fig.6.4, this section presents a Pareto approach to find the global optimal EF and AF configuration. The unified EF and AF settings (EF $=$ 1.40 and AF $=$ 1.30) can be found by gathering the corresponding EF and AF values that constitute the Pareto frontiers in Fig.6.5 and selecting the nearest neighbour values of the average EF and AF values (shown by the two red dashed lines in Fig.6.5). The C-ECMS method with the unified settings is referred to as C-ECMS-U for the remainder of this work, with the capital U standing for "unified."

6.4.3 Evaluation of controlled results with baseline methods

In order to showcase the efficacy of the suggested C-ECMS, a comparative analysis was carried out during five typical driving cycles to assess the vehicle's performance, encompassing fuel efficiency, SoC sustaining precision and reductions in battery capacity. Two types of C-ECMS methods' parameter settings, i.e. 1) CECMS-U with a unified setting (found in the previous section) and 2) C-ECMS-I with independent parameter settings optimised for each cycle are explored. The baseline approaches are an offline DP

computation, the typical ECMS, and a rule-based control mechanism. Table 6.2 shows the specific settings for both baseline and C-ECMS approaches. This study primarily focuses on the charging-sustaining (CS) stage with an initial battery SoC of 0.3 because the functioning of the PHEV in charging-depleting (CD) stages is identical to that of the pure EV.

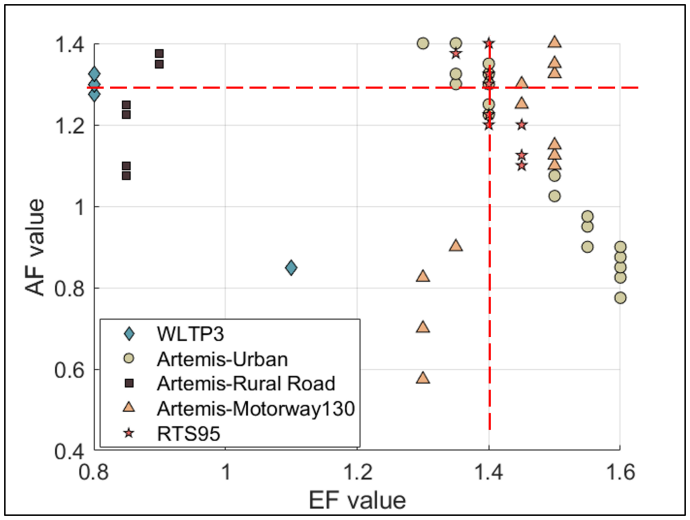

Fig. 6.5. Pareto frontier in five cycles: (a) PF in 3D space; (b) Projection on fuel economy-battery capacity loss coordinates; (c) Projection on SoC error-battery capacity loss coordinates; (d) Projection on SoC error-fuel economy coordinates

Table 6.2
Parameter settings for comparative methods

Control strategy	Working status	Set-up		
		Initial SoC	Discretisation	EF and AF
Rule-based	Hybrid mode switching	0.3	None	None
Standard ECMS	Power distribution (MG1, ICE)	0.3	$m = 30$	Only EF considered
C-ECMS-U	Power distribution (MG1, MG2, ICE)	0.3	$n = m = 30$	Unified parameters
C-ECMS-I	Power distribution (MG1, MG2, ICE)	0.3	$n = m = 30$	Independent parameters
Dynamic programming	Offline optimal calculation	0.3	None	

Table 6.3 compares the vehicle's performance in each of the five driving cycles that were examined. The PHEV's fuel economy ($L/100\ km$), battery capacity loss ($Ah/100\ km$), and SoC sustaining error (%) are all compared, and the relative gains made by the C-ECMS-U and the C-ECMS-I are computed.

When compared to the RB approach, the suggested C-ECMS generally offers notable improvements in SoC sustaining accuracy, fuel efficiency, and battery capacity loss mitigation. In comparison to the normal ECMS approach, the C-ECMS-I results in an average SoC sustaining error of 0.4%, lowers fuel consumption by 8.4%, and reduces battery capacity loss by 10.4%. When compared to the standard ECMS in high-speed driving conditions (the Artemis Motorway 130 cycle and the RTS95 cycle), the improvement in battery-sustaining accuracy is not statistically significant. However, the C-ECMS-I can still reduce the fuel consumption by up to 7.1% and battery capacity loss by 16.7%, for example, under the Artemis-Urban cycles. This is due to the fact that, with properly adjusted parameters, the suggested system can effectively balance both short- and long-term objectives.

Under the presumption that all road information was known beforehand, the DP findings showed the powertrain's theoretically ideal performance. The PHEV managed by the suggested C-ECMS-I, and followed by the C-ECMS-U, is the most similar to the benchmark results attained by DP, according to the results listed in Table 6.3. Compared to the rule-based approach and the conventional ECMS method, both C-ECMS systems have seen significant advancements.

Furthermore, the outcomes show that the suggested C-ECMS-U with the unified configuration performs better than the rule-based approach and the conventional ECMS and adapts effectively to the majority of driving cycles. While the C-ECMS-U may not always be able to match the regular ECMS in terms of best SoC (State of Charge) maintaining accuracy, most driving cycles will find this compromise to be acceptable because it complies with the SAE standard.

Optimising the EF (equivalent factor) and AF (acceleration factor) parameters based on unique cycle characteristics is essential for improved PHEV (Plug-in Hybrid Electric Vehicle) performance. This is the reason the C-ECMS-I method, which uses specific EF and AF settings, consistently performs better than alternative methods.

Table 6.3
Comparison of C-ECMS with baseline methods

Driving cycle	Method	SoC error	Fuel economy*	Fuel consumption reduction**	Battery capacity loss*	Battery capacity loss reduction**
WLTP3	Rule-based	6.3%	4.608	-	10.122	-
	ECMS	2.1%	4.508	-	10.298	-
	C-ECMS-U	2.3%	4.535	-0.6%	7.130	30.8%
	C-ECMS-I	0.3%	3.860	12%	7.959	22.7%
	DP	0.0%	3.840	-	7.779	-
Artemis Urban	Rule-based	1.0%	4.493	-	21.513	-
	ECMS	0.6%	4.570	-	19.265	-
	C-ECMS-U	1.4%	4.245	7.1%	16.042	16.7%
	C-ECMS-I	0.6%	4.215	7.8%	16.039	16.7%
	DP	0.0%	4.206	-	15.983	-
Artemis Rural Road	Rule-based	6.3%	4.503	-	10.988	-
	ECMS	0.0%	4.173	-	11.065	-
	C-ECMS-U	7.5%	4.147	0.6%	9.440	14.7%
	C-ECMS-I	0.5%	3.804	8.8%	9.504	14.1%
	DP	0.0%	3.708	-	9.487	-
Artemis Motorway 130	Rule-based	2.8%	5.267	-	6.728	-
	ECMS	1.6%	5.168	-	6.083	-
	C-ECMS-U	1.0%	4.920	4.8%	6.582	-8.2%
	C-ECMS-I	0.3%	4.927	4.7%	6.474	-6.4%
	DP	0.0%	4.905	-	4.213	-
RTS95	Rule-based	3.3%	5.814	-	12.378	-
	ECMS	0.2%	5.621	-	11.903	-
	C-ECMS-U	0.4%	5.128	8.8%	11.210	5.8%
	C-ECMS-I	0.5%	5.137	8.6%	11.344	4.7%
	DP	0.0%	5.082	-	10.093	-
Average values of C-ECMS-I		0.4%	-	8.4%	-	10.4%

* Fuel economy $(L/100\ km)$ and Battery capacity loss $(10^{-5}Ah/100\ km)$

**The values are calculated based on the results of the standard ECMS.

6.4.4 Processor-in-the-loop (PiL) validation

The Fig.3.2 in the previous section 3.2 provides an illustration of the PiL testing platform that was used for control function verification; with ETAS LABCAR, a real time computer with various I/Os and CAN ports, as the foundation of the PiL platform. Via an Ethernet connection, the host PC downloaded the vehicle model to the LABCAR. The host computer is configured with an NVIDIA GeForce GTX 3070 graphics processor, 16 GB of RAM, and an 11th generation Intel Core i7-11850H CPU running at 2.50 GHz. It runs Windows 10 64-bit. The energy management algorithms were implemented in the controller of the LABCAR for real time validation using C code. The CAN was used to connect the controller and the vehicle plant model, enabling LABCAR to simulate CAN-based automobile communication. In the PiL test, data was transferred in real time between the controller and the vehicle plant model, and a data file was created for the assessment of the vehicle's performance. The control algorithm's highest memory usage during real time control is 78 kb, and the control calculation takes 0.06 s for every time step of 1 s.

In Fig. 6.6, the DP offline simulation results are compared with the PiL results of the PHEV operated by the RB technique, standard ECM, and C-ECMS under the WLTP3 cycle. An EF and AF configuration that is ideal for the WLTP3 cycle is implemented by the C-ECMS. As shown in Fig. 6.6(b), all four techniques regulate the final SoC in proximity to the intended sustaining level. The fuel economy can be greatly increased by the C-ECMS, as shown in Fig.6.6(c). The fuel consumption per 100 km is reduced to 3.880 $L/100\ km$, which is close to the DP results of 3.840 $L/100km$. This is 15.5% less than the RB methods (4.592 $L/100\ km$) and 13.9% less than the conventional ECMS (4.506 $L/100\ km$). In comparison to the other baseline techniques, Figs. 6.6(e) and (f) demonstrate how the C-ECMS assigns MG2 with lower torque commands in the high-speed idle areas and assigns larger torque compensations to the ICE. The

proposed C-ECMS can lower battery capacity loss by 21.5% and 22.9%, respectively, when compared to the RB technique and regular ECMS, as shown in Fig. 6.6(d). As can be seen in Fig. 6.6, the powertrain managed by the C-ECMS displays a distinct SoC trend at the 1500, 3250, and 5000 s times, displaying a discharge-before-charge pattern in contrast to the usual approach. This is a result of the C-ECMS's superior sense of control over battery deterioration. During these times, leaving the battery discharged to power the MG2 will assist in preventing battery capacity degradation more than routinely charging and discharging. As shown in Fig. 6.6(d), this led to reduced battery capacity loss with the suggested C-ECMS in comparison to previous approaches.

6.5 | Chapter summary

For multi-mode PHEVs, the cuboid equivalent consumption minimisation strategy (C-ECMS) is proposed in this chapter. In order to better understand 1) the effect of Hamiltonian matrix dimensions on SoC control accuracy and 2) the effect of EF and AF settings on the Pareto frontier while taking fuel efficiency, SoC accuracy, and battery ageing into consideration, experiments are carried out under five driving cycles. The rule-based approach and the standard ECMS implemented in the same PHEV are contrasted with the C-ECMS-U with a unified setting produced by the numerical analysis and the C-ECMS-I with separate settings from Pareto frontier analysis of the cycles. The research led to the following conclusions:

1) The optimal Hamiltonian matrix in terms of SoC sustaining accuracy and computational effort is found to be a 30-by-30 matrix, according to the orthogonal experiment on the number of elements in the matrix.

2) Pareto frontier analysis is used to determine the unified AF and EF settings based on 5×5600 groups of individual testing with various combinations of AF and EF choices. It is indicated that with the unified settings fixed for real time control, the studied PHEV may be adjusted to most driving conditions.

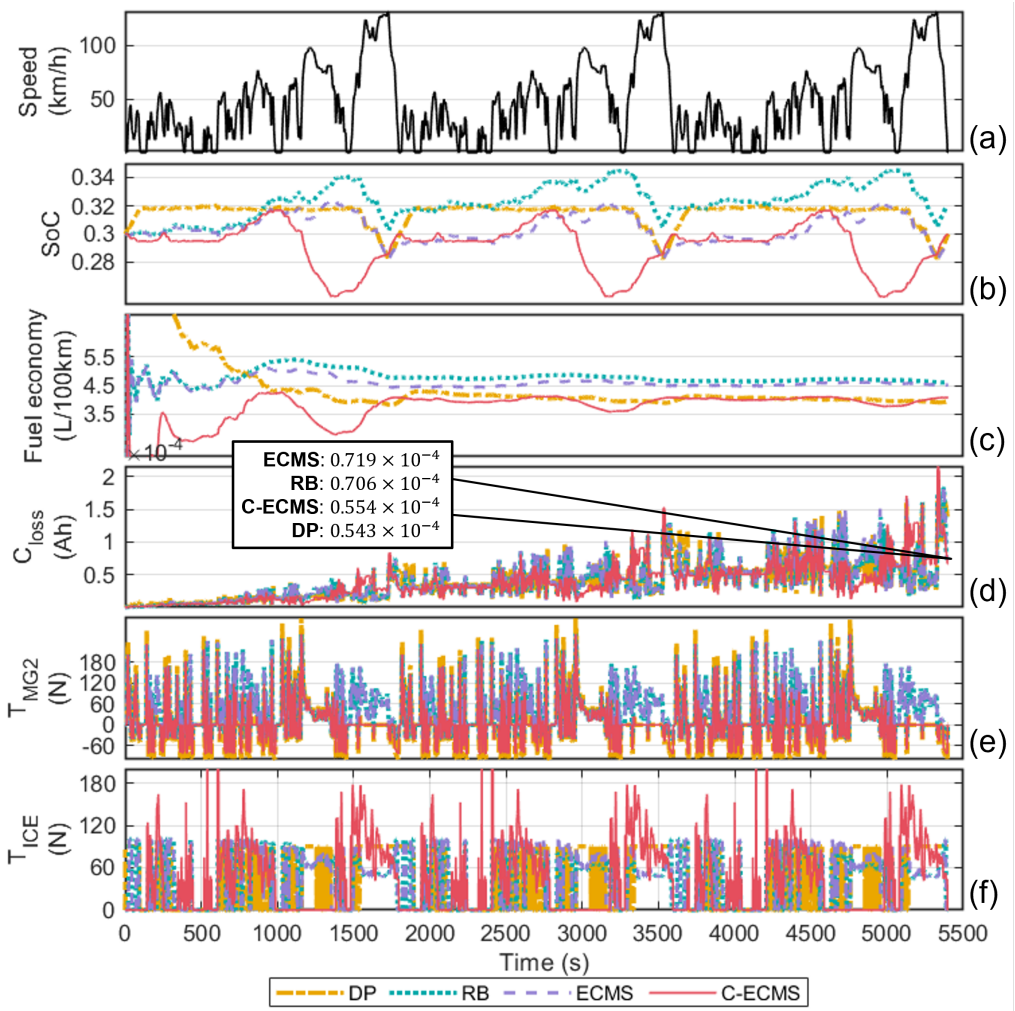

Fig. 6.6. Comparison of PHEV's performances based on three control strategy and DP offline simulation: (a) Test driving cycle; (b) SoC variations; (c) Fuel economies of the PHEV; (d) Battery capacity losses; (e) Torque generated by MG2; (f) Torque generated by ICE

3) In comparison to the rule-based approach and the standard ECMS, the C-ECMS-U utilising the unified configuration performs better by introducing the ageing factor (AF) and is adaptive to most driving cycles. In the Artemis Urban cycle, for example, it can reduce fuel consumption by up to 7.1% and battery capacity loss by 16.7% when compared to the normal ECMS approach.

CHAPTER 7

Conclusion and Future work

This thesis presents a framework for using state-of-the-art artificial intelligence technologies and modelling approaches to solve complicated engineering challenges. This chapter reviews the research impact, presents the key findings from the PhD study, and explores potential directions for future research.

7.1 | Conclusion

For the purpose of designing and optimising the energy management control of a multi-mode plug-in hybrid electric vehicle (PHEV), artificial intelligence (AI) methodologies, optimal control methods, and advanced digital modelling approaches have been developed. For this study, digital twin and artificial intelligence (AI) technologies, such as machine learning and evolutionary computing, were employed. The following findings of this thesis are drawn in accordance with the pertinent chapters:

1). **The proposed dedicated APSO for offline optimisation based on the digital twin improves the optimality and reliability of the EMS control for PHEVs.** According to the research conducted in Chapter 4, the DAPSO was developed based on a comprehensive assessment of the system's optimality, computation efficiency, and success rate in order to maximise the performance of the plug-in hybrid electric vehicle (PHEV) based on an objective function that assesses fuel usage and battery SoC maintenance.

When it comes to optimal control settings, the DAPSO performs better than the conventional PSO algorithms, which were also employed to track the performance of plug-in hybrid electric vehicles (PHEVs) during experimental evaluations. conclusions can be made as:

a) The DAPSO method can increase optimality over baseline algorithms for PHEVs by promoting more local searching for the appropriate threshold. This is done via an adaptive inertia factor adjusted by viewing the swarm's instant findings, which shows that the DAPSO performs better at managing the final SoC while reducing fuel consumption.

b) The DAPSO reduces processing time compared to baseline techniques by providing a state machine that regulates the exploitation-to-exploration ratio and terminates the DT-based PHEV optimisation.

c) According to the cross-validation testing of simulated real-world driving, the EMS settings gathered during the highway cycle utilising DAPSO can be used to create a uniform set-up for the investigated PHEV.

2). **The proposed intelligent digital model of a battery for real-time status estimation improves functionality with complex automotive battery working conditions**

Chapter 5 focuses primarily on the development of digital models for electric car batteries, with the goal of supporting intelligent energy management in advanced hybrid vehicles via real-time applications. By focusing on the complicated working conditions of battery operations, both model-based and data-driven approaches were applied across multiple aspects of direct/indirect SoH health indicators during the charging or discharging process. The findings of this chapter can be summarised as:

a) For the direct health indicators in the battery charging process, the proposed online double-layer system identification (ODSI) scheme enables real-time battery modelling. It offers immediate feedback through a closed-loop approach, eliminating the need for

retraining. This efficient system combines an offline 2-RC model with an online deep convolutional neural network (DCNN) to estimate battery health quickly. Moreover, the proposed ODSI structure allows accurate capacity loss predictions by incorporating existing data.

b) For the direct health indicators in the battery's random discharging process, the proposed asynchronous system of joint estimation for battery status provides real-time battery prediction and monitoring during discharge, making it suitable for online applications. Real-time data improves SoC estimation due to the LSTM 1's open-loop prediction, reducing the need for an additional battery model to conserve computational resources. The LSTM 2 predicts the time the battery takes to complete discharge to the cut-off voltage, allowing for easy SoH calculation via correlation. This method improves adaptability and reliability in real time applications, particularly when uncertainties exist while driving.

c) For the indirect health indicators in the battery charging process, the proposed multi-kernel ARD-GPR frame was employed and adapted for data-driven SoH estimation. With the experimental database, the best compromise of construction for multi-kernel functions with complex temperatures was determined with an optimal allocation ratio of 0.96; with this setting, the proposed multi-kernel ARD-GPR achieved an average 7.1% lower RMSE compared to the conventional GPR methods. Subsequently, an analysis of the variations in ARD lengths during the degradation process revealed that the multi-kernel ARD-GPR framework is capable of estimating degradation levels based on kernel ARD length scales and attributing the importance of operational performance, which makes it a practical and easily applicable approach in EV applications.

3) **For multi-mode PHEVs, the proposed cuboid equivalent consumption minimisation strategy (C-ECMS) leads to superior performance for the online optimal management while considering multiple objectives from various time scales**

In Chapter 6, C-ECMS's advantage appears in its ability to optimise PHEV operation by establishing a balance between fuel efficiency, battery health, and SoC control accuracy, resulting in increased overall performance and efficiency in real-world driving scenarios. Conclusions can be drawn as:

a) The best Hamiltonian matrix for maintaining the accuracy of the SoC and processing effort is a 30-by-30 matrix, as determined by an orthogonal experiment on matrix elements.

b) The combined AF and EF settings are determined using Pareto frontier analysis, based on 5×5600 testing groups with different AF and EF combinations. Adjusting the unified parameters for real-time control allows the PHEV to adapt to various driving situations.

c) The C-ECMS-U, which uses a unified configuration, outperforms the rule-based and standard ECMS approaches by incorporating an ageing factor (AF) and adapting to most driving cycles. The C-ECMS-U can reduce fuel usage by up to 7.1% and battery capacity degradation by 16.7% compared to traditional ECMS methods.

7.2 | Research contributions and academic impact

The principal contributions and research impact of this PhD research project for both the industry and the academic community are presented as below:

7.2.1 contributions of the thesis

1) **Research part 1: Dedicated APSO for offline optimisation based on the digital twin of EVs**

- A collaborative project has been completed, in part with Jiangsu Industrial Technology Research Institute (JITRI) and in part with the State Key Laboratory of Automotive Safety and Energy (Tsinghua University) under *Project KF2029*.

- A Part of research has been presented and published in the 6th IFAC Conference on Engine and Powertrain Control, Simulation and Modeling (*Aug 2021, E-COSM 2021, Tokyo/Virtual Conference*) [375].

- The entire research has been published in *IEEE Transactions on Transportation Electrification*, [26] which is a top journal (*IF=7, JCR Q1*) in the field of propulsion and power and energy conversion for all kinds of electrified vehicles.

2) **Research part 2: Intelligent digital model of a battery and real-time status estimation**

- The proposed online double-layer system identification scheme (ODSI) has been presented and published in the 13th International Conference on Applied Energy (*Dec 2021, ICAE 2021, Bangkok/ Virtual Conference*) [27].

- The asynchronous system of joint estimation has been presented in the Applied Energy symposium: Low carbon cities & Urban energy systems (*Dec 2022, ICAE CUE 2022, MATSUE, JAPAN/ONLINE*).

- The research of multi-kernel ARD-GPR frame has been submitted to the journal *IEEE Transactions on Industrial Informatics* (Top journal in informatics theory and practice in industrial settings, with *IF=12.3, JCR Q1*, under reviewing).

3) **Research part 3: Online optimal control of cuboid-ECMS for multi-mode PHEVs considering multiple objectives in diverse time scales**

- Collaborative research with MAHLE Corporation was conducted on the prototype of a multi-mode PHEV, for advanced online optimal control.

- The proposed Cuboid euivalent consumption minimisation strategy (C-ECMS) has been published by the journal *Applied Energy*, [28] a top journal in the field of

the optimal use of energy resources and the analysis and optimisation of energy processes, with *IF=11.2, JCR Q1*.

7.2.2 Academic impact

For the research community, the published results are widely cited by research papers, i.e. [376]–[379] or reviewed papers, i.e. [380]–[382]. Also, the work in Chapter 4 has been translated into software and has been actively employed in industrial applications at JITRI (Jiangsu Industrial Technology Research Institute). Additionally, a portion of the PhD research has been evaluated for possible market and industrial uses. The research content in Chapters 4 and 6 has served as the basis for a relative business strategy, and has been widely entered in several competitions. A national silver award in an entrepreneurship competition was won by a team under the leadership of the author.

7.3 Future work

Several possible areas for further work and research have been identified based on this study's design and optimisation of a multi-mode plug-in hybrid electric vehicle's (PHEV) energy management control using digital twin technologies and artificial intelligence (AI) methodologies:

1) To improve energy forecasting models by taking into account variables like weather, traffic, and driver behaviour in order to maximise energy management in a variety of real-world situations.

2) To include PHEVs in smart grids and investigate how AI can support bilateral interaction for demand response, grid management, and vehicle battery monitoring.

3) To address the issues of cyber-security and safety related to multi-mode powertrains, such as preventing cyber-attacks and guaranteeing safe communication between car parts.

4) To develop commercialisation and cost-cutting strategies in order to lower the cost of multi-mode powertrains and increase their availability to a larger spectrum of users and sectors.

5) To examine user behaviour and driving patterns to develop customised energy management profiles that enable plug-in hybrid electric vehicles (PHEVs) to adjust their powertrain operating to suit the demands and habits of individual drivers.

6) To develop methods for employing multi-mode PHEVs in fleet electrification, which can significantly save fuel and emissions in fleets of government and commercial vehicles.

References

[1] IEA, "CO2 Emissions in 2022," International Energy Agency, Paris, Tech. Rep., 2023.

[2] Z. Liu, Z. Deng, S. Davis & P. Ciais, "Monitoring global carbon emissions in 2022," *Nature Reviews Earth & Environment*, vol. 4, no. 4, pp. 205–206, 2023.

[3] S. Bouckaert, A. F. Pales, C. McGlade, U. Remme, B. Wanner, L. Varro, D. D'Ambrosio & T. Spencer, "Net zero by 2050: A roadmap for the global energy sector," 2021.

[4] IEA, "Global EV Outlook 2023," International Energy Agency, Paris, Tech. Rep., 2023.

[5] M. Ovaere & S. Proost, "Cost-effective reduction of fossil energy use in the European transport sector: An assessment of the Fit for 55 Package," *Energy Policy*, vol. 168, p. 113 085, 2022.

[6] PwC, "Digital Auto Report 2023," PwC, Tech. Rep., 2023.

[7] B. Ondrej, D. Johannes, G. Michael & K. Martin, "Outlook on the automotive software and electronics market through 2030," McKinsey & Company, Tech. Rep., 2023.

[8] Templeton & Partners, "Digital Transformation in Automotive Market report 2023," Templeton & Partners, Tech. Rep., 2023.

[9] KPMG, "The Digitalisation of the UK Automotive Industry," KPMG, Tech. Rep., 2017.

[10] A. Vălean, *Key technologies to boost the digitalisation of transport*.

[11] D.-D. Tran, M. Vafaeipour, M. El Baghdadi, R. Barrero, J. Van Mierlo & O. Hegazy, "Thorough state-of-the-art analysis of electric and hybrid vehicle powertrains: Topologies and integrated energy management strategies," *Renewable and Sustainable Energy Reviews*, vol. 119, p. 109 596, 2020.

[12] W. Zhuang, S. Li, X. Zhang, D. Kum, Z. Song, G. Yin & F. Ju, "A survey of powertrain configuration studies on hybrid electric vehicles," *Applied Energy*, vol. 262, p. 114 553, 2020.

[13] D. S. Cardoso, P. O. Fael & A. Espirito-Santo, "A review of micro and mild hybrid systems," *Energy reports*, vol. 6, pp. 385–390, 2020.

[14] Y. Yang, X. Hu, H. Pei & Z. Peng, "Comparison of power-split and parallel hybrid powertrain architectures with a single electric machine: Dynamic programming approach," *Applied energy*, vol. 168, pp. 683–690, 2016.

[15] Y. Xie, J. Zhang, D. Jiang, Z. Liu & L. Tian, "Emulation of Integrated Starter/Generator Using Power Electronic Devices," *IEEE Transactions on Industry Applications*, 2023.

[16] S. Onori, L. Serrao & G. Rizzoni, *Hybrid Electric Vehicles Energy Management Strategies*. Springer, 2016.

[17] A. M. Andwari, A. Pesiridis, S. Rajoo, R. Martinez-Botas & V. Esfahanian, "A review of Battery Electric Vehicle technology and readiness levels," *Renewable and Sustainable Energy Reviews*, vol. 78, pp. 414–430, 2017.

[18] W. Cai, X. Wu, M. Zhou, Y. Liang & Y. Wang, "Review and development of electric motor systems and electric powertrains for new energy vehicles," *Automotive Innovation*, vol. 4, pp. 3–22, 2021.

[19] N. Higuchi, Y. Sunaga, M. Tanaka & H. Shimada, "Development of a new two-motor plug-in hybrid system," *SAE International Journal of Alternative Powertrains*, vol. 2, no. 1, pp. 135–145, 2013.

[20] Y. Wang, A. Biswas, P. G. Anselma, A. Rathore, J. Toller, O. Rane, B. Wasacz, J. Roeleveld, Z. K. Motamed & A. Emadi, "Adaptive Real-Time Energy Management of a Multi-Mode Hybrid Electric Powertrain," SAE Technical Paper, Tech. Rep., 2022.

[21] R. R. Kumar & K. Alok, "Adoption of electric vehicle: A literature review and prospects for sustainability," *Journal of Cleaner Production*, vol. 253, p. 119 911, 2020.

[22] A. A. Habib, M. K. Hasan, G. F. Issa, D. Singh, S. Islam & T. M. Ghazal, "Lithium-Ion Battery Management System for Electric Vehicles: Constraints, Challenges, and Recommendations," *Batteries*, vol. 9, no. 3, p. 152, 2023.

[23] C. Xu, P. Behrens, P. Gasper, K. Smith, M. Hu, A. Tukker & B. Steubing, "Electric vehicle batteries alone could satisfy short-term grid storage demand by as early as 2030," *Nature Communications*, vol. 14, no. 1, p. 119, 2023.

[24] A. W. Thompson, "Economic implications of lithium ion battery degradation for Vehicle-to-Grid (V2X) services," *Journal of Power Sources*, vol. 396, pp. 691–709, 2018.

[25] A. Breiter, T. Schuldt, M. Linder, G. Siccardo & N. Vekić, "Battery recycling takes the driver's seat," 2023.

[26] C. Zhang, Q. Zhou, B. Shuai, H. Williams, Y. Li, L. Hua & H. Xu, "Dedicated Adaptive Particle Swarm Optimization Algorithm for Digital Twin Based Control Optimization of the Plug-in Hybrid Vehicle," *IEEE Transactions on Transportation Electrification*, 2022.

[27] C. Zhang, Q. Zhou, M. Hua, C. Wang & H. Xu, "Online double-layer system identification scheme for battery state-of-health prediction," in *Proceedings of the International Conference on Applied Energy, Thailand/Virtual*, vol. 24, 2021.

[28] C. Zhang, Q. Zhou, M. Hua, H. Xu, M. Bassett & F. Zhang, "Cuboid equivalent consumption minimization strategy for energy management of multi-mode plug-in hybrid vehicles considering diverse time scale objectives," *Applied Energy*, vol. 351, p. 121 901, 2023.

[29] F. Tao, H. Zhang, A. Liu & A. Y. Nee, "Digital twin in industry: State-of-the-art," *IEEE Transactions on industrial informatics*, vol. 15, no. 4, pp. 2405–2415, 2018.

[30] Z. Zhang, Z. Zhu, J. Zhang & J. Wang, "Construction of intelligent integrated model framework for the workshop manufacturing system via digital twin," *The International Journal of Advanced Manufacturing Technology*, pp. 1–14, 2022.

[31] X. Sun, J. Bao, J. Li, Y. Zhang, S. Liu & B. Zhou, "A digital twin-driven approach for the assembly-commissioning of high precision products," *Robotics and Computer-Integrated Manufacturing*, vol. 61, p. 101 839, 2020.

[32] R. Ala-Laurinaho, J. Autiosalo, A. Nikander, J. Mattila & K. Tammi, "Data link for the creation of digital twins," *IEEE Access*, vol. 8, pp. 228 675–228 684, 2020.

[33] P. Aivaliotis, K. Georgoulias & G. Chryssolouris, "The use of Digital Twin for predictive maintenance in manufacturing," *International Journal of Computer Integrated Manufacturing*, vol. 32, no. 11, pp. 1067–1080, 2019.

[34] N. Nikolakis, K. Alexopoulos, E. Xanthakis & G. Chryssolouris, "The digital twin implementation for linking the virtual representation of human-based production tasks to their physical counterpart in the factory-floor," *International Journal of Computer Integrated Manufacturing*, vol. 32, no. 1, pp. 1–12, 2019.

[35] S. H. Choi, K.-B. Park, D. H. Roh, J. Y. Lee, M. Mohammed, Y. Ghasemi & H. Jeong, "An integrated mixed reality system for safety-aware human-robot collaboration using deep learning and digital twin generation," *Robotics and Computer-Integrated Manufacturing*, vol. 73, p. 102 258, 2022.

[36] W. Jia, W. Wang & Z. Zhang, "From simple digital twin to complex digital twin Part I: A novel modeling method for multi-scale and multi-scenario digital twin," *Advanced Engineering Informatics*, vol. 53, p. 101 706, 2022.

[37] A. Rasheed, O. San & T. Kvamsdal, "Digital twin: Values, challenges and enablers from a modeling perspective," *Ieee Access*, vol. 8, pp. 21 980–22 012, 2020.

[38] F. Tao & M. Zhang, "Digital twin shop-floor: a new shop-floor paradigm towards smart manufacturing," *IEEE access*, vol. 5, pp. 20 418–20 427, 2017.

[39] Y. Zheng, L. Chen, X. Lu, Y. Sen & H. Cheng, "Digital twin for geometric feature online inspection system of car body-in-white," *International Journal of Computer Integrated Manufacturing*, vol. 34, no. 7-8, pp. 752–763, 2021.

[40] Y. Wei, T. Hu, T. Zhou, Y. Ye & W. Luo, "Consistency retention method for CNC machine tool digital twin model," *Journal of Manufacturing Systems*, vol. 58, pp. 313–322, 2021.

[41] F. Boulfani, X. Gendre, A. Ruiz-Gazen & M. Salvignol, "Anomaly detection for aircraft electrical generator using machine learning in a functional data framework," in *2020 Global Congress on Electrical Engineering (GC-ElecEng)*, IEEE, 2020, pp. 27–32.

[42] R. M. Scheffel, A. A. Fröhlich & M. Silvestri, "Automated fault detection for additive manufacturing using vibration sensors," *International Journal of Computer Integrated Manufacturing*, vol. 34, no. 5, pp. 500–514, 2021.

[43] D. Jones, C. Snider, A. Nassehi, J. Yon & B. Hicks, "Characterising the Digital Twin: A systematic literature review," *CIRP journal of manufacturing science and technology*, vol. 29, pp. 36–52, 2020.

[44] F. TAO, X. MA, Q. QI, W. LIU, H. ZHANG & C. ZHANG, "Theory and key technologies of digital twin connection and interaction," *Computer Integrated Manufacturing System*, vol. 29, no. 1, p. 1, 2023.

[45] N. BEISHEIM, M. RÄDLE, J. REICHWALD, M. LINDE, T. OTTa, S. AMANN & K. KASTNER, "Simultaneous Interdisciplinary Teamwork on Digital Twins in a 3D Collaborative Environment," in *Transdisciplinarity and the Future of Engineering: Proceedings of the 29th International Society of Transdisciplinary Engineering (ISTE) Global Conference, July 5–July 8, 2022, Cambridge, MA, USA*, IOS Press, vol. 28, 2022, p. 380.

[46] A. Tabbah, G. Fischl & M. Aries, "Evaluating Digital Twin light quantity data exchange between a virtual and physical environment," in *E3S Web of Conferences*, EDP Sciences, vol. 362, 2022.

[47] A. A. Malik & A. Brem, "Digital twins for collaborative robots: A case study in human-robot interaction," *Robotics and Computer-Integrated Manufacturing*, vol. 68, p. 102 092, 2021.

[48] E. Bottani, A. Cammardella, T. Murino, S. Vespoli, et al., "From the Cyber-Physical System to the Digital Twin: the process development for behaviour modelling of a Cyber Guided Vehicle in M2M logic," *XXII Summer School Francesco TurcoIndustrial Systems Engineering*, pp. 1–7, 2017.

[49] R. Ala-Laurinaho, J. Autiosalo, A. Nikander, J. Mattila & K. Tammi, "Data link for the creation of digital twins," *IEEE Access*, vol. 8, pp. 228 675–228 684, 2020.

[50] F. Tao, J. Cheng, Q. Qi, M. Zhang, H. Zhang & F. Sui, "Digital twin-driven product design, manufacturing and service with big data," *The International Journal of Advanced Manufacturing Technology*, vol. 94, pp. 3563–3576, 2018.

[51] Z. Liu, N. Meyendorf & N. Mrad, "The role of data fusion in predictive maintenance using digital twin," in *AIP conference proceedings*, AIP Publishing, vol. 1949, 2018.

[52] M. Zhang, F. Tao, B. Huang, A. Liu, L. Wang, N. Anwer & A. Nee, "Digital twin data: methods and key technologies," *Digital Twin*, vol. 1, p. 2, 2022.

[53] F. Tao, M. Zhang, Y. Liu & A. Y. Nee, "Digital twin driven prognostics and health management for complex equipment," *Cirp Annals*, vol. 67, no. 1, pp. 169–172, 2018.

[54] F. Tao, Q. Qi & A. Y. C. Nee, *Digital twin driven service*. Academic Press, 2022.

[55] Z. Lei, H. Zhou, X. Dai, W. Hu & G.-P. Liu, "Digital twin based monitoring and control for DC-DC converters," *Nature Communications*, vol. 14, no. 1, p. 5604, 2023.

[56] Y. Zhou, Z. Fu, J. Zhang, W. Li & C. Gao, "A digital twin-based operation status monitoring system for port cranes," *Sensors*, vol. 22, no. 9, p. 3216, 2022.

[57] J. Wang, L. Ye, R. X. Gao, C. Li & L. Zhang, "Digital Twin for rotating machinery fault diagnosis in smart manufacturing," *International Journal of Production Research*, vol. 57, no. 12, pp. 3920–3934, 2019.

[58] J. Liu, S. Wang, X. Lu & T. Li, "Research on online status evaluation technology for main equipment of power transmission and transformation based on digital twin," in *2021 IEEE 5th Conference on Energy Internet and Energy System Integration (EI2)*, IEEE, 2021, pp. 3368–3373.

[59] Y. Yang, W. Meng & S. Zhu, "A digital twin simulation platform for multi-rotor UAV," in *2020 7th International Conference on Information, Cybernetics, and Computational Social Systems (ICCSS)*, IEEE, 2020, pp. 591–596.

[60] M. Schluse & J. Rossmann, "From simulation to experimentable digital twins: Simulation-based development and operation of complex technical systems," in *2016 IEEE international symposium on systems engineering (ISSE)*, IEEE, 2016, pp. 1–6.

[61] Z. Liu, N. Meyendorf & N. Mrad, "The role of data fusion in predictive maintenance using digital twin," in *AIP conference proceedings*, AIP Publishing, vol. 1949, 2018.

[62] D. Yang, Y. Cui, Q. Xia, F. Jiang, Y. Ren, B. Sun, Q. Feng, Z. Wang & C. Yang, "A digital twin-driven life prediction method of lithium-ion batteries based on adaptive model evolution," *Materials*, vol. 15, no. 9, p. 3331, 2022.

[63] w. Zhang et al., "Digital Twin Based Optimization Design Method for Aerospace Electric Thruster," *Journal of Astronautics*, vol. 43, no. 4, p. 518, 2022.

[64] R. Ward, C. Sun, J. Dominguez-Caballero, S. Ojo, S. Ayvar-Soberanis, D. Curtis & E. Ozturk, "Machining Digital Twin using real-time model-based simulations and lookahead function for closed loop machining control," *The International Journal of Advanced Manufacturing Technology*, vol. 117, no. 11-12, pp. 3615–3629, 2021.

[65] M. Liu, S. Fang, H. Dong & C. Xu, "Review of digital twin about concepts, technologies, and industrial applications," *Journal of Manufacturing Systems*, vol. 58, pp. 346–361, 2021.

[66] Q. Zhou, C. Zhang, Y. Li, et al., "Robust optimization of energy management strategy in hybrid vehicles based on digital twin and PSO algorithm," *J. Automot. Saf. Energy*, vol. 13, pp. 517–525, 2022.

[67] R. N. Bolton, J. R. McColl-Kennedy, L. Cheung, A. Gallan, C. Orsingher, L. Witell & M. Zaki, "Customer experience challenges: bringing together digital, physical and social realms," *Journal of service management*, vol. 29, no. 5, pp. 776–808, 2018.

[68] A. Rasheed, O. San & T. Kvamsdal, "Digital twin: Values, challenges and enablers from a modeling perspective," *Ieee Access*, vol. 8, pp. 21 980–22 012, 2020.

[69] A. Fuller, Z. Fan, C. Day & C. Barlow, "Digital twin: Enabling technologies, challenges and open research," *IEEE access*, vol. 8, pp. 108 952–108 971, 2020.

[70] W. Li, M. Rentemeister, J. Badeda, D. Jöst, D. Schulte & D. U. Sauer, "Digital twin for battery systems: Cloud battery management system with online state-of-charge and state-of-health estimation," *Journal of energy storage*, vol. 30, p. 101 557, 2020.

[71] Q. Zhou, C. Wang, Z. Sun, J. Li, H. Williams & H. Xu, "Human-knowledge-augmented Gaussian process regression for state-of-health prediction of lithium-ion batteries with charging curves," *Journal of Electrochemical Energy Conversion and Storage*, vol. 18, no. 3, p. 030 907, 2021.

[72] H. Li, M. B. Kaleem, I.-J. Chiu, D. Gao & J. Peng, "A digital twin model for the battery management systems of electric vehicles," in *2021 IEEE 23rd Int Conf on High Performance Computing & Communications; 7th Int Conf on Data Science & Systems; 19th Int Conf on Smart City; 7th Int Conf on Dependability in Sensor, Cloud & Big Data Systems & Application (HPCC/DSS/SmartCity/DependSys)*, IEEE, 2021, pp. 1100–1107.

[73] S. Venkatesan, K. Manickavasagam, N. Tengenkai & N. Vijayalakshmi, "Health monitoring and prognosis of electric vehicle motor using intelligent-digital twin," *IET Electric Power Applications*, vol. 13, no. 9, pp. 1328–1335, 2019.

[74] F. Toso, R. Torchio, A. Favato, P. G. Carlet, S. Bolognani & P. Alotto, "Digital twins as electric motor soft-sensors in the automotive industry," in *2021 IEEE International Workshop on Metrology for Automotive (MetroAutomotive)*, IEEE, 2021, pp. 13–18.

[75] Y. Liu, Z. Wang, K. Han, Z. Shou, P. Tiwari & J. H. Hansen, "Sensor fusion of camera and cloud digital twin information for intelligent vehicles," in *2020 IEEE Intelligent Vehicles Symposium (IV)*, IEEE, 2020, pp. 182–187.

[76] B. Yu, C. Chen, J. Tang, S. Liu & J.-L. Gaudiot, "Autonomous vehicles digital twin: A practical paradigm for autonomous driving system development," *Computer*, vol. 55, no. 9, pp. 26–34, 2022.

[77] C. Llopis-Albert, F. Rubio & S. Zeng, "Multiobjective optimization framework for designing a vehicle suspension system. A comparison of optimization algorithms," *Advances in Engineering Software*, vol. 176, p. 103 375, 2023.

[78] X. Wang, R. Yu, M. Ye & M. Hao, "Enhancing Digital Twin Model for Connected Vehicles by Powertrain and Longitudinal Dynamics," in *2023 IEEE/CIC International Conference on Communications in China (ICCC)*, IEEE, 2023, pp. 1–6.

[79] C. Grasselli, A. Melis, R. Girau & F. Callegati, "A digital twin for enhanced cybersecurity in connected vehicles," in *2023 23rd International Conference on Transparent Optical Networks (ICTON)*, IEEE, 2023, pp. 1–4.

[80] M. Ali, G. Kaddoum, W.-T. Li, C. Yuen, M. Tariq & H. V. Poor, "A smart digital twin enabled security framework for vehicle-to-grid cyber-physical systems," *IEEE Transactions on Information Forensics and Security*, 2023.

[81] S. Shadrin, D. Makarova, A. Ivanov & N. Maklakov, "Safety Assessment of Highly Automated Vehicles Using Digital Twin Technology," in *2021 Intelligent*

Technologies and Electronic Devices in Vehicle and Road Transport Complex (TIRVED), IEEE, 2021, pp. 1–5.

[82] B. Wang, C. Zhang, M. Zhang, C. Liu, Z. Xie & H. Zhang, "Digital Twin Analysis for Driving Risks Based on Virtual Physical Simulation Technology," *IEEE Journal of Radio Frequency Identification*, vol. 6, pp. 938–942, 2022.

[83] Y. Gao, S. Yang, Y. Chen, W. Li, J. Yang & F. Yi, "Multi-physical cooperative control of plug-in hybrid electric vehicles via cyber hierarchy and interactional network," *Communications in Nonlinear Science and Numerical Simulation*, vol. 120, p. 107 158, 2023.

[84] C. Yang, R. Chen, W. Wang, Y. Li, X. Shen & C. Xiang, "Cyber-Physical Optimization-based Fuzzy Control Strategy for Plug-in Hybrid Electric Buses Using Iterative Modified Particle Swarm Optimization," *IEEE Transactions on Intelligent Vehicles*, 2023.

[85] Y. Ye, B. Xu, J. Zhang, B. Lawler & B. Ayalew, "Reinforcement Learning-Based Energy Management System Enhancement Using Digital Twin for Electric Vehicles," in *2022 IEEE Vehicle Power and Propulsion Conference (VPPC)*, IEEE, 2022, pp. 1–6.

[86] Y. Li, S. Wang, X. Duan, S. Liu, J. Liu & S. Hu, "Multi-objective energy management for Atkinson cycle engine and series hybrid electric vehicle based on evolutionary NSGA-II algorithm using digital twins," *Energy Conversion and Management*, vol. 230, p. 113 788, 2021.

[87] C. Zhang, Q. Zhou, B. Shuai, H. Williams, Y. Li, L. Hua & H. Xu, "Dedicated Adaptive Particle Swarm Optimization Algorithm for Digital Twin Based Control Optimization of the Plug-in Hybrid Vehicle," *IEEE Transactions on Transportation Electrification*, 2022.

[88] Y. Wang, J. Tian, Z. Sun, L. Wang, R. Xu, M. Li & Z. Chen, "A comprehensive review of battery modeling and state estimation approaches for advanced battery management systems," *Renewable and Sustainable Energy Reviews*, vol. 131, p. 110 015, 2020.

[89] K. Liu, K. Li, Q. Peng & C. Zhang, "A brief review on key technologies in the battery management system of electric vehicles," *Frontiers of mechanical engineering*, vol. 14, pp. 47–64, 2019.

[90] K. Liu, Y. Gao, C. Zhu, K. Li, M. Fei, C. Peng, X. Zhang & Q.-L. Han, "Electrochemical modeling and parameterization towards control-oriented management of lithium-ion batteries," *Control Engineering Practice*, vol. 124, p. 105 176, 2022.

[91] R. Guo & W. Shen, "A review of equivalent circuit model based online state of power estimation for lithium-ion batteries in electric vehicles," *Vehicles*, vol. 4, no. 1, pp. 1–29, 2021.

[92] M.-F. Ng, J. Zhao, Q. Yan, G. J. Conduit & Z. W. Seh, "Predicting the state of charge and health of batteries using data-driven machine learning," *Nature Machine Intelligence*, vol. 2, no. 3, pp. 161–170, 2020.

[93] J. Zhou, B. Xing & C. Wang, "A review of lithium ion batteries electrochemical models for electric vehicles," in *E3S Web of Conferences*, EDP Sciences, vol. 185, 2020, p. 04 001.

[94] N. Baba, H. Yoshida, M. Nagaoka, C. Okuda & S. Kawauchi, "Numerical simulation of thermal behavior of lithium-ion secondary batteries using the enhanced single particle model," *Journal of Power Sources*, vol. 252, pp. 214–228, 2014.

[95] Z. Cen & P. Kubiak, "Lithium-ion battery SOC/SOH adaptive estimation via simplified single particle model," *International Journal of Energy Research*, vol. 44, no. 15, pp. 12 444–12 459, 2020.

[96] Y. Liu, R. Ma, S. Pang, L. Xu, D. Zhao, J. Wei, Y. Huangfu & F. Gao, "A nonlinear observer SOC estimation method based on electrochemical model for lithium-ion battery," *IEEE Transactions on Industry Applications*, vol. 57, no. 1, pp. 1094–1104, 2020.

[97] L. Oca, E. Miguel, E. Agirrezabala, A. Herran, E. Gucciardi, L. Otaegui, E. Bekaert, A. Villaverde & U. Iraola, "Physico-chemical parameter measurement and model response evaluation for a pseudo-two-dimensional model of a commercial lithium-ion battery," *Electrochimica Acta*, vol. 382, p. 138 287, 2021.

[98] Y. Gao, K. Liu, C. Zhu, X. Zhang & D. Zhang, "Co-estimation of state-of-charge and state-of-health for lithium-ion batteries using an enhanced electrochemical model," *IEEE Transactions on Industrial Electronics*, vol. 69, no. 3, pp. 2684–2696, 2021.

[99] R. Yang, Z. Li, Z. Chen, M. S. Ali & G. Chen, "Fast State-of-Charge Estimation for Lithium-Ion Batteries Using a Simplified Electrochemical Model without Initial State Restrictions," *IEEE Transactions on Transportation Electrification*, 2023.

[100] S. Nejad, D. Gladwin & D. Stone, "A systematic review of lumped-parameter equivalent circuit models for real-time estimation of lithium-ion battery states," *Journal of Power Sources*, vol. 316, pp. 183–196, 2016.

[101] X. Lai, W. Gao, Y. Zheng, M. Ouyang, J. Li, X. Han & L. Zhou, "A comparative study of global optimization methods for parameter identification of different equivalent circuit models for Li-ion batteries," *Electrochimica Acta*, vol. 295, pp. 1057–1066, 2019.

[102] B. Y. Liaw, G. Nagasubramanian, R. G. Jungst & D. H. Doughty, "Modeling of lithium ion cells—A simple equivalent-circuit model approach," *Solid state ionics*, vol. 175, no. 1-4, pp. 835–839, 2004.

[103] V. Pizarro-Carmona, S. Castano-Solis, M. Cortes-Carmona, J. Fraile-Ardanuy & D. Jimenez-Bermejo, "GA-based approach to optimize an equivalent electric circuit model of a Li-ion battery-pack," *Expert Systems with Applications*, vol. 172, p. 114 647, 2021.

[104] Y. Li, K. Liu, A. M. Foley, A. Zülke, M. Berecibar, E. Nanini-Maury, J. Van Mierlo & H. E. Hoster, "Data-driven health estimation and lifetime prediction of lithium-ion batteries: A review," *Renewable and sustainable energy reviews*, vol. 113, p. 109 254, 2019.

[105] K. A. Severson, P. M. Attia, N. Jin, N. Perkins, B. Jiang, Z. Yang, M. H. Chen, M. Aykol, P. K. Herring, D. Fraggedakis, et al., "Data-driven prediction of battery cycle life before capacity degradation," *Nature Energy*, vol. 4, no. 5, pp. 383–391, 2019.

[106] D. Castanho, M. Guerreiro, L. Silva, J. Eckert, T. Antonini Alves, Y. d. S. Tadano, S. L. Stevan Jr, H. V. Siqueira & F. C. Corrêa, "Method for SoC estimation in lithium-ion batteries based on multiple linear regression and particle swarm optimization," *Energies*, vol. 15, no. 19, p. 6881, 2022.

[107] S. S. Mansouri, P. Karvelis, G. Georgoulas & G. Nikolakopoulos, "Remaining useful battery life prediction for UAVs based on machine learning," *IFAC-PapersOnLine*, vol. 50, no. 1, pp. 4727–4732, 2017.

[108] J. Wen & Z. He, "Charge Time Prediction Model of Power Battery based on Random Forest algorithm," in *2022 34th Chinese Control and Decision Conference (CCDC)*, IEEE, 2022, pp. 2631–2636.

[109] I. A. Majid, R. F. Rahman, N. A. Setiawan & A. I. Cahyadi, "Electric vehicle battery dynamics modelling using support vector machine," in *2013 Joint International Conference on Rural Information & Communication Technology and Electric-Vehicle Technology (rICT & ICeV-T)*, IEEE, 2013, pp. 1–3.

[110] L. Zhang, K. Li, D. Du, C. Zhu & M. Zheng, "A sparse least squares support vector machine used for SOC estimation of Li-ion Batteries," *IFAC-PapersOnLine*, vol. 52, no. 11, pp. 256–261, 2019.

[111] G. Dziechciaruk, M. Michalczuk, B. Ufnalski & L. M. Grzesiak, "Dynamic model of a lithium-ion cell using an artificial feedforward neural network with dynamical signal preprocessing," *Journal of Energy Storage*, vol. 31, p. 101 503, 2020.

[112] S. Saxena, L. Ward, J. Kubal, W. Lu, S. Babinec & N. Paulson, "A convolutional neural network model for battery capacity fade curve prediction using early life data," *Journal of Power Sources*, vol. 542, p. 231 736, 2022.

[113] G. Capizzi, F. Bonanno & G. M. Tina, "Recurrent neural network-based modeling and simulation of lead-acid batteries charge–discharge," *IEEE Transactions on Energy Conversion*, vol. 26, no. 2, pp. 435–443, 2011.

[114] A. R. Yuliani, A. Ramdan, V. Zilvan, A. A. Supianto, D. Krisnandi, R. S. Yuwana, D. Prajitno & H. Pardede, "Remaining Useful Life Prediction of Lithium-Ion Battery Based on LSTM and GRU," in *Proceedings of the 2021 International Conference on Computer, Control, Informatics and Its Applications*, 2021, pp. 21–25.

[115] Y.-J. He, J.-N. Shen, J.-F. Shen & Z.-F. Ma, "State of health estimation of lithium-ion batteries: A multiscale G aussian process regression modeling approach," *AIChE Journal*, vol. 61, no. 5, pp. 1589–1600, 2015.

[116] X. Zheng & X. Deng, "State-of-health prediction for lithium-ion batteries with multiple Gaussian process regression model," *IEEE Access*, vol. 7, pp. 150 383–150 394, 2019.

[117] V. Pop, H. J. Bergveld, J. O. het Veld, P. Regtien, D. Danilov & P. Notten, "Modeling battery behavior for accurate state-of-charge indication," *Journal of The Electrochemical Society*, vol. 153, no. 11, A2013, 2006.

[118] Q. Yu, Y. Huang, A. Tang, C. Wang & W. Shen, "OCV-SOC-Temperature Relationship Construction and State of Charge Estimation for a Series-Parallel Lithium-Ion Battery Pack," *IEEE Transactions on Intelligent Transportation Systems*, 2023.

[119] Y. Bao, W. Dong & D. Wang, "Online internal resistance measurement application in lithium ion battery capacity and state of charge estimation," *Energies*, vol. 11, no. 5, p. 1073, 2018.

[120] Z. Pang, K. Yang, Z. Song, G. Chen & P. Niu, "Research on SOC Estimation of Lithium Battery Based on Electrochemical Impedance Spectroscopy," in *2023 6th International Conference on Energy, Electrical and Power Engineering (CEEPE)*, IEEE, 2023, pp. 1638–1643.

[121] Y. Zhang, W. Song, S. Lin & Z. Feng, "A novel model of the initial state of charge estimation for LiFePO4 batteries," *Journal of Power Sources*, vol. 248, pp. 1028–1033, 2014.

[122] H. Suryoatmojo, S. Anam, Z. Rahmawan, D. A. Asfani, M. A. Faurahmansyah & P. Prabowo, "State of Charge (SOC) Estimation on Lead-Acid Batteries Using the Coulomb Counting Method," in *2022 10th International Conference on Smart Grid and Clean Energy Technologies (ICSGCE)*, IEEE, 2022, pp. 78–84.

[123] M. Hossain, M. Haque & M. T. Arif, "Kalman filtering techniques for the online model parameters and state of charge estimation of the Li-ion batteries: A comparative analysis," *Journal of Energy Storage*, vol. 51, p. 104 174, 2022.

[124] C. Jiang, A. Taylor, C. Duan & K. Bai, "Extended Kalman Filter based battery state of charge (SOC) estimation for electric vehicles," in *2013 IEEE Transportation Electrification Conference and Expo (ITEC)*, IEEE, 2013, pp. 1–5.

[125] J. Hu, S. Wu, Y. Wang, F. Lu & D. Liu, "Lithium battery soc estimation based on improved unscented kalman filter," in *2020 15th IEEE Conference on Industrial Electronics and Applications (ICIEA)*, IEEE, 2020, pp. 511–515.

[126] M. Wu, L. Qin & G. Wu, "State of charge estimation of Power lithium-ion battery based on an Affine Iterative Adaptive Extended Kalman Filter," *Journal of Energy Storage*, vol. 51, p. 104 472, 2022.

[127] J. Luo, J. Peng & H. He, "Lithium-ion battery SOC estimation study based on Cubature Kalman filter," *Energy Procedia*, vol. 158, pp. 3421–3426, 2019.

[128] D. Jiani, W. Youyi & W. Changyun, "Li-ion battery SOC estimation using particle filter based on an equivalent circuit model," in *2013 10th IEEE International Conference on Control and Automation (ICCA)*, IEEE, 2013, pp. 580–585.

[129] M. Lagraoui, S. Doubabi & A. Rachid, "SOC estimation of Lithium-ion battery using Kalman filter and Luenberger observer: A comparative study," in *2014 International renewable and sustainable energy conference (IRSEC)*, IEEE, 2014, pp. 636–641.

[130] T. He, D. Li, Z. Wu, Y. Xue & Y. Yang, "A modified luenberger observer for SOC estimation of lithium-ion battery," in *2017 36th Chinese Control Conference (CCC)*, IEEE, 2017, pp. 924–928.

[131] I.-S. Kim, "The novel state of charge estimation method for lithium battery using sliding mode observer," *Journal of Power Sources*, vol. 163, no. 1, pp. 584–590, 2006.

[132] J. Xu, C. C. Mi, B. Cao, J. Deng, Z. Chen & S. Li, "The state of charge estimation of lithium-ion batteries based on a proportional-integral observer," *IEEE Transactions on Vehicular Technology*, vol. 63, no. 4, pp. 1614–1621, 2013.

[133] R. Xiong, Q. Yu, C. Lin, et al., "A novel method to obtain the open circuit voltage for the state of charge of lithium ion batteries in electric vehicles by using H infinity filter," *Applied energy*, vol. 207, pp. 346–353, 2017.

[134] Z. Cui, L. Wang, Q. Li & K. Wang, "A comprehensive review on the state of charge estimation for lithium-ion battery based on neural network," *International Journal of Energy Research*, vol. 46, no. 5, pp. 5423–5440, 2022.

[135] D. Saji, P. S. Babu & K. Ilango, "SoC estimation of lithium ion battery using combined coulomb counting and fuzzy logic method," in *2019 4th International Conference on Recent Trends on Electronics, Information, Communication & Technology (RTEICT)*, IEEE, 2019, pp. 948–952.

[136] I. Essiet & Y. Sun, "Parameter Optimization of EV Battery SOC Model with Aggregator Using Evolutionary Algorithms," in *2021 International Conference on Electrical, Computer and Energy Technologies (ICECET)*, IEEE, 2021, pp. 1–5.

[137] L. Zhang, K. Li, D. Du, C. Zhu & M. Zheng, "A sparse least squares support vector machine used for SOC estimation of Li-ion Batteries," *IFAC-PapersOnLine*, vol. 52, no. 11, pp. 256–261, 2019.

[138] G. O. Sahinoglu, M. Pajovic, Z. Sahinoglu, Y. Wang, P. V. Orlik & T. Wada, "Battery state-of-charge estimation based on regular/recurrent Gaussian process regression," *IEEE Transactions on Industrial Electronics*, vol. 65, no. 5, pp. 4311–4321, 2017.

[139] M.-F. Ge, Y. Liu, X. Jiang & J. Liu, "A review on state of health estimations and remaining useful life prognostics of lithium-ion batteries," *Measurement*, vol. 174, p. 109 057, 2021.

[140] Y. Li, K. Liu, A. M. Foley, A. Zülke, M. Berecibar, E. Nanini-Maury, J. Van Mierlo & H. E. Hoster, "Data-driven health estimation and lifetime prediction

of lithium-ion batteries: A review," *Renewable and sustainable energy reviews*, vol. 113, p. 109 254, 2019.

[141] Z. Wang, G. Feng, D. Zhen, F. Gu & A. Ball, "A review on online state of charge and state of health estimation for lithium-ion batteries in electric vehicles," *Energy Reports*, vol. 7, pp. 5141–5161, 2021.

[142] D.-I. Stroe & E. Schaltz, "SOH estimation of LMO/NMC-based electric vehicle lithium-ion batteries using the incremental capacity analysis technique," in *2018 IEEE energy conversion congress and exposition (ECCE)*, IEEE, 2018, pp. 2720–2725.

[143] M. Maures, A. Capitaine, J.-Y. Delétage, J.-M. Vinassa & O. Briat, "Lithium-ion battery SoH estimation based on incremental capacity peak tracking at several current levels for online application," *Microelectronics Reliability*, vol. 114, p. 113 798, 2020.

[144] J. Tian, R. Xiong & Q. Yu, "Fractional-order model-based incremental capacity analysis for degradation state recognition of lithium-ion batteries," *IEEE Transactions on Industrial Electronics*, vol. 66, no. 2, pp. 1576–1584, 2018.

[145] C. Weng, Y. Cui, J. Sun & H. Peng, "On-board state of health monitoring of lithium-ion batteries using incremental capacity analysis with support vector regression," *Journal of Power Sources*, vol. 235, pp. 36–44, 2013.

[146] L. Wang, C. Pan, L. Liu, Y. Cheng & X. Zhao, "On-board state of health estimation of LiFePO4 battery pack through differential voltage analysis," *Applied energy*, vol. 168, pp. 465–472, 2016.

[147] S. Zhang, X. Guo, X. Dou & X. Zhang, "A rapid online calculation method for state of health of lithium-ion battery based on coulomb counting method and differential voltage analysis," *Journal of Power Sources*, vol. 479, p. 228 740, 2020.

[148] B. Wu, V. Yufit, Y. Merla, R. F. Martinez-Botas, N. P. Brandon & G. J. Offer, "Differential thermal voltammetry for tracking of degradation in lithium-ion batteries," *Journal of power sources*, vol. 273, pp. 495–501, 2015.

[149] Z. Wang, C. Yuan & X. Li, "Lithium battery state-of-health estimation via differential thermal voltammetry with Gaussian process regression," *IEEE Transactions on Transportation Electrification*, vol. 7, no. 1, pp. 16–25, 2020.

[150] J. Li, K. Adewuyi, N. Lotfi, R. G. Landers & J. Park, "A single particle model with chemical/mechanical degradation physics for lithium ion battery State of Health (SOH) estimation," *Applied energy*, vol. 212, pp. 1178–1190, 2018.

[151] J. Cannarella & C. B. Arnold, "State of health and charge measurements in lithium-ion batteries using mechanical stress," *Journal of Power Sources*, vol. 269, pp. 7–14, 2014.

[152] J. Shen, Y. He & Z. Ma, "Progress of model based SOC and SOH estimation methods for lithium-ion battery," *CIESC Journal*, vol. 69, no. 1, pp. 309–316, 2018.

[153] Z. Huang, M. Best, J. Knowles & A. Fly, "Adaptive piecewise equivalent circuit model with SOC/SOH estimation based on extended Kalman filter," *IEEE Transactions on Energy Conversion*, 2022.

[154] S. Amir, M. Gulzar, M. O. Tarar, I. H. Naqvi, N. A. Zaffar & M. G. Pecht, "Dynamic equivalent circuit model to estimate state-of-health of lithium-ion batteries," *IEEE Access*, vol. 10, pp. 18 279–18 288, 2022.

[155] Y. Gao, K. Liu, C. Zhu, X. Zhang & D. Zhang, "Co-estimation of state-of-charge and state-of-health for lithium-ion batteries using an enhanced electrochemical model," *IEEE Transactions on Industrial Electronics*, vol. 69, no. 3, pp. 2684–2696, 2021.

[156] A. Bartlett, J. Marcicki, S. Onori, G. Rizzoni, X. G. Yang & T. Miller, "Electrochemical model-based state of charge and capacity estimation for a composite electrode lithium-ion battery," *IEEE Transactions on control systems technology*, vol. 24, no. 2, pp. 384–399, 2015.

[157] Y. Jiang, J. Zhang, L. Xia & Y. Liu, "State of health estimation for lithium-ion battery using empirical degradation and error compensation models," *Ieee Access*, vol. 8, pp. 123 858–123 868, 2020.

[158] K. Li, Y. Wang & Z. Chen, "A comparative study of battery state-of-health estimation based on empirical mode decomposition and neural network," *Journal of Energy Storage*, vol. 54, p. 105 333, 2022.

[159] S. Yang, C. Zhang, J. Jiang, W. Zhang, L. Zhang & Y. Wang, "Review on state-of-health of lithium-ion batteries: Characterizations, estimations and applications," *Journal of Cleaner Production*, vol. 314, p. 128 015, 2021.

[160] P.-Y. Lee & J. Kim, "Impact analysis of deterioration and SOH estimation based on multiple regression analysis," in *2019 IEEE Transportation Electrification Conference and Expo, Asia-Pacific (ITEC Asia-Pacific)*, IEEE, 2019, pp. 1–6.

[161] E. Y. Ang & Y. C. Paw, "Linear Model for Online State of Health Estimation of Lithium-ion Batteries Using Segmented Discharge Profiles," *IEEE Transactions on Transportation Electrification*, 2022.

[162] V. Klass, M. Behm & G. Lindbergh, "A support vector machine-based state-of-health estimation method for lithium-ion batteries under electric vehicle operation," *Journal of Power Sources*, vol. 270, pp. 262–272, 2014.

[163] X. Feng, C. Weng, X. He, X. Han, L. Lu, D. Ren & M. Ouyang, "Online state-of-health estimation for Li-ion battery using partial charging segment based on support vector machine," *IEEE Transactions on Vehicular Technology*, vol. 68, no. 9, pp. 8583–8592, 2019.

[164] L. Qian, L. Xuan & J. Chen, "Battery SOH Estimation Based on Decision Tree and Improved Support Vector Machine Regression Algorithm," *Frontiers in Energy Research*, vol. 11, p. 1 218 580,

[165] R. Pan, T. Liu, W. Huang, Y. Wang, D. Yang & J. Chen, "State of health estimation for lithium-ion batteries based on two-stage features extraction and gradient boosting decision tree," *Energy*, p. 129 460, 2023.

[166] K. S. Mawonou, A. Eddahech, D. Dumur, D. Beauvois & E. Godoy, "State-of-health estimators coupled to a random forest approach for lithium-ion battery aging factor ranking," *Journal of Power Sources*, vol. 484, p. 229 154, 2021.

[167] N. Yang, Z. Song, H. Hofmann & J. Sun, "Robust State of Health estimation of lithium-ion batteries using convolutional neural network and random forest," *Journal of Energy Storage*, vol. 48, p. 103 857, 2022.

[168] T. Berghout, M. Benbouzid, Y. Amirat & G. Yao, "Lithium-ion Battery State of Health Prediction with a Robust Collaborative Augmented Hidden Layer Feedforward Neural Network Approach," *IEEE Transactions on Transportation Electrification*, 2023.

[169] G. Lee, D. Kwon & C. Lee, "A convolutional neural network model for SOH estimation of Li-ion batteries with physical interpretability," *Mechanical Systems and Signal Processing*, vol. 188, p. 110 004, 2023.

[170] X. Shu, J. Shen, G. Li, Y. Zhang, Z. Chen & Y. Liu, "A flexible state-of-health prediction scheme for lithium-ion battery packs with long short-term memory network and transfer learning," *IEEE Transactions on Transportation Electrification*, vol. 7, no. 4, pp. 2238–2248, 2021.

[171] G. Cheng, X. Wang & Y. He, "Remaining useful life and state of health prediction for lithium batteries based on empirical mode decomposition and a long and short memory neural network," *Energy*, vol. 232, p. 121 022, 2021.

[172] R. Li, W. Li & H. Zhang, "State of Health and Charge Estimation Based on Adaptive Boosting integrated with particle swarm optimization/support vector machine (AdaBoost-PSO-SVM) Model for Lithium-ion Batteries," *International Journal of Electrochemical Science*, vol. 17, no. 2, p. 220 212, 2022.

[173] S. Sun, J. Sun, Z. Wang, Z. Zhou & W. Cai, "Prediction of battery soh by cnn-bilstm network fused with attention mechanism," *Energies*, vol. 15, no. 12, p. 4428, 2022.

[174] Z. Zhu, Q. Yang, X. Liu & D. Gao, "Attention-based CNN-BiLSTM for SOH and RUL estimation of lithium-ion batteries," *Journal of Algorithms & Computational Technology*, vol. 16, p. 17 483 026 221 130 598, 2022.

[175] Y. Li, K. Li, Y. Xie, J. Liu, C. Fu & B. Liu, "Optimized charging of lithium-ion battery for electric vehicles: Adaptive multistage constant current–constant voltage charging strategy," *Renewable energy*, vol. 146, pp. 2688–2699, 2020.

[176] X. Lin, X. Hao, Z. Liu & W. Jia, "Health conscious fast charging of Li-ion batteries via a single particle model with aging mechanisms," *Journal of Power Sources*, vol. 400, pp. 305–316, 2018.

[177] T. M. Padovani, M. Debert, G. Colin & Y. Chamaillard, "Optimal energy management strategy including battery health through thermal management for hybrid vehicles," *IFAC Proceedings Volumes*, vol. 46, no. 21, pp. 384–389, 2013.

[178] C. Jia, J. Zhou, H. He, J. Li, Z. Wei, K. Li & M. Shi, "A novel energy management strategy for hybrid electric bus with fuel cell health and battery thermal-and health-constrained awareness," *Energy*, vol. 271, p. 127 105, 2023.

[179] N. Yan, Y.-B. Yao, Z.-D. Jia, L. Liu, C.-T. Dai, Z.-G. Li, Z.-H. Zhang, W. Li, L. Wang & P.-F. Wang, "Online battery health diagnosis for electric vehicles based on DTW-XGBoost," *Energy Reports*, vol. 8, pp. 121–128, 2022.

[180] S. Ebbesen, P. Elbert & L. Guzzella, "Battery state-of-health perceptive energy management for hybrid electric vehicles," *IEEE Transactions on Vehicular Technology*, vol. 61, no. 7, pp. 2893–2900, 2012.

[181] H. Fang, Y. Wang & J. Chen, "Health-aware and user-involved battery charging management for electric vehicles: Linear quadratic strategies," *IEEE Transactions on Control Systems Technology*, vol. 25, no. 3, pp. 911–923, 2016.

[182] S. Li, P. Zhao, C. Gu, D. Huo, J. Li & S. Cheng, "Linearizing battery degradation for health-aware vehicle energy management," *IEEE Transactions on Power Systems*, 2022.

[183] S. Xie, S. Qi, K. Lang, X. Tang & X. Lin, "Coordinated management of connected plug-in hybrid electric buses for energy saving, inter-vehicle safety, and battery health," *Applied energy*, vol. 268, p. 115 028, 2020.

[184] C. Gehbauer, D. R. Black & P. Grant, "Advanced control strategies to manage electric vehicle drivetrain battery health for Vehicle-to-X applications," *Applied Energy*, vol. 345, p. 121 296, 2023.

[185] D.-D. Tran, M. Vafaeipour, M. El Baghdadi, R. Barrero, J. Van Mierlo & O. Hegazy, "Thorough state-of-the-art analysis of electric and hybrid vehicle powertrains: Topologies and integrated energy management strategies," *Renewable and Sustainable Energy Reviews*, vol. 119, p. 109 596, 2020.

[186] Q. Zhang, W. Deng, S. Zhang, J. Wu, et al., "A rule based energy management system of experimental battery/supercapacitor hybrid energy storage system for electric vehicles," *Journal of Control Science and Engineering*, vol. 2016, 2016.

[187] B. Duan, Q. Wang, J. Wang, X. Li & T. Ba, "Calibration efficiency improvement of rule-based energy management system for a plug-in hybrid electric vehicle," *International Journal of Automotive Technology*, vol. 18, pp. 335–344, 2017.

[188] Y. Li, J. Tao & K. Han, "Rule and Q-learning based Hybrid Energy Management for Electric Vehicle," in *2019 Chinese Automation Congress (CAC)*, IEEE, 2019, pp. 51–56.

[189] T. Mesbahi, N. Rizoug, P. Bartholomeüs, R. Sadoun, F. Khenfri & P. Le Moigne, "Optimal energy management for a li-ion battery/supercapacitor hybrid energy storage system based on a particle swarm optimization incorporating Nelder–Mead simplex approach," *IEEE Transactions on Intelligent Vehicles*, vol. 2, no. 2, pp. 99–110, 2017.

[190] G. Li & D. Gorges, "Energy management strategy for parallel hybrid electric vehicles based on approximate dynamic programming and velocity forecast," *Journal of the Franklin Institute*, vol. 356, no. 16, pp. 9502–9523, 2019.

[191] G. Li & D. Görges, "Ecological adaptive cruise control and energy management strategy for hybrid electric vehicles based on heuristic dynamic programming," *IEEE Transactions on Intelligent Transportation Systems*, vol. 20, no. 9, pp. 3526–3535, 2018.

[192] X. Tang, Y. Xie, B. Wang, L. Shi & X. Wu, "Energy management strategy for hydraulic hybrid system with compound accumulator based on dynamic programming," *Proceedings of the Institution of Mechanical Engineers, Part D: Journal of Automobile Engineering*, vol. 237, no. 8, pp. 1819–1829, 2023.

[193] Y. Wang, Z. Wu, Y. Chen, A. Xia, C. Guo & Z. Tang, "Research on energy optimization control strategy of the hybrid electric vehicle based on Pontryagin's minimum principle," *Computers & Electrical Engineering*, vol. 72, pp. 203–213, 2018.

[194] Z. Yuan, L. Teng, S. Fengchun & H. Peng, "Comparative study of dynamic programming and Pontryagin's minimum principle on energy management for a parallel hybrid electric vehicle," *Energies*, vol. 6, no. 4, pp. 2305–2318, 2013.

[195] N. Robuschi, M. Salazar, N. Viscera, F. Braghin & C. H. Onder, "Minimum-fuel energy management of a hybrid electric vehicle via iterative linear programming," *IEEE Transactions on Vehicular Technology*, vol. 69, no. 12, pp. 14 575–14 587, 2020.

[196] R. Ghaderi, M. Kandidayeni, L. Boulon & J. P. Trovão, "Quadratic programming based energy management in a multi-stack fuel cell hybrid electric vehicle," in *2021 IEEE Vehicle Power and Propulsion Conference (VPPC)*, IEEE, 2021, pp. 1–6.

[197] C. Yang, M. Wang, W. Wang, Z. Pu & M. Ma, "An efficient vehicle-following predictive energy management strategy for PHEV based on improved sequential quadratic programming algorithm," *Energy*, vol. 219, p. 119 595, 2021.

[198] X. Wu, X. Hu, X. Yin, L. Li, Z. Zeng & V. Pickert, "Convex programming energy management and components sizing of a plug-in fuel cell urban logistics vehicle," *Journal of power sources*, vol. 423, pp. 358–366, 2019.

[199] P. Saiteja & B. Ashok, "Critical review on structural architecture, energy control strategies and development process towards optimal energy management in hybrid vehicles," *Renewable and Sustainable Energy Reviews*, vol. 157, p. 112 038, 2022.

[200] J. H. Holland, "Genetic algorithms," *Scientific american*, vol. 267, no. 1, pp. 66–73, 1992.

[201] A. Panday & H. O. Bansal, "Energy management strategy for hybrid electric vehicles using genetic algorithm," *Journal of Renewable and Sustainable Energy*, vol. 8, no. 1, 2016.

[202] X. Lü, Y. Wu, J. Lian, Y. Zhang, C. Chen, P. Wang & L. Meng, "Energy management of hybrid electric vehicles: A review of energy optimization of fuel cell hybrid power system based on genetic algorithm," *Energy Conversion and Management*, vol. 205, p. 112 474, 2020.

[203] T. Liu, X. Tang, H. Wang, H. Yu & X. Hu, "Adaptive hierarchical energy management design for a plug-in hybrid electric vehicle," *IEEE Transactions on Vehicular Technology*, vol. 68, no. 12, pp. 11 513–11 522, 2019.

[204] J. Tao, R. Zhang, Z. Qiao & L. Ma, "Q-Learning-based fuzzy energy management for fuel cell/supercapacitor HEV," *Transactions of the Institute of Measurement and Control*, vol. 44, no. 10, pp. 1939–1949, 2022.

[205] Y. Li, S. Wang, X. Duan, S. Liu, J. Liu & S. Hu, "Multi-objective energy management for Atkinson cycle engine and series hybrid electric vehicle based on evolutionary NSGA-II algorithm using digital twins," *Energy Conversion and Management*, vol. 230, p. 113 788, 2021.

[206] T. Deng, C. Lin, J. Luo & B. Chen, "NSGA-II multi-objectives optimization algorithm for energy management control of hybrid electric vehicle," *Proceedings of the Institution of Mechanical Engineers, Part D: Journal of Automobile Engineering*, vol. 233, no. 4, pp. 1023–1034, 2019.

[207] S. Kirkpatrick, C. D. Gelatt Jr & M. P. Vecchi, "Optimization by simulated annealing," *science*, vol. 220, no. 4598, pp. 671–680, 1983.

[208] Z. Chen, C. C. Mi, B. Xia & C. You, "Energy management of power-split plug-in hybrid electric vehicles based on simulated annealing and Pontryagin's minimum principle," *Journal of Power Sources*, vol. 272, pp. 160–168, 2014.

[209] B. Wang, J. Xu, B. Cao & B. Ning, "Adaptive mode switch strategy based on simulated annealing optimization of a multi-mode hybrid energy storage system for electric vehicles," *Applied Energy*, vol. 194, pp. 596–608, 2017.

[210] J. Kennedy & R. Eberhart, "Particle swarm optimization," in *Proceedings of ICNN'95-international conference on neural networks*, IEEE, vol. 4, 1995, pp. 1942–1948.

[211] M. Boujneh, N. Majdoub, T. Ladhari & A. Sakly, "Optimal control strategy parameters of parallel hybrid electric vehicles based on particle swarm optimization," in *2020 20th International Conference on Sciences and Techniques of Automatic Control and Computer Engineering (STA)*, IEEE, 2020, pp. 107–112.

[212] Y.-H. Cheng, C.-M. Lai & J. Teh, "Application of particle swarm optimization to design control strategy parameters of parallel hybrid electric vehicle with fuel economy and low emission," in *2018 International Symposium on Computer, Consumer and Control (IS3C)*, IEEE, 2018, pp. 342–345.

[213] Z. Chen, R. Xiong & J. Cao, "Particle swarm optimization-based optimal power management of plug-in hybrid electric vehicles considering uncertain driving conditions," *Energy*, vol. 96, pp. 197–208, 2016.

[214] I. Rahman, P. M. Vasant, B. S. M. Singh & M. Abdullah-Al-Wadud, "On the performance of accelerated particle swarm optimization for charging plug-in hybrid electric vehicles," *Alexandria Engineering Journal*, vol. 55, no. 1, pp. 419–426, 2016.

[215] Q. Zhou, S. Guo, L. Xu, X. Guo, H. Williams, H. Xu & F. Yan, "Global optimization of the hydraulic-electromagnetic energy-harvesting shock absorber for road vehicles with human-knowledge-integrated particle swarm optimization scheme," *IEEE/ASME Transactions on Mechatronics*, vol. 26, no. 3, pp. 1225–1235, 2021.

[216] W. Li, M. Rentemeister, J. Badeda, D. Jöst, D. Schulte & D. U. Sauer, "Digital twin for battery systems: Cloud battery management system with online state-of-charge and state-of-health estimation," *Journal of energy storage*, vol. 30, p. 101 557, 2020.

[217] w. Geng, d. Lou & t. Zhang, "Multi-objective energy management strategy for hybrid electric vehicle based on particle swarm optimization," *JOURNAL OF*

TONGJI UNIVERSITY(NATURAL SCIENCE), vol. 48, no. 7, pp. 1030–1039, 2020.

[218] X. Xiao, Y. Pan, L. Lv & Y. Shi, "Scheduling multi–mode resource–constrained tasks of automated guided vehicles with an improved particle swarm optimization algorithm," *IET Collaborative Intelligent Manufacturing*, vol. 3, no. 2, pp. 93–104, 2021.

[219] Y. Huang, H. Wang, A. Khajepour, H. He & J. Ji, "Model predictive control power management strategies for HEVs: A review," *Journal of Power Sources*, vol. 341, pp. 91–106, 2017.

[220] W. Touil, Z. Li, R. Outbib, D. Hissel & S. Jemei, "Model predictive control energy management strategy of fuel cell hybrid electric vehicle," in *IECON 2022–48th Annual Conference of the IEEE Industrial Electronics Society*, IEEE, 2022, pp. 1–8.

[221] H. Wang, Y. Huang, A. Soltani, A. Khajepour & D. Cao, "Cyber-physical predictive energy management for through-the-road hybrid vehicles," *IEEE Transactions on Vehicular Technology*, vol. 68, no. 4, pp. 3246–3256, 2019.

[222] S. Zhang, R. Xiong & F. Sun, "Model predictive control for power management in a plug-in hybrid electric vehicle with a hybrid energy storage system," *Applied energy*, vol. 185, pp. 1654–1662, 2017.

[223] Y. Zhang, L. Chu, Y. Ding, N. Xu, C. Guo, Z. Fu, L. Xu, X. Tang & Y. Liu, "A hierarchical energy management strategy based on model predictive control for plug-in hybrid electric vehicles," *Ieee Access*, vol. 7, pp. 81 612–81 629, 2019.

[224] G. Jinquan, H. Hongwen, P. Jiankun & Z. Nana, "A novel MPC-based adaptive energy management strategy in plug-in hybrid electric vehicles," *Energy*, vol. 175, pp. 378–392, 2019.

[225] H. He, Y. Wang, R. Han, M. Han, Y. Bai & Q. Liu, "An improved MPC-based energy management strategy for hybrid vehicles using V2V and V2I communications," *Energy*, vol. 225, p. 120 273, 2021.

[226] Y. Huang, H. Wang, A. Khajepour, H. He & J. Ji, "Model predictive control power management strategies for HEVs: A review," *Journal of Power Sources*, vol. 341, pp. 91–106, 2017.

[227] G. Paganelli, S. Delprat, T.-M. Guerra, J. Rimaux & J.-J. Santin, "Equivalent consumption minimization strategy for parallel hybrid powertrains," in *Vehicular Technology Conference. IEEE 55th Vehicular Technology Conference. VTC Spring 2002 (Cat. No. 02CH37367)*, IEEE, vol. 4, 2002, pp. 2076–2081.

[228] Z. Chen, Y. Liu, M. Ye, Y. Zhang & G. Li, "A survey on key techniques and development perspectives of equivalent consumption minimisation strategy for hybrid electric vehicles," *Renewable and Sustainable Energy Reviews*, vol. 151, p. 111 607, 2021.

[229] C. Zheng, G. Xu, S.-W. Cha & Q. Liang, "Numerical comparison of ECMS and PMP-based optimal control strategy in hybrid vehicles," *International Journal of Automotive Technology*, vol. 15, pp. 1189–1196, 2014.

[230] Q. Zheng, H. Yuan, J. Wu & B. Gao, "Equivalent consumption minimization strategy based on dynamic programming for plug-in hybrid electric vehicle," *IFAC-PapersOnLine*, vol. 51, no. 31, pp. 612–617, 2018.

[231] C. Wei, Y. Chen, X. Sun & Y. Zhang, "Optimal equivalent consumption minimization strategy for plug-in hybrid electric vehicle with improved genetic algorithm," *SAE International Journal of Electrified Vehicles*, vol. 9, no. 2, pp. 143–154, 2020.

[232] Z. Wang & X. Jiao, "Optimization of the powertrain and energy management control parameters of a hybrid hydraulic vehicle based on improved multi-objective particle swarm optimization," *Engineering Optimization*, vol. 53, no. 11, pp. 1835–1854, 2021.

[233] Z. Fu, X. Liu, H. Li & Z. Li, "Equivalent consumption minimization strategy based on a variable equivalent factor," in *2017 Chinese Automation Congress (CAC)*, IEEE, 2017, pp. 4215–4219.

[234] X. Sun, Z. Jin, M. Xue & X. Tian, "Adaptive ECMS with Gear Shift Control by Grey Wolf Optimization Algorithm and Neural Network for Plug-in Hybrid Electric Buses," *IEEE Transactions on Industrial Electronics*, 2023.

[235] K. Choi, J. Byun, S. Lee & I. G. Jang, "Adaptive equivalent consumption minimization strategy (A-ECMS) for the HEVs with a near-optimal equivalent factor considering driving conditions," *IEEE Transactions on Vehicular Technology*, vol. 71, no. 3, pp. 2538–2549, 2021.

[236] K. Gao, P. Luo, J. Xie, B. Chen, Y. Wu & R. Du, "Energy management of plug-in hybrid electric vehicles based on speed prediction fused driving intention and LIDAR," *Energy*, vol. 284, p. 128 535, 2023.

[237] X. Lin, J. Zhang & L. Su, "A trip distance adaptive real-time optimal energy management strategy for a plug-in hybrid vehicle integrated driving condition prediction," *Journal of Energy Storage*, vol. 52, p. 105 055, 2022.

[238] Y. Zeng, J. Sheng, M. Li, et al., "Adaptive real-time energy management strategy for plug-in hybrid electric vehicle based on simplified-ECMS and a novel driving pattern recognition method," *Mathematical Problems in Engineering*, vol. 2018, 2018.

[239] H. He, Y. Shou & J. Song, "An improved A-ECMS energy management for plug-in hybrid electric vehicles considering transient characteristics of engine," *Energy Reports*, vol. 10, pp. 2006–2016, 2023.

[240] R. Vignesh & B. Ashok, "Intelligent energy management through neuro-fuzzy based adaptive ECMS approach for an optimal battery utilization in plugin parallel hybrid electric vehicle," *Energy Conversion and Management*, vol. 280, p. 116 792, 2023.

[241] H. Li, A. Ravey, A. N'Diaye & A. Djerdir, "Online adaptive equivalent consumption minimization strategy for fuel cell hybrid electric vehicle considering power sources degradation," *Energy conversion and management*, vol. 192, pp. 133–149, 2019.

[242] T. Park & H. Lee, "Optimal supervisory control strategy for a transmission-mounted electric drive hybrid electric vehicle," *International journal of automotive technology*, vol. 20, pp. 663–677, 2019.

[243] S. Onori, L. Serrao & G. Rizzoni, *Hybrid electric vehicles: Energy management strategies*. Springer, 2016.

[244] Y. Yang, Y. Zhang, J. Tian & T. Li, "Adaptive real-time optimal energy management strategy for extender range electric vehicle," *Energy*, vol. 197, p. 117 237, 2020.

[245] T. Deng, P. Tang & J. Luo, "A novel real-time energy management strategy for plug-in hybrid electric vehicles based on equivalence factor dynamic optimization method," *International Journal of Energy Research*, vol. 45, no. 1, pp. 626–641, 2021.

[246] Y. Li, X. Jiao & Y. Jing, "A real-time energy management strategy combining rule-based control and ECMS with optimization equivalent factor for HEVs," in *2017 Chinese automation congress (CAC)*, IEEE, 2017, pp. 5988–5992.

[247] S. Wang, X. Huang, J. M. López, X. Xu & P. Dong, "Fuzzy adaptive-equivalent consumption minimization strategy for a parallel hybrid electric vehicle," *IEEE Access*, vol. 7, pp. 133 290–133 303, 2019.

[248] K. V. Singh, H. O. Bansal & D. Singh, "Development of an adaptive neuro-fuzzy inference system–based equivalent consumption minimisation strategy to improve fuel economy in hybrid electric vehicles," *IET Electrical Systems in Transportation*, vol. 11, no. 3, pp. 171–185, 2021.

[249] S. Xie, X. Hu, S. Qi & K. Lang, "An artificial neural network-enhanced energy management strategy for plug-in hybrid electric vehicles," *Energy*, vol. 163, pp. 837–848, 2018.

[250] A. H. Ganesh & B. Xu, "A review of reinforcement learning based energy management systems for electrified powertrains: Progress, challenge, and potential solution," *Renewable and Sustainable Energy Reviews*, vol. 154, p. 111 833, 2022.

[251] Z. Chen, L. Li, X. Hu, B. Yan & C. Yang, "Temporal-difference learning-based stochastic energy management for plug-in hybrid electric buses," *IEEE Transactions on Intelligent Transportation Systems*, vol. 20, no. 6, pp. 2378–2388, 2018.

[252] L. Bo, L. Han, C. Xiang, H. Liu & T. Ma, "A Q-learning fuzzy inference system based online energy management strategy for off-road hybrid electric vehicles," *Energy*, vol. 252, p. 123 976, 2022.

[253] S. Shen, S. Gao, Y. Liu, Y. Zhang, J. Shen, Z. Chen & Z. Lei, "Real-Time Energy Management for Plug-in Hybrid Electric Vehicles via Incorporating Double-Delay Q-Learning and Model Prediction Control," *IEEE Access*, vol. 10, pp. 131 076–131 089, 2022.

[254] C. Zheng, D. Zhang, Y. Xiao & W. Li, "Reinforcement learning-based energy management strategies of fuel cell hybrid vehicles with multi-objective control," *Journal of Power Sources*, vol. 543, p. 231 841, 2022.

[255] S. Ghode & M. Digalwar, "A Novel Model based Energy Management Strategy for Plug-in Hybrid Electric Vehicles using Deep Reinforcement Learning," in *Proceedings of the 2023 Fifteenth International Conference on Contemporary Computing*, 2023, pp. 289–293.

[256] H. Wang, H. He, Y. Bai & H. Yue, "Parameterized deep Q-network based energy management with balanced energy economy and battery life for hybrid electric vehicles," *Applied Energy*, vol. 320, p. 119 270, 2022.

[257] C. Zheng, W. Li, Y. Xiao, D. Zhang & S. W. Cha, "A Deep Deterministic Policy Gradient-Based Energy Management Strategy for Fuel Cell Hybrid Vehicles," in *2021 IEEE Vehicle Power and Propulsion Conference (VPPC)*, IEEE, 2021, pp. 1–6.

[258] C. Qi, C. Song, F. Xiao & S. Song, "Generalization ability of hybrid electric vehicle energy management strategy based on reinforcement learning method," *Energy*, vol. 250, p. 123 826, 2022.

[259] Y. Wang, Y. Wu, Y. Tang, Q. Li & H. He, "Cooperative energy management and eco-driving of plug-in hybrid electric vehicle via multi-agent reinforcement learning," *Applied Energy*, vol. 332, p. 120 563, 2023.

[260] N. Yang, S. Ruan, L. Han, H. Liu, L. Guo & C. Xiang, "Reinforcement learning-based real-time intelligent energy management for hybrid electric vehicles in a model predictive control framework," *Energy*, vol. 270, p. 126 971, 2023.

[261] L. Shi, M. Zheng & F. Li, "The energy management strategy for parallel hybrid electric vehicles based on MNN," *Multimedia Tools and Applications*, vol. 79, pp. 5321–5333, 2020.

[262] S. Li, M. Hu, C. Gong, S. Zhan & D. Qin, "Energy management strategy for hybrid electric vehicle based on driving condition identification using KGA-means," *Energies*, vol. 11, no. 6, p. 1531, 2018.

[263] C. Wei, Y. Chen, X. Li & X. Lin, "Integrating intelligent driving pattern recognition with adaptive energy management strategy for extender range electric logistics vehicle," *Energy*, vol. 247, p. 123 478, 2022.

[264] Y. Wang, Y. Zhang, C. Zhang, J. Zhou, D. Hu, F. Yi, Z. Fan & T. Zeng, "Genetic algorithm-based fuzzy optimization of energy management strategy for fuel cell vehicles considering driving cycles recognition," *Energy*, vol. 263, p. 126 112, 2023.

[265] J. Liu, P. Shi & J. Fan, "Electric Vehicle Energy Consumption Model Based on Working Condition Recognition and K-means Cluster Analysis," in *2022 International Conference on Manufacturing, Industrial Automation and Electronics (ICMIAE)*, IEEE, 2022, pp. 130–134.

[266] I. Miri, A. Fotouhi & N. Ewin, "Electric vehicle energy consumption modelling and estimation—A case study," *International Journal of Energy Research*, vol. 45, no. 1, pp. 501–520, 2021.

[267] S. Li, P. Zhao, C. Gu, D. Huo, J. Li & S. Cheng, "Linearizing battery degradation for health-aware vehicle energy management," *IEEE Transactions on Power Systems*, 2022.

[268] Y. Zheng, F. He, X. Shen & X. Jiang, "Energy control strategy of fuel cell hybrid electric vehicle based on working conditions identification by least square support vector machine," *Energies*, vol. 13, no. 2, p. 426, 2020.

[269] J. Hu, J. Hu, H. Lin, X. Li, C. Jiang, X. Qiu & W. Li, "State-of-charge estimation for battery management system using optimized support vector machine for regression," *Journal of Power Sources*, vol. 269, pp. 682–693, 2014.

[270] Y. Y. Chia, L. H. Lee, N. Shafiabady & D. Isa, "A load predictive energy management system for supercapacitor-battery hybrid energy storage system in solar application using the Support Vector Machine," *Applied Energy*, vol. 137, pp. 588–602, 2015.

[271] X. Guo, X. Yan, Z. Chen & Z. Meng, "A novel closed-loop system for vehicle speed prediction based on APSO LSSVM and BP NN," *Energies*, vol. 15, no. 1, p. 21, 2021.

[272] X. Li, Y. Wang, D. Yang & Z. Chen, "Adaptive energy management strategy for fuel cell/battery hybrid vehicles using Pontryagin's Minimal Principle," *Journal of Power Sources*, vol. 440, p. 227 105, 2019.

[273] Y. Li, S. Zhou, J. Liu, J. Tong, J. Dang, F. Yang & M. Ouyang, "Multi-objective optimization of the Atkinson cycle gasoline engine using NSGA III coupled with support vector machine and back-propagation algorithm," *Energy*, vol. 262, p. 125 262, 2023.

[274] F. Millo, L. Rolando, L. Tresca & L. Pulvirenti, "Development of a neural network-based energy management system for a plug-in hybrid electric vehicle," *Transportation Engineering*, vol. 11, p. 100 156, 2023.

[275] Z. Lu, H. Tian, R. Li, G. Tian, et al., "Neural network energy management strategy with optimal input features for plug-in hybrid electric vehicles," *Energy*, vol. 285, p. 129 399, 2023.

[276] M. A. Kamoona, O. C. Kivanc & O. A. Ahmed, "Intelligent Energy Management System Evaluation of Hybrid Electric Vehicle Based on Recurrent Wavelet Neural Network and PSO Algorithm.," *International Journal of Intelligent Engineering & Systems*, vol. 16, no. 1, 2023.

[277] Z. Chen, C. Yang & S. Fang, "A convolutional neural network-based driving cycle prediction method for plug-in hybrid electric vehicles with bus route," *IEEE Access*, vol. 8, pp. 3255–3264, 2019.

[278] Y. Xing & C. Lv, "Dynamic state estimation for the advanced brake system of electric vehicles by using deep recurrent neural networks," *IEEE Transactions on Industrial Electronics*, vol. 67, no. 11, pp. 9536–9547, 2019.

[279] W. Zhu, "Optimization strategies for real-time energy management of electric vehicles based on LSTM network learning," *Energy Reports*, vol. 8, pp. 1009–1019, 2022.

[280] A. M. Billert, S. Erschen, M. Frey & F. Gauterin, "Predictive battery thermal management using quantile convolutional neural networks," *Transportation Engineering*, vol. 10, p. 100 150, 2022.

[281] J. Wang, J. Zhou & D. Xu, "A real-time predictive energy management strategy of fuel cell/battery/ultra-capacitor hybrid energy storage system in electric vehicle," in *2020 Chinese Automation Congress (CAC)*, IEEE, 2020, pp. 3951–3954.

[282] Y. Wu, Y. Zhang, G. Li, J. Shen, Z. Chen & Y. Liu, "A predictive energy management strategy for multi-mode plug-in hybrid electric vehicles based on multi neural networks," *Energy*, vol. 208, p. 118 366, 2020.

[283] F. Morlock & O. Sawodny, "An economic model predictive cruise controller for electric vehicles using gaussian process prediction," *IFAC-PapersOnLine*, vol. 51, no. 31, pp. 876–881, 2018.

[284] J. W. Bae & K.-K. K. Kim, "Gaussian process approximate dynamic programming for energy-optimal supervisory control of parallel hybrid electric vehicles," *IEEE Transactions on Vehicular Technology*, vol. 71, no. 8, pp. 8367–8380, 2022.

[285] Q. Zhou, Y. Li, D. Zhao, J. Li, H. Williams, H. Xu & F. Yan, "Transferable representation modelling for real-time energy management of the plug-in hybrid vehicle based on k-fold fuzzy learning and Gaussian process regression," *Applied energy*, vol. 305, p. 117 853, 2022.

[286] F. Guo, Z. Chen, F. Xiao, A. Li & J. Shi, "Real-time energy performance benchmarking of electric vehicle air conditioning systems using adaptive neural network and Gaussian process regression," *Applied Thermal Engineering*, vol. 222, p. 119 931, 2023.

[287] N. Higuchi, Y. Sunaga, M. Tanaka & H. Shimada, "Development of a new two-motor plug-in hybrid system," *SAE International Journal of Alternative Powertrains*, vol. 2, no. 1, pp. 135–145, 2013.

[288] Y. Wu, Y. Zhang, G. Li, J. Shen, Z. Chen & Y. Liu, "A predictive energy management strategy for multi-mode plug-in hybrid electric vehicles based on multi neural networks," *Energy*, vol. 208, p. 118 366, 2020.

[289] Y. Li & X. Jiao, "Energy management strategy for hybrid electric vehicles based on adaptive equivalent consumption minimization strategy and mode switching with variable thresholds," *Science Progress*, vol. 103, no. 1, p. 0 036 850 419 874 992, 2020.

[290] W. Zhuang, X. Zhang, Y. Ding, L. Wang & X. Hu, "Comparison of multi-mode hybrid powertrains with multiple planetary gears," *Applied energy*, vol. 178, pp. 624–632, 2016.

[291] M. Seyfi, M. Alinaghian, E. Ghorbani, B. Çatay & M. S. Sabbagh, "Multi-mode hybrid electric vehicle routing problem," *Transportation Research Part E: Logistics and Transportation Review*, vol. 166, p. 102 882, 2022.

[292] T. J. BARLOW, S. Latham, I. McCrae & P. Boulter, "A reference book of driving cycles for use in the measurement of road vehicle emissions," *TRL Published Project Report*, 2009.

[293] S. Tsiakmakis, G. Fontaras, C. Cubito, J. Pavlovic, K. Anagnostopoulos, B. Ciuffo, et al., "From nedc to wltp: Effect on the type-approval co2 emissions of light-duty vehicles," *Publications Office of the European Union: Luxembourg*, vol. 50, 2017.

[294] D. Naber, A. Kufferath, M. Krüger, R. Maier, S. Scherer & H. Schumacher, "Measures to fulfill "real driving emission (rde)" with diesel passenger cars," in *17. Internationales Stuttgarter Symposium: Automobil-und Motorentechnik*, Springer, 2017, pp. 423–446.

[295] D. G. Kooijman, A. E. Balau, S. Wilkins, N. Ligterink & R. Cuelenaere, "WLTP random cycle generator," in *2015 IEEE Vehicle Power and Propulsion Conference (VPPC)*, IEEE, 2015, pp. 1–6.

[296] B. Saha & K. Goebel, "Battery data set," *NASA AMES prognostics data repository*, 2007.

[297] G. Mohan, F. Assadian & S. Longo, "Comparative analysis of forward-facing models vs backwardfacing models in powertrain component sizing," in *IET hybrid and electric vehicles conference 2013 (HEVC 2013)*, IET, 2013, pp. 1–6.

[298] A. Seaman, T.-S. Dao & J. McPhee, "A survey of mathematics-based equivalent-circuit and electrochemical battery models for hybrid and electric vehicle simulation," *Journal of Power Sources*, vol. 256, pp. 410–423, 2014.

[299] M. Chen & G. A. Rincon-Mora, "Accurate electrical battery model capable of predicting runtime and IV performance," *IEEE transactions on energy conversion*, vol. 21, no. 2, pp. 504–511, 2006.

[300] J. Wang, P. Liu, J. Hicks-Garner, E. Sherman, S. Soukiazian, M. Verbrugge, H. Tataria, J. Musser & P. Finamore, "Cycle-life model for graphite-LiFePO4 cells," *Journal of power sources*, vol. 196, no. 8, pp. 3942–3948, 2011.

[301] Z. Hu, J. Li, L. Xu, Z. Song, C. Fang, M. Ouyang, G. Dou & G. Kou, "Multi-objective energy management optimization and parameter sizing for proton exchange membrane hybrid fuel cell vehicles," *Energy Conversion and Management*, vol. 129, pp. 108–121, 2016.

[302] W. Li, M. Rentemeister, J. Badeda, D. Jöst, D. Schulte & D. U. Sauer, "Digital twin for battery systems: Cloud battery management system with online state-of-charge and state-of-health estimation," *Journal of energy storage*, vol. 30, p. 101 557, 2020.

[303] G. Bhatti, H. Mohan & R. R. Singh, "Towards the future of smart electric vehicles: Digital twin technology," *Renewable and Sustainable Energy Reviews*, vol. 141, p. 110 801, 2021.

[304] S. Venkatesan, K. Manickavasagam, N. Tengenkai & N. Vijayalakshmi, "Health monitoring and prognosis of electric vehicle motor using intelligent-digital twin," *IET Electric Power Applications*, vol. 13, no. 9, pp. 1328–1335, 2019.

[305] Y. Liu, Z. Wang, K. Han, Z. Shou, P. Tiwari & J. H. Hansen, "Sensor fusion of camera and cloud digital twin information for intelligent vehicles," in *2020 IEEE Intelligent Vehicles Symposium (IV)*, IEEE, 2020, pp. 182–187.

[306] Q. Zhou, S. Guo, L. Xu, X. Guo, H. Williams, H. Xu & F. Yan, "Global optimization of the hydraulic-electromagnetic energy-harvesting shock absorber for road vehicles with human-knowledge-integrated particle swarm optimization scheme," *IEEE/ASME Transactions on Mechatronics*, vol. 26, no. 3, pp. 1225–1235, 2021.

[307] Q. Zhou, C. Wang, Z. Sun, J. Li, H. Williams & H. Xu, "Human-knowledge-augmented gaussian process regression for state-of-health prediction of lithium-ion batteries with charging curves," *Journal of Electrochemical Energy Conversion and Storage*, vol. 18, no. 3, p. 030 907, 2021.

[308] M. Liu, S. Fang, H. Dong & C. Xu, "Review of digital twin about concepts, technologies, and industrial applications," *Journal of Manufacturing Systems*, vol. 58, pp. 346–361, 2021.

[309] A. Rasheed, O. San & T. Kvamsdal, "Digital twin: Values, challenges and enablers from a modeling perspective," *Ieee Access*, vol. 8, pp. 21 980–22 012, 2020.

[310] A. Fuller, Z. Fan, C. Day & C. Barlow, "Digital twin: Enabling technologies, challenges and open research," *IEEE access*, vol. 8, pp. 108 952–108 971, 2020.

[311] Q. Zhou, Y. He, D. Zhao, J. Li, Y. Li, H. Williams & H. Xu, "Modified particle swarm optimization with chaotic attraction strategy for modular design of hybrid powertrains," *IEEE transactions on transportation electrification*, vol. 7, no. 2, pp. 616–625, 2020.

[312] Q. Zhou, W. Zhang, S. Cash, O. Olatunbosun, H. Xu & G. Lu, "Intelligent sizing of a series hybrid electric power-train system based on chaos-enhanced accelerated particle swarm optimization," *Applied Energy*, vol. 189, pp. 588–601, 2017.

[313] J. Li, Q. Zhou, H. Williams & H. Xu, "Back-to-back competitive learning mechanism for fuzzy logic based supervisory control system of hybrid electric vehicles," *IEEE Transactions on Industrial Electronics*, vol. 67, no. 10, pp. 8900–8909, 2019.

[314] C. A. C. Coello & G. B. Lamont, *Applications of multi-objective evolutionary algorithms*. World Scientific, 2004, vol. 1.

[315] J. Kennedy & R. Eberhart, "Particle swarm optimization," in *Proceedings of ICNN'95-international conference on neural networks*, IEEE, vol. 4, 1995, pp. 1942–1948.

[316] Y. Del Valle, G. K. Venayagamoorthy, S. Mohagheghi, J.-C. Hernandez & R. G. Harley, "Particle swarm optimization: Basic concepts, variants and applications in power systems," *IEEE Transactions on evolutionary computation*, vol. 12, no. 2, pp. 171–195, 2008.

[317] A. Rezaee Jordehi & J. Jasni, "Particle swarm optimisation for discrete optimisation problems: A review," *Artificial Intelligence Review*, vol. 43, pp. 243–258, 2015.

[318] I. N. Laboratory, "2014 bmw i3 with range extender (rex) advanced vehicle testing—baseline vehicle testing results," 2016.

[319] C. Zhang, Q. Zhou, Y. Li, L. Hua & H. Xu, "The digital twin modelling of the electrified vehicle based on a hybrid terminating control of particle swarm optimization," *IFAC-PapersOnLine*, vol. 54, no. 10, pp. 552–557, 2021.

[320] J. Jeong, W. Lee, N. Kim, K. Stutenberg & A. Rousseau, "Control analysis and model validation for bmw i3 range extender," SAE Technical Paper, Tech. Rep., 2017.

[321] C. Musardo, G. Rizzoni, Y. Guezennec & B. Staccia, "A-ecms: An adaptive algorithm for hybrid electric vehicle energy management," *European journal of control*, vol. 11, no. 4-5, pp. 509–524, 2005.

[322] X.-S. Yang, *Nature-inspired optimization algorithms*. Academic Press, 2020.

[323] K. Zielinski & R. Laur, "Stopping criteria for differential evolution in constrained single-objective optimization," in *Advances in differential evolution*, Springer, 2008, pp. 111–138.

[324] N. M. Kwok, Q. P. Ha, D. Liu, G. Fang & K. C. Tan, "Efficient particle swarm optimization: A termination condition based on the decision-making approach," in *2007 IEEE Congress on Evolutionary Computation*, IEEE, 2007, pp. 3353–3360.

[325] W. Pedrycz, A. Sillitti & G. Succi, *Computational intelligence: an introduction*. Springer, 2016.

[326] D. G. Kooijman, A. E. Balau, S. Wilkins, N. Ligterink & R. Cuelenaere, "Wltp random cycle generator," in *2015 IEEE Vehicle Power and Propulsion Conference (VPPC)*, IEEE, 2015, pp. 1–6.

[327] G. Suri & S. Onori, "A control-oriented cycle-life model for hybrid electric vehicle lithium-ion batteries," *Energy*, vol. 96, pp. 644–653, 2016.

[328] X. Han, L. Lu, Y. Zheng, X. Feng, Z. Li, J. Li & M. Ouyang, "A review on the key issues of the lithium ion battery degradation among the whole life cycle," *ETransportation*, vol. 1, p. 100 005, 2019.

[329] S. Shen, M. Sadoughi, X. Chen, M. Hong & C. Hu, "Online estimation of lithium-ion battery capacity using deep convolutional neural networks," in *International Design Engineering Technical Conferences and Computers and Information in Engineering Conference*, American Society of Mechanical Engineers, vol. 51753, 2018, V02AT03A058.

[330] S. Shen, M. Sadoughi & C. Hu, "Online estimation of lithium-ion battery capacity using transfer learning," in *2019 IEEE Transportation Electrification Conference and Expo (ITEC)*, IEEE, 2019, pp. 1–4.

[331] C. Vidal, P. Kollmeyer, E. Chemali & A. Emadi, "Li-ion battery state of charge estimation using long short-term memory recurrent neural network with transfer learning," in *2019 IEEE transportation electrification conference and expo (ITEC)*, IEEE, 2019, pp. 1–6.

[332] *Prognostics center of excellence - data repository*.

[333] N. Srivastava, G. Hinton, A. Krizhevsky, I. Sutskever & R. Salakhutdinov, "Dropout: A simple way to prevent neural networks from overfitting," *Journal of Machine Learning Research*, vol. 15, pp. 1929–1958, 2014.

[334] D. Liu, Y. Song, L. Li, H. Liao & Y. Peng, "On-line life cycle health assessment for lithium-ion battery in electric vehicles," *Journal of cleaner production*, vol. 199, pp. 1050–1065, 2018.

[335] X. Qu, Y. Song, D. Liu, X. Cui & Y. Peng, "Lithium-ion battery performance degradation evaluation in dynamic operating conditions based on a digital twin model," *Microelectronics Reliability*, vol. 114, p. 113 857, 2020.

[336] L. Lu, X. Han, J. Li, J. Hua & M. Ouyang, "A review on the key issues for lithium-ion battery management in electric vehicles," *Journal of Power Sources*, vol. 226, pp. 272–288, 2013.

[337] T. Kalogiannis, D. I. Stroe, J. Nyborg, K. Nørregaard, A. E. Christensen & E. Schaltz, "Incremental Capacity Analysis of a Lithium-Ion Battery Pack for Different Charging Rates," *ECS Meeting Abstracts*, vol. MA2017-01, no. 5, pp. 439–439, 2017.

[338] X. Hu, Y. Che, X. Lin & S. Onori, "Battery Health Prediction Using Fusion-Based Feature Selection and Machine Learning," *IEEE Transactions on Transportation Electrification*, vol. 7, no. 2, pp. 382–398, 2021.

[339] D. Yang, X. Zhang, R. Pan, Y. Wang & Z. Chen, "A novel Gaussian process regression model for state-of-health estimation of lithium-ion battery using charging curve," *Journal of Power Sources*, vol. 384, no. March, pp. 387–395, 2018.

[340] Y. Zhou, M. Huang, Y. Chen & Y. Tao, "A novel health indicator for on-line lithium-ion batteries remaining useful life prediction," *Journal of Power Sources*, vol. 321, pp. 1–10, 2016.

[341] K. A. Severson, P. M. Attia, N. Jin, N. Perkins, B. Jiang, Z. Yang, M. H. Chen, M. Aykol, P. K. Herring, D. Fraggedakis, M. Z. Bazant, S. J. Harris, W. C. Chueh & R. D. Braatz, "Data-driven prediction of battery cycle life before capacity degradation," *Nature Energy*, vol. 4, no. 5, pp. 383–391, 2019.

[342] D. Zhou, L. Xue, Y. Song & J. Chen, "On-line remaining useful life prediction of lithium-ion batteries based on the optimized gray model GM(1,1)," *Batteries*, vol. 3, no. 3, 2017.

[343] L. Ren, L. Zhao, S. Hong, S. Zhao, H. Wang & L. Zhang, "Remaining Useful Life Prediction for Lithium-Ion Battery: A Deep Learning Approach," *IEEE Access*, vol. 6, pp. 50 587–50 598, 2018.

[344] D. Liu, Y. Song, L. Li, H. Liao & Y. Peng, "On-line life cycle health assessment for lithium-ion battery in electric vehicles," *Journal of Cleaner Production*, vol. 199, pp. 1050–1065, 2018.

[345] Y. Zhang & B. Guo, "Online capacity estimation of lithium-ion batteries based on novel feature extraction and adaptive multi-kernel relevance vector machine," *Energies*, vol. 8, no. 11, pp. 12 439–12 457, 2015.

[346] L. Ren, L. Zhao, S. Hong, S. Zhao, H. Wang & L. Zhang, "Remaining Useful Life Prediction for Lithium-Ion Battery: A Deep Learning Approach," *IEEE Access*, vol. 6, pp. 50 587–50 598, 2018.

[347] C. Weng, Y. Cui, J. Sun & H. Peng, "On-board state of health monitoring of lithium-ion batteries using incremental capacity analysis with support vector regression," *Journal of Power Sources*, vol. 235, pp. 36–44, 2013.

[348] B. Ospina Agudelo, W. Zamboni & E. Monmasson, "Application domain extension of incremental capacity-based battery SoH indicators," *Energy*, vol. 234, p. 121 224, 2021.

[349] T. Goh, M. Park, M. Seo, J. G. Kim & S. W. Kim, "Capacity estimation algorithm with a second-order differential voltage curve for li-ion batteries with nmc cathodes," *Energy*, vol. 135, pp. 257–268, 2017.

[350] T. Shibagaki, Y. Merla & G. J. Offer, "Tracking degradation in lithium iron phosphate batteries using differential thermal voltammetry," *Journal of Power Sources*, vol. 374, pp. 188–195, 2018.

[351] B. Ospina Agudelo, W. Zamboni, F. Postiglione & E. Monmasson, "Battery State-of-Health estimation based on multiple charge and discharge features," *Energy*, vol. 263, no. PA, p. 125 637, 2023.

[352] J. zhen Kong, F. Yang, X. Zhang, E. Pan, Z. Peng & D. Wang, "Voltage-temperature health feature extraction to improve prognostics and health management of lithium-ion batteries," *Energy*, vol. 223, p. 120 114, 2021.

[353] D. Gong, Y. Gao, Y. Kou & Y. Wang, "State of health estimation for lithium-ion battery based on energy features," *Energy*, vol. 257, p. 124 812, 2022.

[354] Kevin P. Murphy, *Machine Learning: A Probabilistic Perspective*. MIT press, 2012, vol. 20, pp. 35–43.

[355] D. Lin, X. Zhang, L. Wang & B. Zhao, "State of health estimation of lithium-ion batteries based on a novel indirect health indicator," *Energy Reports*, vol. 8, pp. 606–613, 2022, ICPE 2021 - The 2nd International Conference on Power Engineering.

[356] R. R. Richardson, M. A. Osborne & D. A. Howey, "Gaussian process regression for forecasting battery state of health," *Journal of Power Sources*, vol. 357, pp. 209–219, 2017. arXiv: 1703.05687.

[357] R. C. E. C. K. I. Williams, *Gaussian processes for machine learning*. 2004, vol. 14, pp. 69–106.

[358] E. Brochu, V. M. Cora & N. de Freitas, "A tutorial on bayesian optimization of expensive cost functions, with application to active user modeling and hierarchical reinforcement learning," 2010. arXiv: 1012.2599 [cs.LG].

[359] J. Li, Y. Liu, D. Qin, G. Li & Z. Chen, "Research on equivalent factor boundary of equivalent consumption minimization strategy for phevs," *IEEE Transactions on Vehicular Technology*, vol. 69, no. 6, pp. 6011–6024, 2020.

[360] S. Xie, X. Hu, S. Qi & K. Lang, "An artificial neural network-enhanced energy management strategy for plug-in hybrid electric vehicles," *Energy*, vol. 163, pp. 837–848, 2018.

[361] K. R. Bouwman, T. H. Pham, S. Wilkins & T. Hofman, "Predictive energy management strategy including traffic flow data for hybrid electric vehicles," *IFAC-PapersOnLine*, vol. 50, no. 1, pp. 10 046–10 051, 2017.

[362] Z. Song, H. Hofmann, J. Li, J. Hou, X. Han & M. Ouyang, "Energy management strategies comparison for electric vehicles with hybrid energy storage system," *Applied Energy*, vol. 134, pp. 321–331, 2014.

[363] Y. Liang & S. Makam, "Phev hybrid vehicle system efficiency and battery aging optimization using a-ecms based algorithms," SAE Technical Paper, Tech. Rep., 2020.

[364] S. Sarvaiya, S. Ganesh & B. Xu, "Comparative analysis of hybrid vehicle energy management strategies with optimization of fuel economy and battery life," *Energy*, vol. 228, p. 120 604, 2021.

[365] G. Suri & S. Onori, "A control-oriented cycle-life model for hybrid electric vehicle lithium-ion batteries," *Energy*, vol. 96, pp. 644–653, 2016.

[366] Q. Zhou, J. Li, B. Shuai, H. Williams, Y. He, Z. Li, H. Xu & F. Yan, "Multi-step reinforcement learning for model-free predictive energy management of an electrified off-highway vehicle," *Applied Energy*, vol. 255, p. 113 755, 2019.

[367] G. Paganelli, S. Delprat, T.-M. Guerra, J. Rimaux & J.-J. Santin, "Equivalent consumption minimization strategy for parallel hybrid powertrains," in *Vehicular Technology Conference. IEEE 55th Vehicular Technology Conference. VTC Spring 2002 (Cat. No. 02CH37367)*, IEEE, vol. 4, 2002, pp. 2076–2081.

[368] Z. Song, J. Li, X. Han, L. Xu, L. Lu, M. Ouyang & H. Hofmann, "Multi-objective optimization of a semi-active battery/supercapacitor energy storage system for electric vehicles," *Applied Energy*, vol. 135, pp. 212–224, 2014.

[369] Z. Song, H. Hofmann, J. Li, X. Han, X. Zhang & M. Ouyang, "A comparison study of different semi-active hybrid energy storage system topologies for electric vehicles," *Journal of Power Sources*, vol. 274, pp. 400–411, 2015.

[370] E. Toolbox, "Fuels-higher and lower calorific values," *The Engineering ToolBox Available: https://www. engineeringtoolbox. com/fuels-higher-calorific-values-d_169. html [Accessed 14/08/2022]*, 2003.

[371] C. Musardo, G. Rizzoni, Y. Guezennec & B. Staccia, "A-ecms: An adaptive algorithm for hybrid electric vehicle energy management," *European journal of control*, vol. 11, no. 4-5, pp. 509–524, 2005.

[372] S. Onori, L. Serrao & G. Rizzoni, "Hybrid electric vehicles: Energy management strategies," 2016.

[373] Isidor, B.. "Battery university: Safety of lithium-ion batteries. "2017.

[374] L. Tang, G. Rizzoni & S. Onori, "Energy management strategy for hevs including battery life optimization," *IEEE Transactions on Transportation Electrification*, vol. 1, no. 3, pp. 211–222, 2015.

[375] C. Zhang, Q. Zhou, Y. Li, L. Hua & H. Xu, "The Digital Twin Modelling of the Electrified Vehicle Based on a Hybrid Terminating Control of Particle Swarm Optimization," *IFAC-PapersOnLine*, vol. 54, no. 10, pp. 552–557, 2021.

[376] Z. Huang, X. Xiao, Y. Gao, Y. Xia, T. Dragicevic & P. Wheeler, "Emerging Information Technologies for the Energy Management of Onboard Microgrids in Transportation Applications," *Energies*, vol. 16, no. 17, p. 6269, 2023.

[377] G. Zhang, R. Wang, M. Gao, H. Yu & R. Qiu, "A Power Flow Dynamic Deduction Method for Urban Rail Traction Power Supply System Considering the Fluctuation of Train Passenger Load," *IEEE Transactions on Transportation Electrification*, 2024.

[378] Z. Xu, J. Xu, Z. Guo, H. Wang, Z. Sun & X. Mei, "Design and optimization of a novel microchannel battery thermal management system based on digital twin," *Energies*, vol. 15, no. 4, p. 1421, 2022.

[379] A. M. Jasim, B. H. Jasim, B.-C. Neagu & S. Attila, "Electric Vehicle Battery-Connected Parallel Distribution Generators for Intelligent Demand Management in Smart Microgrids," *Energies*, vol. 16, no. 6, p. 2570, 2023.

[380] M. Hua, B. Shuai, Q. Zhou, J. Wang, Y. He & H. Xu, "Recent Progress in Energy Management of Connected Hybrid Electric Vehicles Using Reinforcement Learning," *arXiv preprint arXiv:2308.14602*, 2023.

[381] R. Mao, Y. Li & H. Zhang, "Simulation Method in Automotive, Aviation and Maritime Industries for Digital Twin: A Brief Survey," in *2023 IEEE 18th Conference on Industrial Electronics and Applications (ICIEA)*, IEEE, 2023, pp. 1442–1447.

[382] D. E. R. de Gauna, L. E. Sanchez, A. Ruiz-Iniesta, C. Villalonga & M. A. Serrano, "Towards an integrated swarm intelligence framework for urban mobility: A systematic review and proposed theoretical model," *Journal of King Saud University-Computer and Information Sciences*, p. 101 836, 2023.